ERASMUS MUNDUS MSC PROGRAMME

COASTAL AND MARINE ENGINEERING AND MANAGEMENT
COMEM

VIDEO-BASED NEARSHORE BATHYMETRY ESTIMATION FOR RIP CURRENT FORECASTING ON A MACROTIDAL BEACH

Roberto Sasso Steele
4128702

Delft University of Technology
June 2012

The Erasmus Mundus MSc Coastal and Marine Engineering and Management is an integrated programme organized by five European partner institutions, coordinated by Delft University of Technology (TU Delft).
The joint study programme of 120 ECTS credits (two years full-time) has been obtained at three of the five CoMEM partner institutions:

- Norges Teknisk- Naturvitenskapelige Universitet (NTNU) Trondheim, Norway
- Technische Universiteit (TU) Delft, The Netherlands
- City University London, Great Britain
- Universitat Politècnica de Catalunya (UPC), Barcelona, Spain
- University of Southampton, Southampton, Great Britain

The first year consists of the first and second semesters of 30 ECTS each, spent at NTNU, Trondheim and Delft University of Technology respectively.
The second year allows for specialization in three subjects and during the third semester courses are taken with a focus on advanced topics in the selected area of specialization:

- Engineering
- Management
- Environment

In the fourth and final semester an MSc project and thesis have to be completed.
The two year CoMEM programme leads to three officially recognized MSc diploma certificates. These will be issued by the three universities which have been attended by the student. The transcripts issued with the MSc Diploma Certificate of each university include grades/marks for each subject. A complete overview of subjects and ECTS credits is included in the Diploma Supplement, as received from the CoMEM coordinating university, Delft University of Technology (TU Delft).

Information regarding the CoMEM programme can be obtained from the programme coordinator and director

Prof. Dr. Ir. Marcel J.F. Stive
Delft University of Technology
Faculty of Civil Engineering and geosciences
P.O. Box 5048
2600 GA Delft
The Netherlands

VIDEO-BASED NEARSHORE BATHYMETRY ESTIMATION FOR RIP CURRENT FORECASTING ON A MACROTIDAL BEACH

By:
Roberto Sasso Steele
June, 2012

Graduation committee:

Prof.dr.ir. M.J.F. Stive	Chairman, Delft University of Technology
Dr.ir. A.R. van Dongeren	Deltares
Dr.ir. J.S.M van Thiel de Vries	Deltares/ Delft University of Technology
Dr. Martin Austin	Plymouth University
Ir. P.B. Smit	Delft University of Technology

This thesis was prepared both at the offices of

Stichting Deltares
Rotterdamsweg 185, 2629HD,
Delft, the Netherlands

and at

The School of Marine Science and Engineering
Plymouth University
United Kingdom

Spending two of the available five months at the latter. This thesis is in partial fulfillment of the requirements of the degree

Erasmus Mundus Master in Coastal and Marine Engineering and Managament (CoMEM)

which is coordinated by

Prof.dr.ir. M. J. F. Stive
Faculty of Civil Engineering and Geosciences
Delft University of Technology (TU Delft)
Delft, The Netherlands

And includes the following educational institutions

Norwegian University of Science and Technology (NTNU)
Trondheim, Norway

Polytechnic University of Catalonia (UPC)
Barcelona, Spain.

Delft University of Technology (TU Delft)
Delft, The Netherlands

At which the graduate has studied.

ABSTRACT

Rip currents are seaward directed flows of water that traverse the surf zone, and in many cases pose potentially dangerous conditions for swimmers and beach users. The present study is carried out focusing on Perranporth beach, UK, which is known to present quite strong rip current events that have been the culprits of large numbers of incidents or rescues (in some cases more than 65 in a single day) in the past (Scott et al., 2009). The main objective of this work is related to the forecasting of rip currents, particularly in helping to develop, calibrate, and validate an operational swimmer safety model for Perranporth beach, UK. This main objective is divided into several specific objectives, which look into answering both general scientific questions and specific details for the implementation of the model at the study site.

The tool used for the estimation of bathymetries is the data-model assimilation scheme *Beach Wizard*, which uses video-derived information to adjust an initial bathymetry into an updated bathymetry. The Beach Wizard model is run with the numerical model XBeach, assimilating the hydrodynamic model output with video-derived measures of wave dissipation (imaps). Specific model formulations and parameters of Beach Wizard are varied and tested as to determine the effects of each, as well as to obtain the best working model for Perranporth, UK. Two systematic estimation errors that were originally pointed out by van Dongeren et al. (2008) are looked into, resulting in the implementation of a variation in the bed updating process, by introducing a time-dependent bed change factor. The changes applied to the model formulations and the adjustments of default parameters resulted in accurate estimations of bathymetries over a three month period (April-June 2011) during which video derived input and five measured bathymetries are available at Perranporth.

The importance of video derived input (timex images) is analyzed in detail, by defining several criteria concerning the quality, quantity, and temporal regularity of images used as input. The quality criteria is divided into two separate indicators, in this manner differentiating between actual image quality (if the camera lens is clean or dirty, or if there is foggy conditions, etc.) and dissipation map (imap) quality (if the dissipation patterns are good or not). With this, it was found that imap quality stands over image quality, meaning that it is more important to have favorable wave breaking conditions than perfect image resolution. As well as this, image regularity was found to be important in maintaining the models predictive ability, due to large temporal gaps between consecutive images increasing the bed uncertainty significantly (resulting in very large, and possibly erroneous bed changes if the corresponding imap is not perfect). The final criteria looked at was image quantity, which turned out not to be of great importance as long as the image regularity is

maintained; presenting even improved results for a case using a smaller total amount of input with the same temporal spacing.

The effects of the above mentioned variations in video derived input were quantified in two overall manners, firstly by computing Brier skill scores and RMS errors over the resulting bathymetries for each case, and secondly by using the computed bathymetries in a non-stationary hydrodynamic XBeach model and comparing the resulting nearshore flows to the nearshore flows computed over measured bathymetries. Both of these methods resulted in the same conclusions mentioned above.

In using estimated bathymetries from the Beach Wizard model for the modeling of rip currents, it was found that very promising similarities are seen between said currents and the currents modeled over measured bathymetries. The use of estimated bathymetries show clear improvements over using an outdated measured bathymetry for the prediction of rip currents, essentially validating the use of the Beach Wizard tool in the eventual implementation of an operational rip current forecasting system at Perranporth beach.

Keywords: Rip current forecasting, bathymetry estimation, Beach Wizard, data-model assimilation, Perranporth.

ACKNOWLEDGEMENTS

First of all I would like to thank my thesis committee for all their valuable input over the past 6 months. In particular Ap van Dongeren, Jaap van Thiel de Vries and Marin Austin who were all extremely helpful. As well as my official committee, I would like to thank Leo Sembiring for all his help during my stay at Deltares and Robert McCall for his helpful contributions during my two months in Plymouth.

I would like to thank and acknowledge Deltares and Plymouth University, both of whom hosted me during this work. This project was funded by Flood Control 2015 (Realtime Safety on Sedimentary Coasts program).

I would also like to acknowledge and thank everyone that has made the CoMEM program possible, in particular Prof. dr. ir. Marcel Stive, who's support and feedback during my work is also greatly appreciated, as well as Mariette van Tilburg and Madelon Burgmeijer for all their planning and organization. I have thoroughly enjoyed my last two years in this program, and would also like to acknowledge all of the universities at which I studied: NTNU (Trondheim, Norway), TU Delft (Delft, the Netherlands), and UPC (Barcelona, Spain).

Finally I thank all my friends and family back home for all their support and encouragement over the last couple of years. To my mum and dad, even though you were far away, your support and encouragement have been fantastic. And finally, to the person who has undoubtedly been my biggest supporter (even though she had no idea) and the reason I have tried so hard to do my best and hurry home, my beautiful daughter, Emilia. Thank-you.

Roberto Sasso Steele
Delft, June 2012

1 INTRODUCTION

1.1 Statement

Rip currents are seaward directed flows of water that traverse the surf zone, and are generally characterised by being extremely unstable and difficult to predict due to the wide range of variables which influence their behaviour. Our understanding of the behaviour and mechanics of rip currents has been greatly expanded over the last fifteen years or so due to a series of field and laboratory experiments (reviewed by MacMahan et al., 2006). However, many of these experiments were carried out for micro-tidal beaches, which are known to behave very differently to macro-tidal beaches.

This project is based on a specific macro-tidal case study at Perranporth beach, on the southwest coast of England, which presents high incidence of rip currents due to its specific hydrodynamic and morphological characteristics. Perranporth is characterized as a low tide bar/rip beach type or "LTBR" (Scott et al., 2007), which is an intermediately dissipative beach, with a macro-tidal tide, having a maximum range at spring tide of approximately 6.5 m.

The main problem addressed in this study is with regard to accurately estimating bathymetries in a macrotidal environment for use in modelling rip currents and assessing swimmer safety levels. One of the major difficulties in predicting and modelling rip currents lies in obtaining the bathymetrical information of the study area, which can be very dynamic and unstable in many cases. It is known that surf zone morphodynamics are quite complex, proving widely movable bathymetries in short periods of time, which can greatly affect the generation and behaviour of rip currents. Because of this, and due to the fact that the bathymetry and bottom contours are one of the governing factors influencing rip currents, the ability to properly model and predict rip currents relies on accurate and up to date bathymetric information of the beach and surf zone.

Another issue particular to the present study is the characteristics of rip currents on macrotidal beaches. It has been shown that tidal variations of rip currents generally show a significant increase in strength during mid to low tides; particularly on macrotidal beaches (Austin et al., 2010). The exact reason for this strengthening of the currents during outgoing lower tides is not completely known, although there are several factors that are known to influence this phenomenon, the "weight" or importance of each factor is what remains uncertain. Considering these temporal fluctuations in rip strength, it is clear that the prediction of rip currents should be able to include the proper approximation of rip strength as well as its timing and duration.

1.2 Importance

This project is directly related to swimmer safety, specifically at Perranporth beach in the southwest of the UK. This in itself can be looked at as the main importance or substantiating grounds for the carrying out of this work, along with the obvious benefits of widening our scientific and theoretical understanding of rip currents and bathymetrical updating systems in macro-tidal environments.

Rip currents account for the vast majority of rescues or "incidents" at lifeguard monitored beaches all around the world; the records taken at 62 beaches in the southwest of England from the Royal National Lifeboat Institution (RNLI) showed that during spring and summer (1 May to 1 Oct) in 2005, rip currents were responsible for 71% of all recorded incidents (Scott et al, 2007).

It is quite clear that in order to provide a far safer beach environment for its users, action must be taken in regard to the dangers of rip currents. These actions are quite restricted, in that in most cases physical action (construction of physical structures, hard or soft) is not feasible. Therefore, forecasting and beach safety education come into the picture as having major roles. The creation of an accurate warning system for beach users and life guard associations would be of enormous value if it could eventually come to save lives in its implementation.

Of particular distress in the southwest of the UK are mass rescue events, during which massive simultaneous rescues at beaches in the area are undertaken. A project on rip current variability and hazard on the southwest coast of the UK by Scott et al (2009)

showed this phenomenon of mass rescue events, which in almost all cases were quite spatially varied (occurring at more that 10 beaches at a time). This spatial variation of the events shows the importance of the hydrodynamic forcing (waves/tides), due to the fact that these forces are generally the same for neighbouring beaches. These mass rescue events showed up to 151 rescues per day (at over 10 beaches), and in certain cases around 65 incidents per day at a single beach (Scott et al, 2009).

Beach safety education and awareness is of great importance in controlling rip current related accidents. A survey conducted on beachgoers in two regional areas of New South Wales, Australia, showed that 20% did not know what a rip current looked like, 80% thought they could identify a rip current (but only 40% could actually do so), and 50% pointed out a rip current as the safest place to swim (Hatfield et al, 2007). Looking at these results, and considering that Australia is a country with quite high levels of beach safety education, it is clear that there is room for improvement in this area. The development of an operational swimmer safety model, which users and lifeguard institutions can access along with educational information on how to identify rips as well as how to react to them in case of an emergency, would be an immense contribution to the goal of preventing rip related incidents around the world.

1.3 Objectives

The general objective of the present master´s thesis is to help develop, calibrate and validate an operational swimmer safety model for Perranporth beach, located in the south west of the UK. With this project's general objective in mind, a set of specific objectives are defined that will envelope the entirety of the work to be carried out; and are shown in bullet form below.

- Analyse the importance of up to date bathymetrical information for the correct modelling of rip currents and associated level of swimmer safety at Perranporth beach. This is done by analysing the variation of measured bathymetries, knowing that the accurate modelling of rip currents is directly related to the input bathymetry (real bathymetries producing quite good model results).

- Set up and calibrate an operational bathymetry updating system for Perranporth beach, using Argus video information, offshore SWAN output, tidal information, and measured bathymetries (all available between April and July 2011). The method to be used for said bathymetry updating will be the data-model assimilation method Beach Wizard (Van Dongeren et al., 2008).
- Analyse the Beach Wizard model formulations and parameter settings, as well as issues concerning the spatial (cross shore direction) variability in the model's behaviour.
- Analyse the behaviour of the aforementioned bathymetry updating system with regards to the frequency, quality, and quantity of input (Argus images) necessary to achieve accurate estimates resembling real measured bathymetries.
- Analyse the temporal variability (in the order of months) of the bathymetry calculation's error, with the objective of determining the relative importance of specific individual inputs (Argus images); possibly depending on the occurrence of variable storm events.
- Validate the bathymetry updating system with regards to rip current dynamics, by utilizing the obtained bathymetries as input to a non-stationary hydrodynamic XBeach model (which is available for Perranporth beach from Austin et al., (in press)) and comparing with the obtained flows using the same model and measured bathymetries.

1.4 Theoretical and practical background

Extensive research has been undertaken on the topic of rip current dynamics, however, due to the high complexity level of these systems it can be said that much work is yet to be done on the matter at hand. Rip current theory dates back to around 1940, when the first attempts to describe rip currents arose (Shepard, Emery and La Fond, 1941), followed by the first description of these; which was that the onshore mass transport by waves over an alongshore bar exits most efficiently through a rip channel (Munk, 1949 a,b). Following this, the theory of rip currents and their

behaviour has been widely expanded; a good general review of these developments is described by MacMahan et al. (2006).

As well as theoretical advances in rip current theory, a series of field and laboratory experiments have been undertaken as to acquire a solid basis for these theories. Much of the current knowledge and experimental results regarding rip currents has been undertaken in the last ten to fifteen years or so (MacMahan et al, 2006), which isn't really much time at all considering the complexity of these systems.

As it was mentioned previously, one of the topics to be addressed in the present study is the temporal variability of rip current circulation on a macro-tidal beach. This problem has not been greatly studied, with the exception of Austin et al. (2010) and Bruneau et al. (2009). A field experiment on the same beach as the present study (Perranporth, UK) was carried out by Austin et al. (2010) to examine rip dynamics over a LTBR system in response to changing wave and tide conditions. One of the aims of this study by Austin et al. (2010) was to look at the importance of the spatial and temporal distribution of wave dissipation, and the distribution of morphodynamic flow constrictions, both of which had been previously linked to the tidal modulation of rip current flow, ultimately resulting in that with decrease in tidal levels higher rip current flows are expected (Shepard et al., 1941; Scott et al., 2009; MacMahan et al., 2006; Bruneau et al., 2009). Austin et al. (2010) concluded that both variations in wave dissipation and morphological control seem to force the rip current flow, however, the importance of each process is variant.

A topic of great importance in the scope of the present study is that related to video-imaging and the benefits and possibilities of the different techniques applied in this field. The use of video imaging for the study of coastal processes dates back to the early 1930's, when aerial photographs were beginning to be used for this effect. More recently, in 1980, the Coastal Imaging Lab (CIL) at Oregon State University began the first attempts at remote sensing, using time-lapsed video images of wave runup for the study of infragravity wave motions (Holman and Stanley, 2007). Having thought of using these time-exposed images for the study of infragravity wave motions (although for that purpose the results were inconclusive) ended up opening the doors to what is one of the main products of the Argus system. During this experiment clear

bands of wave breaking were observed, which turned out to be related to an offshore sand bar. That observation was then extensively studied until a relationship between the time-exposure images and sand bar location was demonstrated in tests at Duck, North Carolina (Lippmann and Holman, 1989). Following this initial discovery of the applicability of time-exposure images to the study of the dynamics of the nearshore coastal zone, the first un-manned Argus video-imaging station was set up in 1992 at Yaquina head, Oregon, after which two newer generations have been developed (now working with the third generation of Argus). The Argus system has been widely expanded and improved over the years, and now has many capabilities in providing valuable information on the nearshore coastal zone, which has obvious benefits in comparison to other data collection methods (field surveys).

In the past, the obtaining of bathymetrical information was limited by excessive costs and time-consuming procedures. As it was mentioned in the objectives of the present work, nearshore bathymetrical information will be obtained using a relatively new technique, combining video-imaging and a data-model assimilation method called "Beach Wizard" (Van Dongeren et al., 2008), which will be described in the next section of this report. This bathymetry estimation method follows the work of Aarninkhof et al., (2005a), where the basis of the remote sensing technique used in Beach Wizard was developed in a 1D format, operating on a time series of cross-shore intensity profiles to resolve the pattern in depth change on a morphological timescale.

The use of numerical models for the approximation of hydrodynamic behaviour in the nearshore zone has seen vast improvements in recent years, and is currently under development. In the present work the numerical model XBeach (Roelvink et al., 2009) will be employed to simulate rip dynamics (the basis of this model will be explained in further detail in the upcoming section of this report). Over the years the capabilities of hydrodynamic models have seen large improvements, to a point in which now if accurate bathymetry and forcing conditions are available, the skill of these models is quite good (Sutherland et al., 2004; Van Rijn et al., 2003). The importance of good and up to date bathymetrical information is thought to be of great importance in obtaining good results (Van Dongeren et al., 2008).

The development of operational models in the coastal zone, specifically with respect to morphodynamics and hydrodynamics is a topic yet to be greatly studied. MICORE (Morphological Impacts and Coastal Risks Induced by Extreme Storm Events) is a European Union project, which aims (amongst others) to develop real time systems for the prediction of storm impacts. The MICORE project analysed storm response approaches in nine European countries, concluding that a great improvement would be the implementation of operational coastal risk assessment methods. Baart et al. (2009) describes the architecture of the proposed system by MICORE, which is a real-time system taking into account morphodynamic processes. The implementation of an operational model of this kind requires the coupling of several models, with different scales and objectives, ideally resulting in real time results for the specified users on a web server. In addition, Sembiring (2010) evaluated the performance of an operational model and the Beach Wizard scheme, for Egmond Beach on the north Dutch coast, finding that the implementation of an operational model in combination with Beach Wizard is feasible.

2 THEORETICAL FRAMEWORK

2.1 Rip currents

2.1.1 *Definition*

A rip current can be defined as a seaward directed flow of water that is generated in the surf zone, converges through a narrow channel, and finally widens past the breaker line. This is obviously a crude approximation for the sake of a general description of a rip current, which can also be seen schematically in Figure 2-1. As it is shown in Figure 2-1, the general form of a rip current consists of alongshore feeder currents near the shoreline that converge to form the rip, which flows through the rip neck and broadens into the rip head past the breaker zone. The presence of alongshore variations in wave breaking bring variations in the onshore directed flows, which in turn will contribute to the aforementioned feeder currents that converge into a rip current (MacMahan et al., 2006).

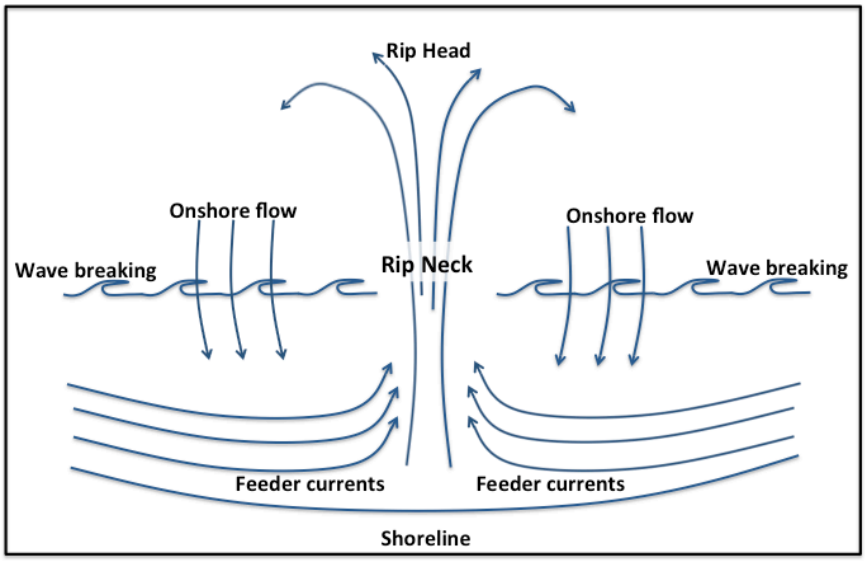

Figure 2-1. Rip current schematization (based on MacMahan et al. 2006)

For near normally incident waves at beaches presenting rip current systems, it is common for these to present closed circulation cells. This meaning that the water that exits via the rip head returns onshore and forms a closed circulation pattern. Rip currents may present one or two circulation cells (rotating in opposite directions), and in some cases with very strong alongshore currents no circulation cells at all. Not knowing the exact characteristics of rip currents at every beach poses danger for

swimmers, as different types of circulation will call for different reactions from swimmers to exit a rip current.

2.1.2 *Generation and forcing*

A simple way of looking at the generation of rip currents is by considering that where waves break, the water surface moves shoreward, and it is clear that this shoreward moving water must somehow return offshore. Now, this return flow can either present itself as undertow (a return flow at intermediate depth under breaking waves), or as rip currents. The deciding factor on whether the return flow will be as undertow or as a rip current will depend on a series of elements, such as the alongshore distribution of wave breaking, the presence of bars, channels or other morphological flow constrictors, and the hydrodynamic conditions. Bowen (1969) showed that alongshore variations in bathymetry produce variations in wave height, which in turn generate rip currents.

Both morphological confinement and hydrodynamic forcing are key factors in the generation of rip currents, presenting for a certain combination of these an "optimum" rip. The modulation of rip current flow due to distribution of wave dissipation and distribution of morphological flow constrictions was studied by Austin et al. (2010), and concluded that both factors influence rip modulation at different scales depending on other variables (the importance of each process was not clearly found). Wave conditions play a key role in rip intensity, presenting a general finding that follows the most basic description of rip currents, that is for larger, more energetic waves, rip intensities will be higher (MacMahan et al., 2006) due to a larger amount of water exiting the surf zone. However, this is a generalization, since rip intensity depends on a series of other factors (morphodynamic), and not necessarily all the water exiting the surf zone will do so in the form of rip currents (undertow may be the main component in many cases).

The forcing used in dynamical rip current models is based on alongshore wave height variations, which generate variations in the alongshore momentum flux. The excess momentum flux due to the presence of waves is known as radiation stress (Longuet-Higgins and Stewart, 1964), and the horizontal gradients in these give rise to a wave

induced force on the water. From these wave induced forces come water level variations as well as currents (both in cross shore and longshore directions); this can be seen considering the momentum balance equations (MacMahan et al., 2006). For a simplified case with normally incident waves on an alongshore uniform beach, the regions with larger breaking waves have larger set up and set down, which generate currents away from these regions of high waves towards regions with lower breaking waves. The alongshore momentum equation can be viewed as follows (MacMahan et al., 2006).

$$Fy = -\frac{dS_{yy}}{dy} - \rho g(h+\eta)\frac{d\eta}{dy} \quad (1)$$

where Fy is the alongshore forcing, S_{yy} is the alongshore radiation stress, ρ is the density if seawater, g is gravitational acceleration, h is the still water level, and η is the surface elevation. Considering as well that in shallow water S_{yy} = E/2 and wave height is depth restricted by a breaking coefficient γ, where E is the wave energy ($E=1/8\ \rho g H^2$), we obtain the following alongshore momentum balance (MacMahan et al., 2006).

$$Fy = -\frac{1}{8}\rho g\gamma^2(h+\eta)\frac{d(h+\eta)}{dy} - \rho g(h+\eta)\frac{d\eta}{dy} \quad (2)$$

In this case shown in Equation (2) (supposing a small and negligible shear component of the radiation stress), the radiation stress forcing is of the same magnitude and direction as the pressure gradient, resulting in a convergence of flows in areas of low waves, exiting the surf zone in the form of a rip.

2.1.3 *Types*

Rip currents can be divided into two general groups, being those that are generated by morphological constriction (Dalrymple, 1978) and those that are not (Dalrymple et al., 2011). Morphologically constrained rip currents have been identified as the most common type of rip current (Dalrymple, 1978). They are also characterised as being stronger than non-morphologically constrained (or transient) rip currents. Morphological confinement or restriction of rip currents refers to the rip current flow being driven by a physical characteristic, may it be topographical (due to the shape of the beach or bay), bathymetrical (due to bars and channels on the seabed), or even hard coastal structures (breakwaters or groynes). Due to the fact that the beach

studied in this thesis (Perranporth, UK) is an intermediately dissipative beach (Wright et al., 1984; Scott et al., 2007) with a macro-tidal tide, some of the characteristic rip current systems for these environments will be described below.

Research on rip currents in macro-tidal environments (Scott et al., 2007,2009; Austin et al., 2010) have shown that beaches presenting clear rip channel morphologies tend to present the highest risk or intensity of these seaward flows. Rip channel morphologies refers to the beach configuration, which will also depend on the beach state (Wright et al., 1984; Scott et al., 2007). Beach states as defined by Wright et al. (1984) can be divided into 3 major groups, dissipative beaches, reflective beaches, and intermediate beaches. The so-called intermediate beach states are in turn divided into four generalised states, being longshore bar trough (LBT), rhythmic bar and beach (RBB), transverse bar and rip (TBR), and ridge runnel or low tide terrace (RR or LTT). These four beach states can be seen schematically in Figure 2-2.

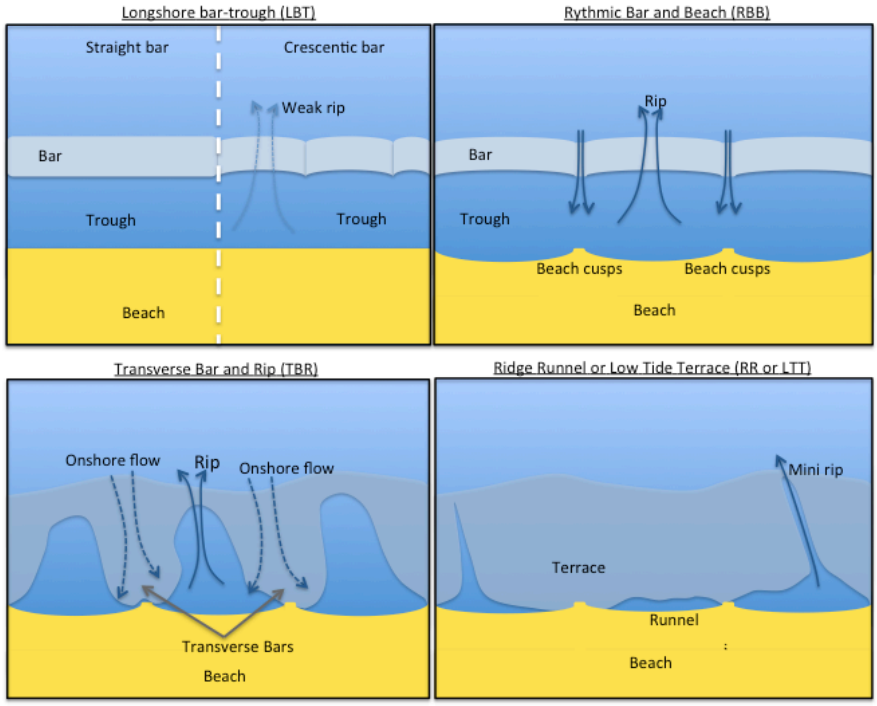

Figure 2-2. The four intermediate beach states (Modified from Wright et al. (1984)).

On the Atlantic coast of the UK around 90% or rip current related incidents recorded by the Royal National lifeboat Institution (RNLI) were due to the contribution of beaches presenting identifiable rip channel morphologies, more specifically low tide terrace and bar/rip (LTT+R), and low tide bar/rip (LTBR) morphologies (Scott et al.,

2009). These two beach types are variations of the previously mentioned four intermediate beach states according to Wright et al. (1984). The term "low-tide" in the name of these two beach states refers to the fact that the state of the beach varies in time, and during low tides is when the particular morphologies (terrace and bar/rip or bar/rip) are present. These two beach types just mentioned have a tendency to present rhythmic bar and rip current systems around low tide (when bars and/or terraces are present), and it was shown by Scott et al. (2007) that the type with highest calculated rip current risk in the UK falls under LTBR beaches.

2.1.4 *Characteristics*

Rip currents have several known forcing processes or mechanisms that produce fluctuations at different time scales (MacMahan et al, 2006). These pulsations are composed of infragravity motions (Reniers et al., 2007), modulations of wave group energy (Reniers et al., 2004), shear instabilities (Haller and Dalrymple, 2001), and tides (Bruneau et al., 2009; Austin et al., 2010). These pulsations of rip current flow velocity can reach quite high variation levels, showing in some cases variations from typical velocities of 0.3-0.6 m/s in the rip neck to velocities of 2 m/s (MacMahan et al., 2006) in a matter of minutes. As well as these rather fast fluctuations in rip velocity, longer timescales also affect rips. As it was mentioned earlier, tidal elevation is a crucial parameter for rip strength, particularly at macro-tidal beaches. In most cases where large tidal ranges are present, highest rip intensity is observed around low water, due to increased wave breaking because of shallower water depths as well as heightened morphological flow constriction (presence of bars and channels).

Seasonal variation of rip currents is also a factor in many places, for which some key drivers were found (for rip intensity) for LTBR and LTT+R beaches in the south of the UK by Scott et al. (2009). These drivers include relatively small long-period swell waves, low- and mid-tide bar/rip morphologies and spring tidal ranges (Scott et al., 2009). With regards to seasonal variations it can then be said that spring/summer months (presenting small, long-period waves) tend to promote and develop accretionary bar/rip systems. Long period swell waves also allow shoaling to extend further to the inner bars, therefore generating increased alongshore gradients in

dissipation and consequently stronger rips. As well as this, long-term tidal cycles influence rip intensity, as extreme low tides may present high incidence of rip current risk. The large tidal variations don't necessarily produce stronger rip currents, but increase the rate of alongshore transition or "movement" of these, reducing the possible reaction time for lifeguards.

As well as being temporally variable, rip currents are spatially variable, depending mainly on bathymetric features and hydrodynamic forcing variations. Rip current spacing is a topic that has not been greatly studied for macro-tidal beaches, and the attempts that have been made to correlate rip spacing with wave height, period and sediment characteristics have not been successful (Ranasinghe et al., 2002). Models however, have shown that there is a correlation between rip spacing and the alongshore length scale of wave group energy and the wave direction. Although it might seem plausible for rip intensity to be dependent on rip spacing, this is not the case; rip currents have only a limited capacity, and increasing the spacing only redistributes the composition of the return flow (undertow is a major factor).

Rip currents can present serious danger for swimmers in many cases. Considering that an excellent swimmer in peak physical condition can barely reach a swimming speed of 1m/s, and that in certain cases current speeds of around 2m/s have been recorded (MacMahan et al., 2006), its clear that rips pose a definite threat. As to present some general measured characteristics of rip currents from different locations around the world, Table 2-1presents just this, adapted from MacMahan et al. (2006).

Table 2-1. Characteristic field measurements of rip currents (* estimated to MSL), where U_r is mean rip current cross shore velocity, U_{max} is the maximum rip velocity, λ_r is the rip spacing, w_r is the rip channel width, h_r^* is the channel depth, h_b^* is the bar height, H_{mo} is the significant wave height, and D_{50} is the mean sediment size. Adapted from MacMahan et al. (2006).

Location	U_r (m/s)	U_{max} (m/s)	λ_r (m)	w_r (m)	h_r^* (m)	h_b^* (m)	H_{mo} (m)	T_p (s)	D_{50} (mm)
Skallingen, NED	0.3	1.7	90	150	1.25	1	0.8	8	0.25
Pal Beach, AUS	0.4	2	200	60	1.8	1	0.75	10	0.35
Muriwai, NZL	0.65	2	500	150	1.5	1	1.5	14	0.25
Moreton Islan, AUS	0.4	1	300	35	1.4	1	0.5	10	0.2
Torrey Pines, USA	0.2	1	300	100	1.25	1	0.5	12	0.1
Monterrey, USA	0.3	2	125	60	1.5	1	1.5	12	0.35
Sea Grove, USA	0.35	1.25	60	30	0.8	0.3	0.5	8	0.3

2.2 Numerical modeling of rip currents (XBeach)

It was mentioned earlier that in the present study the numerical model "XBeach" will be used to model rip current dynamics. This model is an open source software, currently under development by UNESCO | IHE, Deltares, Delft University of Technology, and University of Miami. XBeach was originally developed to study the nearshore response to hurricane impacts (Roelvink et al., 2009), and will be used here for the modelling of rip current flows and as the model base for the bathymetry updating scheme Beach Wizard. The XBeach model has been tested against field measurements, and has proven to give good results in the modelling of rip currents (Jacobs, 2010, Winter, 2011). The model includes wave breaking, surf and swash zone processes, dune erosion, overwashing and breaching (where the important processes for this particular study are in wave breaking and surf hydrodynamics). The important processes for the modelling of surf zone dynamics are resolved employing a two-dimensional horizontal description of the wave groups and accompanying infragravity waves over a certain bathymetry (Roelvink et al., 2009). For the modelling of rip current flows, the wave group forcing is computed from a non-stationary wave-action balance with a dissipation model and a roller model according to Roelvink et al. (1993), all of which will be briefly described shortly. As well as this, the short wave model may be run in stationary mode (which will be implemented for the Beach Wizard scheme), applying the wave dissipation formulation of Baldock et al (1998). XBeach can also simulate sediment transport and associated morphodynamics, but will not be used in the present application.

The functionalities of the model mentioned above are separated into a number of modules, where the main ones are the hydrodynamic module and the morphodynamic module, and are in turn divided into four sub-modules. These sub modules are the short wave module and flow module (under the hydrodynamic module), and the morphology module and sediment transport module (under the morphodynamic module). Figure 2-3 shows how the previously mentioned modules interact with each other, where the arrows symbolize connectivity and the terms in italics are relevant output parameters for each module. In this figure an arrow going from one module to another indicates the use of output from the former in the latter.

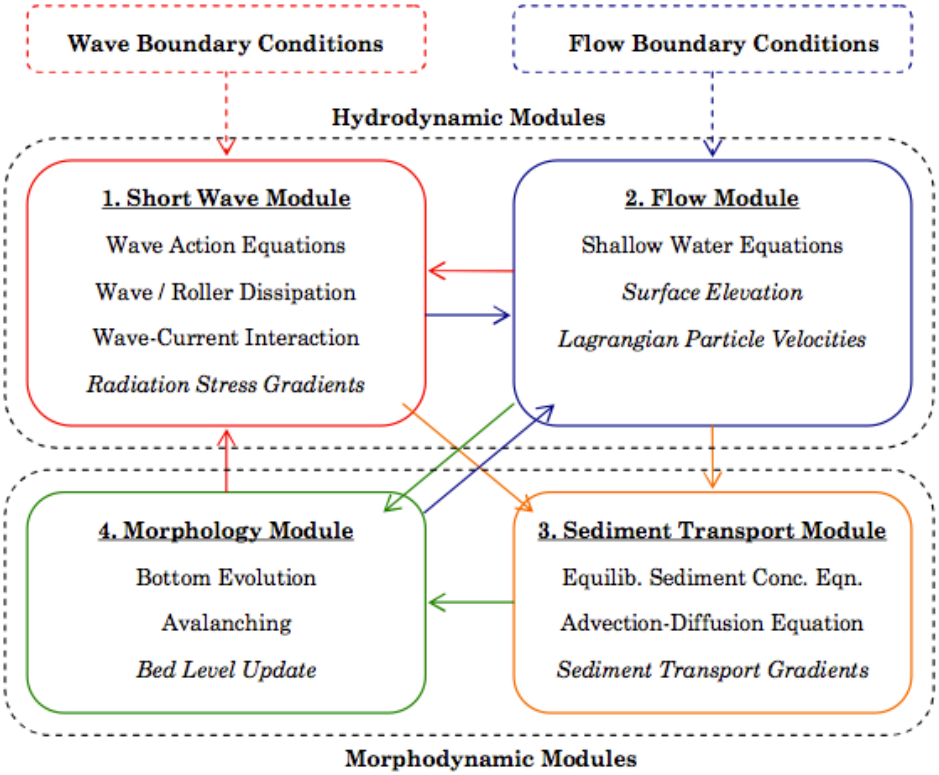

Figure 2-3. XBeach component modules (Daly, 2009)

The following model formulations are taken and summarised from Roelvink et al. (2009), which use a coordinate system where the x-axis is towards the coast (perpendicular) and the y-axis is alongshore, this is depicted below in Figure 2-4. The grid used is a staggered grid, where water levels, water depths, bed levels and concentrations are defined in cell centres and velocities and sediment transport rates are defined at the cell interfaces (*u*- and *v*- points). As well as this, in the energy balance, the energy, roller energy and radiation stress are defined at cell centres, and the radiation stress gradients are defined at cell interfaces.

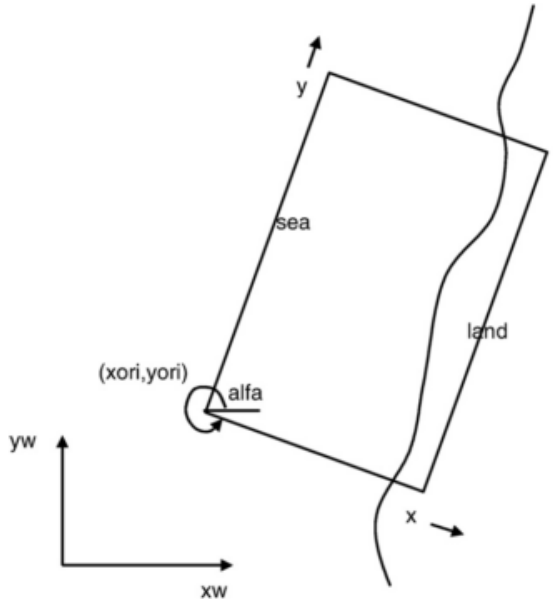

Figure 2-4. XBeach coordinate system (Roelvink et al., 2009)

2.2.1 *Wave-action equations*

The wave-action balance basically shows that the spatial-temporal variations of wave action are equal to the wave energy dissipation over the intrinsic wave frequency (the model reduces the frequency space to one representative frequency), and is shown as follows.

$$\frac{\partial A}{\partial t} + \frac{\partial c_x A}{\partial x} + \frac{\partial c_y A}{\partial y} + \frac{\partial c_\phi A}{\partial \phi} = -\frac{D_w}{\sigma} \quad (3)$$

Where A is the wave action, D_w is the energy dissipation, σ is the intrinsic wave frequency, c is the propagation speed of the wave action, and ϕ is the angle of wave incidence with respect to the x-axis. Here the wave action is equal to the wave energy density over the intrinsic wave frequency. The propagation speeds are given by,

$$c_x(x,y,t,\phi) = c_g \cos(\phi) + u^L \quad (4)$$

$$c_y(x,y,t,\phi) = c_g \sin(\phi) + v^L \quad (5)$$

$$c_\phi(x,y,t,\phi) = \frac{\sigma}{\sinh 2kh}\left(\frac{\partial h}{\partial x} sin\phi - \frac{\partial h}{\partial y} cos\phi\right) + cos\phi\left(sin\phi \frac{\partial u}{\partial x} - cos\phi \frac{\partial u}{\partial y}\right) + sin\phi\left(sin\phi \frac{\partial v}{\partial x} - cos\phi \frac{\partial v}{\partial y}\right) \quad (6)$$

where u and v are cross shore and alongshore depth averaged velocities, and the superscript L symbolizes Lagrangian velocities. Equation (6) takes into account both bottom refraction (first term on RHS) and current refraction (second and third term on RHS). The wave number is calculated with the eikonal equations, which say that the variation in time of a wave number vector (k_x or k_y) plus the variation of the absolute radial frequency (ω) in the coordinate of the considered wave number vector

must be equal to zero. The absolute radial frequency is equal to the intrinsic wave frequency plus the product of the wave number and the Lagrangian velocity.

The calculation of the wave dissipation can be done in several manners, either following the formulation of Roelvink (1993), Baldock et al (1998), or Roelvink and Daly (2010). The total wave energy dissipation as defined by Roelvink (1993) due to wave breaking is as follows.

$$\overline{D_w} = \frac{\alpha}{\pi} Q_b \sigma E_w \quad (7)$$

Where α=O(1) is a calibration coefficient, Q_b is the fraction of breaking waves, and E_w is the wave energy. As well as this, a wave height or breaking parameter can be added to this formulation (H_{rms}/h), or the fraction of breaking waves can be taken as defined by Roelvink and Daly (2010); which says that the waves are fully breaking (Q_b=*1*) if the wave height exceeds a certain threshold or not breaking (Q_b=*0*) if the wave height is below another threshold.

In the case of a stationary model run, the Baldock formulation is used to calculate the wave dissipation, and is defined as is shown below in Equation (8).

$$\overline{D_w} = \frac{1}{4} \propto Q_b \rho g f_{rep} (H_b^2 + H_{rms}^2) \quad (8)$$

Where f_{rep} is a representative intrinsic frequency, H_b is the breaking wave height, H_{rms} is the root means square wave height, and the rest of the variables are consistent with the definitions in the present report. The wave energy dissipation can be distributed proportionally over the wave directions, by multiplying the total dissipation by the ratio of the energy density (of each direction) over the total wave energy. Having the spatial distribution of the wave energy the radiation stresses can be found using linear wave theory, as a function of the angle of incidence, the group velocity, and the energy density.

2.2.2 ***Roller energy balance***

The roller energy balance and the wave action balance (described above) go hand in hand, as the resulting wave energy dissipation from the wave action/energy balance is input into the roller energy balance. As is assumed in the wave action balance, the directional distribution of the roller energy is considered, while the frequency

spectrum is simplified to a single representative frequency. The roller energy balance is as follows,

$$\frac{\partial S_r}{\partial t} + \frac{\partial c_x S_r}{\partial x} + \frac{\partial c_y S_r}{\partial y} + \frac{\partial c_\phi S_r}{\partial \phi} = -D_r + D_w \quad (9)$$

where the roller energy is $S_r(x,y,t,\phi)$. The roller energy propagation speeds have virtually the same formulations as the wave energy propagation speeds (Equations (4), (5) and (6)), except for the difference that the group speed is changed for the celerity (equal to the wave frequency over the wave number). Now, the total roller energy dissipation is taken as (Renier et al., 2004; Roelvink et al., 2009),

$$\overline{D_r} = \frac{2g\beta_r E_r}{c} \quad (10)$$

Where β_r is a roller calibration coefficient, and choosing this coefficient the roller energy can be solved for from Equation (8), knowing also that the directionally distributed roller energy is found in the same way as the directionally distributed wave energy. Now the contribution to the radiation stress of the roller energy is found, with which (in addition to the radiation stress from the wave action) the wave forcing is found, and presented as follows.

$$F_x(x,y,t) = -\left(\frac{\partial(S_{xx,w}+S_{xx,r})}{\partial x} + \frac{\partial(S_{xy,w}+S_{xy,r})}{\partial y}\right) \quad (11)$$

$$F_y(x,y,t) = -\left(\frac{\partial(S_{xy,w}+S_{xy,r})}{\partial x} + \frac{\partial(S_{yy,w}+S_{yy,r})}{\partial y}\right) \quad (12)$$

2.2.3 *Non-linear shallow water equations*

Shallow water equations are used when considering the low-frequency and mean flows. These low-frequency and mean flows are used in a depth averaged formulation where the momentum and continuity equations are set in terms of the Lagrangian velocities (this is known as a Generalized Lagrangian Mean (GLM) formulation) (Andrews and McIntyre, 1978). The Lagrangian velocity is the distance a water particle travels during one wave period, divided by that period; and is equal to the summation of the Eulerian velocity and the Stokes drift (Stokes, 1847). This Stokes drift can be calculated using the short-wave energy and direction from the wave-action balance, and are shown below for *x*- and *y*-direction respectively (Phillips, 1977).

$$u^S = \frac{E_w cos\phi}{\rho hc} \quad ; \quad v^S = \frac{E_w sin\phi}{\rho hc} \tag{13}$$

Now, as it was mentioned above, the Lagrangian velocities are used in the GLM-equations, which include bed shear stresses and wave-induced stresses. It is also worth mentioning that the Eulerian velocity is used in calculating the bottom shear stresses as opposed to the Lagrangian velocity, since the Eulerian velocities are what the seabed will react to.

2.3 Nearshore bathymetry Estimation (Beach Wizard)

The nearshore bathymetry that will be used as input for the modeling of rip current dynamics is calculated using the nearshore bathymetry estimation method "Beach Wizard", which assimilates model computations and remote sensing observations (Van Dongeren et al., 2008). By integrating this method in the XBeach model, along with data obtained from Argus images, updated nearshore bathymetries are calculated. Inputs to the model are a series of data extracted from Argus video images, which can be roller dissipation maps, intertidal bathymetries, and/or wave celerities. The model essentially updates a given input bathymetry (which could be anything from a measured bathymetry to a uniform plane bed) by assimilating the hydrodynamic model computations to the observed quantities (derived from Argus video information), which ideally results in bed updates toward the real bathymetry.

2.3.1 *Beach Wizard data assimilation model*

The Beach Wizard data-model assimilation method (Van Dongeren et al., 2008) calculates updated bathymetries using Argus video imagery information as its main input along with model computations (using XBeach in the present case). The model formulations presented here are taken and summarized from Van Dongeren et al. (2008). The bathymetry is updated using an optimal least-squares estimator, and is computed in the following manner.

$$h_{update} = h_{prior} + \alpha(h_{obs} - h_{prior}) \tag{14}$$

Where h_{update} is the updated bathymetry, h_{prior} is the prior (or input) bathymetry, h_{obs} is the indirectly obtained (using Argus observations) bathymetry, and α is the optimal weighting coeficient. Since the input data is not directly bathymetry

measurements, rather wave celerity or wave dissipation (or intertidal bathymetry), an inverse model is used to relate the input data to the bathymetry.

$$h - h_{obs} = \left(\frac{df}{dh}\right)^{-1} (f - f_{obs}) \tag{15}$$

Here the f_{obs} refers to a measured quantity (wave celerity or dissipation), f is a computed quantity, and h refers to the bathymetry elevation (with the same meaning for the sub indices). The computed quantity f is a result of the hydrodynamical model, and the corresponding gradients (df/dh) are computed in the bed update routine of Beach Wizard. For the case when the computed quantity is wave dissipation, the gradients are calculated as the derivative of the organized wave dissipation since the derivative of the roller dissipation with respect to depth cannot be computed analytically. These derivatives are shown in Appendix E.

The uncertainties of both the prior bathymetry (h_{prior}) and the new estimates (h_{obs}) are needed to find the optimal weighting coefficient α as follows.

$$\alpha = \left(\frac{\sigma_{prior}^2}{\frac{T_S}{\Delta t}\sigma_{obs}^2 + \sigma_{prior}^2}\right) \tag{16}$$

Where the σ^2 terms refer to the uncertainty of both the prior and observed (Argus-derived) bathymetries, T_S is the simulation time, and Δt is the time step duration. The uncertainty of the observed (Argus-derived) bathymetry is calculated in a way that it is dependent on a certain measurement error (ε), on the difference between the observed and computed quantities ($f_i - f_{i,obs}$), and on the gradient with respect to depth of the computed quantity (df/dh), as follows.

$$\sigma_{obs}^2 = \frac{\varepsilon^2 + (f - f_{obs})^2}{\left(\frac{df}{dh}\right)^2 + \delta^2} \tag{17}$$

As well as this, the uncertainty of the updated bathymetry (σ_{prior}^2) is calculated for every numerical time step in Beach Wizard by multiplying the uncertainty of the observation (σ_{obs}^2) by the weighting coefficient, and also by the simulation duration (T_S) over the numerical time step (Δt) due to the observations being not statistically independent. Now using Equations (14) and (15) the time-update scheme of the bathymetry is written as,

$$h(t + \Delta t) = h(t) - \alpha \sum_{i=1}^{S} \frac{\frac{df_i}{dh}}{\left(\frac{df_i}{dh}\right)^2 + \delta_i^2} (f_i - f_{i,obs}) \tag{18}$$

Where the subscript "*update*" from Equation (14) refers to the time level $t + \Delta t$, and the subscript "*prior*" refers to the time level t. Also, the index i refers to the source (wave energy dissipation, intertidal bathymetry, and/or wave celerity).

As well as calculating an updated bathymetry uncertainty for every time step during a specific Beach Wizard simulation, the updated uncertainty is calculated between consecutive simulations as well. This is done to increase the uncertainty between simulations for increasing periods of time between simulations, meaning that for larger times between simulations, the prior uncertainty will grow towards a certain "natural" uncertainty. This will be further elaborated on and explained in sections 5.1.3 and 5.3.2.

The overall scheme of how the model works is presented in Figure 2-5 below.

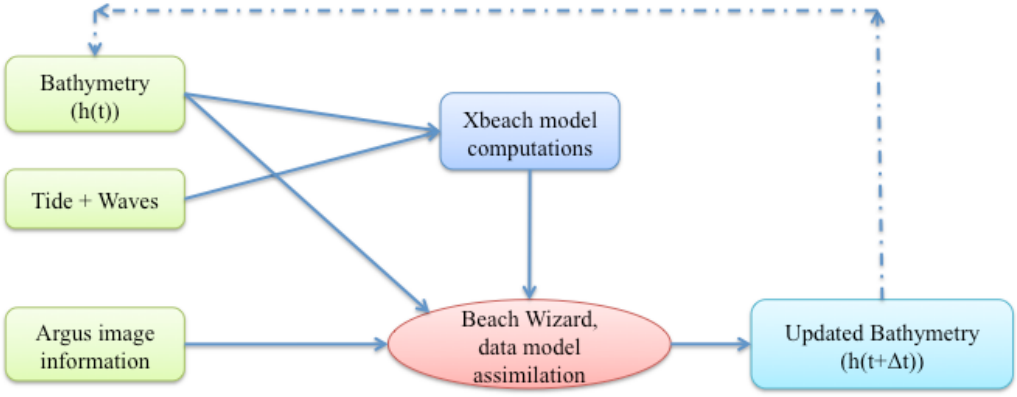

Figure 2-5. Beach Wizard data-model assimilation method

Figure 2-5 shows one simulation of the Beach Wizard model. It is clear from the previous figure that for one simulation only one set of Argus image information and one set of tide and wave information are input to the system, while the bathymetry is updated for every time step. It is important to point out that in the present study, only the hydrodynamic module of XBeach is used, and not the morphodynamic module.

2.3.2 *Argus image pre-processing*

The raw images obtained from Argus stations must be pre-processed in order to extract the desired information to be used as input for the aforementioned model. Here the process for obtaining roller dissipation maps (Aarninkhof et al., 2005b) and intertidal bathymetries (Aarninkhof et al., 2003) will be briefly explained.

Figure 2-6 presents a schematic view of the processes involved in obtaining wave roller dissipation maps from raw Argus images.

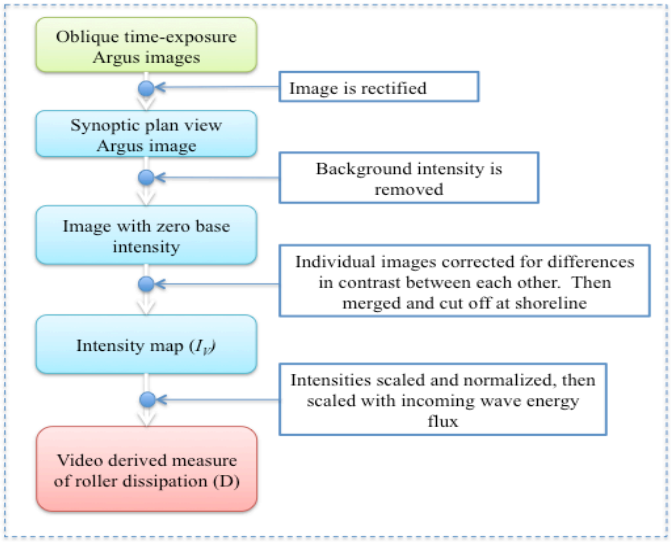

Figure 2-6. Process for obtaining roller dissipation maps from Argus images

The procedure to obtain roller dissipation maps begins with rectifying the oblique Argus time-exposure images, which means converting them to a plan view format. Once this is done, the base intensity is removed, which results in an image where the offshore areas with no wave breaking have zero intensity. After these zero-base intensity images are obtained, all the available images (from the different cameras) must be merged together. In order to merge the images, the intensities of the individual images must be corrected for possible differences in image intensity arising from the conditions of each individual camera. Having the merged images, a very important step is now to cut off the image at the shoreline, which may result in difficulties, especially at dissipative beaches with very low slopes. These difficulties are due to there possibly being exposed bars and other features near the shoreline, which can be confused for breaking waves in a time-exposure image. Next the image is scaled as for it to represent a quantitatively correct gauge of wave roller dissipation. The intensities (I_v) in this dissipation map are then normalized, and scaled with the current incoming wave energy flux (Ec_g) at the time of taking of the images, and a final measure of roller dissipation (D) is found as follows (Aarninkhof et al., 2005b).

$$D(x,y) = \left(\frac{I_V(x,y)}{\int_x \int_y I_V dxdy}\right) \int_y Ec_g cos\theta dy \qquad (19)$$

Argus time averaged images can be used for the calculating of intertidal beach bathymetries, following the methods of the Intertidal Beach Mapper (IBM, Aarninkhof et al., 2003). A schematic view of the IBM is shown below in Figure 2-7.

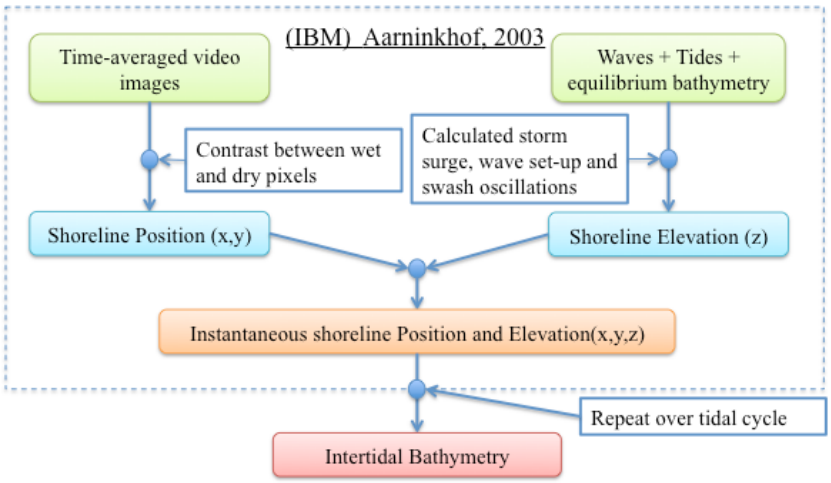

Figure 2-7. Intertidal Beach Mapper schematic view

The process shown in Figure 2-7 shows that the required input for the IBM are time-averaged Argus images on one hand, and on the other hand wave and tide information at the same time as when the image was taken, along with an equilibrium profile for the specific site location. Firstly, the images must be rectified into plan view (as was described previously for the obtaining of dissipation maps), then a contrast is found between wet and dry parts of the beach. This is done by sampling the intensities of the image (near the shoreline, both sub-aqueous and sub-aerial) and converting to hue saturation value (HSV), which is a cylindrical coordinate system representing a red green blue (RGB) colour system. These HSV are plotted in a histogram, which will present two peaks, representing wet and dry pixels, and the folding point (saddle point) will represent the shoreline. This now provides an instantaneous shoreline position. A more detailed description of this process is presented by Aarninkhof et al. 2003. Once the instantaneous shoreline position is found, the shoreline elevation is found by calculating storm surge, wave induced set-up, and swash oscillations at the time when the image was taken. This results in a shoreline elevation, and repeating both of the aforementioned processes over a tidal cycle a 3D intertidal bathymetry is obtained.

3 SITE DESCRIPTION AND BATHYMETRICAL VARIATION

The present chapter will provide an overview of the general characteristics of Perranporth beach. This specifically includes location and general information with regards to wave conditions, tidal range, morphological characteristics; a description of the type of rip currents presented at Perranporth; and a description of the morphological variations that occur at Perranporth on different timescales.

3.1 Perranporth Beach

3.1.1 *Location and general information*

Perranporth beach is located in the south-west of the UK, as is shown in Figure 3-1. The beach faces west-northwest, due to which the predominant waves are swell waves from the North Atlantic, as well as locally generated wind waves. The wave conditions are quite seasonably variable, generally presenting more energetic and higher waves during winter months and smaller swell waves during summer months, with a yearly average in significant wave height and peak period of H_s = 1.6 m and T_p = 10.5 s respectively.

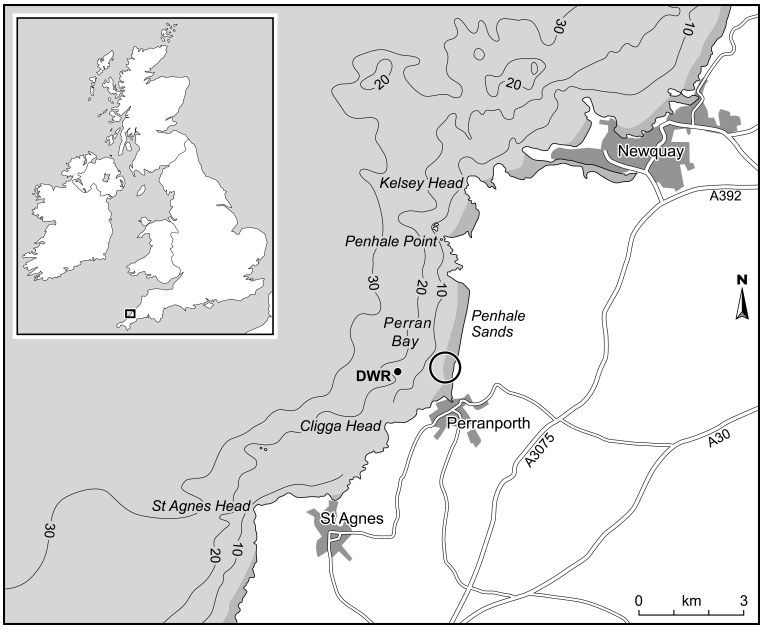

Figure 3-1. Perranporth beach location.

The tidal regime is semi-diurnal with a mean spring tide of around 6.3m, which classifies as a macrotidal range. The beach is composed mainly of medium sized quartz (D_{50} = 0.28 – 0.34mm). Due to the combination of the just mentioned characteristics and general forcing conditions, Perranporth beach is classified as a LTBR morphology, as it was described in section 2.1.3 of the present report. The upper intertidal shoreface is quite flat ($\tan\beta$ = 0.015 – 0.025) and featureless, while around low-water levels the beach presents complex bar-rip channel morphologies. As to appreciate the large tidal variation and the flat featureless characteristics of the upper intertidal shoreface, Figure 3-2 presents two snapshot images taken from camera 1 at the Droskyn Argus station during low tide (left) and high tide (right) on April 2nd 2011. It is clear from this image that the occurrence of rip currents during high water levels at Perranporth is not generally an issue, due to the lack of rip and bar morphologies at the upper portion of the beach.

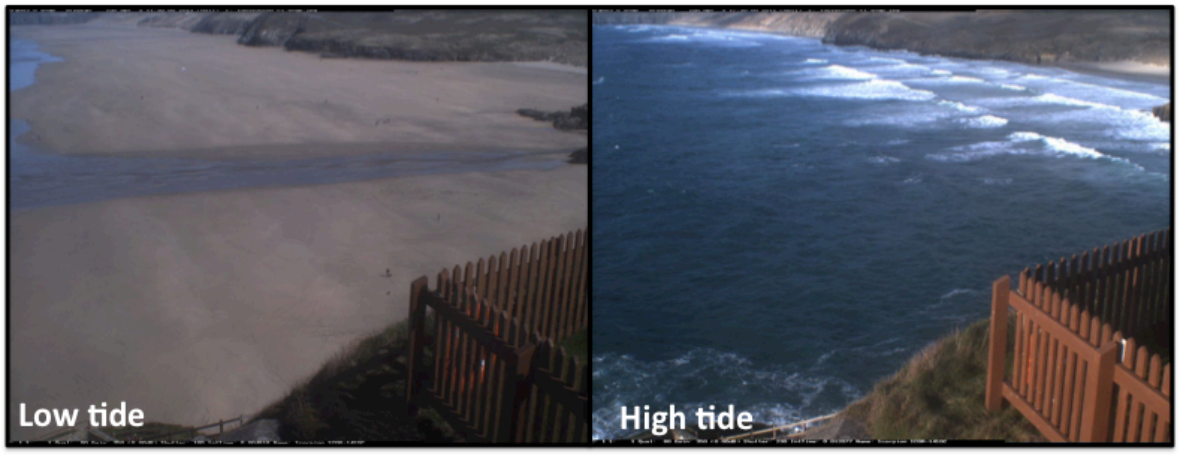

Figure 3-2. Perranporth beach during low tide (left) and high tide (right).

Perranporth is quite a seasonal town, meaning that during winter months very low activity is present and has a large amount of tourists and visitors coming during the summer months of the year. This beach is quite a popular one in the UK, and swimming (when the weather allows) and other water sports are quite popular. Due to the presence of rip currents and the large amounts of people in the water during summer months, the importance of beach monitoring and understanding of rip currents goes without saying. The occurrence of rip currents and the related

characteristics of these at Perranporth beach will be described in the coming section of the present report.

3.1.2 *Rip currents at Perranporth*

Rip currents account for the majority of incidents and rescues carried out by the RNLI lifeguards (Scott et al., 2009) at Perranporth. Here the focus will be on the physical characteristics of rip currents at Perranporth rather than the associated risk due to these. As it has been mentioned in the present report, Perranporth generally is representative of a LTBR beach, and is prone to quite strong rip currents. Figure 3-3 shows an image of Perranporth beach near low water, where several major rips can be seen.

Figure 3-3. Rip currents at Perranporth beach (www.ripcurrents.co.uk). Rip currents marked by red lines and arrows, and onshore directed flow marked by light blue lines and arrows.

The figure presented above shows several major offshore directed flows of water (rips), which can be spotted out as the dark jets of water extending through the surf zone, marked by red lines and arrows. This image shows the rhythmic bar and rip morphology present around low tide at Perranporth, where the undulations along the coastline are clear, as well as several major transverse bars. The transverse bars (where most of the people are in the picture) have large amounts of water moving over them due to wave breaking (light blue arrows in Figure 3-3), which near the

shoreline turns into the feeder channels and returns offshore in the form of rip currents.

A good description of the rip currents and their temporal variability at Perranporth is presented by Austin et al (2010), where field measurements are used to describe said phenomena. Here the general findings of that field experiment and overall study (Austin et al., 2010) will be mentioned, providing an overview of the general characteristics of Perranporth's rip currents.

The aforementioned study was based on a field experiment carried out between the 1st and 8th of August 2008, covering a spring-neap tidal cycle and presenting summer swell conditions and a low tide transverse bar/rip system (ideal conditions for the generation of rip currents). It was found that the rip currents seem to "activate" around low tides, specifically when the local water depth falls below ~ 3 m. It was found that generally when the rip currents are activated, the circulation patterns present circular eddies of size in the order of 200 m, and when the tides are higher the longshore current is dominant and little or no offshore directed currents are present. Both Eulerian and Lagrangian flow velocity measurements were taken during the experiment. The mean flow speeds recorded by drifters in the circulation system ranged between 0.01 – 1.27 ms^{-1}, with the highest values recorded during low water levels (the days with spring tides) and high wave conditions. Figure 3-4 shows the circulation pattern from one of the drifter deployment days during which the significant wave height, peak period, wave angle, and tidal range were Hs = 0.84 m, Tp = 9.1 s, θ = 280^0, and η = 6.2 m respectively. This image shows a counter clockwise rotation of the rip current flow, with a well confined circulation cell.

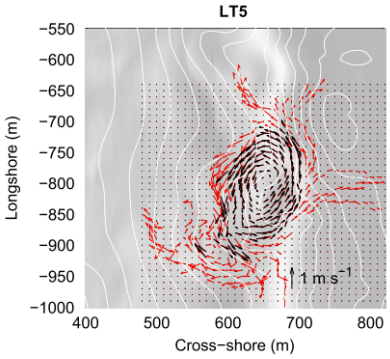

Figure 3-4. Rip current circulation during drifter deployment LT5, where the vectors represent current velocity and direction for all (red) and statistically significant (black) observations (Austin et al., 2010).

The circular circulation pattern depicted in the above figure is representative of the activated rip currents at Perranporth during the field experiment. However, the activation of said currents was the matter of interest, and varied widely with semidiurnal variations in water depth, spring-neap tidal variations, and forcing conditions. An important conclusion by Austin et al (2010) was that the presence of rip currents at Perranporth generally occurs at local water depths shallower than ~ 3 m. With this it was also found that the variation from spring to neap tides is of great importance, since during neap tides the low water level generally would not be low enough as to activate the rip current systems.

3.2 Bathymetrical variation at Perranporth Beach

As it was mentioned in the previous section of this report, Perranporth beach generally will present a LTBR beach state, meaning that it has a quite flat and featureless upper shoreface, and pronounced rip/bar morphologies around low water. Several bathymetrical surveys have been conducted over the past years at Perranporth beach, twelve of which are presented in Appendix A, for dates ranging between the 15th of October 2010 and the 17th of January 2012. A simple overview of the shapes presented by the contour lines in the figures presented in Appendix A show the variability in the bathymetry at Perranporth. A good example of how the bathymetry could possibly vary can be seen by visually comparing Figure A-2 (measured on 30/10/2010) and Figure A-4 (measured on 28/04/2011), where the appearance of two pronounced rip channels can be seen on the 28th of April 2011, which were not present at all on the 30th of October 2010.

It has been demonstrated in several instances (Jacobs, 2010; Winter, 2011; Sutherland et al., 2004; Van Rijn et al., 2003) that given accurate bathymetrical information along with correct hydrodynamic forcing conditions, rip currents can be accurately approximated using hydrodynamical models. As it was stated previously in the present report, this is considered to be a valid assumption; therefore, the importance of having up to date bathymetrical information for the correct modelling of rip currents at a specific beach is directly related to the physical variations in time of said bathymetry. With this in mind, the temporal variations in bathymetry at Perranporth

will be shown here, concentrating on seven measured bathymetries between March and August 2011. An initial visual inspection of all the available measured bathymetries shown in Appendix A showed clear variations, and now the difference between the observed long term (order of months) and short term (order of days) bathymetrical variations will be looked at.

First the "monthly" variation in bathymetry will be looked at, using 5 measured bathymetries, specifically from the 15th of March, the 25th of April, the 1st of June, the 13th of July, and the 23rd of August. Next the "daily" variations will be looked at, using 3 measured bathymetries from June 2011, specifically surveyed on the 1st of June 2011, the 6th of June 2011 and the 11th of June 2011.

For the correct prediction or modeling of rip currents, a very important aspect of the bathymetry is the locations in alongshore direction of rip channels, as well as the cross shore location of bars or terraces and the depth of these. As to address these aspects, 3 cross sections are chosen both in cross shore direction and in alongshore direction and are plotted for all of the aforementioned bathymetry survey dates. The location of these cross sections was chosen in a way that between the three of them (in each direction) the general characteristics of the morphology at Perranporth can be seen. The chosen cross shore profiles used are shown in Figure 3-5 (left), and the chosen alongshore profiles are shown in Figure 3-5(right), using the measured bathymetry from the 1st of June 2011 as the base image.

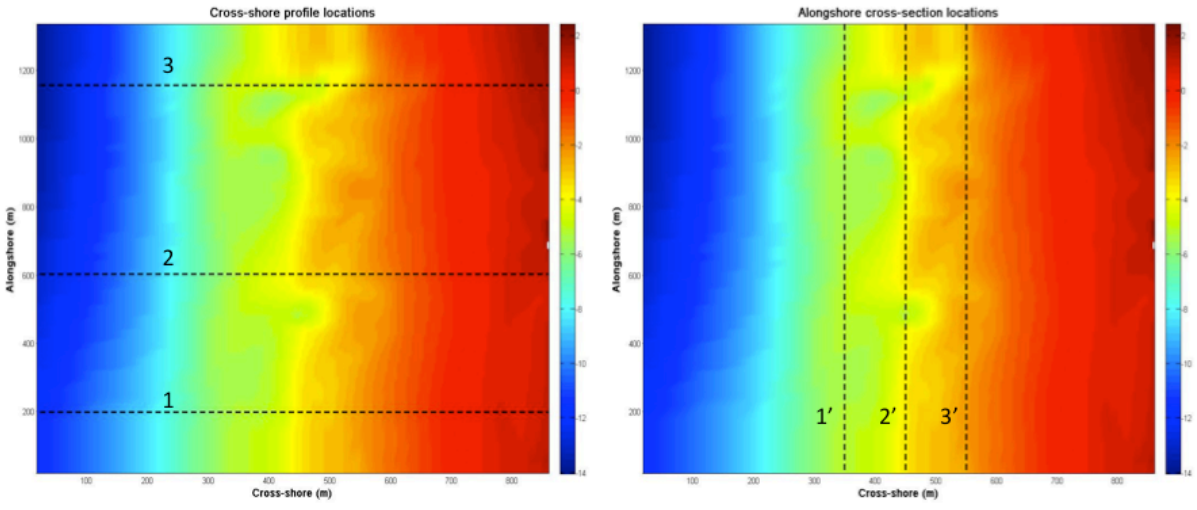

Figure 3-5. Cross-shore (left) and Alongshore (right) profile locations, depth scale in meters (positive up).

The alongshore locations in *y*- (local coordinate system) for the cross shore profiles shown on the left side of Figure 3-5 are 200 m, 602 m, and 1155 m, for profiles 1, 2 and 3 respectively. The cross shore locations in *x*- (local coordinate system) of the alongshore transects shown in the right side of Figure 3-5 are 350 m, 450 m, and 550 m for profiles 1', 2' and 3' respectively. Upon previous inspection, it was noted that the major variations in bathymetry are seen in the zone between 300 m and 600 m in cross shore direction, because of which the locations of profiles 1', 2' and 3' were chosen where they were chosen. The numeration of the profiles shown in Figure 3-5 is consistent with the rest of the figures presented in this section of the report.

The cross-shore profiles for five different survey dates (representing the variations in the order of months) are shown in Figure 3-6, and the cross-shore profiles for three different dates (representing the variations in the order of days) are shown in Figure 3-7. After these, the alongshore cross sections are shown in Figure 3-8 and Figure 3-9, where the first corresponds to the "monthly" and the second the "daily" variations in bathymetry.

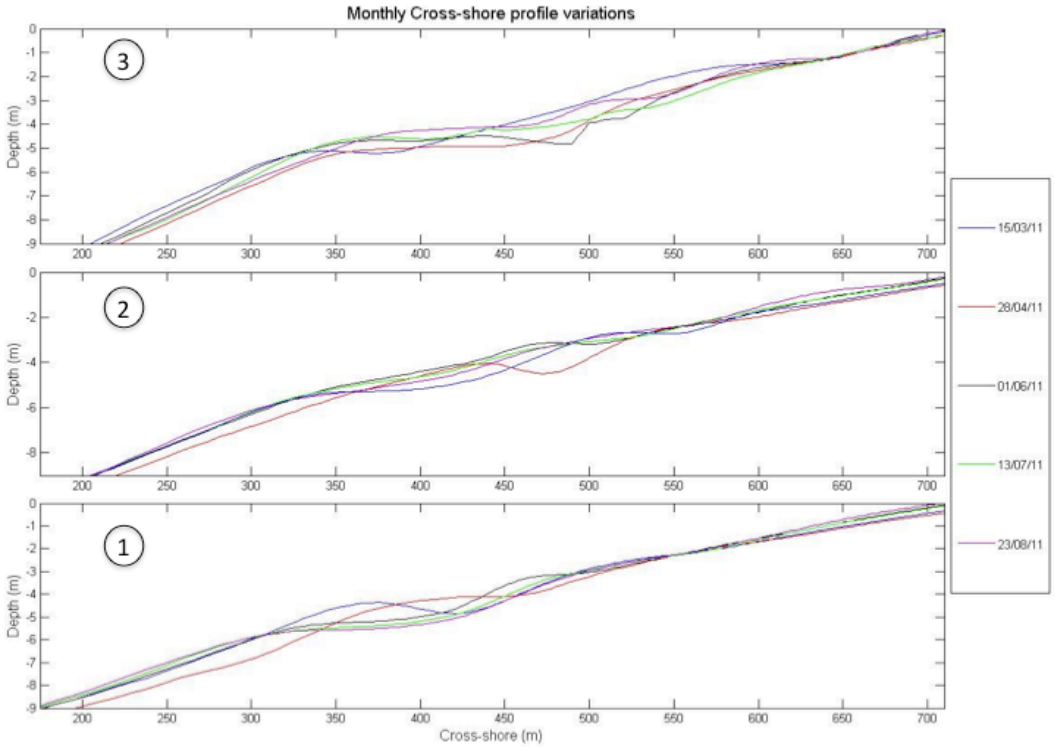

Figure 3-6. Monthly cross-shore variations in bathymetry

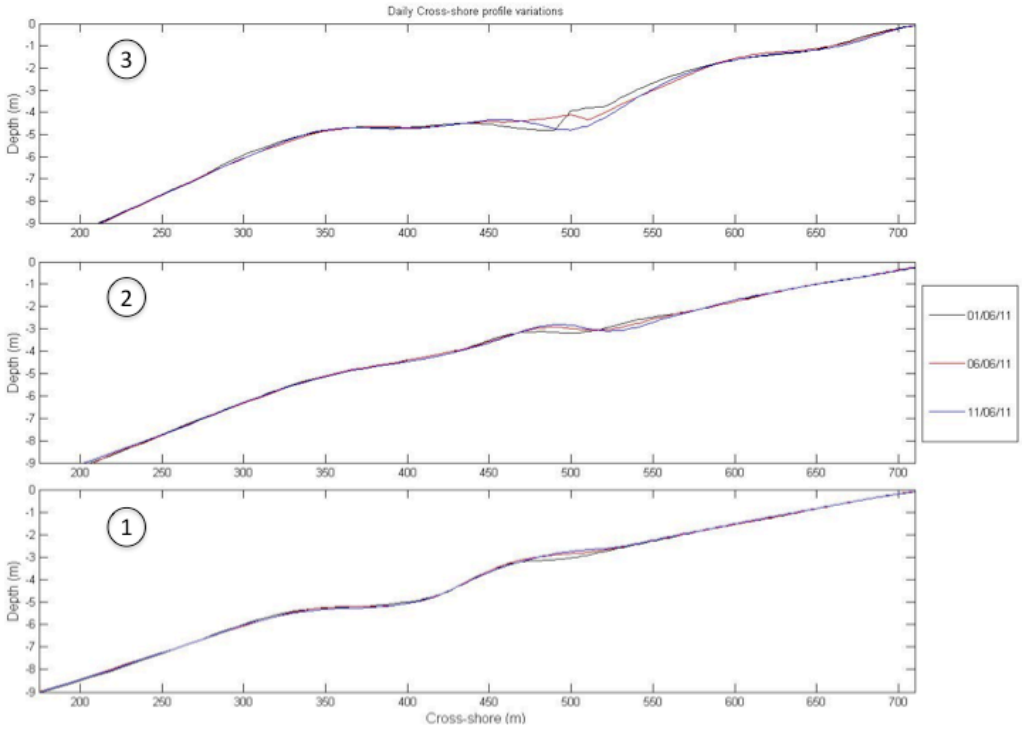

Figure 3-7. Daily cross-shore variations in bathymetry.

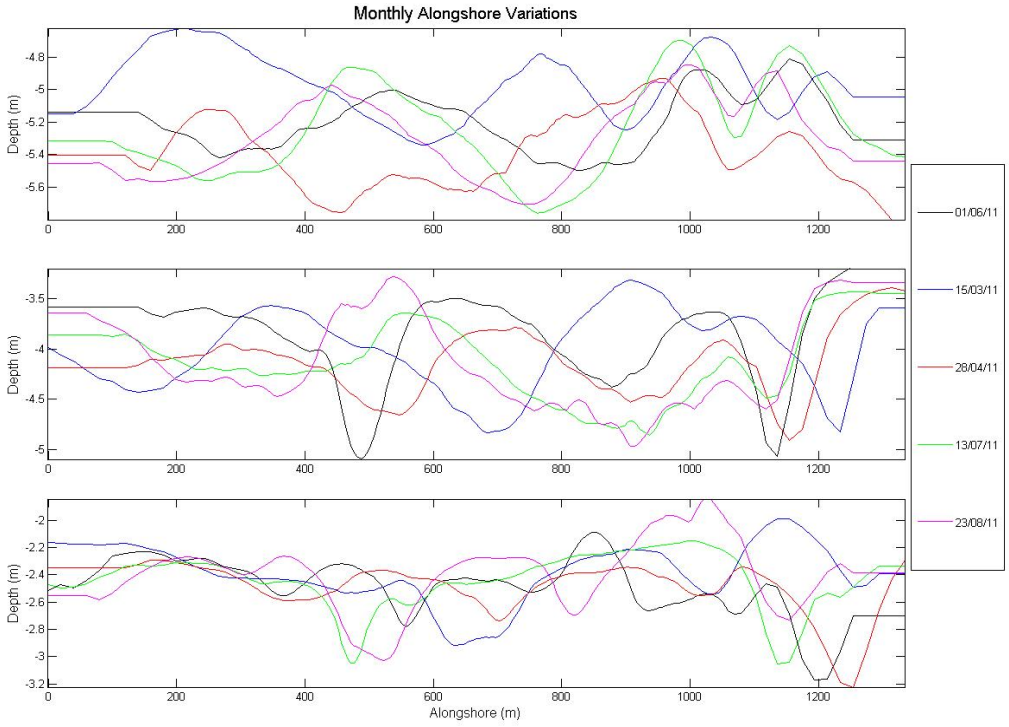

Figure 3-8. Monthly alongshore bathymetry variations

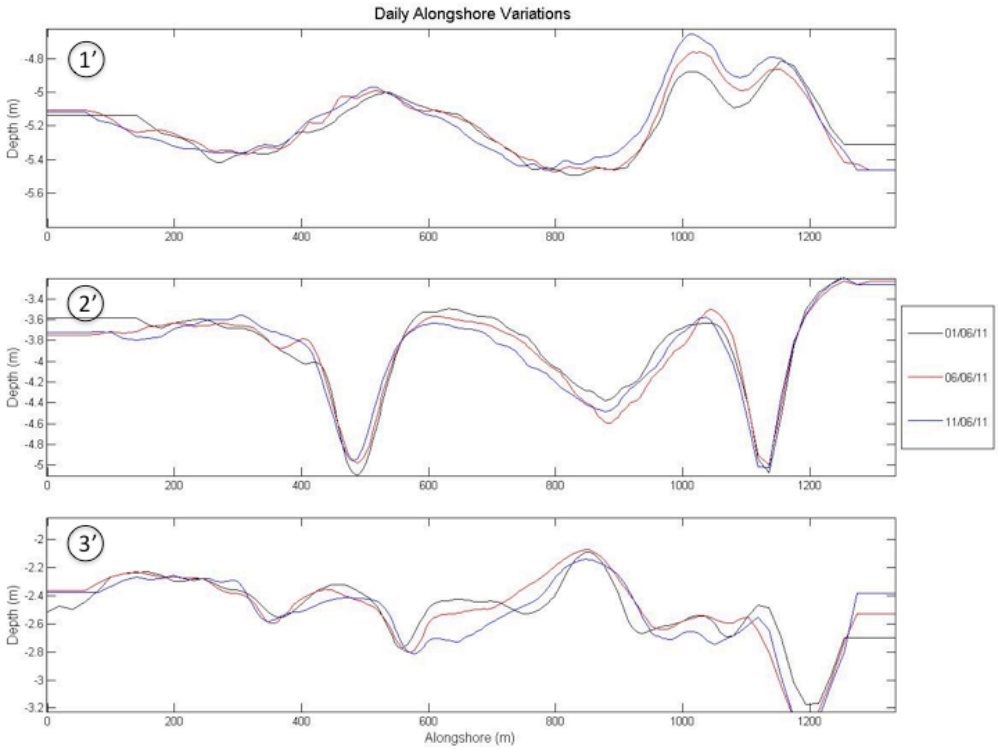

Figure 3-9. Daily alongshore bathymetry variations

Studying Figure 3-6 through Figure 3-9, it can be seen that the bathymetry at Perranporth beach certainly does fluctuate in time, showing considerable changes in time scales in the order of months, and quite small variations in shorter periods of time (in the order of days). From Figure 3-6 it is revealed that bars and troughs fluctuate in cross shore direction with time, showing particular movement mainly between 350 m and 600 m (in local *x*- coordinates). As well as this, the figure shows signs of rise and fall in vertical direction of the bathymetry (in some cases up to 1 m change), pointing out large amounts of sediment transport, fluctuating in time due to varying storm and calm conditions. Figure 3-8 shows a wide scatter of coloured lines which at first may seem overwhelming, however, this irregularity or chaos in the figure is in itself proof that there is substantial variations in the alongshore profile of bathymetry for time scales in the order of months.

The observed variations in bathymetry are in fact an argument for the use of the Beach Wizard bed updating scheme for rip current forecasting. Since it was found that the variations in bathymetry are small for short timescales, one may argue that using an outdated measured bathymetry for the forecasting of rip currents would only

be suitable for short periods of time, during which the variations in bathymetry are very slight; and for longer term situations (in the order of months), outdated bathymetries will not likely resemble real (current) bathymetries.

The finding that the bathymetries vary significantly from month to month and very slightly on time scales in the order of days (up to 10 days) will be used in the calibration of the Beach Wizard model, specifically with respect to the timescale parameter (T_r) which will be described in section 5.3.2.

4 MODEL SET-UP

The initial set-up process for the Beach Wizard model to be used throughout the present study is based on the available XBeach model for Perranporth beach (Austin et al., (in press)). The set-up of the model includes the grid definition (both for the Argus input and the XBeach grids), the processing of a good quality Argus image to use as input, and the adjustment of the matlab scripts and codes as to arrive at a working model. A series of simple test cases are run, with the main objective of proving the general functionality of the initial model set-up, as well as for the analysis of the behavior and governing processes influencing the model output. The set-up of the model is described in the following sections of the present report. As well as this, the selection process and a qualitative ranking system for the video-derived images to be used as input in the long scale model runs that will be carried out in the following chapters of this report will be explained here.

4.1 Model grid and input parameters

As to simplify the model, the Beach Wizard grid is fit to the XBeach grid. This meaning that the plan view Argus images are cropped to match the XBeach grid in size, but not having the same grid spacing. The XBeach grid used is one with variable spacing, with a total length of 860 meters in cross-shore direction (*x*-direction) and 1334m in alongshore direction (*y*-direction). The grid resolution increases towards the centre, having widely spaced cells at the boundaries and finer spaced cells towards the centre. The first and last 200 m in *y*- present an alongshore spacing of 40 m, which then reduces to 20 m, and finally reaches its finest spacing of 10 m for the region of the grid between 300-1000 m in *y*-. The cross shore grid resolution increases from offshore to onshore, starting at a spacing of 35 m on the offshore boundary, and gradually reducing to minimum spacing of 4 m in the shallower regions of the grid. The Beach Wizard grid is defined with the same dimensions in *x*- and *y*- as mentioned above, with a cell spacing of 5 meters in cross-shore direction and 10 meters in alongshore direction, resulting in a 173 x 135 grid size (*x*- and *y*- direction respectively). A local coordinate system is used to visualize the model outputs, with

its origin (0,0) coinciding with the location (174691.5022 , 54835.7957) in Great Britain National Grid coordinates (OSGB36[1]). The implemented grid is located at the southern end of Perranporth beach as for it to cover the field of view of the Perranporth Argus cameras. The grid location is depicted in Figure 4-1, where the dashed blue lines indicate the grid location. The orientation of this grid is defined by the angle alfa (defined in section 2.2), which is 340.95^0.

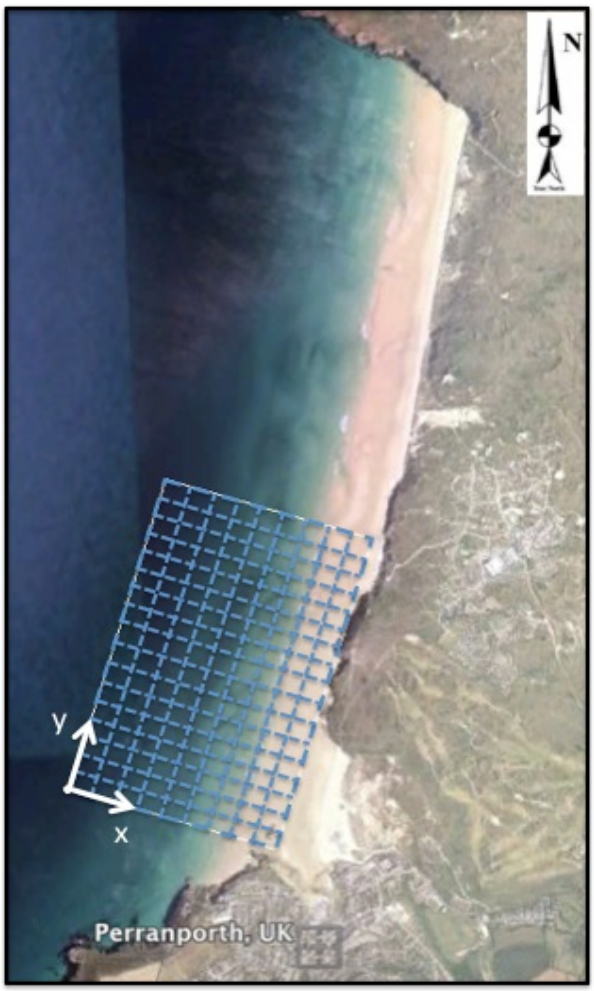

Figure 4-1. Model grid location at Perranporth beach.

Given that the Beach Wizard assimilation method runs in the XBeach system, a series of input parameters must be defined for the hydrodynamic calculations, which are set in an input file (*params.txt*). This input file also contains a keyword (*bchwiz*) which depending on the value entered will run or not run the Beach Wizard module. For

[1] www.ordnancesurvey.co.uk

bchwiz = 0 Beach Wizard is turned off, for *bchwiz* = 1 Beach Wizard is turned on, and for *bchwiz* = 2 both Beach Wizard and physics-based morphology are turned on at the same time. The present study only uses the hydrodynamic module of XBeach, therefore the morphology module must be turned off, and *bcwiz* = 1 is set. The general XBeach input parameters are shown Table 4-1.

Table 4-1. General XBeach input Parameters (*values vary for each simulation)

Parameter	Definition	Value	Units
nx	Number of grid cells in x- direction	136	-
ny	Number of grid cells in y- direction	94	-
xori	x- coordinate of grid origin	174691.5022	OSGB36
yori	y- coordinate of grid origin	54835.7957	OSGB37
depfile*	Bathymetry file	bed.dep	-
xfile	x- grid	x.grd	-
yfile	y- grid	y.grd	-
alfa	Grid orientation	340.9499	degrees
break	Option breaker model	2	-
hmin	Threshold water depth for return flow	0.05	m
gamma	Breaker parameter	0.55	-
beta	Breaker slope coefficient	0.1	-
alpha	Wave dissipation coefficient	1	-
rho	Density of water	1000	kg/m3
g	Gravitational acceleration	9.81	m/s^2
thetamin	Lower directional limit	195	degrees
thetamax	Upper directional limit	345	degrees
dtheta	Directional resolution	10	degrees
dir0*	Direction of wave propagation	Dir_naut	degrees
Hrms*	RMS wave height	H_rms	m
Tm01*	Spectral period	T_peak	s
zs0*	Water level	water_level	m

The XBeach model is run in stationary mode for each Beach Wizard simulation, assuming that the simulation time is short enough (maximum 2 hours) as to represent stationary tidal elevations and wave conditions; this is set by giving a value of 0 to the parameter "*instat*" in the input file (params.txt). Since the model is run in stationary mode, the wave dissipation model to be used is the Baldock model (Baldock et al., 1998), which is set by the parameter "break" = 2. Table 4-1 presents several input parameters denoted with "*", meaning that for each beach Wizard simulation these

parameters can change. Since the Beach Wizard scheme is a bathymetry updating method, the output bathymetry in a given simulation will be the input bathymetry for the next simulation. Also, for each simulation, wave information (direction, wave height, period) and tidal elevations are gathered from the Swan model output and a tidal elevation estimator respectively, providing variable conditions for each simulation; this information is gathered for each Argus time-exposure image at the specific time of its taking.

4.2 Image processing

The beach Wizard data-model assimilation method requires specific input, namely Argus video-derived information (dissipation maps, celerity maps, and/or intertidal bathymetries) coupled with the corresponding forcing and boundary conditions. In the present model only dissipation maps generated from Argus time-exposure images will be used as video-derived input. Scaled dissipation maps may be referred to as "imaps" throughout the remainder of the report. For the time being, the process for generating the required dissipation maps (imaps) is not fully automated, and requires some manual selection processes. The general process for the generation of imaps is described in section 2.3.2 of the present report, and will be explained here in further detail, using a single image (taken on the 9th of June 2011 at 16:30) as a descriptive example. As well as the actual time-exposure images, the Beach Wizard system needs actual wave and tide conditions corresponding to each image, and a series of default values that must also be defined.

As it was mentioned in section 2.3.2, dissipation maps are derived from Timex images. Timex images are images taken with an aperture time of 10 minutes, and are taken every 30 min at the Perranporth Argus station. The Perranporth Argus station counts with 3 individual cameras, located on the southern headland of the beach. Figure 4-2 shows the approximate location of the Perranporth Argus station and the extent of the view of the three cameras, where the camera sits at the southern end of the image, and the green shaded area corresponds to camera 1's view, the red shaded area to camera 2's view, and the blue shaded area to camera 3's view. The variation in extent of the camera's views is due to differences in the cameras and their resolution, where

camera 3 is the newest camera and has higher resolution and therefore has farther extent of view. Camera 3 was mounted after the initial cameras 1 and 2 to get a better merge line between the two, due to the generation of merging problems along the joint line of the two older cameras.

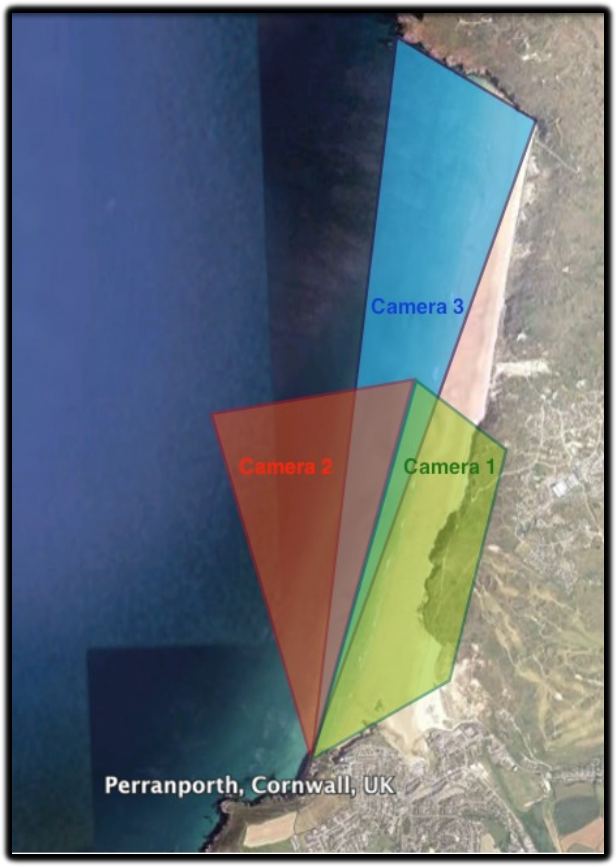

Figure 4-2. Perranporth Argus station location and approximate camera views.

Figure 4-3 shows examples of both the snapshots and timex images for all three cameras, taken on the 9th of June 2011 at 16:30. It can be seen in this figure that in the timex images wave breaking is seen as white bands, which will then be the basis for obtaining a quantitatively correct dissipation map.

The individual images shown in Figure 4-3 must be merged into a single image, as to have one image in which the whole field of view of all three cameras can be seen. This is done by means of a matlab script that reads all three timex images for each date and time, and proceeds to merge them and correct for contrast or differences between cameras. The transformation from the individual image coordinates (u, v) to their corresponding real world coordinates (x, y, z) is done first, by means of a relation

between the individual camera location (x_c, y_c, z_c), the effective focal length f, and the camera orientation (Aarninkhof, 2003). The camera orientation in turn is defined by a series of angles, being the tilt τ, the azimuth ϕ, and the roll σ. The details for the procedure involved in transforming camera coordinates to real world coordinates are described well by Aarninkhof (2003).

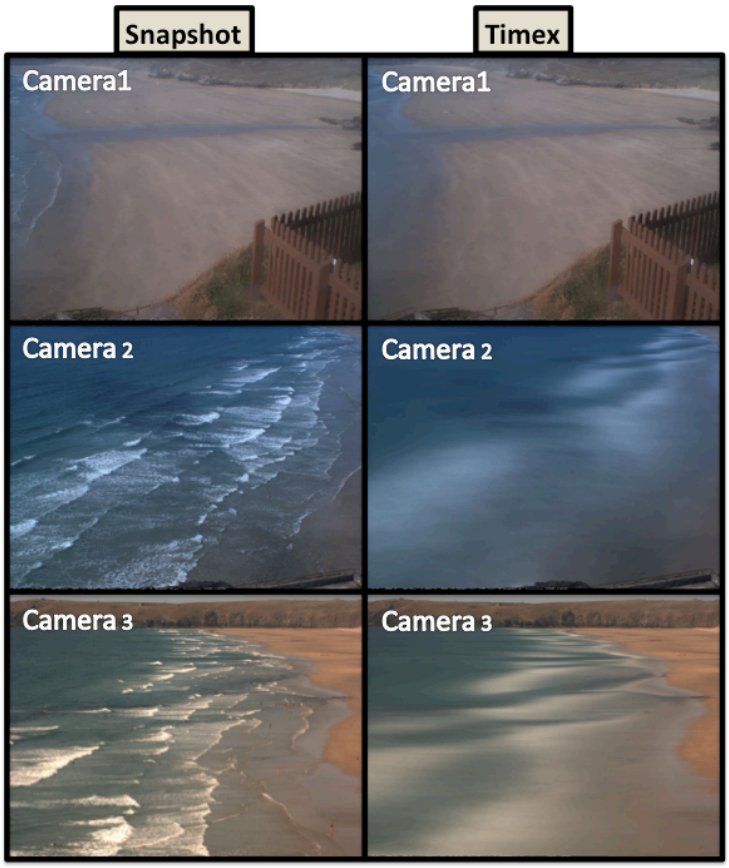

Figure 4-3. Individual snapshots and timex images from 09/06/2011 at 16:30

The correcting between images is done by measuring the mean intensity of a center point in each camera view and adjusting them to a target value. First a merged timex image is obtained (left side of Figure 4-4) from the individual cameras and then this is translated into a colour measure of pixel intensity, and normalized (right side of Figure 4-4) so the maximum value of intensity in the map is unity.

The bottom corners of Figure 4-4 correspond to the parts of the grid which are not in the field of view of any of the cameras. Figure 4-4 is a very nice example of an intensity map, where the dry parts of the beach are represented by a bright yellow colour (high intensity), the offshore area with no wave breaking is blue (low

intensity), and in the surf zone red stripes can be seen which correspond to waves breaking. It is important to re-state that this is an ideal image (in the sense of color contrast and overall image quality) and not very commonly obtained, this will be further discussed later in this report.

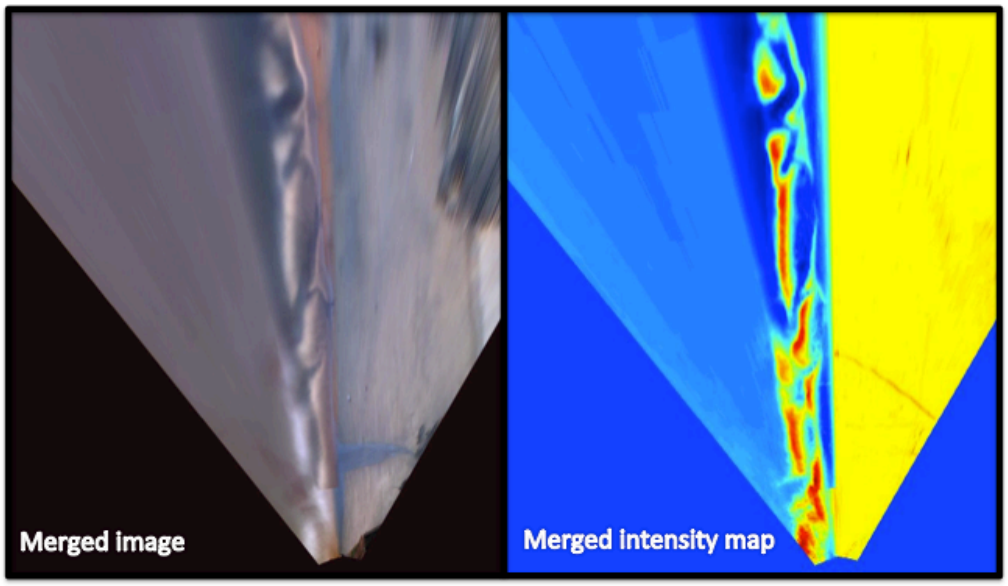

Figure 4-4. Merged timex image (left) and normalized intensity map (right)

As opposed to the common procedure to generate scaled imaps, which involved cutting off the raw intensity map (right side of Figure 4-4) simply along the shoreline and then scaling with the offshore wave conditions, a slight modification was made in the present master's thesis. One problem encountered in making scaled wave energy intensity maps is that the offshore region where there is no wave breaking should ideally show zero intensity, however, this is not always the case. In many circumstances, the offshore area of the intensity maps does not correspond to zero intensity, due primarily to problems in the image merging process. One of the problems with the merging of the three camera's images at Perranporth is related to the fact that all three cameras don't share a common horizon line, and therefore don't have equal base intensities. Because of this, the correction between images sometimes results in the offshore and dry beach areas not having the correct intensities. To overcome this, an interactive shoreline and surf zone extent detection scheme is applied, where the user essentially draws a polygon around the area of interest (surf zone), cutting out the dry beach and the offshore area and giving these

regions an intensity value of zero. This manual delimitation of the surf zone is considered valid due to the subsequent scaling with the incoming wave conditions, ideally providing a good representation of the observed wave dissipation having not considered any possibly false dissipation at the offshore areas.

The remaining step to obtain a quantitatively correct measure of roller dissipation is scaling the intensity map with the incoming wave energy. This is done by simply normalizing the intensity map so that its total sum amounts to unity, and then multiplying by the offshore wave energy flux, as described in Equation (19) in section 2.3.2 of the present report. The obtained scaled roller dissipation map (imap) for the 9th of June 2011 at 16:30 is shown in Figure 4-5, where the colour bar represents the scale of roller dissipation in units of wave energy per square metre (W/m^2).

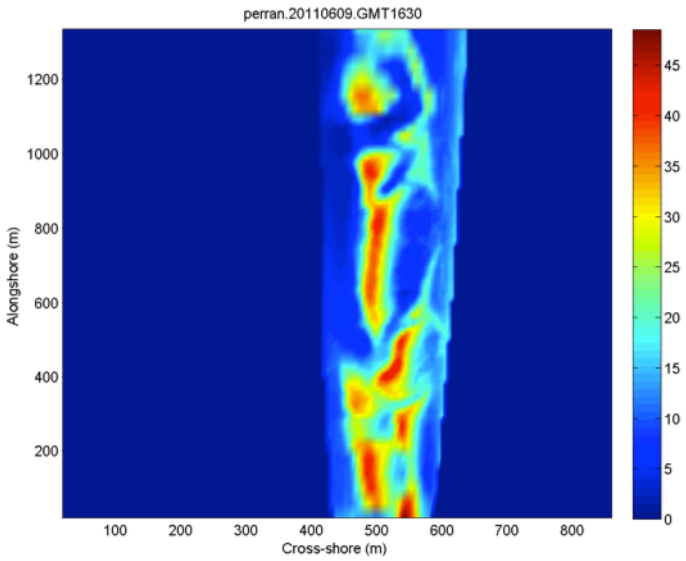

Figure 4-5. Roller dissipation map (imap) on 09/06/11 at 16:30.

4.3 Image selection and ranking

The initial set-up of the Beach Wizard model to be used took as input a single imap, as it was mentioned in the previous section. However, the runs used as the core of this master thesis have a time range spanning between the 1st of April and the 30th of June 2011, for which timex images were selected and processed for these three months. A process for manually selecting the timex images to be used was defined, along with a qualitative ranking scheme for the generated imaps, which will be later used for the analysis of the importance of the image quality in Beach Wizard for the correct

modeling of bathymetries and rip currents. Here the process of image selection and the criteria used will be described.

4.3.1 *Tidal image limitation*

The first filtering process of images to be used was based on tidal elevation, and the fact that Perranporth presents a featureless upper shoreface. Considering Perranporth's general beach state, an upper limit of -1 m (w.r.t MSL) was selected for the tidal levels to be analyzed. With this limit in place, all images corresponding to tidal levels below -1 m and during daylight hours came to be the starting base group of images to be further filtered and processed. This limitation resulted in a total number of images during daylight hours of 538 timex images. It was later decided to test using a higher tidal level as the limiting restriction (+1 m), as to try and solve some estimation errors that were present near the shoreline at -1 m. The additional images were selected for the month of April only, resulting in a total of 188 available timex images between -1 m and +1 m tidal elevation. The further selection process will now be described.

4.3.2 *Image quality*

The second step in the initial image selection process was a visual filtering of images, where each individual camera timex image was looked at alongside the corresponding merged plan-view timex image. The objective of this stage was to eliminate the very poor images, which presented problems due to very dirty camera lenses, extremely foggy or rainy conditions, and any other factor resulting in a completely "unusable" image. Figure 4-6 and Figure 4-7 show examples of what is considered a "good" image and a "bad" or rejected image respectively.

Figure 4-6 shows what was considered a "good" image, showing very clear individual camera resolution, and a clear merged timex image. Figure 4-7 shows very blurry individual camera images, and a very bright merged image. This is due possibly to salt or simply dirty camera lenses, particularly for cameras 1 and 2 (in order from top to bottom in the figure).

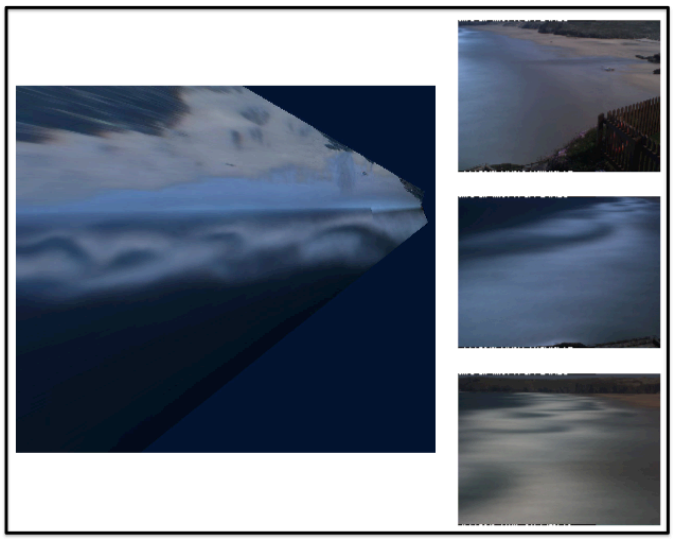

Figure 4-6. Example of "good" merged and individual timex images.

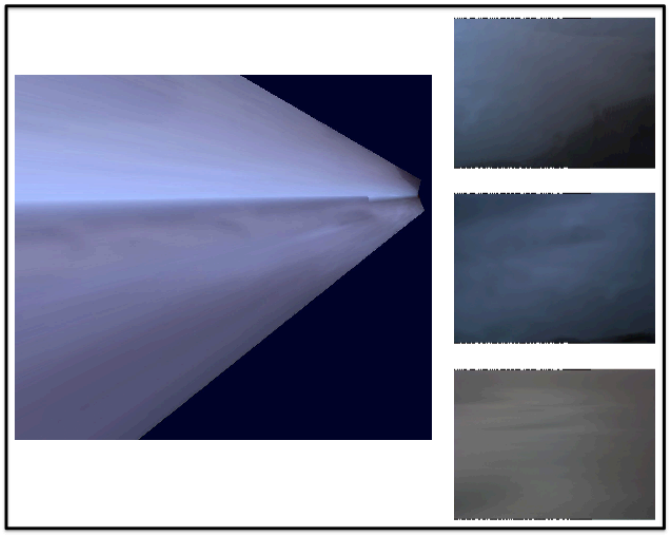

Figure 4-7. Example of "bad" merged and individual timex images

This filtering out of bad images reduced the total amount of images for the time span of interest from 538 to 402 images. Next, these 402 images were processed following the procedure for imap generation that was previously described, obtaining a total of 382 scaled imaps. The difference in 20 images was due to corrupt files and missing corresponding merged *.mat* files; this was not considered an important loss of information.

4.3.3 *Qualitative ranking*

During the generation of the imaps fro the available set of images, each one was assigned a qualitative ranking between 1 and 4, where a 1 corresponds to a "very bad" imap, a 2 is a "bad" imap, a 3 is a "fair" imap, and a 4 is a "good" imap. This ranking is purely qualitative, and subjective judgment considered only the actual quality of the image itself, regardless of wave or tidal conditions. This meaning that an image with very large streaks running through it, or large patches of bad information was called a very bad imap, and an imap that presented very clear dissipation with no noise or image quality related problems was assigned a 4. This ranking essentially ranks the generated imaps based on how well it represents the timex image, and how well this corresponding timex image represents dissipation; in other words, it is a qualitative ranking relating to image quality rather than actual imap quality or dissipation patterns.

Further along in the work of the present thesis, it was decided to include a higher tidal limit; reason for which will be described later in the report. With this, a test was conducted for the month of April, raising the tidal limit of the imaps to be used to +1 m. The available images images between -1m and +1m tidal elevation were 188, and after the same initial filtering out of "unusable" images, 108 usable images were obtained. These images were also ranked using the aforementioned qualitative ranking system, and were kept separate from the rest of the processed imaps for reasons that will shortly be pointed out.

Here the obtained ranking and monthly distribution of all generated imaps between April 1st and Jun 30th 2011 are presented. Figure 4-8 shows the distribution of the ranking of imaps for each month and for the total timeframe. The total number of imaps for April, May, and June is 147, 113 and 122 respectively.

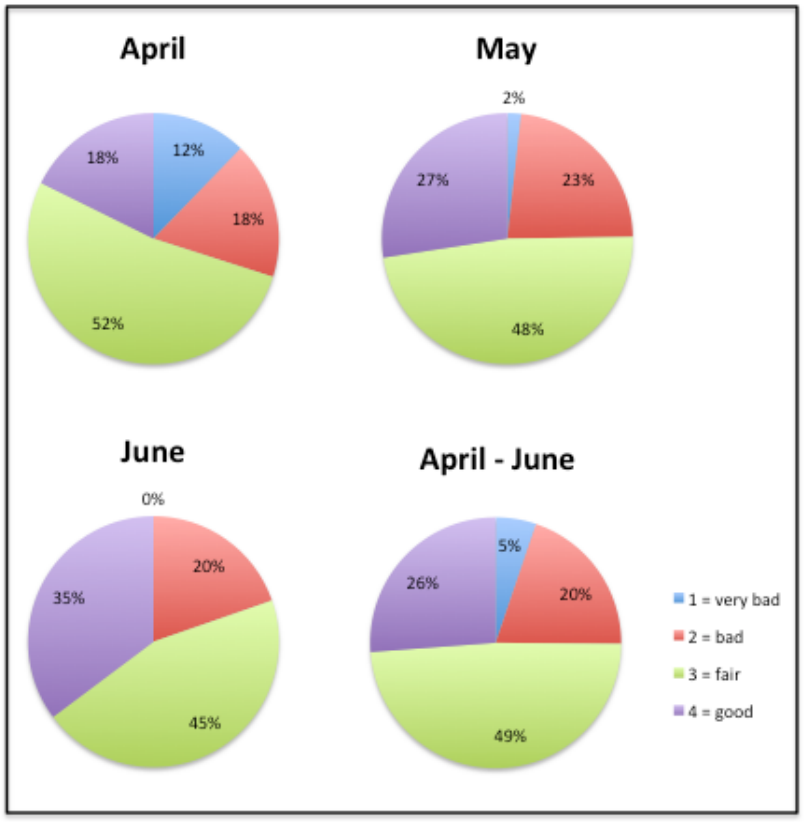

Figure 4-8. Monthly distribution of imaps according to qualitative ranking.

This distribution shows reasonably equal division of imap quality between the three months, meaning that this qualitative ranking system can be considered applicable to a variety of conditions, and tends to provide equal distributions. The distribution of imap quality for higher tidal levels (between -1 m and +1 m) for the month of April is looked at separately, and is shown in Figure 4-9.

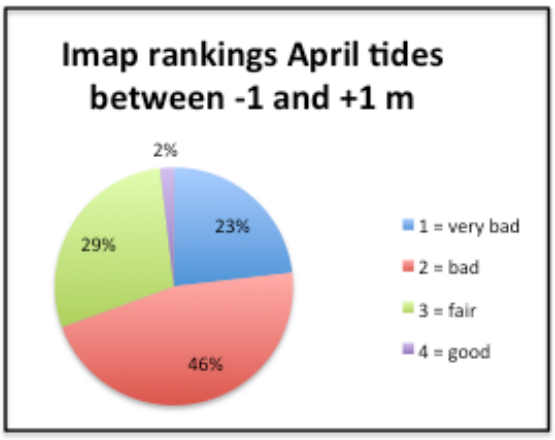

Figure 4-9. Qualitative imap distribution for higher tidal levels (-1 m to +1 m), April 2011.

The reason for looking at the quality of imaps for higher tidal levels is to point out a problem with the generation of these specifically at Perranporth. During the image merging process, there is a problem with the joint between cameras 1 and 2 (Figure 4-2), which sometimes shows up as a bright line in the merged image along this joint. The reason why this problem did not affect the generation of imaps for tidal levels below -1 m is that this tidal elevation coincides almost exactly with this merge line, so the bright line rarely appears at all in these merged images. However, when looking at merged images for higher tides, this bright line may appear in the surf zone, leading Beach Wizard to believe that it's dissipation, while in reality it is an image error. The distribution of image quality for higher tides shown in Figure 4-9 reflects this phenomenon, where almost three quarters of the images are bad or very bad (sowing problems coinciding with the merge line between cameras 1 and 2). An example of this is shown in Figure 4-10, which is a merged timex image and corresponding raw intensity map for the 12th of April, at a tidal elevation of 0.14 m. This image shows a bright vertical line in the merged image, which is reflected as a red line in the intensity map. This causes problems for the detection of the shoreline, and ultimately reduces the quality of the imap due to both a poor representation of the shoreline and an unrealistic sign on dissipation (the red vertical stripe in the imap).

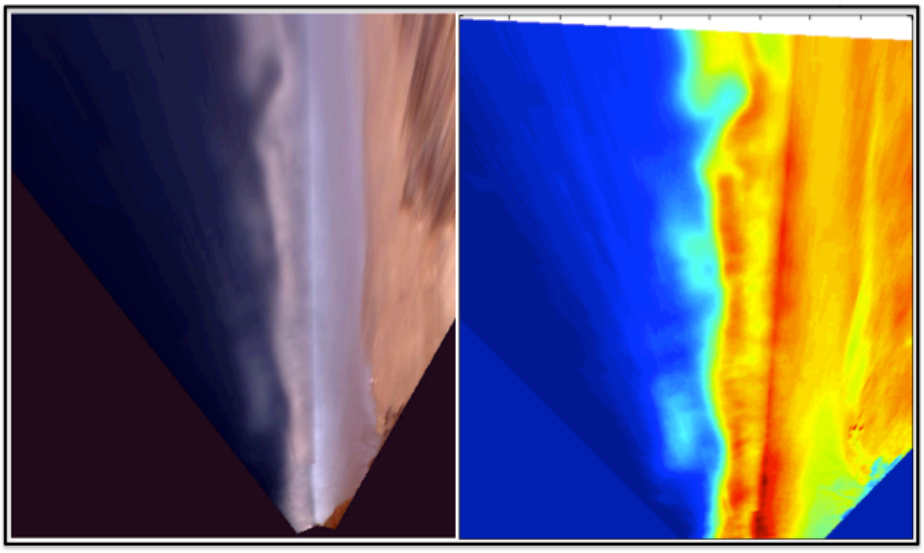

Figure 4-10. Shoreline detection problem at mergeline between cameras 1 and 2. (Left) merged timex image tidal elevation = 0.14 m, (Right) corresponding raw intensity map.

4.4 Specific Beach Wizard input

For the running of a model with the Beach Wizard module functioning, a few specific inputs are required, each having a certain format in which it must be presented. These inputs correspond specifically to the dissipation map information (imaps) and default values of measurement error and uncertainties.

The dissipation maps are input into the model in the form of a text file, where the values of said map are arranged in one single column. The values are taken starting from the grid origin (0,0) moving in cross shore direction, that is, arranging every row in a single column, starting from the first row. As well as this, the first seven lines in said text file correspond to the beach wizard grid origin in *x*- and *y*- in world coordinates, the cross-shore and alongshore spacing in metres, the number of grid cells in cross-shore and alongshore, and the orientation of the grid in degrees (in that order). This file has a name describing its location, date, and exact time of taking of the image, and has the extension ":\.imap.txt". As well as this, another file with the same name and the extension ":\.info.txt" contains the tidal elevation, the wave height, the peak period, and the wave direction.

Another specific input file for the Beach Wizard model is a file (*bwdefaults.inp*) containing default error values for the different input sources. These default measuremet errors are for the observed quantities of dissipation, celerity, bathymetry, and intertidal bathymetry (only dissipation for Perranporth). The use of default measurement errors for dissipation will be looked at in further detail in the following chapter, where a slight variation will be made.

4.5 Conclusions and Recommendations

In setting up the bathymetry updating model, selecting, and processing the timex imges used as input, some general conclusions and recommendations can be pointed out, mainly with regard to the image selection and intensity map generation processes.

The qualitative imap ranking employed is dependent on the quality of associated timex images. The distribution of the different qualitative ranks over the three

months in the study period are quite regular (small variations in ranking distribution between months), meaning that the ranking in fact is dependent on image quality and not linked at all to forcing or tidal conditions.

Two overall problems were found in the timex image merging process. The first problem is frequent errors producing untruthful intensities in the offshore region, where the intensity should in fact be zero (or very near to zero). This problem was addressed by implementing an interactive shoreline and surf zone detection process, in which the user outlines the zone of interest (area presenting wave dissipation) and the rest of the domain is set to zero intensity. Further work is recommended to be put into the merging process, as to obtain proper offshore base intensities. As well as this, the interactive shoreline and surf zone detection process is quite time consuming when processing large amounts of images, so transitioning to a more operational method would be ideal.

The second problem with the merging process is a problematic merge-line between cameras 1 and 2, presenting in many cases a bright line along it. For tidal elevations below -1 m this is not a problem, because the merge-line is above that elevation. However, for higher tidal elevations the problematic merge-line produces bad imaps in many cases, with a bright line through the surf zone (being read by Beach Wizard as wave dissipation, which is not true). Efforts should be made to fix this issue, and in this manner have a larger available set of timex images (for higher tidal levels).

5 BEACH WIZARD BATHYMETRY UPDATING MODEL RESULTS

The present chapter will focus on the functionality of the data-model assimilation method beach Wizard, looking into detailed aspects of the code, model outputs, sensibility to parameter variations and the relative weight or importance of these. During this work, changes were made to the Beach Wizard code and parameters, all of which will be described here. First, the default settings of the code will be explained, along with several important details regarding the assimilation process. Next, the first test cases that were carried out will be described, during which the basic functioning of the model is looked at by using several simplified cases with varying input setups. After this, the long run (April-June 2011) model will be looked at, along with several changes made to the code, and the effects of these changes on the resulting computed bathymetries.

Beach Wizard's general assimilation process and formulations were previously described in the theoretical framework of this report, and here reference will be made to the equations mentioned in said section, also providing further detail into these formulations and parameters.

5.1 Initial default code and parameter settings

The main points looked at in the default Beach Wizard code and parameter settings are with regards to the definition of the measurement error and the uncertainty in observed dissipation, the restrictions applied to the bed update scheme with respect to water depth, and the variation of the uncertainty between simulations. Here the main formulations considered will be described, as well as making reference to the equations presented in section 2.3.1.

5.1.1 *Measurement error and observed bathymetry uncertainty*

In section 2.3.1 the weighting coefficient (α) for the bed update scheme was defined as the ratio between the prior estimate uncertainty and the sum of the observed and prior uncertainties (Equation 16). Since this weighting coefficient directly affects the magnitude of the bed change that will take place, it is clear that the definition of these uncertainties will be critical in the functionality of the bed update scheme.

The uncertainty in bathymetry due to the observed data (σ_{obs}^2), as defined in Equation (17), is as follows for the particular case in which the observed quantity is wave dissipation.

$$\sigma_{obs}^2 = \frac{\varepsilon^2 + (D_{com} - D_{obs})^2}{\left(\frac{dD_{com}}{dh}\right)^2 + \delta^2} \tag{20}$$

Where ε^2 is the measurement error, D is dissipation (subscripts *obs*=observed, *com*=computed), h is water depth, and δ is a noise level. In the default Beach Wizard code, the measurement error is defined as an initial default value that is input to the system as a text file in the run directory, and then is varied twice throughout the code with respect to the observed quantity of dissipation (D_{obs}), wave height, and water depth. The formulation that seemed to alter the default measurement error significantly is the following,

$$\varepsilon = \varepsilon_{def} + \left(100 - \varepsilon_{def}\right) * \left(1 - \tanh\left(\frac{3.7 H_{rms}}{h}\right)^{20}\right) \tag{21}$$

Where ε_{def} is the default measurement error (entered by the user). The effect of this is that at locations where the water depth is more than 3.7 times the wave height, the measurement error is increased from its default value to 100 W/m^2. This increases the measurement error significantly, and therefore reduces the bed change, particularly on days with small wave heights. Since one of the objectives of this thesis is to look at the importance of the quality of input images, not necessarily related to wave conditions, this is not an ideal change to make to the measurement error. The effects of this will be discussed further on; using model results from this default setting compared to changed code configuration results.

5.1.2 *Depth restricted bed change factor*

Another interesting "hard-coded" feature in the default code is a factor that essentially restricts bed updating to water depths greater than 1 m. This is done by means of an extra term multiplying the weighting coefficient in the bed change equation (Equation 18). This extra term directly multiplies the weighting coefficient (α) as follows.

$$h(t + \Delta t) = h(t) - \beta\alpha \sum_{i=1}^{S} \frac{\frac{df_i}{dh}}{\left(\frac{df_i}{dh}\right)^2 + \delta_i^2} (f_i - f_{i,obs}) \tag{22}$$

$$\beta = \tanh(h^{20}) \tag{23}$$

The effect of raising the water depth to the power of 20 is that for depths below 1 m the term β drops rapidly to zero, cutting off any possible bed change. The effects of this will be looked at and explained in more depth in the upcoming section of this report, using several test cases as a basis.

5.1.3 *Modulations in prior bathymetry uncertainty*

Another important factor in the bed update process is the prior uncertainty (σ^2_{prior}), which like the observed uncertainty is updated during each Beach Wizard assimilation loop, and unlike the observed uncertainty it is altered from one simulation to another (one image to the next) with a sigmoid function. The logic behind this rests on wanting to reduce the prior uncertainty for every iteration in one simulation (since the model is assimilating, and reducing the difference between computed and observed quantities, less bed change will occur), and wanting to increase the prior uncertainty from one image to the next, depending on the time between taking of consecutive images. As it was mentioned in section 2.3.1, the updated measurement uncertainty is calculated at the end of each assimilation loop, which then goes on to be the prior uncertainty in the subsequent iteration. This is calculated as follows,

$$\sigma^2_{update} = \alpha \frac{T_s}{\Delta t} \sigma^2_{obs} \tag{24}$$

Where T_s is the simulation length and Δt is the numerical time step (time interval upon which the bed update occurs). Following the implementation of the factor β recently mentioned and shown in Equation (23) (which restricts bed change for depths shallower than 1 m), it is consequently applied to Equation (24) as well in the default Beach Wizard code. Again, the reasoning behind this is that multiplying this factor by the updated uncertainty (prior uncertainty in the next iteration) will make this uncertainty tend to zero at depths shallower than 1 m; again, making the weighting coefficient tend to zero and therefor the bed change as well.

As well as this updating of the measurement uncertainty for every numerical timestep, it is also updated between simulations. This increase in uncertainty between simulations is not carried out in the Beach Wizard code, since each simulation is a separate run in the XBeach model; rather, it is calculated in a matlab script (*runcaseAvD10.m*) that arranges the information for the next simulation. This is

heuristically modeled with a sigmoid function, which is an exponential approach to σ_{evo} (natural uncertainty). This natural uncertainty is set to 1 m, and the rate at which the uncertainty increases towards this depends on the timescale T_r, which depends on the magnitudes of sediment transport rates that are responsible for the bed evolution. This indicates that the mentioned timescale should depend on wave heights and other factors affecting sediment transport rates, however, in this default case a constant value of 5 days is used (the sensitivity of this will be tested further ahead). The function of the uncertainty increase between simulations is as follows.

$$\sigma^2(t_j) = \sigma^2(t_{j-1}) + (\sigma_{evo}^2 - \sigma^2(t_{j-1}))\tanh^2\left(\frac{3}{T_r}(t_j - t_{j-1})\right) \quad (25)$$

Where the subscript *j* corresponds to the beginning of the current simulation, and *j-1* to the end of the previous simulation. The effect of this function is a small increase in measurement uncertainty from one simulation to the next if these are not too far apart in time (ie. consecutive images from the same day), and a larger increase in uncertainty for instances where 2 consecutive simulations are separated by a day or more. This will too be looked at in further detail in the upcoming sections of this report, by looking at the evolution of the measurement uncertainty in time (between simulations) and the differences between having consecutive images on a single day and having images a day or more apart.

5.2 Simplified test runs

A series of initial test runs were conducted with simplified conditions for Perranporth, as to obtain a working model and look into some of the general code and parameter settings mentioned in the previous section. Here a brief description of the simulated simplified cases will be carried out, presenting only what was considered to be the more important findings. The test cases are divided into two major groups depending on the imaps used as input, being runs that use a single imap as input (repeated several times with the same forcing conditions), and runs that use several different imaps taken between the 1st and the 9th of June 2011.

5.2.1 *Single imap test runs*

Several test runs using a single imap taken on the 9th of June 2011 (as described in section 4.2) were carried out, simply to assure that the bed update scheme was working correctly and to look at the effects of the depth limiting factor mentioned previously as well as the impacts of using different initial bathymetries. These test cases used a set of identical imaps repeated every 12 hours with the exact same wave an tide conditions. Using this simplified case with a fixed shoreline gives a clear view of the effects of having a depth limiting update factor in the code, and how this influences the development of the bed during a single simulation.

Figure 5-1 shows the results for a test case using an imap from the 9th of June repeated twice a day over 3 weeks. This result is using all the default parameter and code settings described in the previous section. In this figure all axis coordinates correspond to the local model coordinates system described in the model setup section of this report. What can be taken from this figure is that the computed dissipation is in fact moving towards the observed dissipation, by modifying the bed at every location. This can be seen easily in the two bottom panels of each quadrant of the figure, where these are cross sections of the bed (z) and the wave dissipation (D). The plot showing a cross section of the computed (red line) and observed (blue line) dissipation shows how as the run progresses the dissipation is converging to the observed.

The first two quadrants in Figure 5-1, specifically in the cross section of bathymetry panel (z), show a problem which is recurrently encountered in this course of this thesis, and was also noted by Van Dongeren et al (2008). This problem is the digging down of the bathymetry at the shoreline due to the computed dissipation being higher than the observed dissipation, which in reality might not be correct. This is a systematic estimation error that occurs due to the fact that the bed updating scheme doesn't account for the "history" of wave dissipation from offshore to onshore; this meaning that in reality if there is a bar offshore, there will be wave dissipation over that bar, and therefore less dissipation at the shoreline without the need to deepen the bed at the shoreline. The details of this systematic estimation error will be looked at in detail in section 5.3.3.

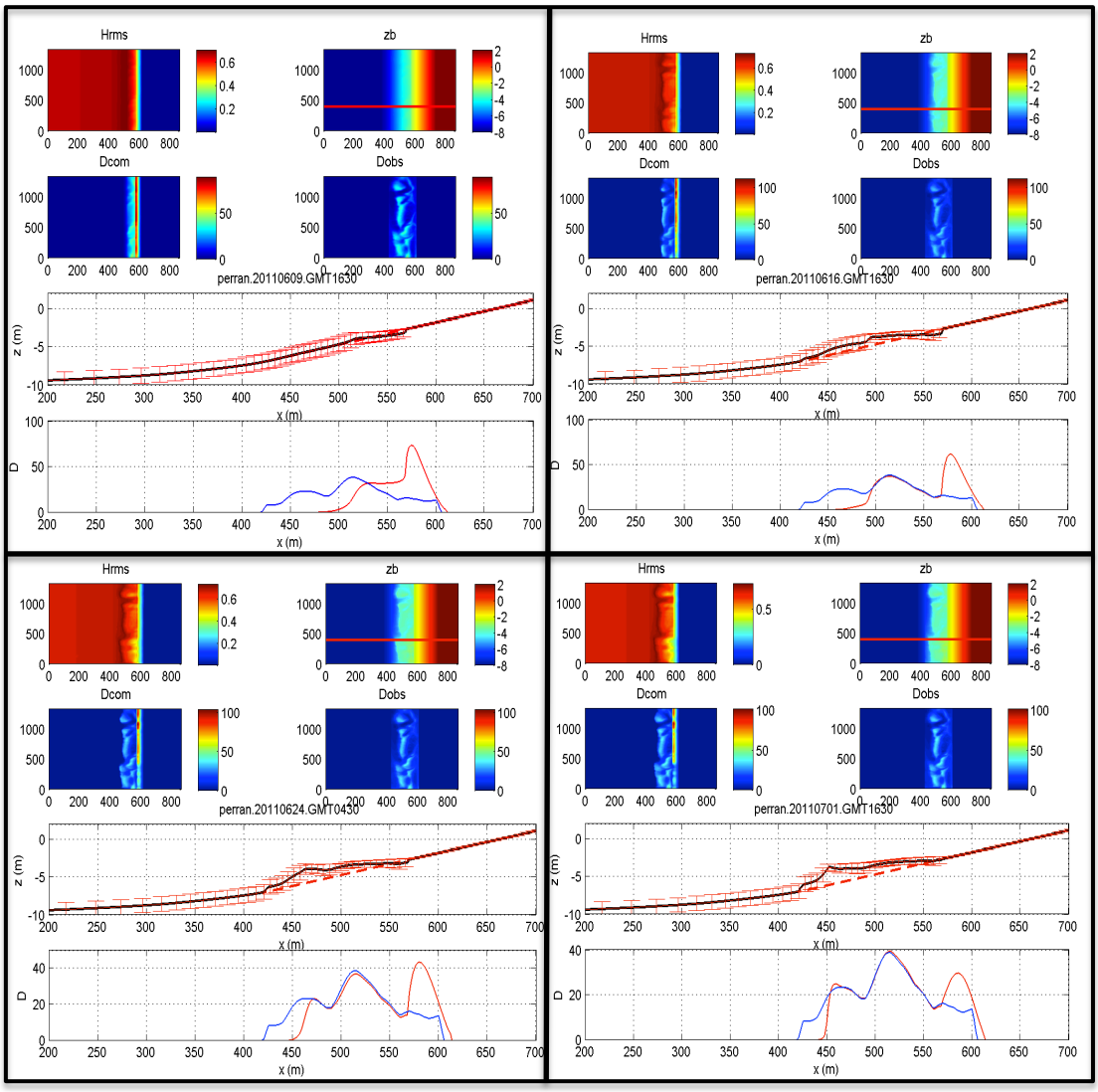

Figure 5-1. Single image repeated over three weeks and plane bed as input. The four quadrants of the figure from top left to bottom right correspond to results at different times during the run, namely 09/06/2011, 16/06/2011, 24/06/2011, and 01/07/2011. Each quadrant presents wave height (Hrms(m)), computed bed elevations (zb(m)), computed dissipation (Dcom(W/m²), observed dissipation (Dobs(W/m²), and a cross section of bed elevation (z (m)) where the dashed red line is the initial bed, the solid black line is current computed bed level, and the red errorbars are uncertainty; and a cross section of dissipation (D (W/m²)) where the blue line is observed dissipation and the red line is computed dissipation.

Another observation from this test run is that the bed updating is zero near the shoreline, for water depths below 1 m. This is expected due to the reason previously explained, where there is a depth limiting factor in both the bed update equation and the uncertainty update equation. This was varied, by reducing the limiting depth to 0.5 m from the original 1 m, by dividing the depth by 0.5 in Equation (23). The result

of this variation was as expected, and simply moved the extent of bed change shoreward. This effect is seen more clearly in the two runs described below.

As to look at the importance of the initial bathymetry, and how different initial bathymetries will react differently to the above mentioned depth restricting factor, a series of runs were carried out using an alongshore uniform bathymetry as the initial model bed. The cross section for this initial bathymetry was taken from a longshore location of y=400m (local model coordinates) on the measured bathymetry on the 1st of June 2011. Below, Figure 5-2 shows the final simulation results for two runs with the initial bathymetry that was just described, and two different depth limited bed update restrictions (1m (left), and 0.5m (right). These two runs used a single imap as input repeated 15 times twice a day.

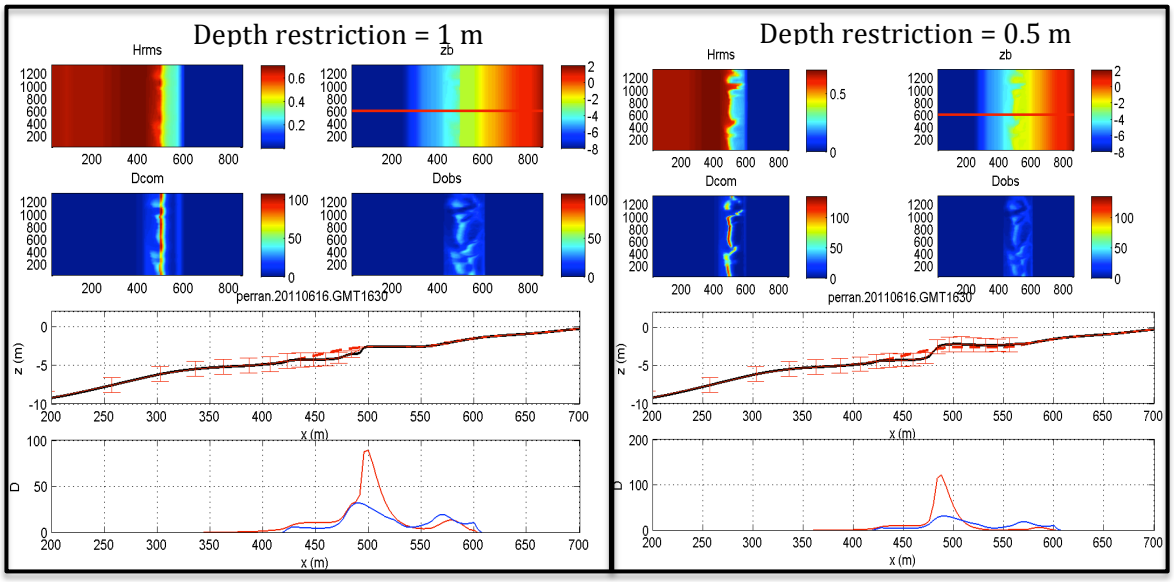

Figure 5-2. (Left) Results of run with 15 repeated imaps twice a day, alongshore uniform barred initial bathymetryand, and bed change restricted to depths deeper than 1 m. (Right) Results of run with 15 repeated imaps twice a day, alongshore uniform barred initial bathymetryand, and bed change restricted to depths deeper than 0.5m. Figure has the same layout as the previous figure.

The interesting observation from the results shown in Figure 5-2 is with respect to the extent in cross shore direction of the bed change that takes place. Since the initial bathymetry presented a bar or kind of nearshore terrace, restricting bed change to depths greater than 1 m has a strong impact in computing the nearshore bathymetry features. The water depth is equal to 1 m right around the 500 m mark in x, leaving quite a large area (from 500 to 600 in –x) out of range for the case shown in the left

side of the figure. This can be seen as a straight vertical line at x=500 in the plot in the left side of the figure marked zb, which is the computed bathymetry. Comparing this with the right side of the figure, which corresponds to a limiting depth of 0.5 m, it is clear that the latter has the ability to calculate the bathymetry to a farther onshore extent, capturing the rip channels observed in the imap, unlike the case with a limiting depth of 1 m (left side of figure).

The dependence and effects of varying the initial bathymetry will be briefly discussed in section 6.5, where the results are more conclusive. For this reason, the test cases carried out in the present phase where the initial bathymetry was varied will not be shown, and it will simply be mentioned that it was found that for a simple test case with 1 imap as input and 1 single forcing condition, the initial bathymetry has a strong impact in the results, particularly when there is depth limiting factors in play. This is due to the possible restriction of bed change in cross shore direction, as well as the previously mentioned systematic estimation error.

Since in the present phase it was found that the importance of having various different images with different waves and boundary conditions is paramount, the next test runs were carried out using 16 different imaps between the 1st and 9th of June 2011. This finding is based on the observation of harmful bed changes (particularly near the shoreline) being progressively amplified between simulations, due to the fact that the shoreline position was at a fixed location and the tidal modulation was disregarded. This leads to believe that having multiple inputs with different forcing conditions and tidal elevations would prevent the amplification of shoreline errors during consecutive simualtions.

5.2.2 *Multiple imap test runs*

The objective of this phase of work is to obtain what is considered a good model version, with the best parameter and code settings possible. For this, it is kept in mind that one of the main objectives of the present thesis is to look at the importance of regularity and quality of imaps used as input, therefore the definition of a "good" model configuration here is one which models the bathymetry well and trusts the input to a sufficient degree. The fact that only dissipation maps are available as input

is another thing to keep in mind, which makes the output of the model rely completely on the images available. As it was mentioned, the test runs carried out in this section will use a total of 16 different imaps between the 1st and 9th of June 2011. It is important to point out that although section 4.3 (image selection and ranking) has already been presented in this report, that section was carried out after these test cases that will be presented here, reason for which the imaps used here do not have associated qualitative rankings.

Start time

A very important finding that arose during this section is with respect to the start-time of the Beach Wizard assimilation scheme in the XBeach computational process. The start-time is manually defined in the matlab script (*runcaseAvD10.m*) that organizes the input and information files for each simulation. For the simulations that were run prior to this stage in the work, this time was set to zero, meaning that the Beach Wizard assimilation process starts with the first XBeach wave calculation. The problem found with this is that at time zero the computed dissipation still hasn't had a chance to develop across the whole domain, while the observed dissipation has already been read by Beach Wizard. Because of this, a large bed change was observed at the start of each simulation, raising the bed at every point where there is observed dissipation. This clearly is a problem, and therefore the start-time was changed to 2 minutes, allowing the XBeach wave computations to "warm up", and reach a fully developed computation by the time the bed update process begins. This can be seen in Figure 5-3, where 3 time instances in a single simulation are shown for both the default case with start-time equal to zero (top) and start-time equal to 2 minutes (bottom). The important observation to take from this figure is the difference in bed change at the first time interval for both cases; where for the case with start-time equal to zero there is an increase in bed level (positive bed change) wherever there is observed dissipation, and for the case with start-time equal to two there is positive bed change where the observed dissipation is lower than the observed and vice versa. It is important to state that the time instance shown in the figure (t=1) corresponds to the first output time in XBeach (defined by *tstart* in *params.txt,* and in this case equal

to the aforementioned start-time) *so* in computational time, the time at t=1 on the top panel is in fact t=1, and on the bottom panel t = 1 is actually t = 2 minutes.

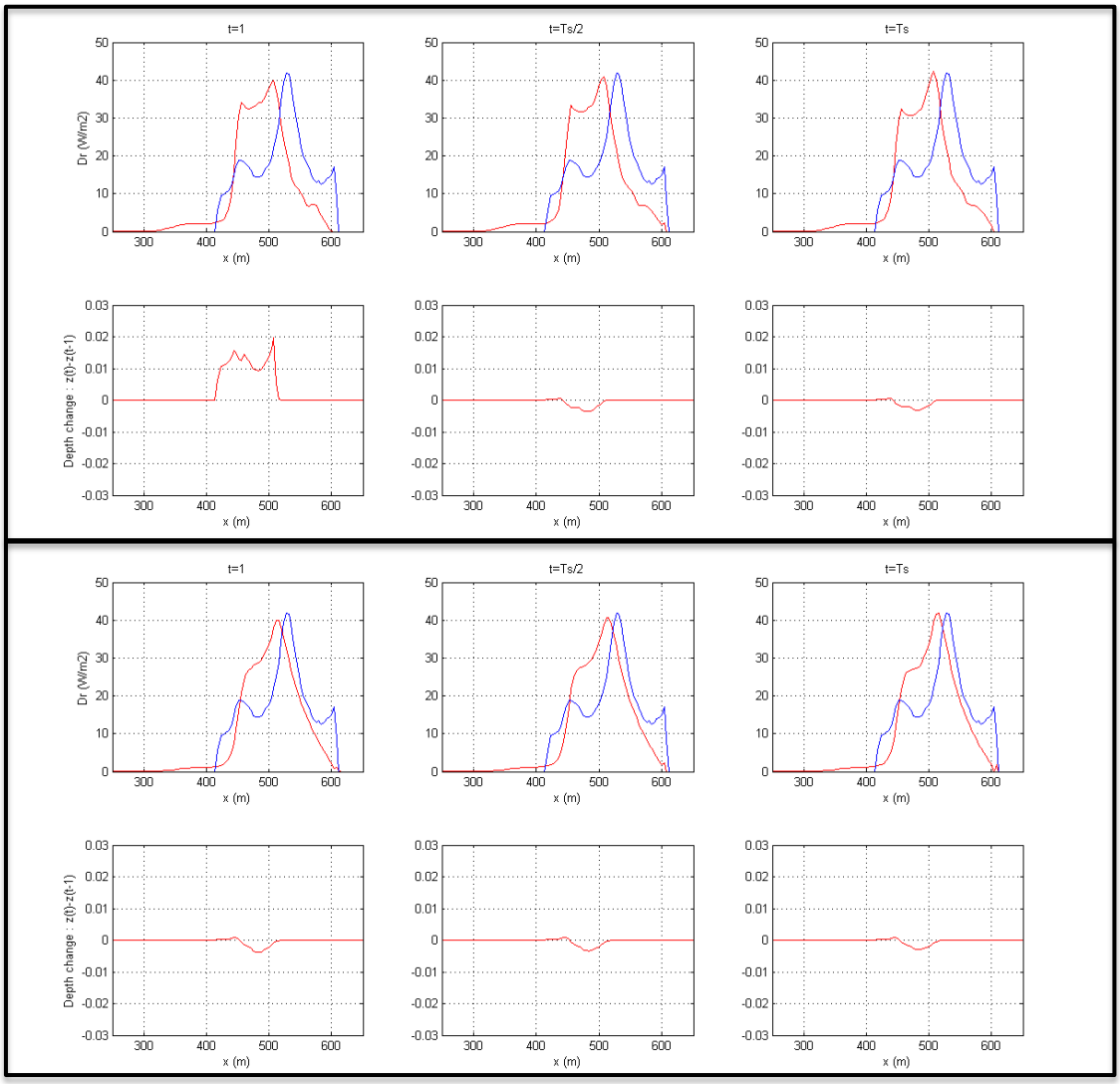

Figure 5-3. (Top) 3 time instances for default single simulation, showing in top panels computed (red line) and observed (blue line) dissipation, and depth change in bottom panels. (Bottom) 3 time instances for single simulation with start-time=2min.

Measurement error

In this phase of work important findings were made with respect to the measurement error. The reason for having observed these findings is due to the fact that variable imaps were used, each with different waves and tidal conditions, as opposed to the fixed uniform conditions used in the previous test runs (using a single imap repeated

several times). The effect of using a constant default measurement error (20 W/m^2 in this case) is that in cases with very variable wave conditions, days with large wave heights will have a different relative uncertainty as days with small waves. More specifically, for the default value of 20 W/m^2 that was given previously to the measurement error, an image taken on a day with large waves (dissipation in the order of 200-300 W/m^2) will be considered far more trustworthy in comparison to an image taken on a day with small waves (dissipation in the order of 30-50 W/m^2). For the purposes of this thesis, it is not desirable to link the measurement error or reliability of input images to wave heights in this manner (at least not at this stage that is), since one of the major questions is with regards to the importance of image quality regardless of forcing conditions. Not wanting to link the measurement error with wave height in this manner is specifically due to the fact that it is not known whether the relative trustworthiness of a given image is directly related to wave height or not. For this reason, it was decided to set a variable (from one simulation to the next) default measurement error corresponding to 15% of the maximum observed dissipation. This may however be looked at as relating the measurement error to wave heights (since dissipation is derived from the offshore wave heights), regardless, this will allow all images irrespective of wave height to have the same relative uncertainty. This should facilitate the further analysis of the importance of regularity and quality of images that is necessary for the Beach Wizard model to function optimally, due to the fact that not the relative uncertainty of an image is not a varying factor.

As well as this addition of a measurement error as a percentage of the maximum observed dissipation, the measurement error variation described previously and shown in Equation (21) was eliminated from the code. The effect of this change is substantial, due to the fact that the increase in measurement error from Equation (21) was essentially making the assimilation process work extremely slowly, not allowing sufficient bed change to occur. This can be seen below, in Figure 5-4.

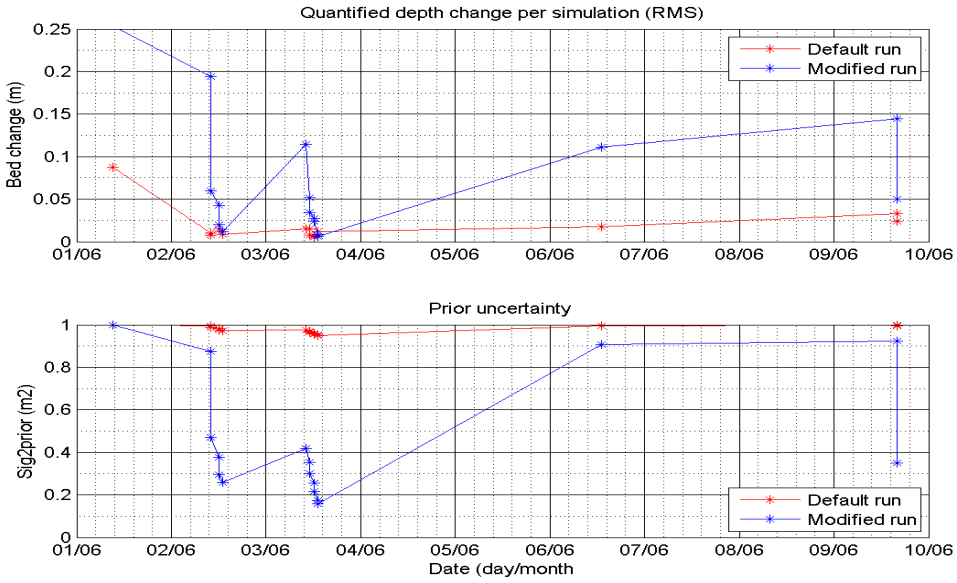

Figure 5-4. (Top) Quantified total depth change per simulation, default case (red) and changed uncertainty (blue). (Bottom) Prior uncertainty at each simulation, default case (red) and changed uncertainty (blue).

Figure 5-4 shows two different runs, the first (red) being the default case (including Equation 21), and the second (blue) being a modified case in which Equation (21) is eliminated and a default measurement error of 15% of the maximum observed dissipation is used. In this figure the top panel corresponds to a quantification of the total bed change per simulation (each marker corresponds to one simulation), calculated as a root mean square of the difference between the initial and final bathymetries in each simulation. The bottom panel in the same figure shows the prior uncertainty at the beginning of each simulation, taken at a single point on the offshore boundary as to only look at the variation of uncertainty due to the general equations of prior or updated uncertainty, and not relate it to the observed uncertainty at all. The difference generated is clear, the change in measurement error allows the model to work much faster, assuming that dissipation maps are more trustworthy, the prior uncertainty becomes much smaller and the bed change per simulation becomes significantly larger.

Another interesting observation worth pointing out from Figure 5-4 is how both the bed change rises and falls in time. The reason for this is the change imposed by Equation (25), where for larger periods of time between simulations the prior

uncertainty tends to the natural uncertainty of 1 m. This shows how on the 2nd and 3rd of June, where several imaps are available very close together in time, the uncertainty drops, and when there are several days between simulations the prior uncertainty rises substantially towards 1 m. This will be discussed again further ahead in this report (section 5.3.2).

Depth limited bed change factor

The final change made to the Beach Wizard code in this phase of the work is with respect to the depth-limiting factor discussed earlier. The factor β in Equation (23) drops from 1 to 0 extremely fast at a limiting water depth of 1 m due to the water depth being raised to the power of 20. For this specific case at Perranporth, this was considered to be too drastic a limitation, since no intertidal bathymetries or any other information to help model the shallow water zones was available. For this reason, the factor β was given a smoother, more gradual progression from 1 to zero, by altering its configuration as shown below.

$$\beta = \tanh\left(\left(\frac{h}{0.85}\right)^5\right) \tag{26}$$

This change can be visualized in Figure 5-5, where it is clear that the new configuration of β provides a smoother reduction of the factor with diminishing water depth. The red line shows the default shape of this depth-limiting factor, and the blue line shows the modified factor, providing a much more gradual reduction with water depth. The difference in the bed computations with and without this change is as expected, simply in that the new factor allows bed changes to occur in shallower water than the previous, and no change at all is seen at regions with water depths greater than 1 m.

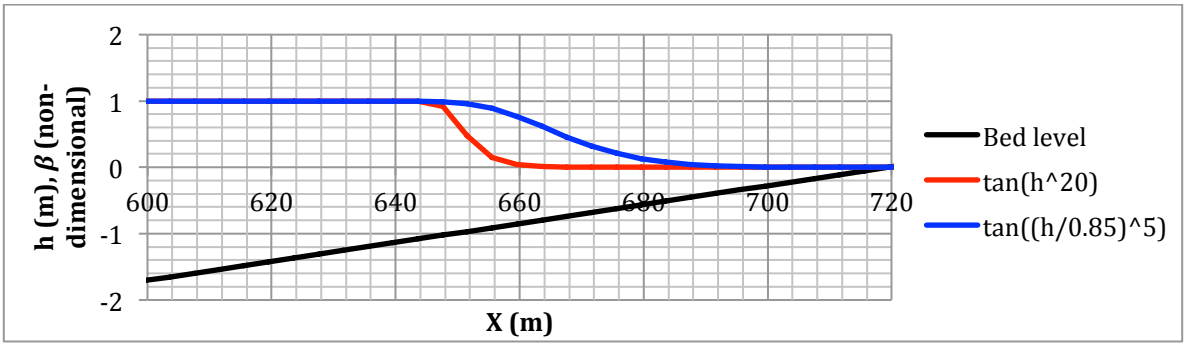

Figure 5-5. Depth-restricting bed change factor.

The resulting bathymetries from the test runs carried out in this section were looked at and considered when making the changes to the code and parameter settings mentioned above, however, these resulting bathymetries will not be presented here. The reason for this being that a better view of the development and estimation of bathymetries can be seen in the upcoming section, where the long term (1st April – 30th June) model runs will be presented and explained.

5.3 Long term model runs

The work carried out in this project phase corresponds to the tuning and sensitivity analysis of the Beach Wizard model formulations and parameter settings with respect to change in bathymetry estimations, using all available images between the 1st of April and the 30th of June 2011. Here "all available images" corresponds to the generated imaps with qualitative rankings 2, 3 and 4 as described in section 4.3 of the present report. This series of images corresponds to a total of 362 imaps for the entire period. Figure 5-6 presents the wave and tide conditions, as well as the qualitative imap rankings for the entire study period (including the imaps ranked 1, which will not be used here).

The impact of the changes implemented to the code or parameters in Beach Wizard during this stage will be quantified based on the quality of the estimated bathymetries in comparison with the available measured bathymetries on the 28th of April, the 1st, 6th and 11th of June, and the 13th of July 2011. The quantification of the variations in estimated bathymetries will be calculated by means of a root means square (RMS) error between the estimated and measured bathymetries, as well as using a Brier skill score (BSS) of the model in question. A Brier skill score is a comparison between the modeled, measured, and the initial (as input into the model) bathymetries, effectively giving a value greater than zero if the model shows an improvement in the bathymetry estimation over the initial input bathymetry and a negative value if the initial bathymetry is actually closer to the measured than the modelled bathymetry. The Brier skill score to be used is as follows (van Rijn et al., 2003),

$$BSS = 1 - \frac{\overline{(h_{mo} - h_{me})^2}}{\overline{(h_0 - h_{me})^2}} \qquad (27)$$

where h_{me} is the measured bathymetry, h_{mo} is the Beach Wizard modelled bathymetry, and h_0 is the initial bathymetry.

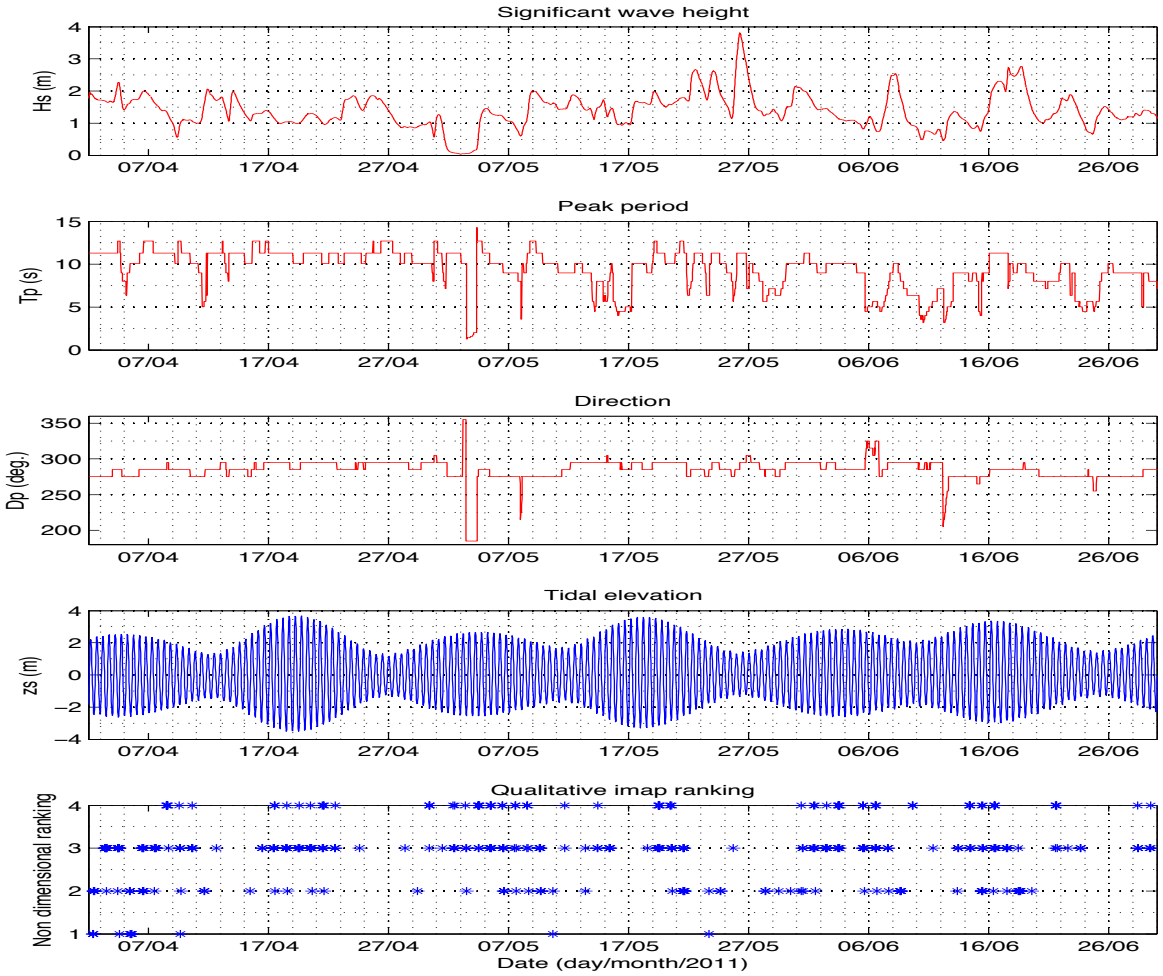

Figure 5-6. Waves, tides, and qualitative imap ranks for whole study period. Listed from top to bottom, (1) significant wave height, (2) peak wave period, (3) wave direction, (4) tidal elevation, (5) qualitative imaps ranking, where each asterisk is one imap.

The Brier skill score will be calculated with the initial bathymetry being the measured bathymetry on the 15th of March 2011, and the modeled and measured bathymetries coinciding on the date of measured bathymetries when it is possible. The skill score for the 30th of June is calculated with the measured bathymetry from the 13th of July (2 weeks after the modeled date), as this is the closest measured bathymetry at the end of the study period. This difference in time should not create too big an error, however, it will be kept in mind that the error can be expected to be larger on the 30th of June than for the other dates, where coinciding dates for measured and modeled bathymetries are used. Both the BSS and the RMS for each simulation will be

calculated for separate sections of the model grid, as to account for differences in model behavior in the cross shore direction. The regions where these calculations are carried out are the entire domain, the inner surf zone, and the outer surf zone. It is important to note that for the entire domain and outer surf zone calculations the region below y=300 m will not be taken into account, due to the persistent deepening seen in this region (because the area seawards of x=400 m and below y=300 m is out of the field of view of the Argus cameras). The limits of the inner and outer surf zones were chosen by looking at the main morphological features, and where wave breaking occurs; ultimately defining the outer surf zone as the region between 250 and 450 m in $-x$, and the inner surf zone between 450 and 600 m in $-x$. The extent of the domains used for the calculation of the BSS and RMS errors is shown in Appendix D.

The first version of the Beach Wizard code to be used is the default version as described previously in this chapter, which essentially includes Equations 21 and 23. Next is the version obtained from the tests carried out in the previous section, which includes using the measurement error as 15% of the maximum observed dissipation, the smoothed depth limiting bed update factor (Equation 26), and the elimination of Equation (21). As well as these two versions, a modification is looked into where the bed change is made time variant in cross shore direction, which addresses the issue of the systematic estimation errors that were mentioned previously. On top of these variations in the code, the effects of varying the timescale factor T_r in Equation (25) will be looked at for the second and third versions of the code just mentioned.

5.3.1 *Default vs. 1st modified model version*

The first results to be presented will be a comparison between the modeled bathymetries obtained with the default model version and the ones obtained with the first modified executable. From here on, in this report the default version will be referred to as executable 1 (Exe. 1) and the first modified version to be looked at here as executable 2 (Exe. 2). As it was mentioned, the difference between executable 1 and 2 is the removal of Equation 21, the implementation of a variable measurement error equal to 15% of the maximum observed dissipation, and the use of the modified depth restricting factor (Equation 25) in executable 2.

Figure 5-7 through Figure 5-11 show the resulting bathymetries for all dates with measured bathymetries during the study period. The results shown in these figures are in the form of computed bathymetries with both model versions, where the color bar at the bottom of each figure represents bed elevation in metres. As well as this, the measured bathymetry on each date and the initial measured bathymetry from the 15th of March are shown, as for comparison between these and the model results. The difference plots shown are the difference between the measured bathymetry and the modeled bathymetry (with each model version) on the corresponding coinciding dates.

The area of interest in the modeled bathymetry plots is everything above approximately y=300 m, due to the deepening of the estimated bathymetry that can be seen at around x=300 m and y=0 m. This deepening is due to the particular region being out of the field of view of the cameras.

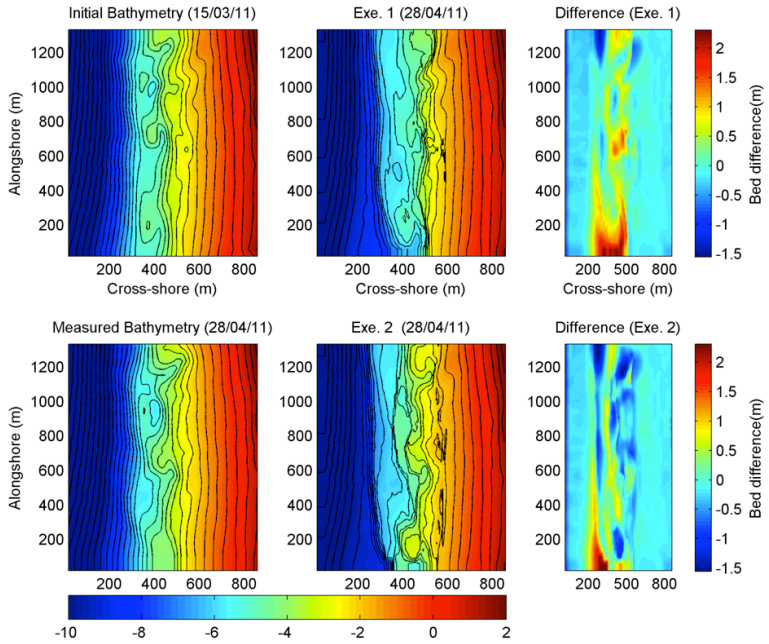

Figure 5-7. Bathymetry (color scale in m) estimation results with Exe.1 and Exe.2. (Top left) Initial measured bathymetry from 15/03/11. (Top centre) Modelled bathymetry with executable 1. (Top right) Difference between measured and modeled bathy. with exe. 1 on 28/04. (Bottom left) Measured bathymetry on 28/04/11. (Bottom centre) Modelled bathymetry with executable 2. (Bottom right) Difference between measured and modeled bathy. with exe. 2 on 28/04/11.

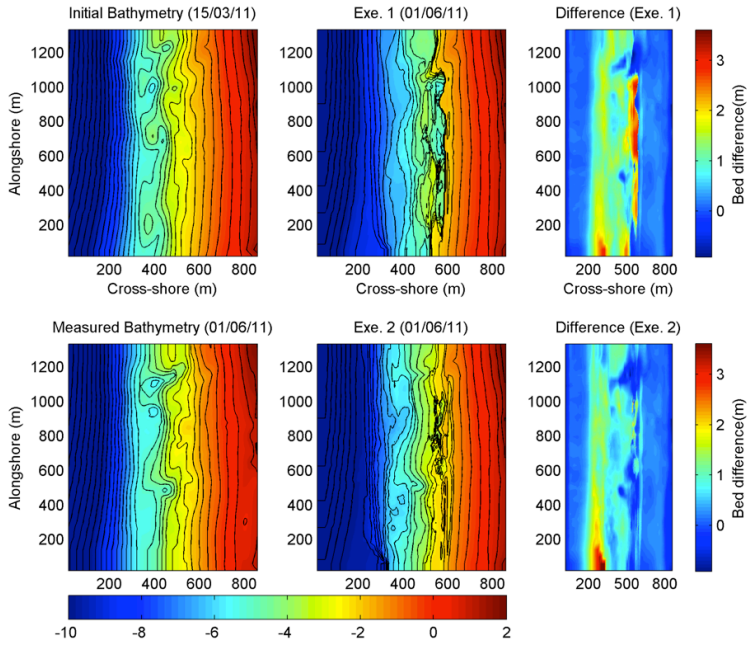

Figure 5-8. Bathymetry (color scale in m) estimation results with Exe.1 and Exe.2. (Top left) Initial measured bathymetry from 15/03/11. (Top centre) Modelled bathymetry with executable 1 on 01/06. (Top right) Difference between measured and modeled bathy. with exe. 1 on 01/06. (Bottom left) Measured bathymetry on 01/06/11. (Bottom centre) Modelled bathymetry with executable 2. (Bottom right) Difference between measured and modeled bathy. with exe. 2.

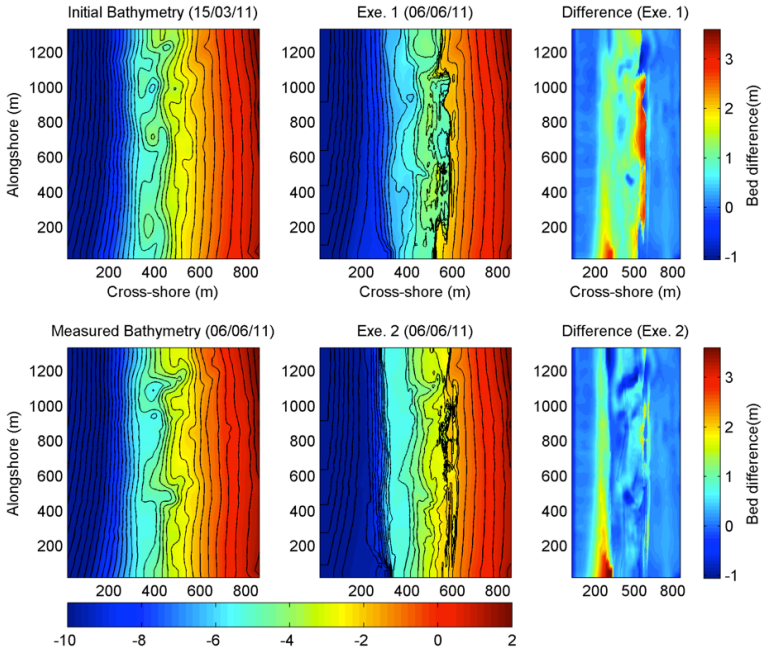

Figure 5-9. Bathymetry (color scale in m) estimation results with Exe.1 and Exe.2. (Top left) Initial measured bathymetry from 15/03/11. (Top centre) Modelled bathymetry with executable 1 on 06/06. (Top right) Difference between measured and modeled bathy. with exe. 1 on 06/06. (Bottom left) Measured bathymetry on 06/06/11. (Bottom centre) Modelled bathymetry with executable 2. (Bottom right) Difference between measured and modeled bathy. with exe. 2.

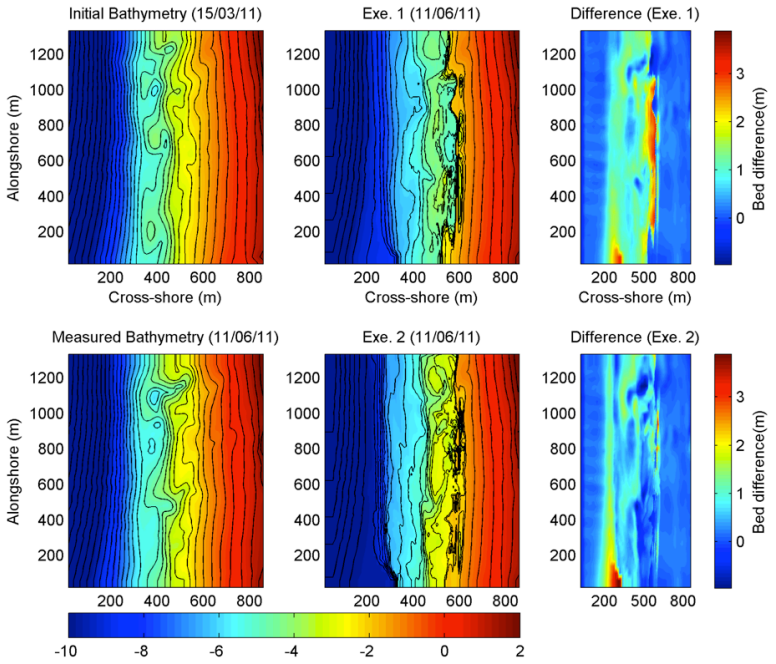

Figure 5-10. Bathymetry (color scale in m) estimation results with Exe.1 and Exe.2. (Top left) Initial measured bathymetry from 15/03/11. (Top centre) Modelled bathymetry with executable 1 on 11/06. (Top right) Difference between measured and modeled bathy. with exe. 1 on 11/06. (Bottom left) Measured bathymetry on 11/06/11. (Bottom centre) Modelled bathymetry with executable 2. (Bottom right) Difference between measured and modeled bathy. with exe. 2

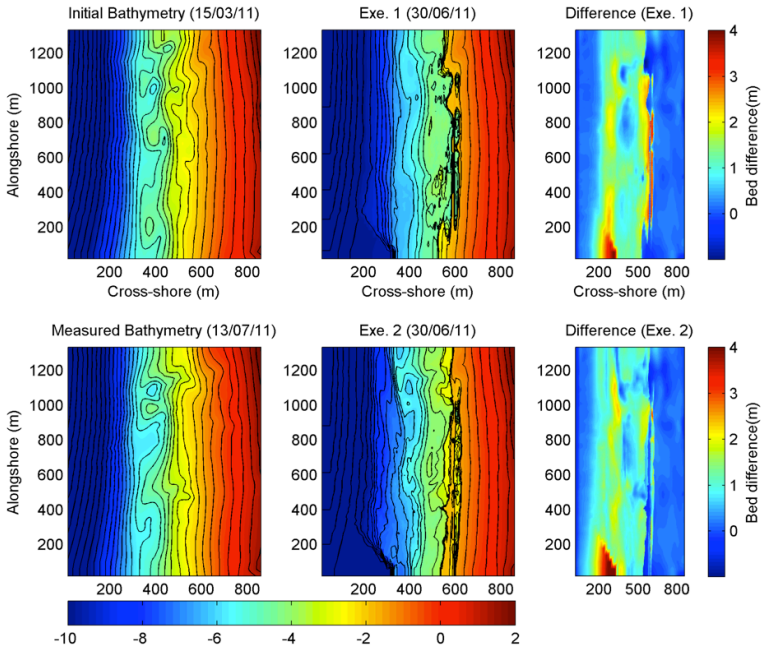

Figure 5-11. Bathymetry (color scale in m) estimation results with Exe.1 and Exe.2. (Top left) Initial measured bathymetry from 15/03/11. (Top centre) Modelled bathymetry with executable 1 on 30/06. (Top right) Difference between measured and modeled bathy. with exe. 1 on 30/06. (Bottom left) Measured bathymetry on 10/07/11. (Bottom centre) Modelled bathymetry with executable 2. (Bottom right) Difference between measured and modeled bathy. with exe. 2.

These resulting bathymetries show quite a significant difference between the results obtained with executable 1 versus the results obtained with executable 2. Firstly, on the first comparison date (28th of April) two major features are observed on the measured bathymetry, which are the channel at the north, and the channel and transverse bar present at around 400-500m in –*x* and 600-700m in –*y*. It is clear from Figure 5-7 that executable 2 seems to catch these main morphological features much better than executable 1. Another thing worth pointing out is that the resulting updated bathymetries are quite rigid or jagged compared to the real bathymetries. The magnitude of the bed change (RMS error) and the Brier skill score for each date and both executable 1 and 2 is shown in Table 5-1, as well as in the bar graphs shown at the end of this chapter in Figure 5-30 and Figure 5-31.

Continuing on to Figure 5-8, the results for the next month of simulation are shown, adding up to a total run length of two month at this point. The resulting bathymetries on the 1st of June show that executable 1 crashed completely, and formed a large step at the shoreline, not providing a reasonable estimate of real bathymetry. The results from executable 2 show a definite improvement over executable 1, however, the main morphological features are not well developed, and some problems at the shoreline are also present. At the shoreline a series of ridges and deep alongshore channels can be seen on the estimated bathymetry from executable 2. The channel at 500m –*x* and 500m –*y* on the measured bathymetry isn't being greatly represented in the estimated bathymetry, however, an indentation in the shoreline is present at the right location, but without sufficient protrusion. The curvature of the shoreline in longshore direction seems to be estimated quite well, despite "missing" the clear rip channels present in the measured bathymetry.

Moving on to the results on the 6th of June, shown in Figure 5-9, the same problem is seen as for the previous date in the case of executable 1. In the case of executable 2, the rip channels seem slightly more pronounced, especially the channel to the north. As well as this, the deep channels and ridges presented at the shoreline are still present, with similar characteristics. On the 11th of June, which is seen in Figure 5-10, the problem with executable 1 persists, and the estimated bathymetry with executable 2 seems to have deteriorated even further from the 6th of June. The

problems at the shoreline are quite pronounced at this date, extending further seawards than on the 6th of June. Finally, on the 30th of June (Figure 5-11), the bathymetry estimation has further deteriorated in comparison with the previous dates. Here executable 1 has clearly shown the same problem as the previous dates, and the bathymetry estimated with executable 2 has continued to dig and create problems at the shoreline, not being able to represent the measured bathymetry in an acceptable manner.

Table 5-1. Brier skill score and RMS error for executables 1 and 2, computed over all domains as defined in Appendix D.

		28.04.2011		01.06.2011		06.06.2011		11.06.2011		30.06.2011	
		BSS	***RMS***	***BSS***	***RMS***	***BSS***	***RMS***	***BSS***	***RMS***	***BSS***	***RMS***
Whole domain	**Exe. 1**	-0.404	0.41	-5.8	0.971	-5.97	0.974	-6.08	0.993	-6.626	1.057
	Exe. 2	0.027	0.3343	-1.381	0.59	-0.489	0.451	-1.364	0.566	-3.865	0.815
Outer surf zone	**Exe. 1**	-0.162	0.66	-2.957	1.198	-1.611	1.012	-1.838	1.036	-1.754	1.248
	Exe. 2	0.341	0.5137	-1.475	0.962	0.173	0.571	-0.781	0.834	-1.576	1.182
Inner surf zone	**Exe. 1**	0.19	0.501	-5.465	1.511	-5.968	1.617	-5.234	1.622	-8.77	1.541
	Exe. 2	0.047	0.397	-0.059	0.652	0.159	0.539	-0.158	0.611	-4.181	1.028

As well as the quality of the estimated bathymetries, the behavior of the model in time was considered here. For this effect, the total bed change per simulation was quantified by means of a root mean square difference between the initial and final bathymetries in each simulation (for each image run). As to try and observe if the model was adjusting the bathymetry in the correct direction, a Brier skill score was also applied for each simulation. This calculation of the *BSS* per simulation follows Equation (27), using the initial and final bathymetries in each simulation as the initial and modeled bathymetries in said equation, and using the nearest measured bathymetry (ahead in time) to the current simulation as the measured bathymetry in this equation. This might not be a correct depiction of whether or not the model is adjusting the bathymetry in the right direction, due to the fact that the nearest measured bathymetry to a certain simulation could be a month away, and the bathymetry during 1 month can fluctuate in many directions. Having said this, the *BSS* per simulation was still looked at, with the hope of finding any clear issues worth pursuing.

Figure 5-12 shows the just mentioned bed change and skill estimations for each simulation during the whole run period for executable 2. The first major observation

is that there are several large peaks in bed change during the simulation, and the fact that they coincide with large values of prior uncertainty and periods when there are several days between images. These observations correspond with the ones made previously in section 5.2.2, and will be looked into further in the following section, where the sensitivity of varying the timescale T_r from Equation (25) will be looked at.

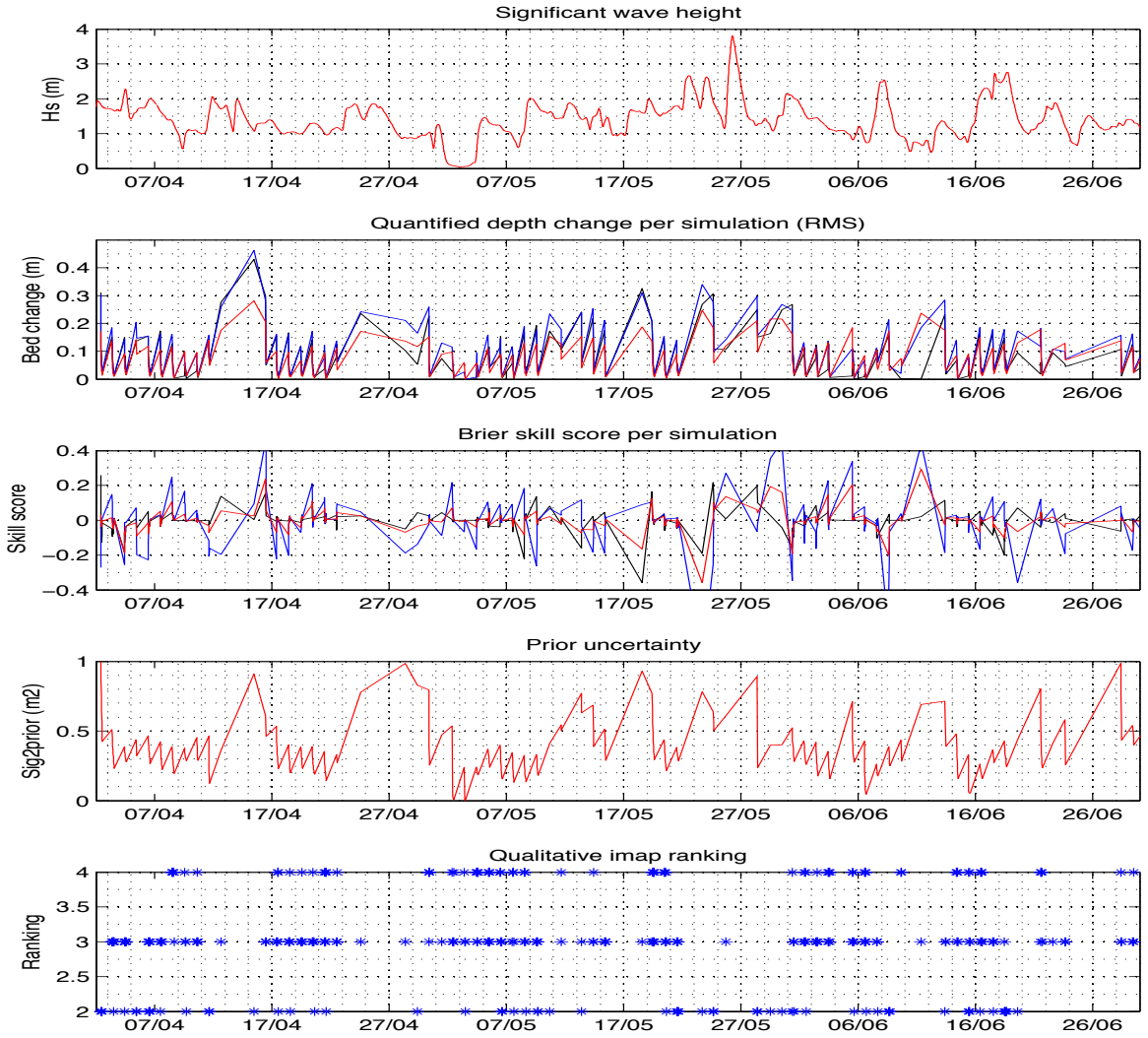

Figure 5-12. Behaviour of Exe. 2 for whole time period. In order from top to bottom, (1) Significant wave height, (2) RMS depth change per simulation, (3) BSS per simulation, (4) prior uncertainty per simulation, (5) qualitative imap rankings.

5.3.2 *Dependence on uncertainty increment parameter (T_r)*

As it was just mentioned, Figure 5-12 shows how the prior uncertainty and the bed change are related, and how large bed changes are seen at several instances during the entire model run. To address this issue, the dependence of the rate of bed change

upon the timescale factor T_r from Equation (25) will be looked into here. The function of said timescale is to increase the prior uncertainty between simulations towards the natural uncertainty with increasing time between simulations. The value of the timescale in the first run with executable 2, which corresponds to the results shown in Figure 5-12, is T_r = 5 days. Considering the general tendency of the bathymetry at Perranporth to fluctuate relatively slowly, which was seen in section 3.2, showing that there was little bed change between the 1st and 11th of June 2011; here longer timescales of both 10 and 15 days will be tested.

The variation in uncertainty for increasing timescales is shown in Figure 5-13, where the vertical axis is the updated uncertainty computed with Equation (25) with a prior uncertainty of 0 m, and the horizontal axis is time (in days) between consecutive simulations. This figure shows that for times between simulations of 2 days or less, the effect of changing the timescale from 5 to 10 days is more than 10 days to 15 days.

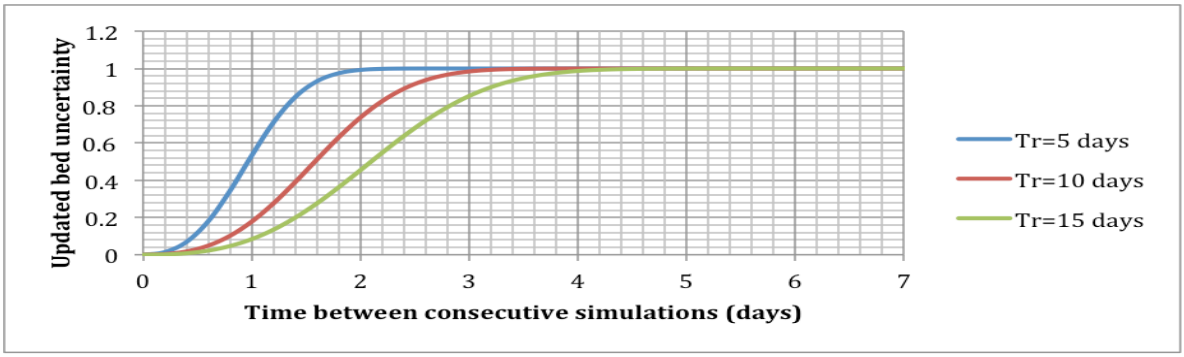

Figure 5-13. Increments in uncertainty for varying uncertainty increment parameter values

Firstly, based on the observed bathymetry changes between the 1st and the 11th of June 2011, an increase in morphological timescale from the initial 5 days to 10 days is tested, looking at the resulting estimated bathymetry and the rate of bed updating observed with the implementation of this change. Figure 5-14 shows the quantified bed change per simulation and the prior uncertainty per simulation for both cases run with executable 2, with T_r = 5 days (blue lines) and T_r = 10 days (red lines). As was expected with this change, the prior uncertainty is decreased, and therefore so is the bed change per simulation. As to present a more detailed view of this change, Figure 5-15 shows the same as Figure 5-14, but on a shorter timescale, from the 14th to the 20th of May. This time frame was chosen because there are days with several images

(14th, 15th and 19th), a day with a single image (18th), and a 3-day gap between consecutive simulations (15th to 18th).

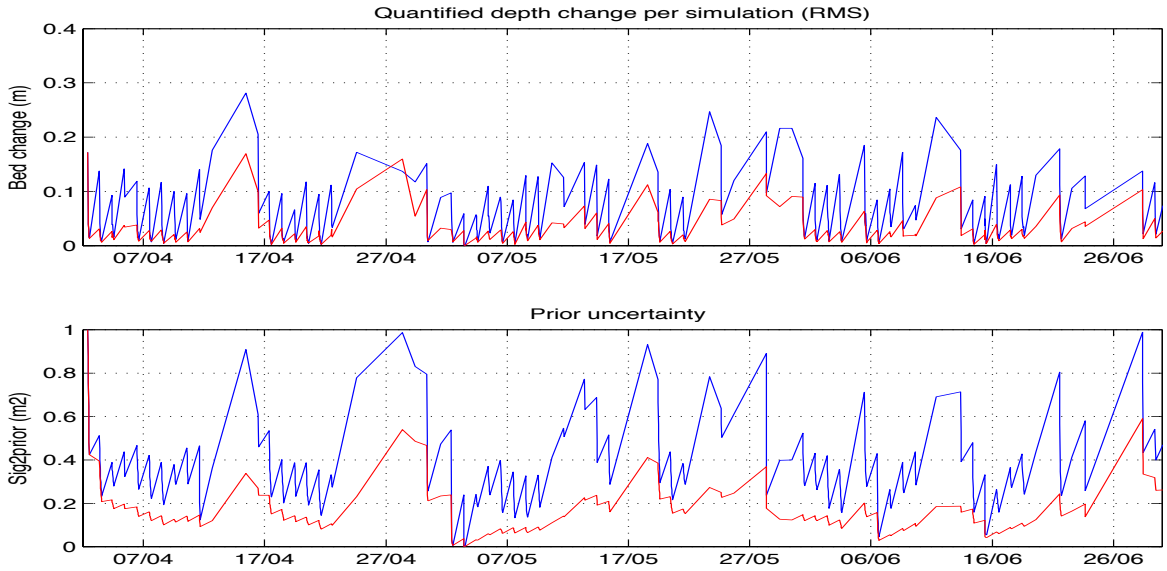

Figure 5-14. RMS bed change and prior uncertainty for variable morphological timescales. (Blue line) executable 2 with Tr=5 days, (red line) executable 2 with Tr=10 days.

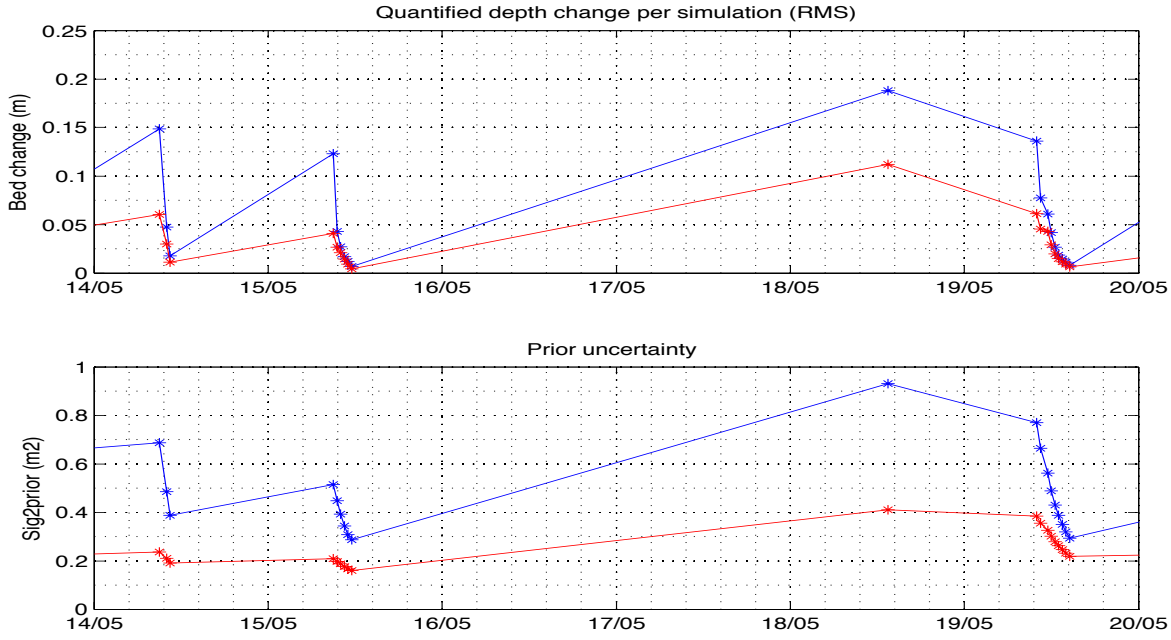

Figure 5-15. RMS bed change per simulation and prior uncertainty per simulation for Tr=5 days (blue lines) and Tr=10 days (red lines), both with executable 2, for the period between the 14th and 20th of May 2011.

The two previously shown figures show the reduction of the prior uncertainty between simulations due to an increased morphological timescale, which ultimately

reduces the rate of change of the bed updating in the Beach Wizard model. The effect of this reduction on the output bathymetry is a smoother bathymetry, with less sharp ridges, due solely to the fact that the lasting effects of having very big bed changes during a single simulation are reduced. The reduction in the increment of the uncertainty between simulations on the 18th of May clearly reflects the trend of increments seen in Figure 5-13.

Figure 5-16 through Figure 5-20 show the resulting bathymetries for the two cases described above, both using executable 2 and with timescales of 5 and 10 days. The plots labeled "Exe. 2 w/tr=10" correspond to the case with a morphological timescale of 10 days, and the one simply labeled as "Exe. 2" corresponds to a morphological timescale of 5 days.

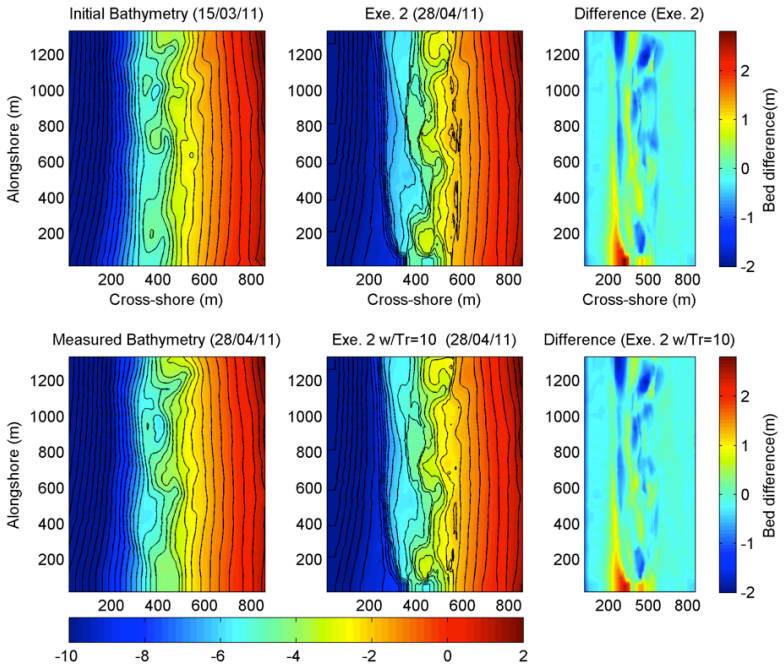

Figure 5-16. Bathymetry (color scale in m) estimation results with Exe 2 and changed Tr. (Top left) Initial measured bathymetry from 15/03/11. (Top centre) Modelled bathymetry with Exe 2 and Tr=5 (28/04/11). (Top right) Difference between measured and Exe 2 with Tr=5 . (Bottom left) Measured bathymetry on 28/04/11. (Bottom centre) Modelled bathymetry with Exe 2 and Tr=10. (Bottom right) Difference between measured and modeled bathy. with exe. 2 and Tr=10 on 28/04/11.

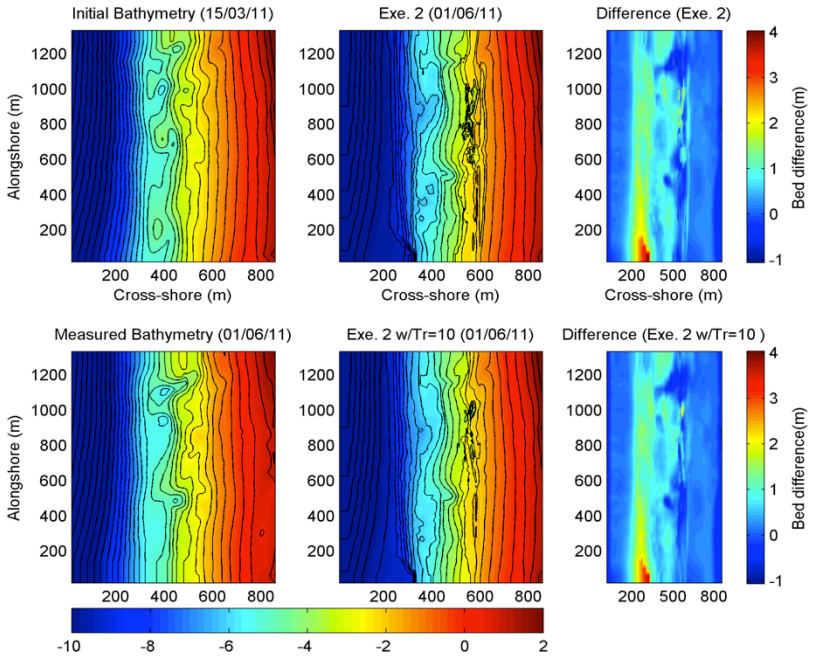

Figure 5-17. Bathymetry (color scale in m) estimation results with Exe 2 and changed Tr. (Top left) Initial measured bathymetry from 15/03/11. (Top centre) Modelled bathymetry with Exe 2 and Tr=5. (Top right) Difference between measured and Exe 2 with Tr=5 on 01/06. (Bottom left) Measured bathymetry on 01/06/11. (Bottom centre) Modelled bathymetry with Exe 2 and Tr=10. (Bottom right) Difference between measured and modeled bathy. with exe. 2 and Tr=10 on 01/06/11.

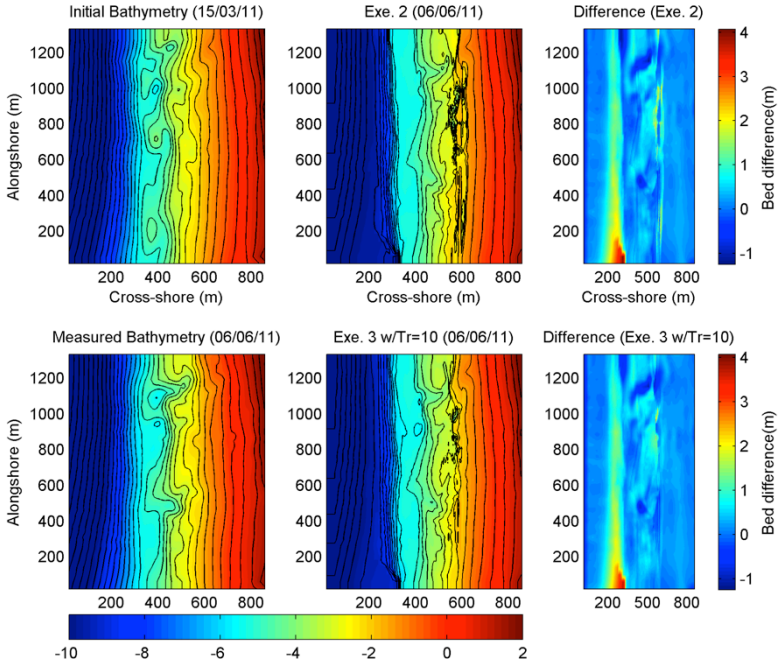

Figure 5-18. Bathymetry (color scale in m) estimation results with Exe 2 and changed Tr. (Top left) Initial measured bathymetry from 15/03/11. (Top centre) Modelled bathymetry with Exe 2 and Tr=5. (Top right) Difference between measured and Exe 2 with Tr=5 on 06/06. (Bottom left) Measured bathymetry on 06/06/11. (Bottom centre) Modelled bathymetry with Exe 2 and Tr=10. (Bottom right) Difference between measured and modeled bathy. with exe. 2 and Tr=10 on 06/06/11

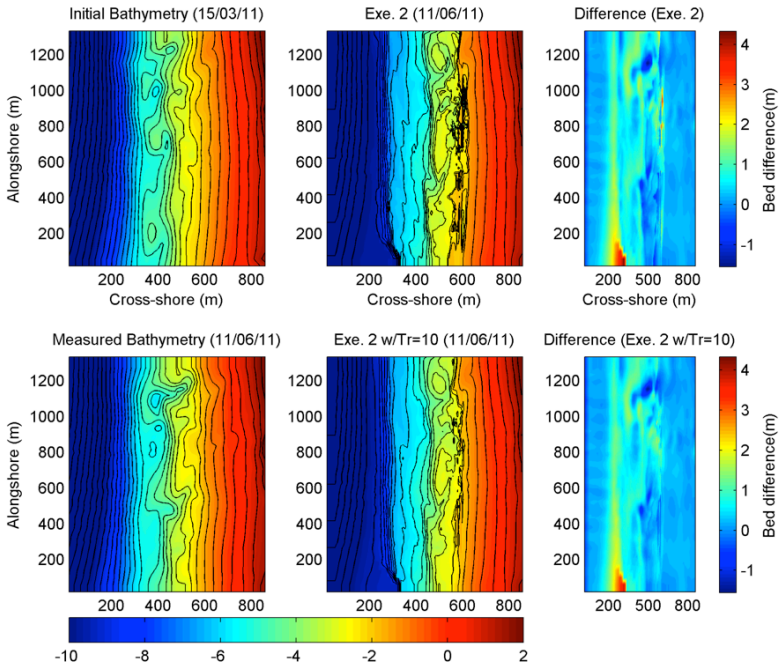

Figure 5-19. Bathymetry (color scale in m) estimation results with Exe 2 and changed Tr. (Top left) Initial measured bathymetry from 15/03/11. (Top centre) Modelled bathymetry with Exe 2 and Tr=5. (Top right) Difference between measured and Exe 2 with Tr=5 on 11/06. (Bottom left) Measured bathymetry on 11/06/11. (Bottom centre) Modelled bathymetry with Exe 2 and Tr=10. (Bottom right) Difference between measured and modeled bathy. with exe. 2 and Tr=10 on 11/06/11.

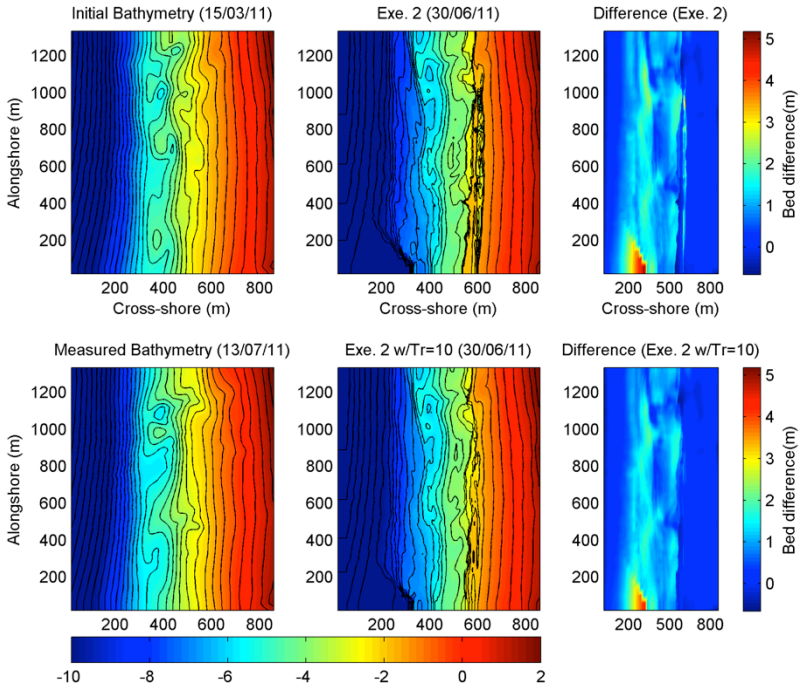

Figure 5-20. Bathymetry (color scale in m) estimation results with Exe 2 and changed Tr. (Top left) Initial measured bathymetry from 15/03/11. (Top centre) Modelled bathymetry with Exe 2 and Tr=5. (Top right) Difference between measured and Exe 2 with Tr=5 on 30/06. (Bottom left) Measured bathymetry on 13/07/11. (Bottom centre) Modelled bathymetry with Exe 2 and Tr=10. (Bottom right) Difference between measured and modeled bathy. with exe. 2 and Tr=10 on 30/06/11.

The five figures presented above show the general effects on the estimated bathymetries due to using a longer uncertainty increment timescale in the equation for uncertainty update between simulations (Equation 25). The effect is a smoother calculated bathymetry, and a clear reduction in the sharp problematic features at the shoreline that were observed with a timescale of 5 days. This effect of smoother resulting bathymetries is primarily noticed at the shoreline, where the main problems are observed. To this effect, the increase of the morphological timescale parameter is considered to be a helpful adjustment for the reduction of bathymetry update errors, particularly at the shoreline. As well as incrementing the T_r to 10 days, a value of 15 days was also tested, as to see if the effects of increasing it even more would be incremental in the reduction of estimation errors. It was found that the difference between using a timescale of 10 days or 15 days was minimal, since the time between simulations rarely goes above a few days. The resulting Brier skill scores and RMS errors for timescales of 5, 10 and 15 days are shown below in Table 5-2, where the three runs are the ones described above, all using the same version of the Beach Wizard model executable (executable 2). These values can also be seen as bar graphs in Figure 5-30 and Figure 5-31 at the end of this chapter.

Table 5-2. BSS and RMS error for varying morphological timescales (Tr), all using Exe. 2

		28.04.2011		**01.06.2011**		**06.06.2011**		**11.06.2011**		**30.06.2011**	
		BSS	***RMS***	***BSS***	***RMS***	***BSS***	***RMS***	***BSS***	***RMS***	***BSS***	***RMS***
Whole domain	**T_r=5**	-0.06	0.35	-1.52	0.60	-0.60	0.47	-1.46	0.57	-4.09	0.83
	T_r=10	0.08	0.32	-1.09	0.55	-0.35	0.43	-0.96	0.51	-3.02	0.75
	T_r=15	0.15	0.30	-1.13	0.55	-0.61	0.47	-1.03	0.52	-2.58	0.71
Outer surf zone	**T_r=5**	0.17	0.57	-1.70	1.00	-0.03	0.65	-0.99	0.88	-1.75	1.24
	T_r=10	0.28	0.51	-1.43	0.94	-0.05	0.65	-0.84	0.84	-1.47	1.19
	T_r=15	0.31	0.50	-1.28	0.91	-0.15	0.67	-0.85	0.83	-1.27	1.14
Inner surf zone	**T_r=5**	0.05	0.40	-0.06	0.65	0.16	0.54	-0.16	0.61	-4.18	1.03
	T_r=10	0.14	0.35	0.16	0.58	0.25	0.51	0.01	0.58	-3.43	0.96
	T_r=15	0.29	0.31	-0.09	0.61	-0.04	0.60	-0.07	0.62	-2.94	0.90

The results presented in Table 5-2 reflect nicely the observed improvement in bathymetry calculation that was seen by visually assessing the resulting bathymetries for cases with varying morphological timescales. By increasing the morphological timescale (T_r), a general tendency for the values of the calculated BSS to increase and the RMS error to decrease is observed. The difference in BSS and RMS error between the case with T_r =5 days and T_r =10 days is larger than the difference observed between T_r =10 days and T_r =15 days. This is due to the general spacing of the available images never being larger than a week or so, therefore increasing T_r over 10 days has little effect.

The improvement with this change is definitely noticeable, however, the estimated bathymetries are still relatively far from the real measured bathymetries, for which some attention will now be paid to the bed update process. The following section will focus on the two systematic estimation errors originally noticed by van Dongeren et al (2008), and again in the present thesis; and will present a modification to the bed change process that addresses these issues.

5.3.3 *Systematic estimation errors*

In the original Beach Wizard paper by van Dongeren et al (2008), two systematic estimation errors were noticed. The same errors were noticed in this work, and are an erroneous deepening ("digging") near the shoreline, and an erroneous building of a terrace near the shoreline. Both of these effects are due to the same problem, and that problem is that the bed update scheme does not account for the "history" of wave dissipation from offshore to onshore. This means that the assimilation process updates the bed on the entire domain at the same time considering only local differences in observed and estimated dissipation, and doesn't take into account the fact that if there is dissipation offshore, then there will be less wave breaking reaching the nearshore. In other words, if in reality there is a bar offshore (which is not present in the model yet), then the wave breaking over that bar will translate to less wave breaking in the nearshore in reality, which will not be accounted for by the model. Figure 5-21 helps understand this, showing a schematization of both the

problematic deepening (left) and building (right) of the shoreline, where the images depict a cross shore profile of the bed and wave dissipation, with the shoreline to the right. In this figure, the dashed black line is the initial modeled bathymetry, the red solid line is the corresponding modeled dissipation, the solid black lines represent the observed dissipation and the properly adjusted bathymetry, and the dashed red lines show the two systematic estimation errors.

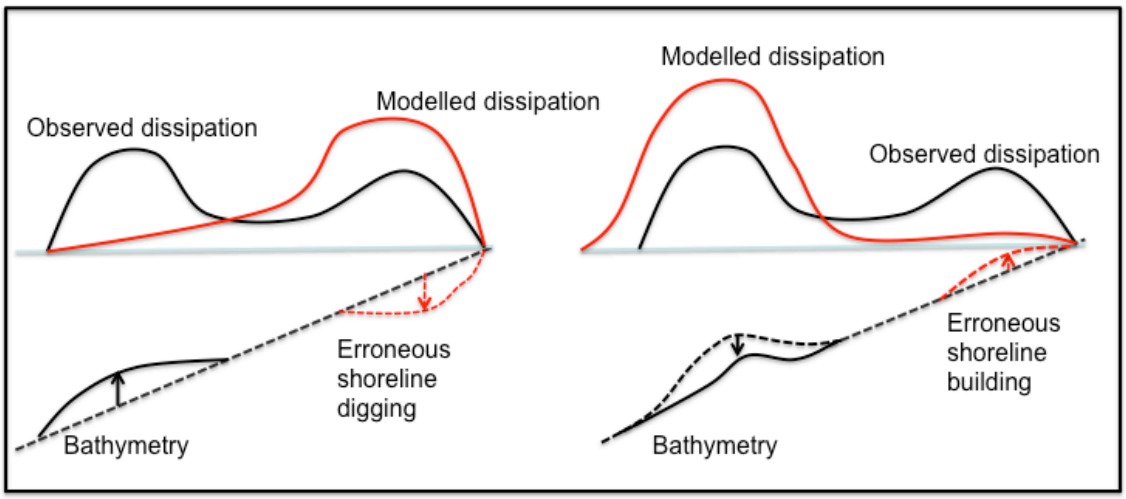

Figure 5-21. Systematic estimation errors.

Taking the left side of Figure 5-21 as an example, the specific reason for this systematic estimation error will be further described, as to not leave any doubts lying on the reasoning behind this phase of work. The reaction of the model to the initial condition shown in this image will be to raise the bed in the offshore region where the modelled dissipation is less than the observed dissipation and lower the bed in the nearshore region where the modeled dissipation is greater than the observed dissipation. The problem here is that the deepening at the shoreline might not be realistic, in that if the offshore bar were to be adjusted towards reality first, then the modeled dissipation would consequently be incremented over the bar, leaving less dissipation in the nearshore region without the local depth in that region having to increase.

An example simulation was chosen from the 15th of April 2011 at 11:00, where a step at the shoreline is already present in the bathymetry as a result from previous simulations, and the shoreline digging effect can be clearly seen. The temporal

evolution of the bed and dissipation of this example case is shown in Figure 5-22. In this figure the top row represents the bed change at a given time step of the Beach Wizard update scheme (where a negative value means an increase in bed level), the second row shows the bed elevation (for each time instance and the initial), and the bottom row shows the computed and observed dissipation. This figure shows how the bed updating occurs over the entire domain at once from the beginning of the simulation, generating continuous digging at the step that is already present at the shoreline. What comes to mind here is that in order to prevent (or at least diminish) this shoreline digging, a possibility would be to update the bed farther offshore first, with the hopes of allowing the dissipation near the shoreline to be reduced without the bed having to be lowered in this region. This will be further explained in the following section, where a time dependent update factor is introduced to the system.

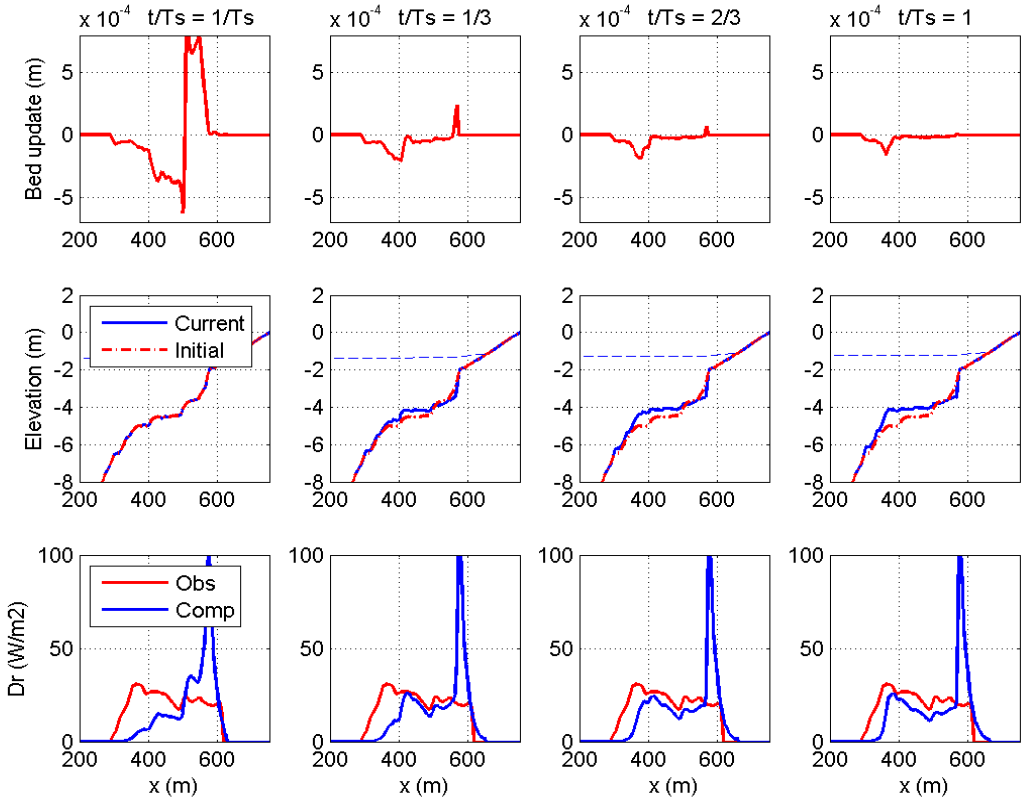

Figure 5-22. Bed updating at 4 time instances during simulation on the 15th of April using executable 2. (Top) Bed update per time step in Beach Wizard. (Middle) Bed elevation, red dashed line = initial bathymetry and blue line = current bathymetry. (Bottom) Wave dissipation, red line = observed, blue line = computed.

5.3.4 *Cross shore time-dependent bed update factor*

The present section looks into the application of a time dependent bed change factor to attempt to resolve or at least diminish the problems generated by the systematic estimation errors described in the previous section. As it was mentioned in the previous section, the systematic errors present in the bed change process are due to the fact that the current bed update scheme in Beach Wizard does not account for the effects of spatial distribution of wave dissipation from offshore to onshore, and only considers local differences in dissipation. On this note, the approach to be described here is the implementation of a factor that will temporally regulate the bed change, moving from offshore to onshore throughout the simulation, ultimately allowing for the areas farther offshore to be updated first; in this manner indirectly adjusting the dissipation nearshore and avoiding the erroneous digging or building at the shoreline. This test is carried out using the latest version of the Beach Wizard model (Exe. 2) with the default value of 5 days for the uncertainty increase timescale ($_{Tr}$). The factor to be applied will be called "γ" here, and multiplies the bed update in Equation (22) in this manner,

$$h(t+\Delta t) = h(t) - \gamma\beta\alpha \sum_{i=1}^{S} \frac{\frac{df_i}{dh}}{\left(\frac{df_i}{dh}\right)^2 + \delta_i^2} (f_i - f_{i,obs}) \tag{28}$$

Several configurations of the new update factor γ were tried, ultimately deciding upon one where it varies from a value of 1 to 0 with a hyperbolic cosine function, which is dependent on the timestep of the Beach Wizard assimilation process. This factor has the following configuration,

$$\gamma = \cosh\left(\left(\frac{1}{100}\left(x - \frac{0.6*t*(x_f - x_i)}{T_s} - x_s\right)\right)^{-10}\right) \tag{29}$$

where x is the –x axis (cross shore), t is the time instance in the simulation, T_s is the simulation length, x_f - x_i is the total length of the –x axis in metres, and x_s is a certain buffer space that can be adjusted by the user (defines at which point in –x the factor begins to move onshore with time). The form of this factor can be seen in Figure 5-23, where the colors represent instances in time during a simulation increasing from left to right in the figure. This figures shows the shape that was chosen for the factor,

which is a smooth curve which moves in time from offshore to onshore, starting at point x_s, which in this case was set equal to 200 m (which is roughly the maximum observed cross shore extent of wave breaking at Perranporth during the study period).

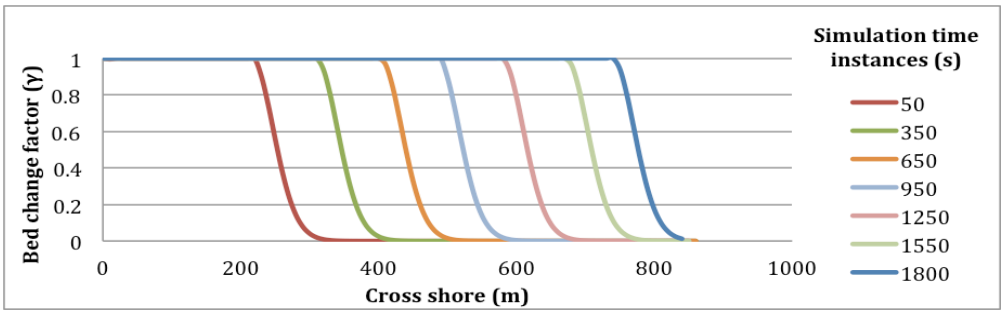

Figure 5-23. Time dependent bed update factor.

For the implementation of this time stepping bed update scheme, the assimilation time step of Beach Wizard was set to every computational time step in XBeach, as opposed to the interval of wave computations which is defined in the parameter file ("wavint" in *params.txt*) for XBeach. The reason for this change was to have a more gradual movement of the factor in time towards the shoreline, without having to decrease the interval of wave computation in XBeach to a very small number (this was found to be more computationally efficient). As to not simply reduce the amount of bed update at the shoreline by cutting the total assimilation time down too much in this region, a criteria was chosen here saying that for at least half of the simulation length γ should have a value equal to 1 for the entire wet domain (providing normal bed updating over the whole domain up to the shoreline for half the simulation). This can be seen in Figure 5-23, where at time 950 (which is just over half the simulation length), the update factor has reached the shoreline, leaving the rest of the simulation time to update the entire domain as it would normally.

The effect of this time dependent update factor was tested on the same simulation for which the systematic errors were described in the previous section, which corresponds to the simulation on the 15th of April 2011. Figure 5-24 shows the effect of the time dependent factor on the just mentioned simulation.

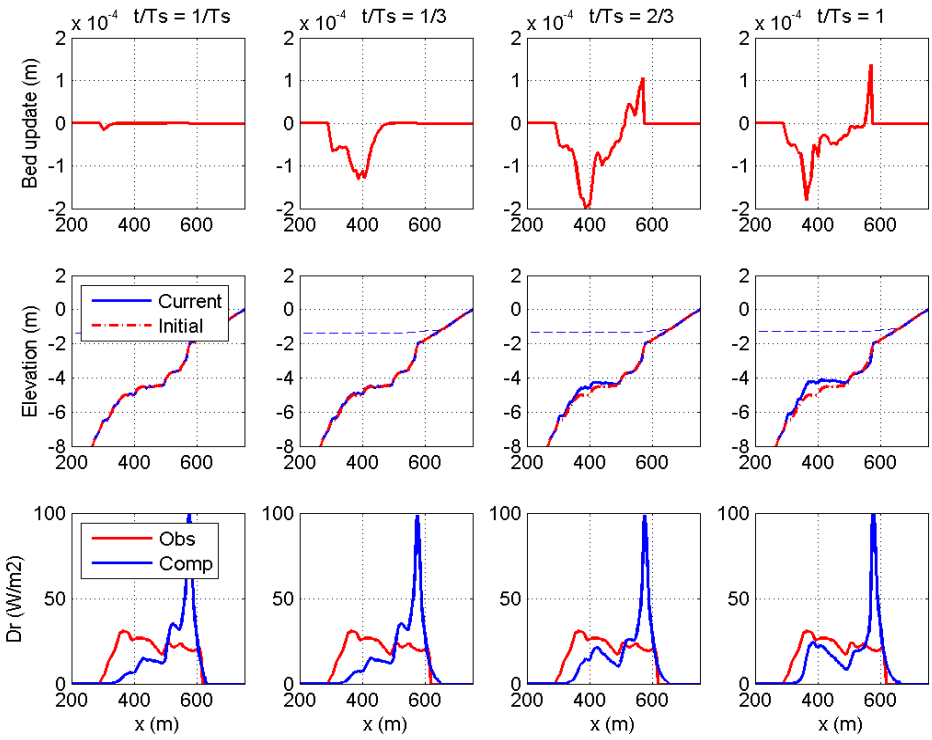

Figure 5-24. Time dependent assimilation process in simulation from the 15th of April 2011. (Top row) Bed change at 4 time instances during the simulation. (Middle row) 4 time instances of bed level (blue line) and initial bed level (dashed red line). (Bottom row) Wave dissipation, blue line = computed , red line = observed.

The figure shown above shows in the first row the bed update at 4 instances in time during the simulation, where a negative value means an increase in bed level. What is noticeable from this is how the assimilation gradually moves shoreward, allowing for the offshore bar in the surfzone (around 400m in –x) to rise before the nearshore area is lowered. The actual difference between this and the prior update scheme (where the entire domain is updated at each time step) can be seen by comparing Figure 5-24 and Figure 5-22. A definite reduction in deepening in the nearshore zone is seen with the implementation of the new time dependent factor.

Having tested the new update factor on a single simulation and obtained seemingly improved results, this new bed change formulation is tested on the entire long term run from the 1st of April to the 30th of June 2011. From this point forward, the new model version with the implemented time dependent bed change factor included will be referred to as executable 3 (Exe. 3). The resulting bathymetries obtained with executable 3 are shown in Figure 5-25 through Figure 5-29, in the same comparative

form that has been recurrently used in the present chapter of this report, which includes the resulting bathymetries from the previous model version (Exe. 2), the measured bathymetries (initial and current), and difference plots between the measured and modeled bathymetries.

By visually comparing the resulting bathymetries with and without the implementation of the time dependent bed change factor (γ), a promising result can be seen, and that is a reduction in shoreline problems that had been observed in the previous runs. The resulting bathymetries have more smoothed features at the shoreline (which is the area of interest in implementing this change) and very slight changes in the farther offshore areas of the bathymetry. This is exactly what was aimed to achieve by introducing this time dependent bed change factor, however, a certain degree of doubt remains as to whether this difference is due to the right reasons. What this means is that part of the reason for the reduced shoreline effects might be attributed simply to there being less available time of the simulation length assigned to updating the bed in those regions.

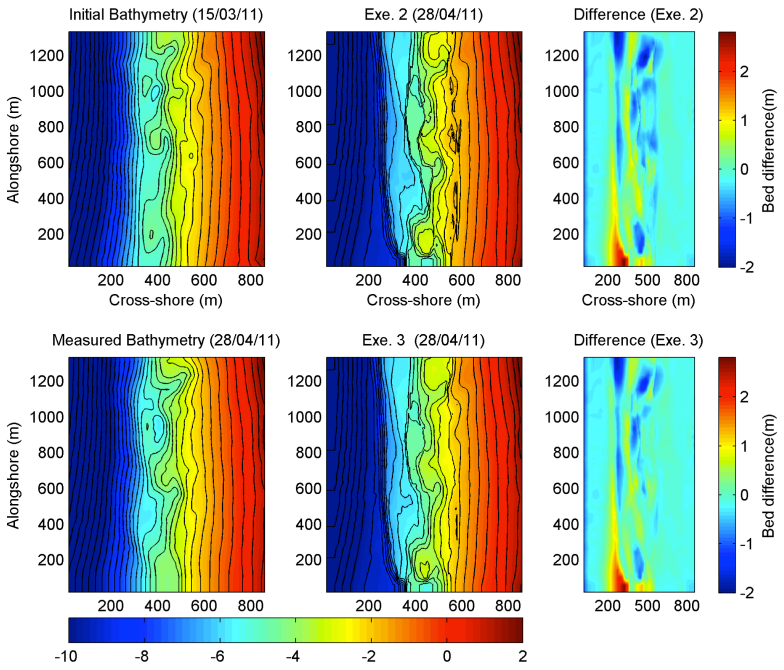

Figure 5-25. Bathymetry (color scale in m) estimation results with Exe 2 and Exe 3. (Top left) Initial measured bathymetry from 15/03/11. (Top centre) Modelled bathymetry with Exe 2 (28/04/11). (Top right) Difference between measured and Exe 2. (Bottom left) Measured bathymetry on 28/04/11. (Bottom centre) Modelled bathymetry with Exe 3. (Bottom right) Difference between measured and modeled bathy. with Exe. 3 on 28/04/11.

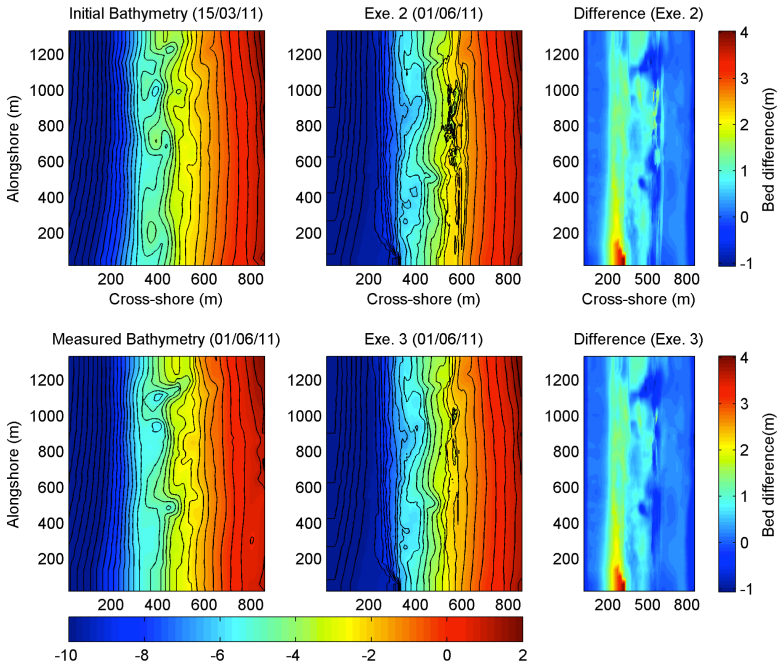

Figure 5-26. Bathymetry (color scale in m) estimation results with Exe 2 and Exe 3. (Top left) Initial measured bathymetry from 15/03/11. (Top centre) Modelled bathymetry with Exe 2 (01/06/11). (Top right) Difference between measured and Exe 2. (Bottom left) Measured bathymetry on 01/06/11. (Bottom centre) Modelled bathymetry with Exe 3. (Bottom right) Difference between measured and modeled bathy. with Exe. 3 on 01/06/11.

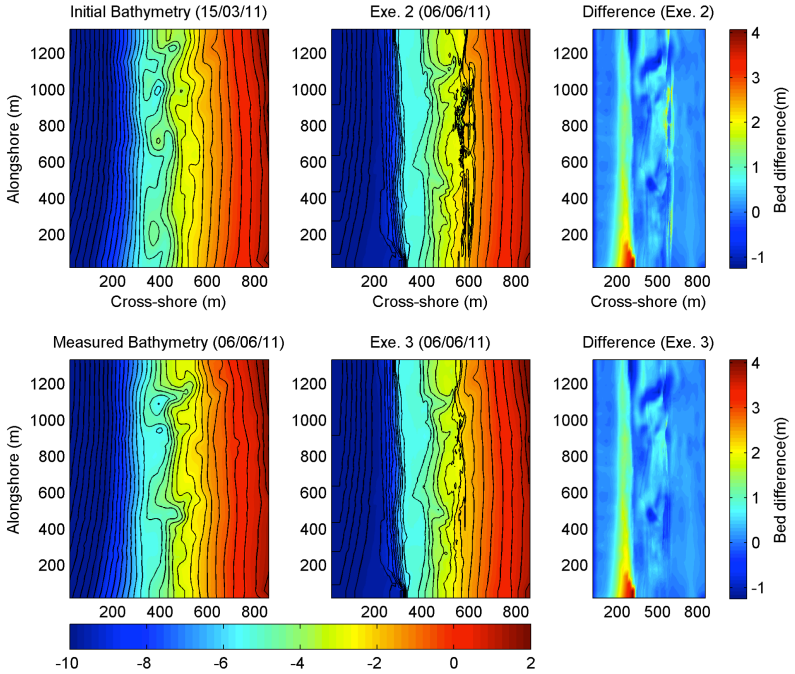

Figure 5-27. Bathymetry (color scale in m) estimation results with Exe 2 and Exe 3. (Top left) Initial measured bathymetry from 15/03/11. (Top centre) Modelled bathymetry with Exe 2 (06/06/11). (Top right) Difference between measured and Exe 2. (Bottom left) Measured bathymetry on 06/06/11. (Bottom centre) Modelled bathymetry with Exe 3. (Bottom right) Difference between measured and modeled bathy. with Exe. 3 on 06/06/11.

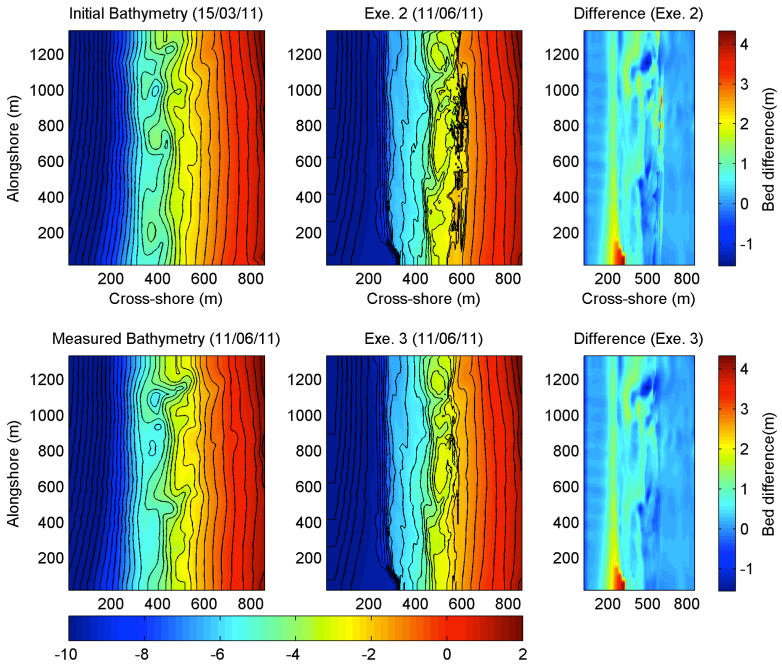

Figure 5-28. Bathymetry (color scale in m) estimation results with Exe 2 and Exe 3. (Top left) Initial measured bathymetry from 15/03/11. (Top centre) Modelled bathymetry with Exe 2 (11/06/11). (Top right) Difference between measured and Exe 2. (Bottom left) Measured bathymetry on 11/06/11. (Bottom centre) Modelled bathymetry with Exe 3. (Bottom right) Difference between measured and modeled bathy. with Exe. 3 on 11/06/11.

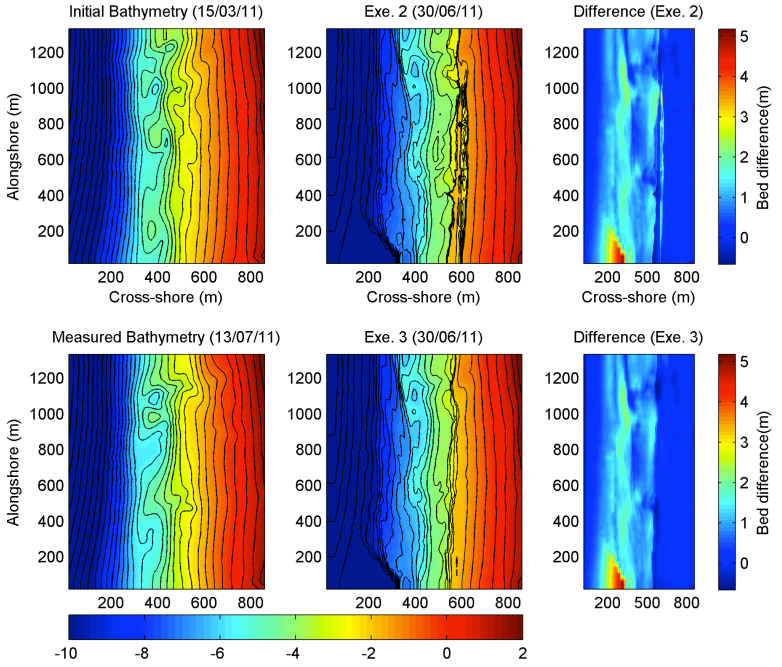

Figure 5-29. Bathymetry (color scale in m) estimation results with Exe 2 and Exe 3. (Top left) Initial measured bathymetry from 15/03/11. (Top centre) Modelled bathymetry with Exe 2 (30/06/11). (Top right) Difference between measured and Exe 2. (Bottom left) Measured bathymetry on 30/06/11. (Bottom centre) Modelled bathymetry with Exe 3. (Bottom right) Difference between measured and modeled bathy. with Exe. 3 on 30/06/11.

A slight variation was tested in the time dependent update factor shown in Equation (29), which was changing the time step factor from 0.6 to 0.65 (the value that directly multiplies by the time). This value controls the rate at which the update factor moves shorewards in time, where a larger value means a faster progression towards the shore. The purpose of this test was to see if there would be a significant difference due to there being more time when the whole domain can be updated. This means determining if the observed changes between using the time dependent update factor or not were due to the dissipation at the shoreline reacting to offshore bed changes or due simply to there being less time allowed to change the bed at the shoreline. The difference between using a time stepping factor of 0.6 and 0.65 were very small, which is good in that it signifies that the difference might be due to the shoreline dissipation reacting to offshore bed changes.

The resulting Brier skill scores and RMS errors for the changes in Beach Wizard code and parameters mentioned in this chapter are shown in the form of a bar graph in Figure 5-30 and Figure 5-31, where each colour corresponds to a different executable and/or parameter value. The numerical values corresponding to these two bar graphs are shown in Appendix B-2, along with the BSS and RMS results divided into the inner and outer surf zones.

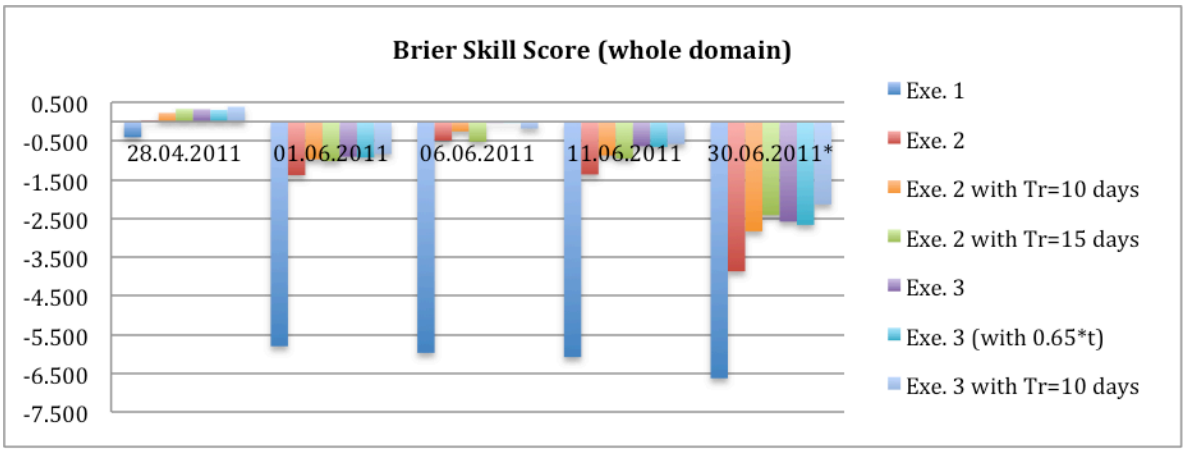

Figure 5-30. Beach Wizard model sensitivity to code and parameter changes, quantified as Brier skill scores (* the BSS is calculated with modeled results on 30/06/11 and measured on 13/07/11).

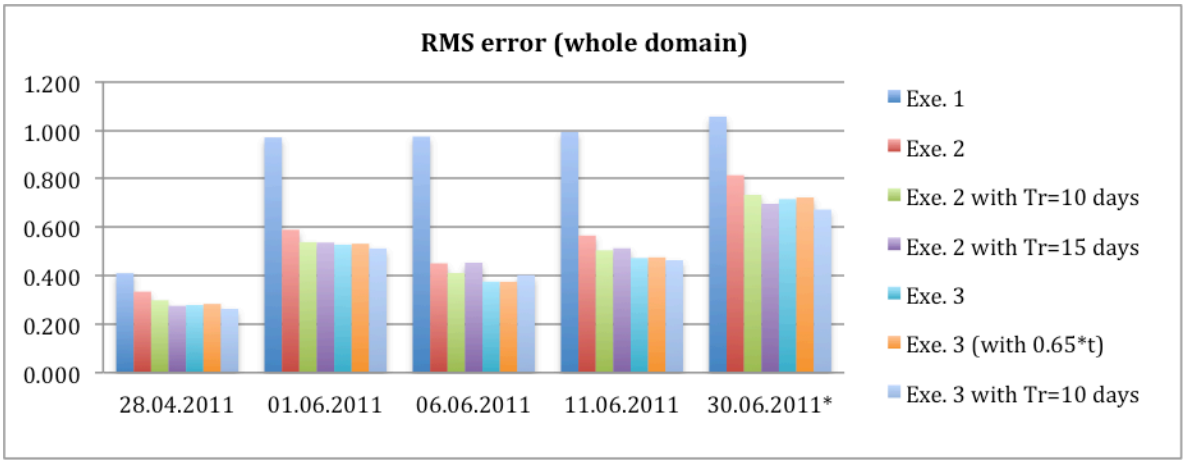

Figure 5-31. Beach Wizard model sensitivity to code and parameter changes, quantified as RMS errors (* the BSS is calculated with modeled results on 30/06/11 and measured on 13/07/11).

The two graphs shown above present the results of the changes made to the Beach Wizard code and variations to the parameters involved, as well as a combination of these. The combination that was chosen was using the model version with time dependent update factor included (Exe. 3) with a time step rate of 0.6, and with an uncertainty increment parameter (T_r) of 10 days. This combination proved to generally present the best resulting bathymetries on the measured dates. The resulting bathymetries using this combination of code and parameter settings is shown in Appendix B-1.

This version of the Beach Wizard code is at this point considered to be the best possible working setup that can be reached during this thesis, and will be used throughout the next chapter of the report. The following chapter will focus on the sensitivity of the necessary video derived input (imaps) for the model to provide the best possible estimated bathymetries.

5.4 Conclusions and Recommendations

Here an overview of the conclusions obtained pertaining to the Beach Wizard model and parameter setting will be presented. As well as this, the recommendations will include specific ideas on possible future work regarding the functionality of the Beach Wizard bathymetry updating scheme.

5.4.1 *Conclusions*

The main objective of the present chapter was to obtain a thorough understanding of the Beach Wizard data-model assimilation scheme, to determine the relevance and importance of the different parameters in the model, to address the systematic estimation errors, and to ultimately obtain the best possible working model for the continuation of the following phases of work.

For the specific case at Perranporth where only dissipation maps are available as input, the depth limiting bed change factor was found to be harmful to the results when it strictly limited bed change to depths greater than 1 m. This was due to there being large areas of the surf zone with depths shallower than 1 m, therefore this factor was modified as to provide a smooth transition from zero bed change to full bed change in the nearshore zone.

The measurement error was found to be an important factor, as the uncertainty and hence the amount of bed change in a simulation is defined as a function of it. In this work two equations which ultimately increased the measurement error were eliminated, and a measurement error equal to a percentage (15%) of the maximum observed dissipation was implemented. This change was found to be a significant improvement in the resulting estimated bathymetries.

The timescale parameter which controls the increment in uncertainty between simulations (T_r) was found to be an important parameter in that it has the capacity to significantly change the prior uncertainty between simulations, and therefore has a large impact on the amount of bed change in a given simulation. Using a timescale of 10 days results in the increment of the uncertainty to the natural uncertainty (1 m) for consecutive simulations separated by 3 or more days. This parameter is dependent on the specific beach type and the amounts of sediment transport that are dominant in the area, therefore said parameter must be defined by the user.

The systematic estimation errors ("digging" and "building" of the shoreline) in the model come forth due to the model considering only local differences in modeled and observed dissipation, not accounting for the "automatic" reaction of the dissipation near the shoreline due to changes in the bed level (and dissipation) farther offshore. A time dependent bed update factor was implemented in the model, and resulted in a

reduction of the systematic errors near the shoreline and overall improved model skill.

The estimated bathymetries obtained using the best found model configuration showed very good results for the first month of simulation, and slightly reduced skill for the remaining two months. The calculated RMS errors for the bathymetries in June (except for the 30th of june) are still relatively low (in the order of 0.5 m or less), and the overall shape of the morphological features look good, which might possibly result in good prediction of rip currents.

5.4.2 *Recommendations*

The persistent error in modeled bathymetries at the lower left corner of the surf zone are due to that particular region being outside of the field of view of the Argus cameras. In order to solve this problem, the imap generation process should set the regions out of camera view as "not a number" (NaN) in stead of setting to zero intensity. In setting these regions to zero intensity rather than NaN, erroneous bed change (deepening) will occur when there is computed dissipation shown over that region.

Due to time constraints it was not possible to explore all aspects and many different configurations with regards to the functionality of the Beach Wizard model. During the work presented in this chapter several ideas were thought of which will be described here as recommendations for future work on this subject.

Firstly, it might be helpful to investigate more into the definition of the measurement error, and how to make this a variable value depending on a number of factors. The measurement error is thought to vary depending on the forcing conditions (waves and tides) and quite possibly on water depth. The measurement error used in the remainder of this work is defined as a percentage of the maximum observed dissipation, which could eventually be an initial (default) value which may be varied in the Beach Wizard code depending on a number of parameters which should be further investigated.

The next recommendation is with regards to the timescale that controls the rate at which the uncertainty increases between simulations (T_r). Van Dongeren et al (2008)

had mentioned that this timescale would ideally be dependent on the gradients of sediment transport and the corresponding wave height, current, and any other factors influencing this transport. In order to make the model more robust, it would be good to define this timescale depending on the mentioned factors, however, it also may be suitable to leave this value to be defined by the user who can analyze the observed rates of morphological change and in this manner define T_r. As it was mentioned, this timescale parameter controls the rate at which the bed uncertainty increases towards the natural uncertainty, which has a default value of 1 m. It is recommendable to test the effects of varying this default value of 1 m to lower values versus increasing the timescale, both of which might have a similar effect on the final outcome.

Perhaps the most important recommendation made here is with regards to the further investigation and implementation of some sort of time dependent bed update scheme (similar to the one presented in this chapter) to address the systematic estimation errors. Several different approaches to obtain a similar effect as is desired with a time dependent bed update factor could be used. One idea is to divide the area of the grid which presents wave breaking into several sections (limited in cross shore direction) and basically run an entire simulation for each section (with bed change restricted to each section), moving progressively from the farthest offshore section towards the shoreline. This would obviously increase run time significantly, however, it might be an improvement in the sense that the model will in this way have exactly the same available time to update each part of the bed (a whole simulation length); allowing the dissipation in the nearshore zone to react to the changes made in the farther offshore areas without necessarily producing bed changes in the nearshore area.

The time dependent bed change factor described in this chapter is basically "hard-coded" to fit the needs of Perranporth beach, for which it is recommended to elaborate on this as to make it applicable to any beach. This could be done by defining the offshore extent of wave breaking for each simulation, using this point as the starting point of the bed change factor (x_s in Equation 29), and progressively moving the bed update region shoreward throughout the simulation. Further investigation

should go into this as to determine the best way to achieve the correction of the systematic estimation errors at the shoreline.

6 IMPORTANCE OF VIDEO-DERIVED INPUT

In order to determine the importance of video-derived input (Timex images) for the accurate prediction of bathymetries using the Beach Wizard bathymetry updating system, a sensitivity analysis was conducted where the input was varied based on a series of different criteria. The objectives set out to be answered in this chapter are the importance of quality, quantity, and regularity of timex images necessary to produce good estimations of bathymetry. In order to achieve this, the meaning of "quality" of a given intensity map must be defined since there are many possible indicators that may be used to define whether an image is "good" or "bad" for the system. The sensitivity analysis carried out in this chapter will use the Beach Wizard model configuration obtained in the previous chapter (Exe. 3 with T_r=10) for all runs. The sensitivity of the model to image input will be quantified in this chapter in the same manner as was described in the previous chapter; by means of Brier skill scores and RMS errors on the calculated bathymetries.

Previously in this report (section 4.3) a qualitative imap ranking was defined and used to rank all of the generated intensity maps between the 1st of April and the 30th of June 2011. This qualitative imap ranking will be used in this chapter as the first indicator of image quality, since a point was made to not link this qualitative imap ranking to any other factors such as wave conditions or tidal elevations. Later on another qualitative filtering of images will take place, which does take into account forcing conditions and not solely image quality. To differentiate between these two criteria of imap quality, the first (following the ranking scheme described in section 4.3) will be referred to as image quality, and the second (which will appear in section 6.4.1) as imap quality. Links between wave climate and tidal elevations to bathymetry estimation capabilities will also be looked into in this chapter, by means of limiting the input based on restrictions such as wave height, period and tidal elevation.

The content of this chapter will first look at the effects of varying imaps with respect to their qualitative imap ranking (image quality), next image frequency or regulatity will be looked into, then image quantity (number of imaps), and finally another look into imap quality will be carried out.

6.1 Image quality

The first stage in the sensitivity analysis carried out in this chapter is with regards to the necessary quality of images to produce the best possible estimates of bathymetry with Beach Wizard. The definition of quality of an imap will follow the criteria outlined in section 4.3, where the quality of an imap is dependent only on the quality of the image itself, and how well the produced intensity map replicates the dissipation observed in a given timex image. For this, two runs will be carried out and compared to the results of the run using all imaps (ranked 2, 3 and 4). These two runs will be first using only imaps ranked 3 and 4, and second using only imaps ranked 4. Since these runs will obviously have different total amounts of imaps used as input, the importance of quantity of imaps will also be partly assessed with the results here generated. Figure 6-1 presents the wave height, tidal elevations, and the qualitative ranking of each imap to be used.

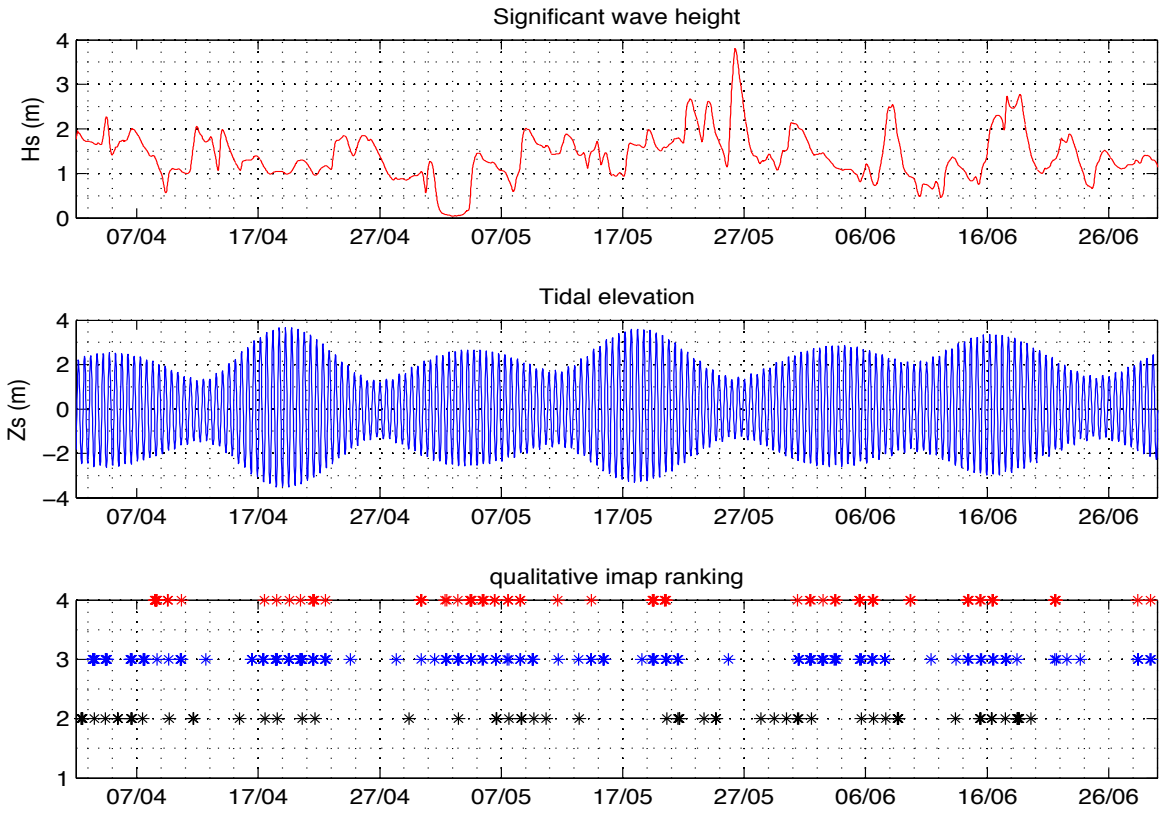

Figure 6-1. (Top) Significant wave heights, (centre) tidal elevations, (bottom) qualitative imap rankings.

The first run carried out in this section will be removing all imaps ranked 2, which corresponds to a total of 76 "bad" imaps, leaving this run with a total of 286 imaps with rankings 3 and 4 (fair and good imaps). As it was mentioned, the resulting bathymetries will be compared to the base case, which for this chapter will be a run using all 362 imaps during the study period with the model version called executable 3 with T_r=10 days (described in the previous chapter).

The resulting bathymetries using only imaps ranked 3 and 4 are plotted alongside the bathymetries calculated using all imaps (ranked 2, 3 and 4), and are shown in Appendix C. The reason for not showing the bathymetry plots in this section in the report is that there are very slight differences, no major changes are observed. On the model results for the 28th of April, there are only minimal differences, concentrating primarily at the shoreline (at about 600 m in –x). The general features in the morphology are the same using all imaps and only imaps ranked 3 and 4, except for a very slight difference in the northern channel, where using all imaps seems to have estimated this feature slightly better than using fewer imaps.

Similarly to the model results from the 28th of April, the results on the 1st and 6th of June present very similar differences. On these dates there are slightly more differences observed in the surf zone (between 300 and 500 m in –x), showing a positive difference (in the difference plot) which means that the resulting bed level computed with only imaps ranked 3 and 4 is lower than the bed level computed using all imaps. Also on these date, the computed bed with only imaps 3 and 4 presents a flatter terrace at the shoreline, but still quite similar to the base case.

The results from the 11th of June seem to present a slight improvement over using all imaps. Again, the difference is minimal, but in this case the main difference is that the detached bar at around 500m –x and 600m –y that was present in the resulting bathymetry using all imaps has now re-attached to the shoreline. Finally, the results from the 30th of June present very similar characteristics to the differences seen on the 1st and 6th of June, showing very little difference, and a flatter shoreline terrace.

The quantification of the variations discussed above are also shown in the form of Brier skill scores and RMS errors for all dates. The BSS are presented in Figure 6-7 through Figure 6-9, which is located after the upcoming results, which will now be

shown and discussed. The results are shown in graph form, and the numerical values of these along with the RMS errors are seen in Appendix C.

The next test to be carried out in this section is one in which only imaps ranked 4 will be used. As it was described previously, a ranking of 4 means that the image is considered "good", and that the intensity map represents well the wave dissipation observed in said image. Using only imaps ranked 4 results in a total of 100 imaps for the entire study period, specifically 26, 31, and 43 imaps for April, May, and June respectively. This is a considerable reduction in the total amount of imaps used as input for the model, therefore the results obtained here should shed some light on the question regarding the importance of quantity as well as quality of imaps necessary to reproduce real bathymetries as well as possible.

The resulting bathymetries will first be presented here in Figure 6-2 through Figure 6-6, where they are plotted alongside the calculated bathymetries using all imaps (base case). As well as this, each figure presents both the initial bathymetry and the current measured bathymetry, and a difference plot showing the difference between the base case using all imaps and the new test case using only "good" imaps (ranked 4).

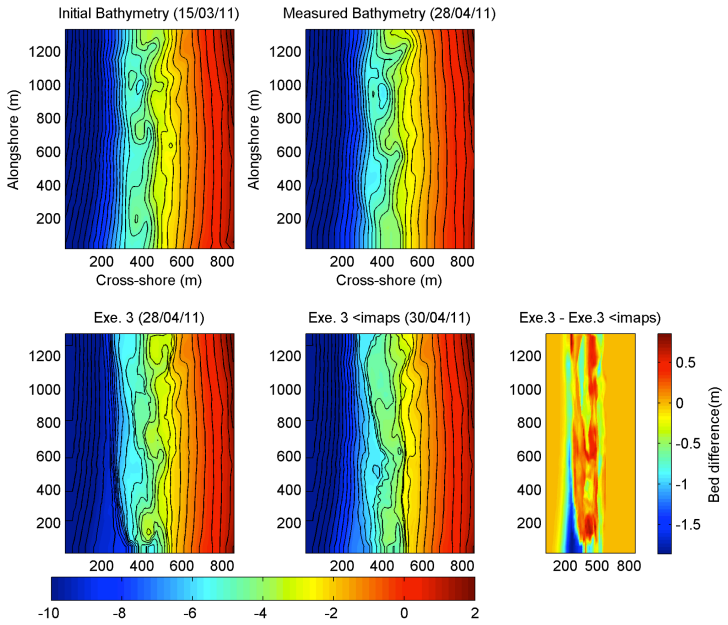

Figure 6-2. Resulting bathymetries using only imaps ranked 4. (Top) Measured bathymetries, initial (15/03/11) and current (28/04/11). (Bottom Left) Modelled bathymetry using all imaps (28/04/11). (Bottom centre) Modelled bathymetry using imaps ranked 4 (30/04/11). (Bottom right) Difference between modeled bathymetries with all imaps and with only imaps ranked 4.

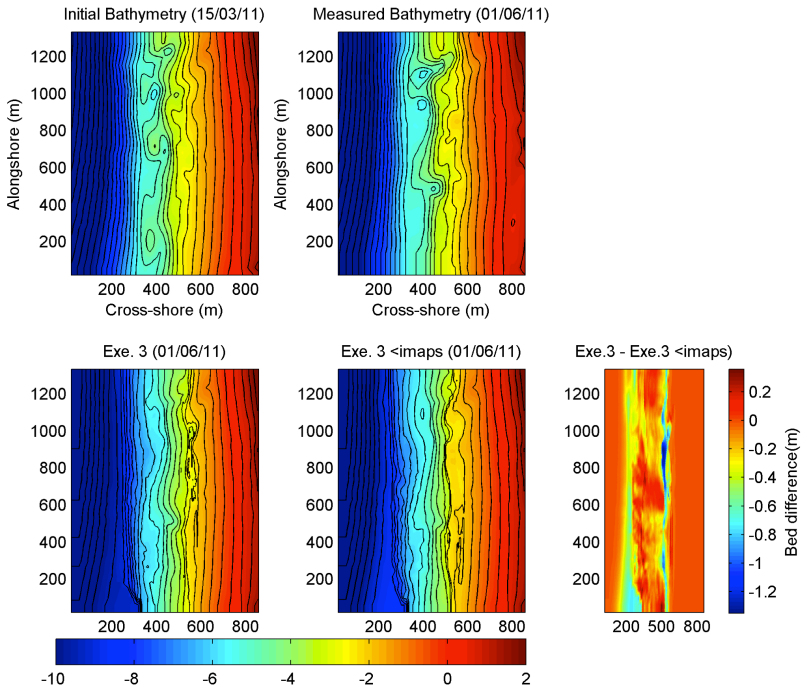

Figure 6-3. Resulting bathymetries using only imaps ranked 4. (Top) Measured bathymetries, initial (15/03/11) and current (01/06/11). (Bottom Left) Modelled bathymetry using all imaps (01/06/11). (Bottom centre) Modelled bathymetry using imaps ranked 4 (01/06/11). (Bottom right) Difference between modeled bathymetries with all imaps and with only imaps ranked 4.

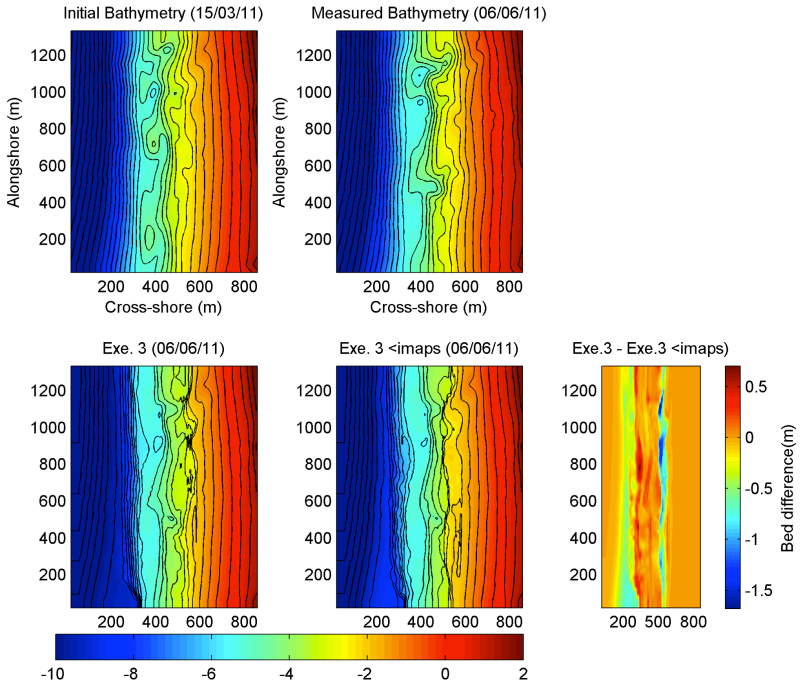

Figure 6-4. Resulting bathymetries using only imaps ranked 4. (Top) Measured bathymetries, initial (15/03/11) and current (06/06/11). (Bottom Left) Modelled bathymetry using all imaps (06/06/11). (Bottom centre) Modelled bathymetry using imaps ranked 4 (06/06/11). (Bottom right) Difference between modeled bathymetries with all imaps and with only imaps ranked 4.

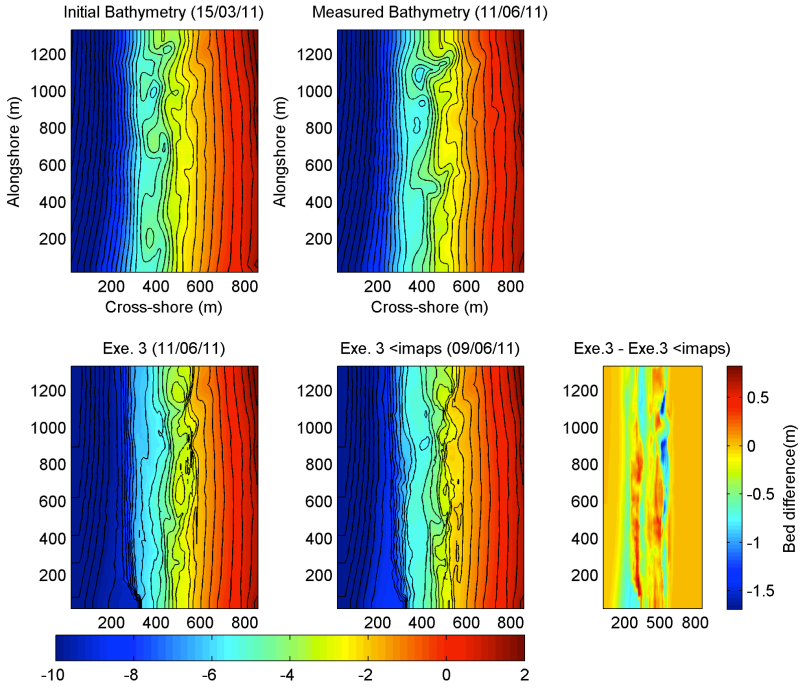

Figure 6-5. Resulting bathymetries using only imaps ranked 4. (Top) Measured bathymetries, initial (15/03/11) and current (11/06/11). (Bottom Left) Modelled bathymetry using all imaps (11/06/11). (Bottom centre) Modelled bathymetry using imaps ranked 4 (09/06/11). (Bottom right) Difference between modeled bathymetries with all imaps and with only imaps ranked 4.

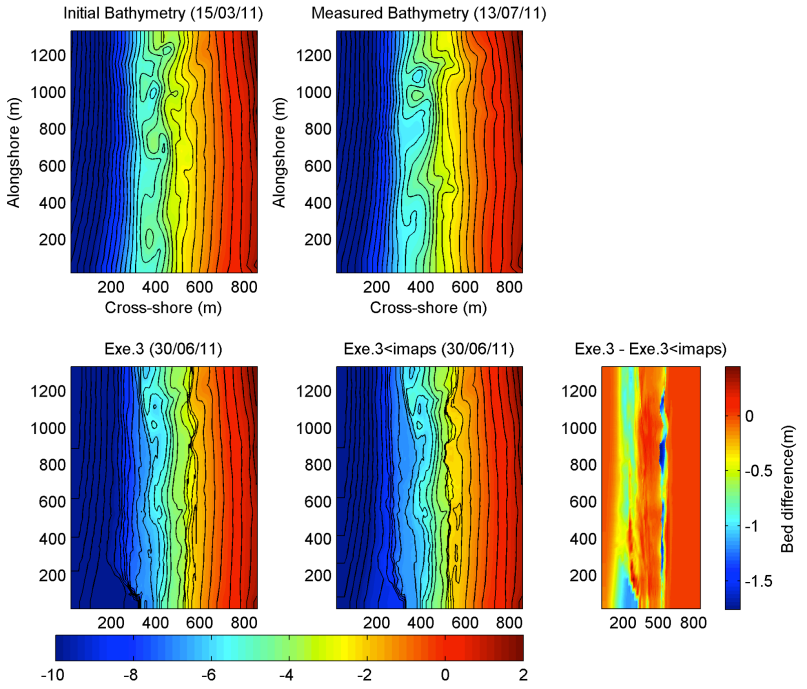

Figure 6-6. Resulting bathymetries using only imaps ranked 4. (Top) Measured bathymetries, initial (15/03/11) and current (30/06/11). (Bottom Left) Modelled bathymetry using all imaps (30/06/11). (Bottom centre) Modelled bathymetry using imaps ranked 4 (30/06/11). (Bottom right) Difference between modeled bathymetries with all imaps and with only imaps ranked 4.

The resulting bathymetries shown in Figure 6-2 correspond to the modeled bathymetries on the 28th of April 2011. It is important to clarify that for the case using only imaps ranked 4, there was no available image on the 28th of April, reason for which the results on the 30th of April are used for comparison (this was the closest date to the measured bathymetry on the 28th of April). The first observation by visually analyzing this figure is that the resulting bathymetry having used only imaps with a ranking of 4 ("good" imaps) presents a less defined channel and transverse bar at around 400-500 m in –x and 600-700 m in –y, as well as a less defined channel at the north. This points towards a possible conclusion that says that image quality is less important than other factors (possibly imap quality, imap quantity and/or regularity). The resulting BSS for the present run are shown along with the resulting scores for the previously described run (using imaps 3 and 4) and the base run (using imaps 2, 3 and 4) in Figure 6-7 through Figure 6-10, where each figure corresponds to a different region of the model domain (Appendix D).

For the modeled bathymetries on the measured dates in June, the results obtained by using only imaps with a ranking of 4 are very similar to the results obtained using imaps with rankings 3 and 4. As it was mentioned, the difference between these two runs (using less imaps) and the base run is mainly near the shoreline, where the modeled bathymetries tend to present a flatter terrace when using less imaps (only 3's and 4's or only 4's). By looking at Figure 6-1, the difference in the spacing and frequency of imaps can be seen for the three cases being compared here (all imaps, imaps 3 and 4, and imaps 4). Since the resulting bathymetries in June do not seem to vary very much between using either imaps 3 and 4 or using just imaps ranked 4, and the resulting bathymetry at the end of April seems to present a more distinguished variation, then the difference between the characteristics of these two periods should be of interest. Looking at the distribution of imaps during the entire study period, the main difference seen between using either imaps ranked 3 and 4 or ranked just 4 lies at the end of April. This difference is that for the case using just imaps ranked 4, there is a gap with no available images between the 22nd and 30th of April, while there are imaps ranked 3 on the 24th, 28th and 29th of April. This difference may have been enough to present a difference in the estimation of the channels and transverse bars

on the 28th of April (30th of April in the case of using only imaps ranked 4), and therefore points towards the importance of regularity of imaps over quality of images (following the definition of quality used in this section).

Figure 6-7 through Figure 6-10 shown below present the calculated Brier skill scores for all modeled dates during the study period for the three cases described in this section, with varying qualitative imap rankings. These Brier skill scores are calculated for different regions in the given domain, which are described and shown in detail in Appendix D.

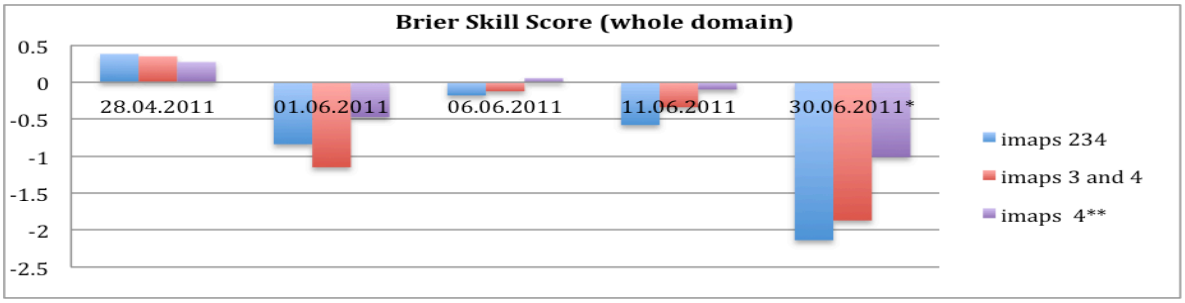

Figure 6-7. Brier Skill Scores over whole domain (excluding region below y=300m) for runs using executable 3, with (blue) imaps ranked 2, 3 and 4, (red) imaps ranked 3 and 4, (purple) imaps ranked 4. *BSS calculated with modelled result on this date with measured bathymetry from 13/07/11. ** No result available on 28/04/11 or 11/06/11; 30/04/11 and 09/06/11 used instead.

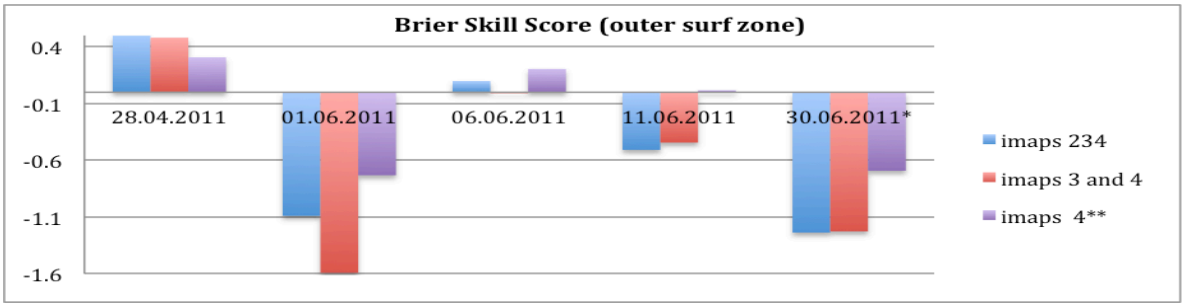

Figure 6-8. Brier Skill Scores for outer surf zone (x=250-450m, y=300-1340m) for runs using executable 3, with (blue) imaps ranked 2, 3 and 4, (red) imaps ranked 3 and 4, (purple) imaps ranked 4. *BSS calculated with modelled result on this date with measured bathymetry from 13/07/11. ** No result available on 28/04/11 or 11/06/11; 30/04/11 and 09/06/11 used instead.

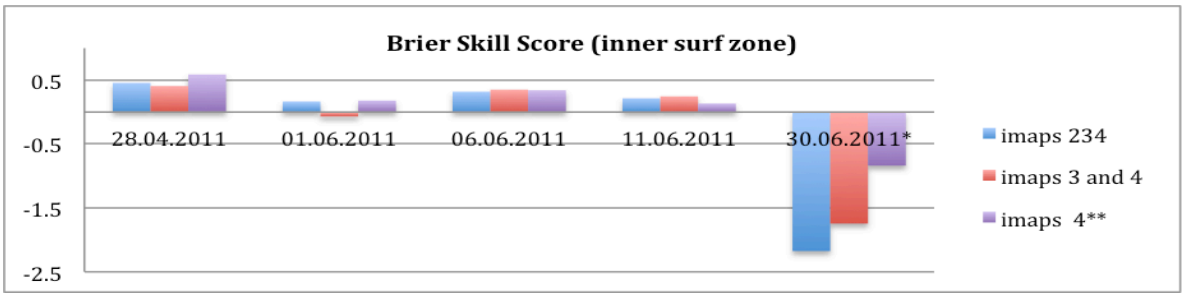

Figure 6-9. Brier Skill Scores for inner surf zone (x=450-600m) for runs using executable 3, with (blue) imaps ranked 2, 3 and 4, (red) imaps ranked 3 and 4, (purple) imaps ranked 4. *BSS calculated with

modelled result on this date with measured bathymetry from 13/07/11. ** No result available on 28/04/11 or 11/06/11; 30/04/11 and 09/06/11 used instead.

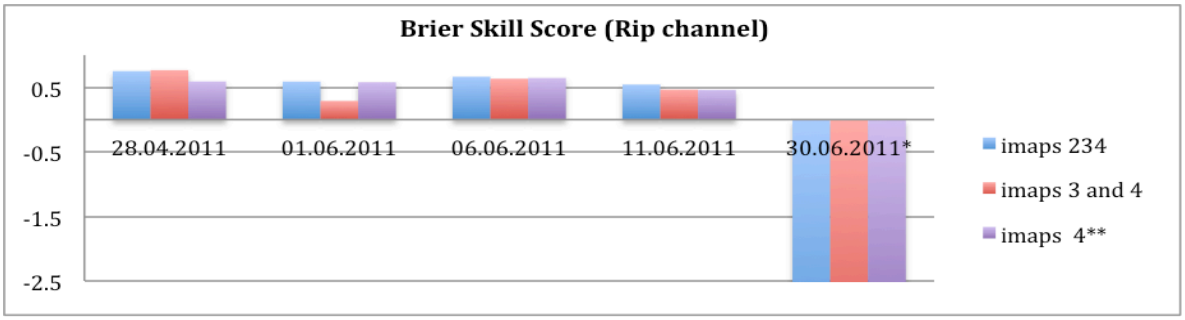

Figure 6-10. Brier Skill Scores at measured channel locations (Appendix D) for runs using executable 3, with (blue) imaps ranked 2, 3 and 4, (red) imaps ranked 3 and 4, (purple) imaps ranked 4. *BSS calculated with modelled result on this date with measured bathymetry from 13/07/11. ** No result available on 28/04/11 or 11/06/11; 30/04/11 and 09/06/11 used instead.

The Brier skill scores just shown, show different results (either increased or reduced skill with respect to base case) for the different dates and for the different calculation regions. Firstly, for the whole domain, the results on the 28th of April show a reduction in skill for both cases (using imaps ranked 3 and 4 and using imaps ranked 4) with respect to the base case (imaps 234). This coincides well with the observed differences seen in the estimated bathymetries, where it was seen that the general morphological features were not estimated as well when eliminating either imaps ranked 2 or imaps ranked 2 and 3. For the dates in the month of June however, the general tendency is an increase in skill for the two cases (except for the case using only imaps ranked 3 and 4 on the 1st of June). The reason for the diminished skill seen when removing only imaps ranked 2 on the 1st of June may be due to a similar problem noticed previously, being the large space in time generated between consecutive images when removing "bad" images. When removing all imaps ranked 2, a large temporal gap with only 1 image available between the 21st and 31st of June is observed (Figure 6-1), potentially missing important video-derived information from those 10 days. However, in the case using only imaps ranked 4, this temporal gap between images is also present (11 days long in this case), and the reduction in skill doesn't occur. The skill on the 1st of June in fact increases for the case using only imaps ranked 4 with respect to the base case (using all imaps), suggesting that there is a kind of "balance" between quality of images and regularity of imaps, where both are important, but perhaps on different scales. This will be further examined in the

upcoming sections of the report, where more sensitivity runs will take place, varying the regularity (temporal spacing), the quantity, and the quality (using a different definition of quality as the one used in this section of the report) of imaps used as input to the model.

The Brier skill scores calculated for the inner surf zone and for the specific channel locations show much more positive results, meaning that the model is showing an improvement over the initial bathymetry towards the real current measured bathymetry in those regions. At the inner surf zone, the BSS calculated on the 28th of April for the case using only imaps ranked 4 is higher than the BSS calculated for the base case, contradicting the results obtained for the whole domain as well as the visual observations previously made. The BSS calculated at the specific channel locations show particularly good results for all dates except for the 30th of June, most likely due to the fact that the modeled results on the 30th of June are compared to a measured bathymetry on the 13th of July (unlike the rest of the dates where the modeled results coincide with measured bathymetry dates).

From the calculated BSS and the visual analysis of the estimated bathymetries, it seems as though the general effect of using higher ranked imaps rather than all imaps is a reduction in model skill, meaning that even though an image is not perfect, the resulting imap may be good for the model. However, the calculated Brier skill scores are quite variable both in the spatial domain and on the different calculated dates, making it difficult to draw definite conclusions with respect to the importance of image quality at this point. To further investigate this, the resulting rip current flows will be studied in the upcoming chapter, and the actual impact of image quality on the modeling of rip currents using estimated bathymetries will be analyzed.

6.2 Temporal regularity of images

The importance of temporal regularity or "frequency" of images (image spacing in time) to be used as input in the Beach Wizard model is analyzed by varying the input of the base model (using all imaps) in two overall manners. The two variations on image input carried out in this section are by using images once per week, and by eliminating instances when there are two or less consecutive images in one day. The

results of the first should give an idea as to whether regularity of images is important or not, without taking into account the quality of said images. The objective of the second run will be to investigate whether having only one or two imaps in a single day is helpful or harmful to the model outcome.

By looking at Figure 6-1 in the previous section, it is clear that the images used are already present in "groups", mainly concentrating around dates coinciding with neap tides. This is due primarily to the fact that the images were originally selected with an upper threshold of tidal elevation set to -1 m, and during neap periods there is consequently less available images that meet that standard. This problem could not be overcome in this thesis due to the problems with the merging of timex images between cameras 1 and 2, presenting problematic resulting imaps for mid to high tides (described in section 4.3). Therefore, considering that the available imaps (ranked 2, 3 and 4) have the maximum possible frequency, the variations on frequency will be carried out on said group of images.

6.2.1 *Input once per week*

The first case run in this section is using all imaps from a single day once per week (roughly) beginning on the 2nd of April until the 30th of June 2011. A point was made to make sure that the selected day had to have several imaps (preferably with varying imap rankings), ultimately setting the limit to more than five images in a single day. For this reason, the spacing between days is not always strictly one week, and varies depending on the specific incidence of images. Figure 6-11 shows the distribution of the selected days for the run using all imaps in a day once per week, where the used imaps correspond to the red marks on the plots. The plots show that the spacing between days used is on average 1 week, except for the last two dates in April, where there is 13 days lapse time (17th-30th of April) due to the fact that the days found in between that period didn't have enough consecutive daily imaps.

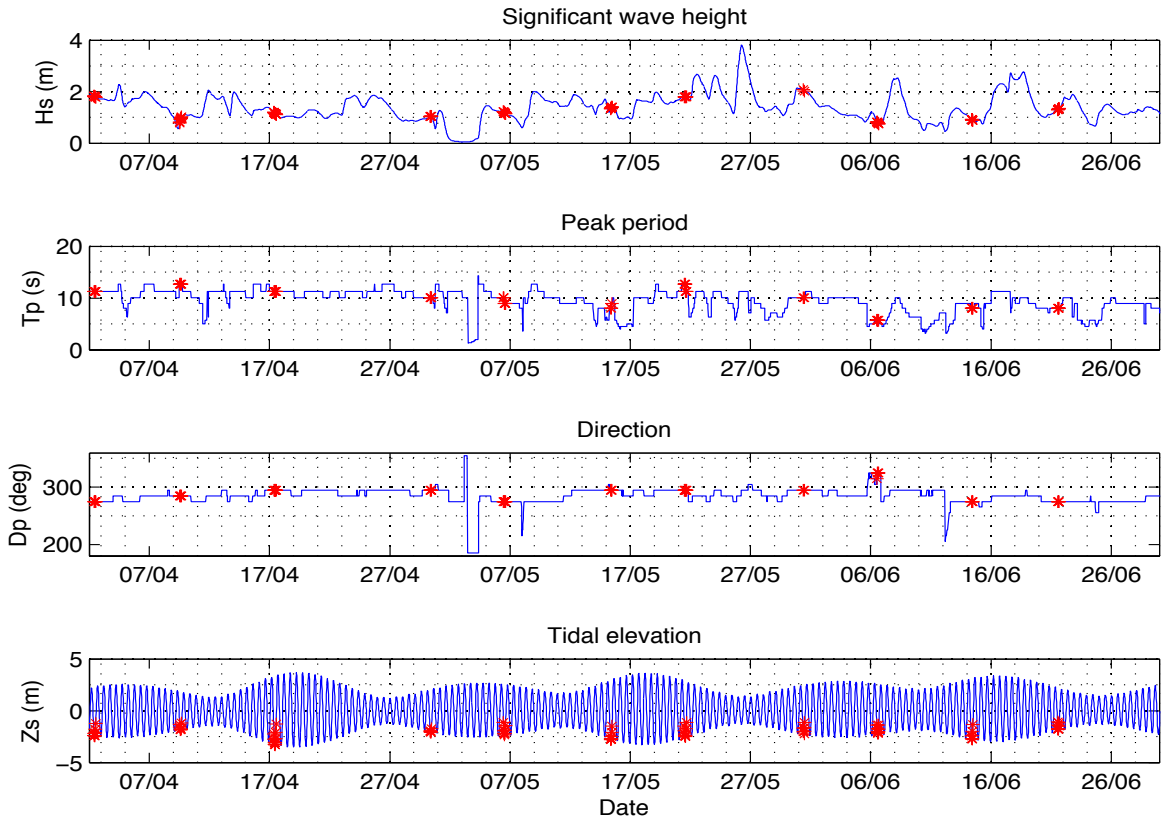

Figure 6-11. Wave and tide forcing and imaps marked with red asterisks for sensitivity run using all imaps in a day once a week.

Some of the chosen dates in this run do not coincide to dates with measured bathymetries, for which the closest date is chosen for the analysis of resulting bathymetries. The model output on the 30th of April will be compared with the measured bathymetry on the 28th of April, the 31st of May with measured bathymetry on the 1st of June, the 14th of June with measured bathymetry on the 11th of June, and the two other dates with measured bathymetries are available in the model results (6th and 30th of June). Figure 6-12 through Figure 6-16 show the resulting bathymetries calculated using imaps distributed to one day per week. The initial and current measured bathymetries are on the top side of each figure, and the bottom row corresponds to modeled bathymeries with all imaps (Exe. 3), modelled with imaps once per week (Exe. 3<imaps), and the difference between these (Exe. 3-Exe.3<imaps).

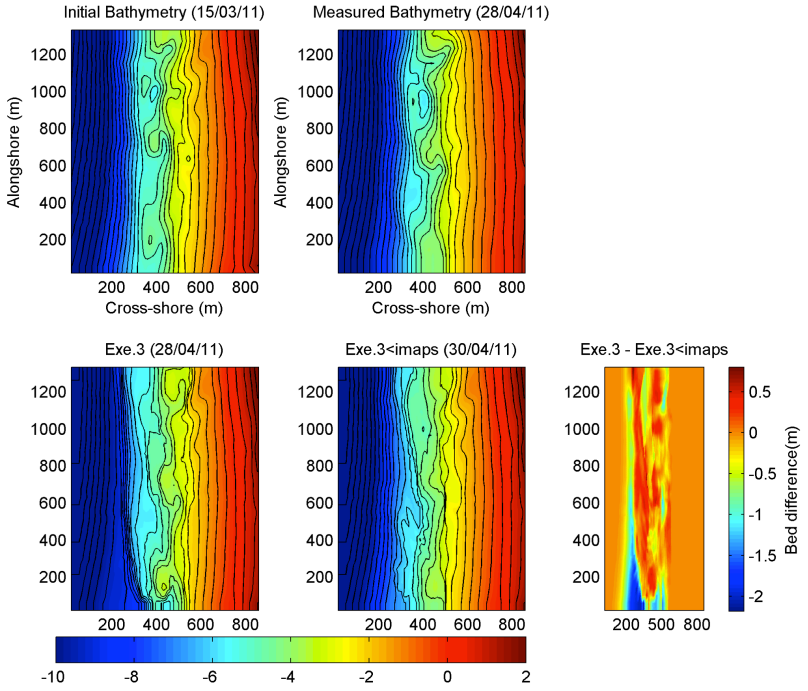

Figure 6-12. Resulting bathymetries using only imaps 1 day per week (Top) Measured bathymetries, initial (15/03/11) and current (28/04/11). (Bottom Left) Modelled bathymetry using all imaps (28/04/11). (Bottom centre) Modelled bathymetry using imaps once per week (30/04/11). (Bottom right) Difference between modeled bathymetries with all imaps and with imaps once per week.

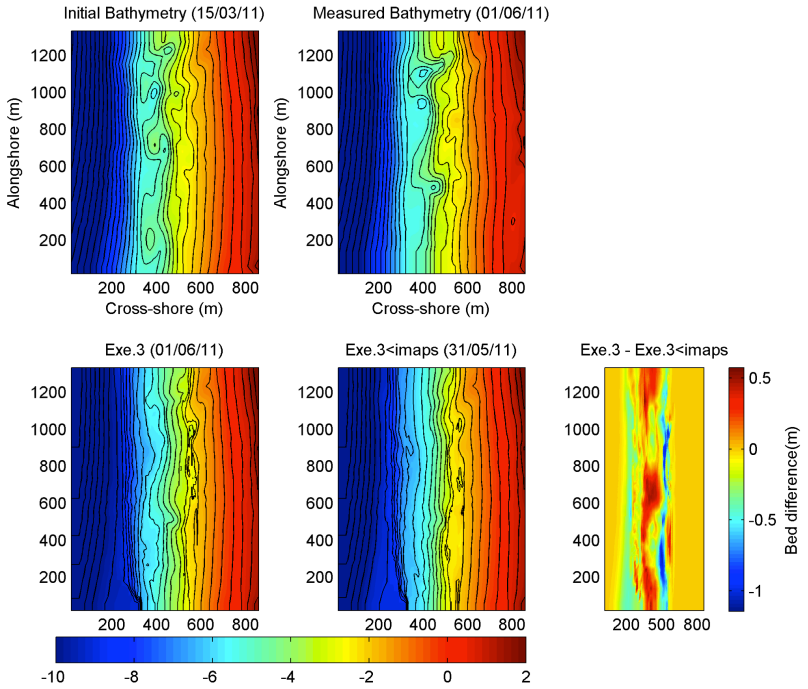

Figure 6-13. Resulting bathymetries using only imaps 1 day per week (Top) Measured bathymetries, initial (15/03/11) and current (01/06/11). (Bottom Left) Modelled bathymetry using all imaps (01/06/11). (Bottom centre) Modelled bathymetry using imaps once per week (31/05/11). (Bottom right) Difference between modeled bathymetries with all imaps and with imaps once per week.

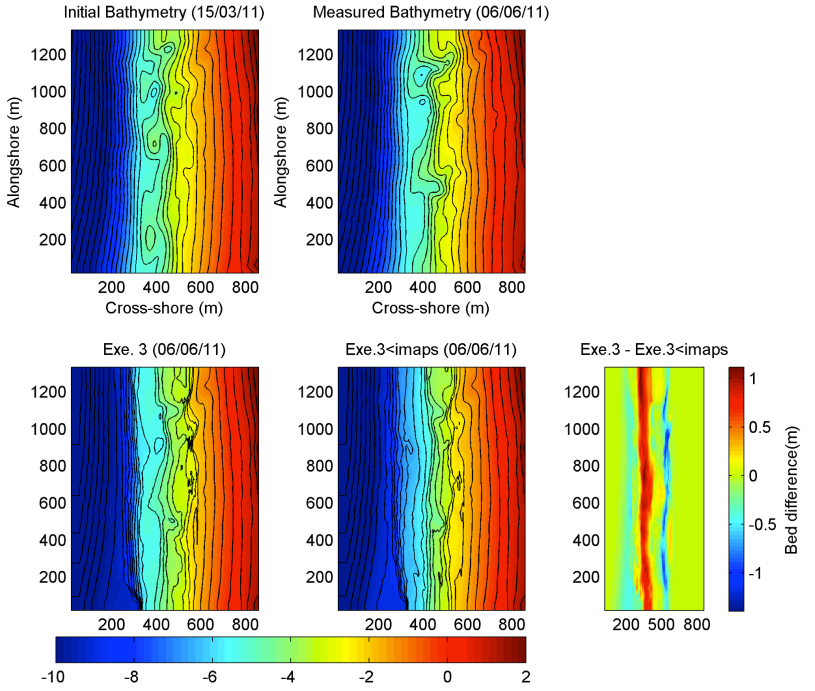

Figure 6-14. Resulting bathymetries using only imaps 1 day per week (Top) Measured bathymetries, initial (15/03/11) and current (06/06/11). (Bottom Left) Modelled bathymetry using all imaps (06/06/11). (Bottom centre) Modelled bathymetry using imaps once per week (06/06/11). (Bottom right) Difference between modeled bathymetries with all imaps and with imaps once per week.

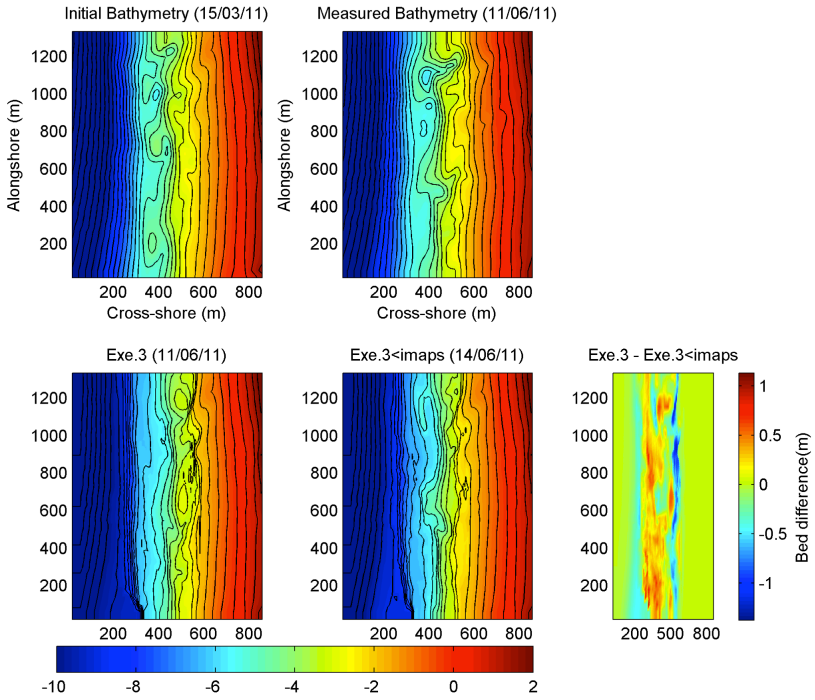

Figure 6-15. Resulting bathymetries using only imaps 1 day per week (Top) Measured bathymetries, initial (15/03/11) and current (11/06/11). (Bottom Left) Modelled bathymetry using all imaps (11/06/11). (Bottom centre) Modelled bathymetry using imaps once per week (14/06/11). (Bottom right) Difference between modeled bathymetries with all imaps and with imaps once per week.

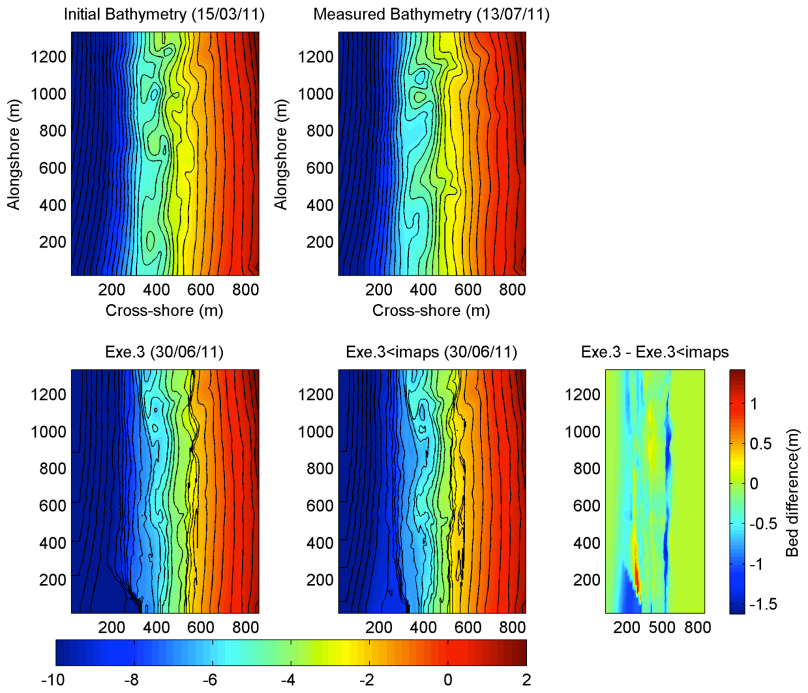

Figure 6-16. Resulting bathymetries using only imaps 1 day per week (Top) Measured bathymetries, initial (15/03/11) and current (13/07/11). (Bottom Left) Modelled bathymetry using all imaps (30/06/11). (Bottom centre) Modelled bathymetry using imaps once per week (30/06/11). (Bottom right) Difference between modeled bathymetries with all imaps and with imaps once per week.

Starting with the resulting bathymetry on the 30th of April using imaps once per week, and comparing this with both the measured bathymetry and the modeled bathymetry using all imaps on the 28th of April, a reduction in the reproduction of the main morphological features is seen. Figure 6-12 shows this comparison, and it is clear that spacing the used imaps to only one day per week has had a negative effect on the resulting bathymetry, since the two main channels and the transverse bar at 400-500 m in x- and 600-700 m in y- are clearly less pronounced than in the case using all available imaps. The problem at this date may be due to the same problem observed in the previous run (where only maps ranked 4 were used), where there is a large temporal gap between the last date in April and the second to last. The time between the two last modeled dates in April is 13 days, which is basically twice the spacing between the rest of the dates. As it was mentioned previously, the reason for this time between used dates being so long is that the days with available images during that period did not have enough images.

The resulting bathymetry from the 31st of May (compared to the measured bathymetry on the 1st of June) also shows a visible decrease in accuracy, where the main channels are even less pronounced than in the bathymetry estimated using all available imaps. The plots shown in Figure 6-13 show the bathymetry in the surf zone between approximately 400-500 m in –x presenting a generally lower bed elevation than in the calculated using all imaps (as well as compared to the measured bathymetry). The other notable difference in the estimated bathymetry on the 1st of June is a higher bed level near the shoreline, with a flatter terrace section (shown by the blue vertical line in the difference plot).

The just mentioned difference at the shoreline is also seen on the estimated bathymetry from the 6th of June, which can be seen Figure 6-14. As well as this, there is a substantial difference in the elevation of the outer bar (at around 400 m in –x), where the estimated bathymetry is consistently around 1 m lower than the bathymetry estimated using all imaps (as well as the measured bathymetry). The difference in elevation of this region would likely generate a large error in the modeling of nearshore currents, due to the change in wave breaking over this region (this will be discussed in the following chapter).

The bathymetry calculated on the 14th of June seems to show a better estimation of the general shoreline shapes in comparison with the case using all imaps (shown in Figure 6-15). However, similar to the observation made for the results on the 6th of June, the estimated bed elevation using imaps once per week is lower than the estimated using all imaps (the difference is a lot less than on the 6th of June). Slight differences could also be attributed to the fact that the modeled date using imaps once per week is three days after the measured bathymetry date, while the modeled bathymetry using all imaps is on the same day as the measured bathymetry.

Figure 6-16 shows the final estimated bathymetries for the run using imaps once per week (on the 30th of June), along with the bathymetry modeled using all imaps, and the corresponding measured bathymetry from the 13th of July. The difference between using all imaps and using imaps once a week is less here than on the rest of the dates, showing the most visible difference at the shoreline. This difference at the shoreline is the same observation that was made on the previous modeled dates, and

is that the modeled bed elevation using imaps once per week is higher and flatter near the shoreline than in the case using all imaps. The Brier skill scores for the resulting bathymetries are shown in Figure 6-19 through Figure 6-22, along with the results from the run that will now be described. The rest of the computed numerical results are shown in Appendix C.

6.2.2 *Impact of "lone" images*

"Lone" images refers to instances in which only two or less images are available in a single day. The purpose of this section lies on determining whether or not using very few images in a single day is helpful to the model results or not. At first thought it could be reasonable to believe that having very few images in a single day would not be helpful to the model. The reasoning behind this is that no smoothing over a tidal cycle could happen on a single day, and because the model might not have a chance to assimilate the bathymetry to the general daily conditions observed. This last observation follows what was observed in the previous chapter, Figure 5-15; where for each day with several imaps the bathymetry converges towards a "final" daily state, and in cases with only one or two images this convergence is not seen. However, this reasoning is what is set out to be analyzed with this model run.

The present model run eliminates any days in which only two or fewer images are available. This corresponds to a total of 21 days during the study period that are eliminated, with a total of 27 removed imaps.

Figure 6-17 shows the forcing conditions and all images used marked with a red asterisk for the present model run. There are three major notable time gaps between days with available imaps for this run, and they coincide with the days around neap tides at the end of each month. At the end of April there are 8 days between consecutive images, and at the end of May and June there are 7 days spacing between the groups of images seen in Figure 6-17.

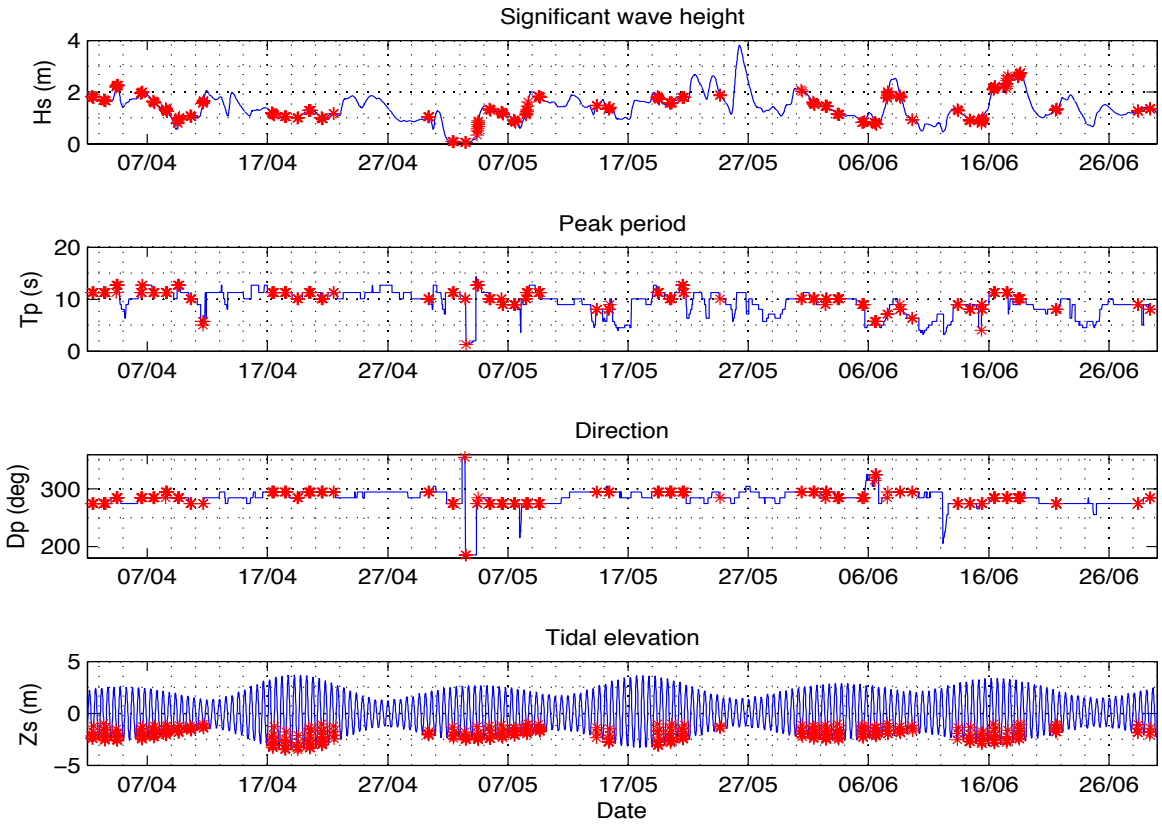

Figure 6-17. Wave and tide forcing and imaps marked with red asterisks for sensitivity run removing days with only two or less imaps.

The resulting bathymetries for the present sensitivity run do not show substantial differences in comparison to the base run (using all imaps), with the exception of the results at the end of April. The modeled bathymetry in this case that is available for comparison with the measured bathymetry on the 28th of April is two days after this date, on the 30th of April. The resulting bathymetry for this date is presented in Figure 6-18, while the rest of the modeled bathymetries for this run are shown in Appendix C. Figure 6-18 shows how the resulting bathymetry from the run having eliminated days with two or less imaps does not reproduce the general morphological characteristics as well as the bas case with all images. By simply observing the contour lines presented in the bathymetry plots, it is clear that by eliminating the days with few imaps impairs the estimation of the two major channels. As well as this, the difference plot shows that there is a large amount of the surf zone where the modeled bed elevation is in the order of half a meter lower than the bathymetry modeled in the base case.

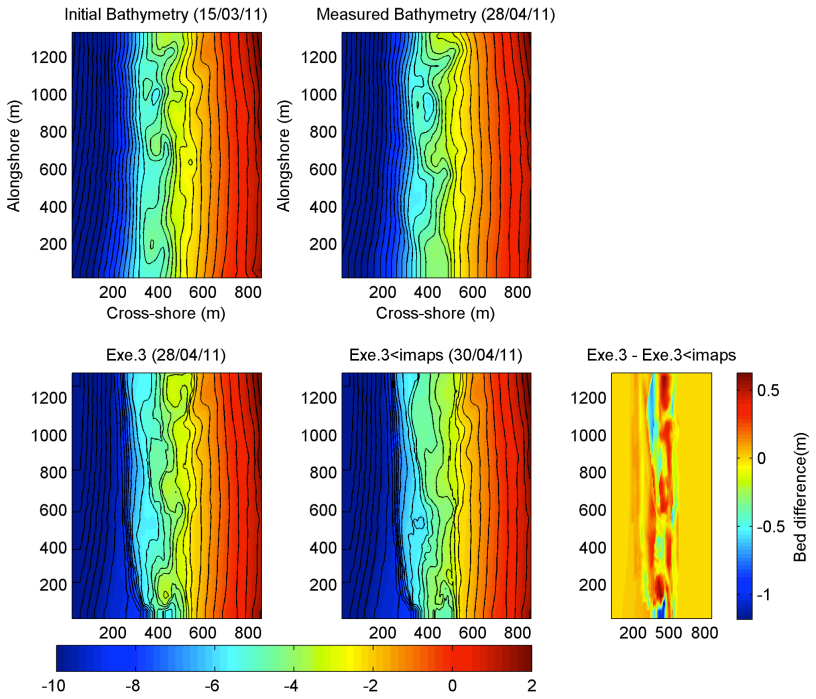

Figure 6-18. Resulting bathymetries using only days with more than 2 imaps per day. (Top) Measured bathymetries, initial (15/03/11) and current (28/04/11). (Bottom Left) Modelled bathymetry using all imaps (28/04/11). (Bottom centre) Modelled bathymetry using days with more than 2 imaps per day (30/04/11). (Bottom right) Difference between modeled bathymetries with all imaps and with days with more than 2 imaps per day.

The importance of temporal regularity of imaps used as input for the Beach Wizard system is expressed in numerical values of Brier skill scores and RMS errors as well as the presented bathymetry plots shown previously in the last two sections of the report. All of these results are presented in Appendix C, with only the Brier skill scores shown as column graphs in this section of the report. Figure 6-19 through Figure 6-22 show the BSS calculated for the base case using all imaps along with the two cases described in this section of the report, being the case with imaps used only once per week, and the case where days with two or less imaps are eliminated (labelled 3 or more consecutive). The skill scores are calculated for different regions of the domain, which are described in Appendix D. The BSS are calculated using the initial measured bathymetry from the 15th of March, the measured bathymetry from each available date, and the modeled bathymetries on the nearest dates to dates with surveyed bathymetries.

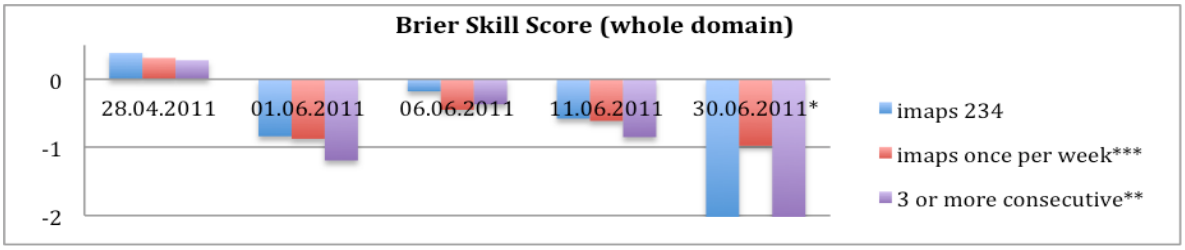

Figure 6-19. Brier Skill Scores over whole domain (excluding region below y=300m) for sensitivity on imap input frequency, with (blue) imaps ranked 2, 3 and 4, (red) imaps used once per week, (purple) days with two or less imaps removed. *BSS calculated with modelled result on this date with measured bathymetry from 13/07/11. ** No result available on 28/04/11 or 11/06/11, 30/04/11 and 09/06/11 used instead. * No result available on 28/04/11, 01/06/11, or 11/06/11; 30/04/11, 31/05/11 and 14/06/11 used.**

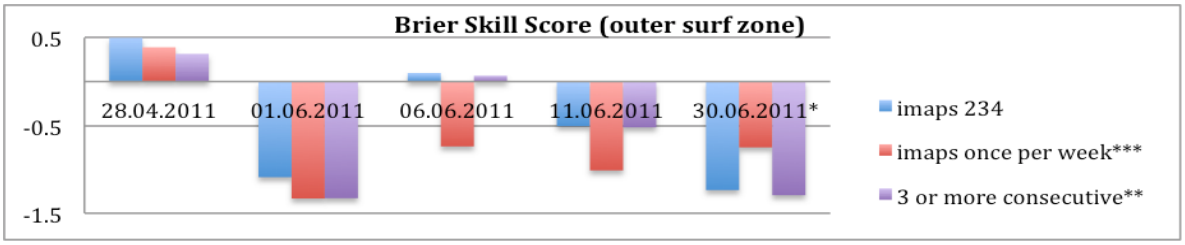

Figure 6-20. Brier Skill Scores in outer surf zone (x=250-450m, y=300-1340m) domain for sensitivity on imap input frequency, with (blue) imaps ranked 2, 3 and 4, (red) imaps used once per week, (purple) days with two or less imaps removed. *BSS calculated with modelled result on this date with measured bathymetry from 13/07/11. ** No result available on 28/04/11 or 11/06/11; 30/04/11 and 09/06/11 used instead. * No result available on 28/04/11, 01/06/11, or 11/06/11; 30/04/11, 31/05/11 and 14/06/11 used instead.**

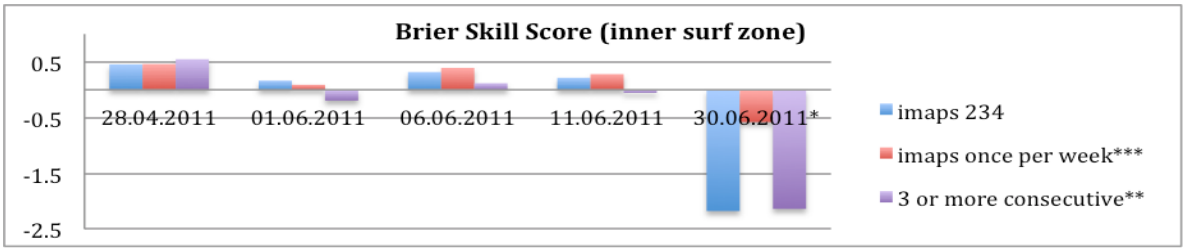

Figure 6-21. Brier Skill Scores in inner surf zone (x=450-600m) for sensitivity on imap input frequency, with (blue) imaps ranked 2, 3 and 4, (red) imaps used once per week, (purple days with two or less imaps removed. *BSS calculated with modelled result on this date with measured bathymetry from 13/07/11. ** No result available on 28/04/11 or 11/06/11; 30/04/11 and 09/06/11 used instead. * No result available on 28/04/11, 01/06/11, or 11/06/11; 30/04/11, 31/05/11 and 14/06/11 used instead.**

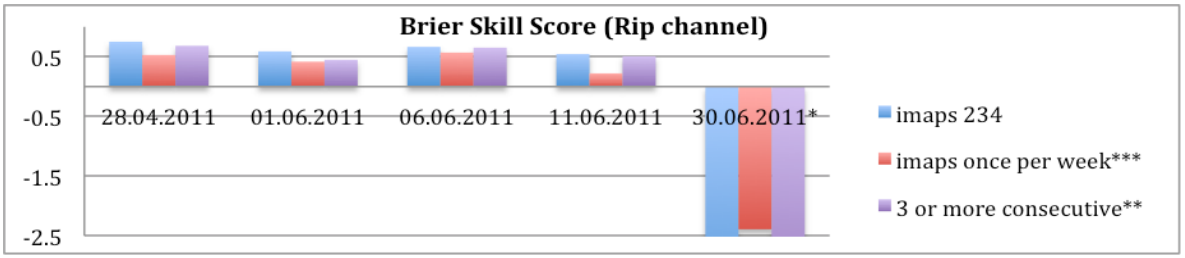

Figure 6-22. Brier Skill Scores at measured channel location (Appendix D) for sensitivity on imaps input frequency, with (blue) imaps ranked 2, 3 and 4, (red) imaps used once per week, (purple days with two or less imaps removed. *BSS calculated with modelled result on this date with measured bathymetry from 13/07/11. ** No result available on 28/04/11 or 11/06/11; 30/04/11 and 09/06/11 used instead. * No result available on 28/04/11, 01/06/11, or 11/06/11; 30/04/11, 31/05/11 and 14/06/11 used instead.**

The calculated BSS for the entire domain and for the outer surf zone concur with what was visually observed in the resulting bathymetries, and that is a reduction in skill for both the case where imaps are used once per week and the case where days with two or less imaps available (labeled "3 or more consecutive") are removed. The skill scores calculated at the specific channel locations also coincide with the previous observations, and also highlights that using imaps once per week is worse than eliminating days with two or less available images.

The general observation from the two sensitivity runs carried out in this section is a reduction in skill with respect to the base case. This is an interesting and useful result, in that it points towards the importance of having high regularity of images (no large spaces between consecutive days). The BSS for the case where days with two or less imaps are eliminated shows that having only one or two images per day is in fact more helpful than harmful to the model. These are preliminary conclusions, which will be further elaborated on in the conclusions and in the upcoming chapter of this report.

Another interesting observation is that the BSS calculated at the location of the channel in each measured bathymetry show positive results. The reason for this is that the channel in the initial bathymetry (15th of March) was located several hundred meters to the north of the channel locations in April and June, therefore any slight resemblance of the channel in the modeled bathymetry to the channel in the measured bathymetries will give positive skill scores (because the initial bathymetry at that location has no channel).

The BSS calculated at the end of June (30th of June) are generally significantly lower than for the other dates. This reduction in skill with respect to the rest of the analyzed dates may be due in part to the fact that the measured bathymetry used for comparison on this date is from the 13th of July (two week after the modeled date).

6.3 Quantity of image input

The necessary amount of images needed as input for the Beach Wizard data-model assimilation process is an important factor to be tested. Here the quantity of images simply refers to the total number of intensity maps used in a certain period of time

during a model run. From the previously run test cases (presented in the portion of the present chapter preceding the current section) an idea on the importance of image quantity can already start being formed. This is due to the fact that the previously run test cases reduced the total amount of imaps in each run, depending on different criteria for each case. It was observed that it is possible to maintain the skill of the model to a certain degree whilst reducing the amount of images used, however, in some of the previous cases the images that were eliminated were not chosen randomly ("bad" images were eliminated). What the present section sets out to determine is the importance of only the quantity of images, without considering the quality or specific characteristics of each image.

Two model runs are carried out, each using a different total number of images. From the previous section it was found that the regularity of images in fact does have an effect on the model outcome, reason for which the tests carried out here will not vary this at all, having images on every available day during the study period. The first scenario to be tested is one in which 3 imaps are used on each available day (if there isn't three available, two or one will still be used), and for the second only one daily image will be used.

The first case where 3 images per day are used generates a reduction of approximately 50% of the total amount of available images (362 total imaps available), resulting in a total of 174 imaps to be used. The second case, using only one imap per day, resulted in a reduction of approximately 80% of the total amount of available imaps, leaving a total of 69 imaps to be used. The resulting calculated bathymetries for both of these runs do not present clear visible differences between them, therefore the resulting bathymetry plots will only be shown here for the second case run (using one imap per day), and the differences will be addressed in the form of Brier skill scores and RMS errors. Figure 6-23 through Figure 6-27 show the estimated modeled bathymetries using a single image per day as input, along with the corresponding initial and current measured bathymetries, the bathymetry calculated in the base case (using all imaps), and a difference plot between the bathymetries using all imaps and using a single imap per day.

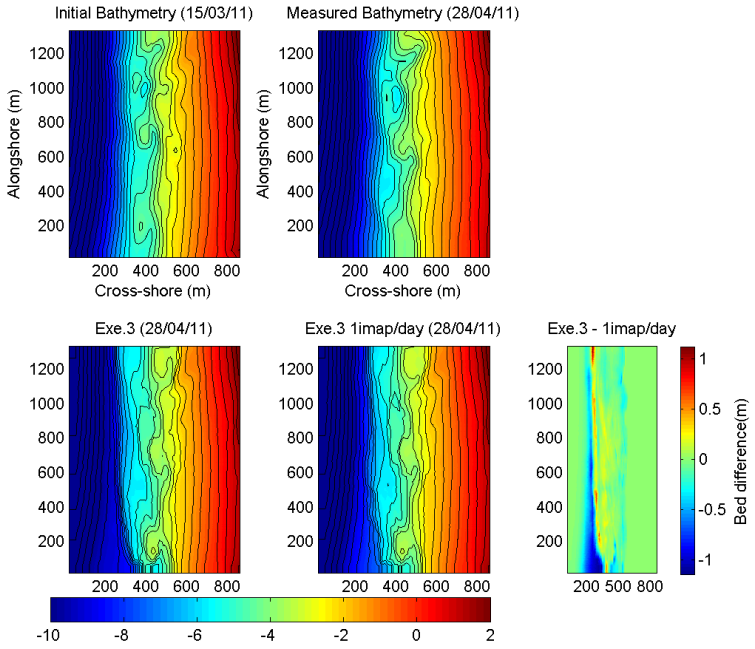

Figure 6-23. Resulting bathymetries using 1 imap per day. (Top) Measured bathymetries, initial (15/03/11) and current (28/04/11). (Bottom Left) Modelled bathymetry using all imaps (28/04/11). (Bottom centre) Modelled bathymetry using 1 imap per day (28/04/11). (Bottom right) Difference between modeled bathymetries with all imaps and with 1 imap per day.

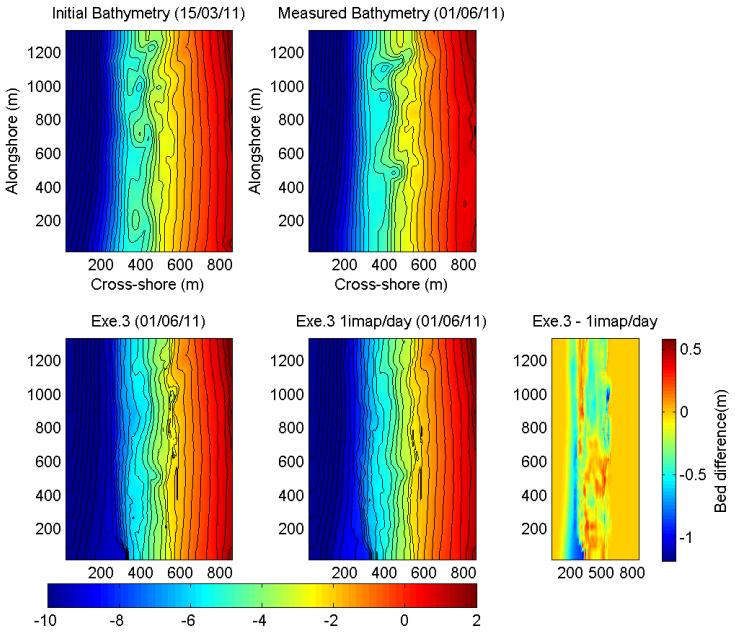

Figure 6-24. Resulting bathymetries using 1 imap per day. (Top) Measured bathymetries, initial (15/03/11) and current (01/06/11). (Bottom Left) Modelled bathymetry using all imaps (01/06/11). (Bottom centre) Modelled bathymetry using 1 imap per day (01/06/11). (Bottom right) Difference between modeled bathymetries with all imaps and with 1 imap per day.

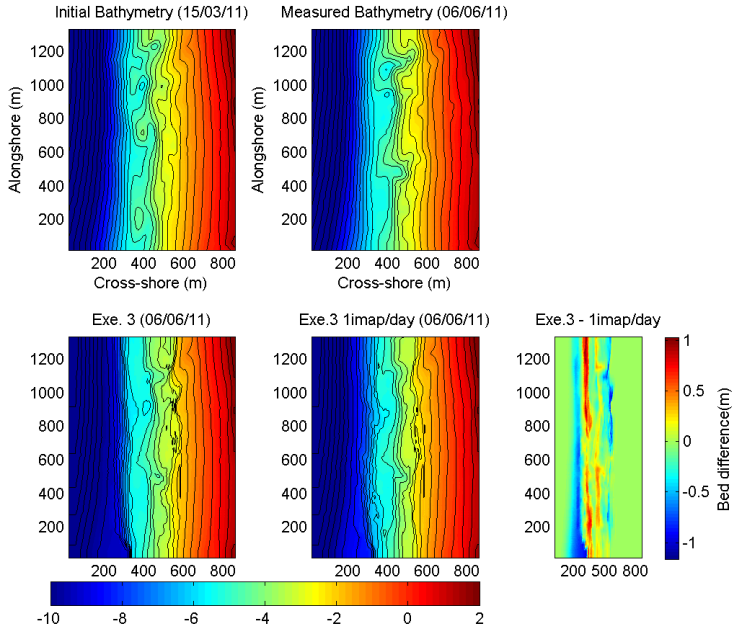

Figure 6-25. Resulting bathymetries using 1 imap per day. (Top) Measured bathymetries, initial (15/03/11) and current (06/06/11). (Bottom Left) Modelled bathymetry using all imaps (06/06/11). (Bottom centre) Modelled bathymetry using 1 imap per day (06/06/11). (Bottom right) Difference between modeled bathymetries with all imaps and with 1 imap per day.

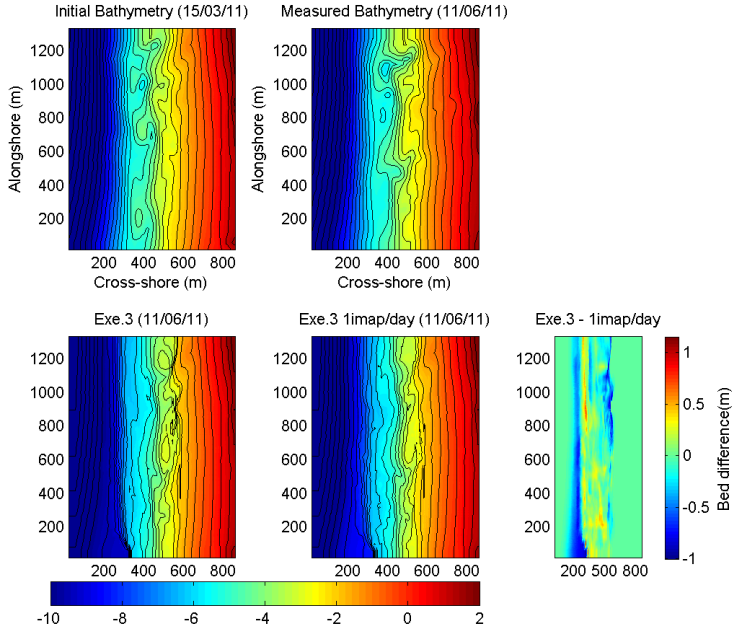

Figure 6-26. Resulting bathymetries using 1 imap per day. (Top) Measured bathymetries, initial (15/03/11) and current (11/06/11). (Bottom Left) Modelled bathymetry using all imaps (11/06/11). (Bottom centre) Modelled bathymetry using 1 imap per day (11/06/11). (Bottom right) Difference between modeled bathymetries with all imaps and with 1 imap per day.

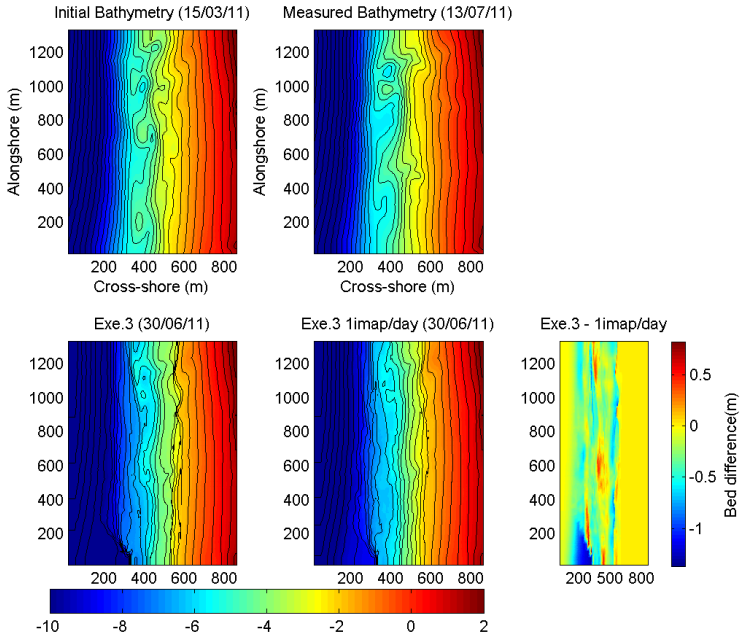

Figure 6-27. Resulting bathymetries using 1 imap per day. (Top) Measured bathymetries, initial (15/03/11) and current (13/07/11). (Bottom Left) Modelled bathymetry using all imaps (30/06/11). (Bottom centre) Modelled bathymetry using 1 imap per day (30/06/11). (Bottom right) Difference between modeled bathymetries with all imaps and with 1 imap per day.

Starting with the bathymetries estimated on the 28th of April (shown in Figure 6-23), it can be seen that there are no significant differences between using all available imaps and using a single imap per day (with respect to modeling the general morphological features present in the measured bathymetry on 28/04/11). The greatest difference seen between the two cases (shown in the mentioned figure) is the dark blue shown at around 300 m in –x and 0 m in –y in the difference plot, which as it has been recurrently mentioned in this report, is due to that particular area being out of the field of view of the Argus cameras, meaning there is no observed data there but there is computed data (generating a deepening of the bathymetry).

Figure 6-24 through Figure 6-27 show the resulting bathymetries from the 1st, 6th, 11th, and 30th of June. These resulting bathymetries show similar results as the previously described for the 28th of April, where little differences between the base case and using a single imap per day are noted. Using a single imap per day actually seems to show slight improvements over using all available imaps, particularly in the

bed elevations being closer to reality, but with the same shape in the contours of the main morphological features.

The effect of reducing the total amount of imaps used can be seen in the form of Brier skill scores on the estimated bathymetries, which are shown in Figure 6-28 through Figure 6-31. The calculation domains for the skill scores follow the regions defined in Appendix D.

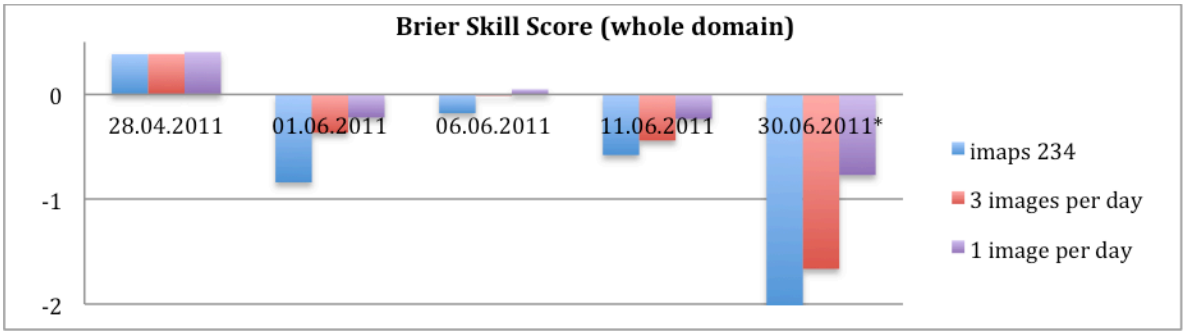

Figure 6-28. Brier Skill Scores over whole domain (excluding region below y=300m) for sensitivity on imap quantity, with (blue) all imaps, (red) 3 imaps per day, (purple) 1 imaps per day. *BSS calculated with modelled result on this date and measured bathymetry from 13/07/11.

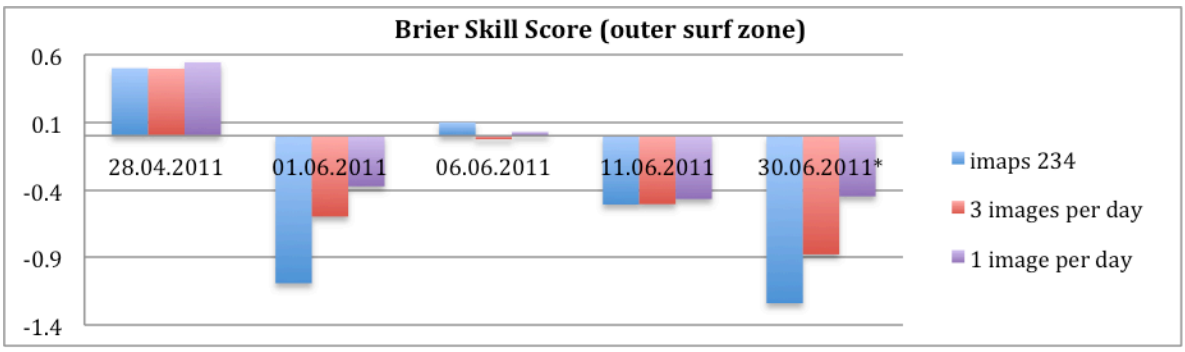

Figure 6-29. Brier Skill Scores for outer surf zone (x=250-450m, y=300-1340m) for sensitivity on imap quantity, with (blue) all imaps, (red) 3 imaps per day, (purple) 1 imaps per day. *BSS calculated with modelled result on this date and measured bathymetry from 13/07/11.

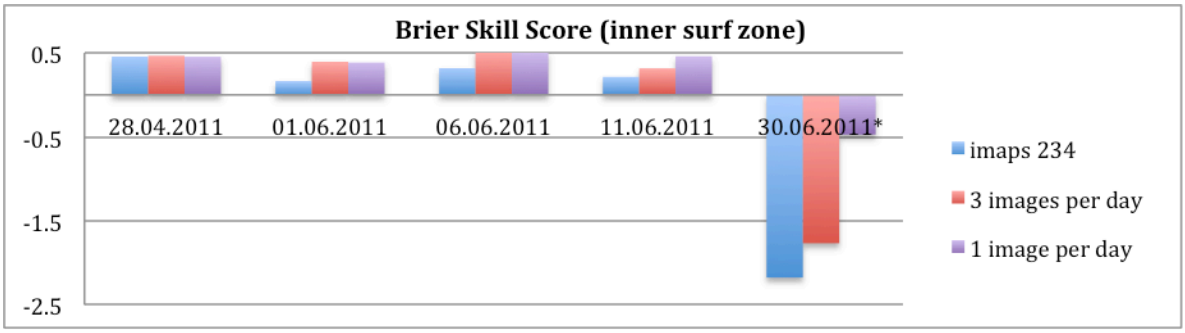

Figure 6-30. Brier Skill Scores for inner surf zone (x=450-600m) for sensitivity on imap quantity, with (blue) all imaps, (red) 3 imaps per day, (purple) 1 imaps per day. *BSS calculated with modelled result on this date and measured bathymetry from 13/07/11.

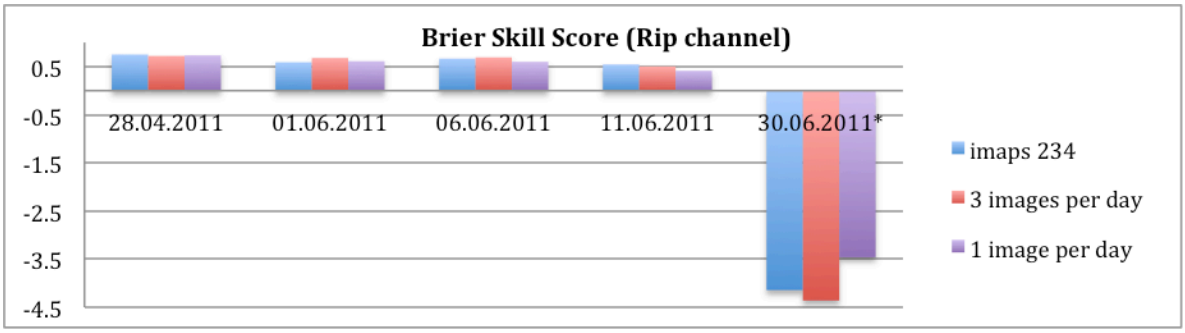

Figure 6-31. Brier Skill Scores for specific measured channel locations (Appendix D) for sensitivity on imap quantity, with (blue) all imaps, (red) 3 imaps per day, (purple) 1 imaps per day. *BSS calculated with modelled result on this date and measured bathymetry from 13/07/11.

The resulting skill scores calculated for the 28th of April show small variations between the two sensitivity runs and the base run, presenting values in the order of 0.5 for all cases and in all calculated domains. The skill of the case using a single image per day as input shows slightly improved results with respect to both the case using all imaps and the case using three imaps per day.

The results calculated on the 1st, 11th, and 30th of June also show an improvement in skill for both cases using less imaps as input. The results on these dates still show negative results for the calculations over the whole domain and in the outer surf zone, but with less negative values for the cases with reduced imaps.

The results for the inner surf zone and at each measured channel location show positive results on all dates (except for the 30th of June, which may be expected). On many of the calculated dates and over different error calculation domains, a trend of increased skill for decreasing number if imaps used per day was found. This result may turn out to be very useful in the future implementation of this system in an operational manner for the forecasting of rip currents, as it shows that a very extensive amount of images is not necessary to obtain the best estimated bathymetries. This will be further commented in the conclusions of this report.

6.4 Imap quality and limited forcing conditions

As it was mentioned previously, imap quality is different from image quality, in that the latter refers to the quality of the timex image, and the first refers to the quality of the imaps which takes into account the distribution of wave breaking, the presence of

rip currents, the tidal elevation, etc. In this chapter the importance of image quality has already been looked into, leaving the importance of imap quality to be looked at here. The present section of this report shows the results obtained by manually choosing "good" imaps as well as two test cases in which the used input is restricted by a limiting wave height and period.

6.4.1 *Imap quality*

Considering the manner in which the Beach Wizard bed update scheme functions, (where local differences in wave dissipation are the main driving force) it may be reasonable to believe that in order to reproduce rip channel morphologies, the imaps used as input should ideally show no wave dissipation over the channel areas. This was not the case in the majority of the timex images during the study period, where many of the obtained dissipation maps showed very little signs of the present rip channels. For this reason, a manual selection of imaps is carried out, in which the ones that present clear alongshore variations in wave dissipation at the location of the rip channels are chosen, and making sure that the dissipation presented in the imaps is consistent and representative of the dissipation observed in the corresponding timex images. It is important to make clear that imap and image quality are not linked together, meaning that in the upcoming model run using manually selected "good" imaps, the qualitative rankings of the images are varied (2, 3 and 4) and not necessarily only ranked 4. The wave and tide conditios for the selected imaps to be used in testing the importance of imap quality are shown in Figure 6-32, where the red marks correspond to each selected imap.

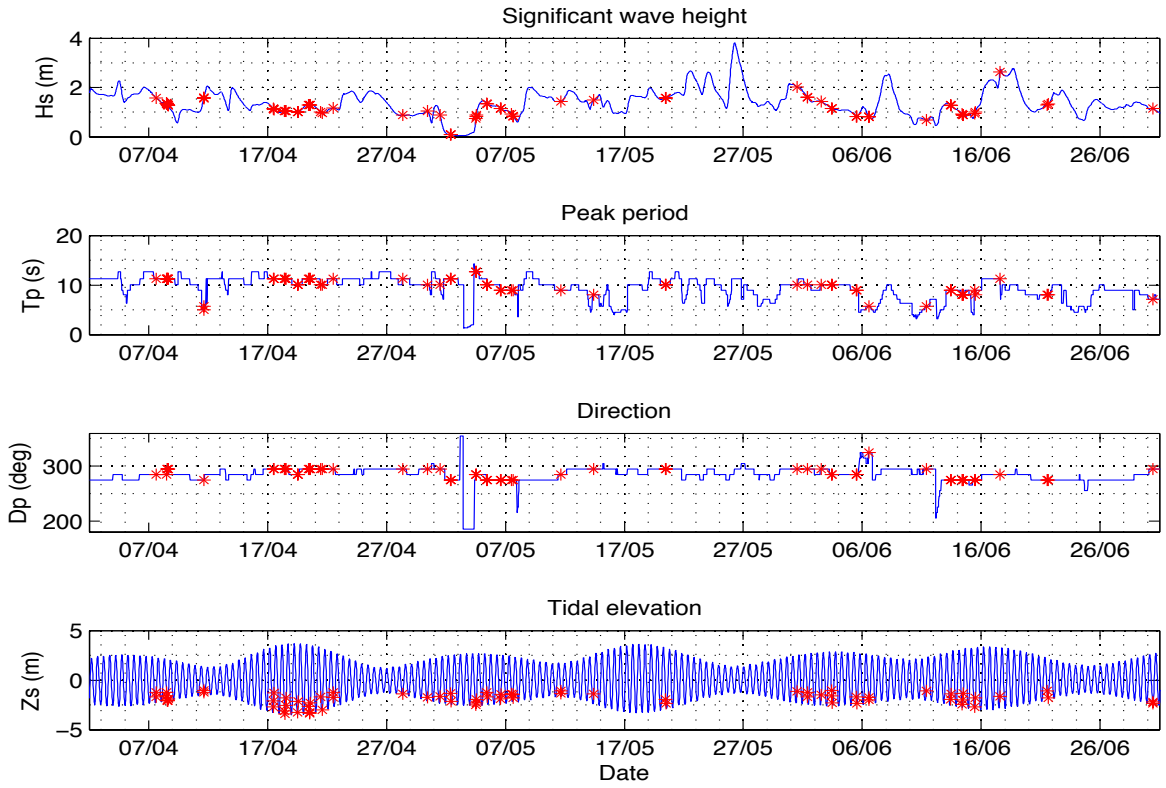

Figure 6-32. Wave and tide forcing and imaps marked with red asterisks for sensitivity run on imap quality, by manually selecting "good" imaps.

Similarly to some of the previous runs, the spacing of used imaps shown in Figure 6-32 presents large time gaps around neap tides, particularly around the neap tide at the end of May and at the end of June for this case. The time between consecutive imaps is particularly long at the end of may, where there is no chosen imaps between the 20th and the 31st of May. The mentioned manual selection of "good" imaps resulted in a total of 71 imaps, of which 29 are from the month of April, 19 from May, and 23 from June. This reduction in imaps results in the use of approximately 20% of the total available amount of imaps. In the previous sections it was determined that the actual quantity of imaps used does not reduce the skill of the model in predicting bathymetries, however, the temporal spacing between consecutive imaps has shown to produce problems. A point of interest in this section is to determine if large gaps between images will affect the model negatively even if said images correspond to the best possible imaps (in the sense that the dissipation represents the main morphological features well). Figure 6-33 through Figure 6-37 show the resulting bathymetries for the presently described sensitivity case.

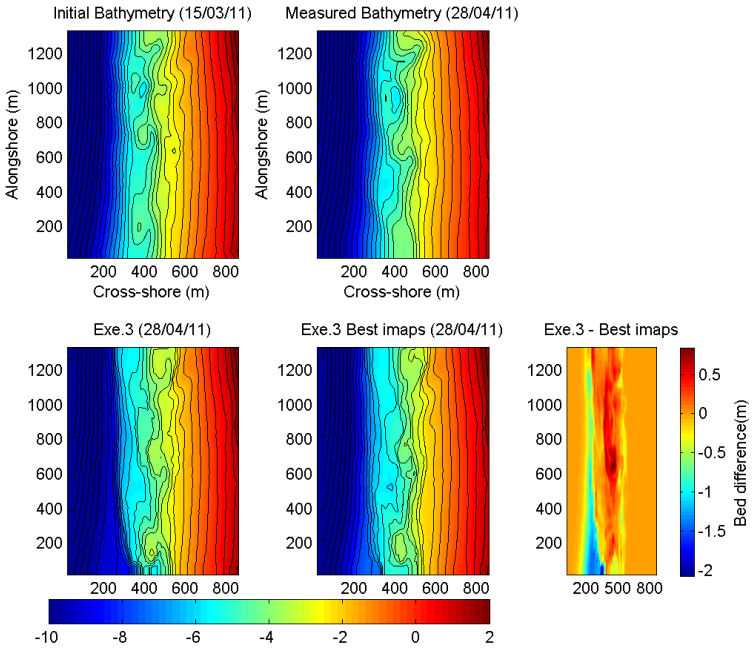

Figure 6-33. Resulting bathymetries for hand selected good imaps. (Top) Measured bathymetries, initial (15/03/11) and current (28/04/11). (Bottom Left) Modelled bathymetry using all imaps (28/04/11). (Bottom centre) Modelled bathymetry using best imaps (28/04/11). (Bottom right) Difference between modeled bathymetries with all imaps and with best imaps.

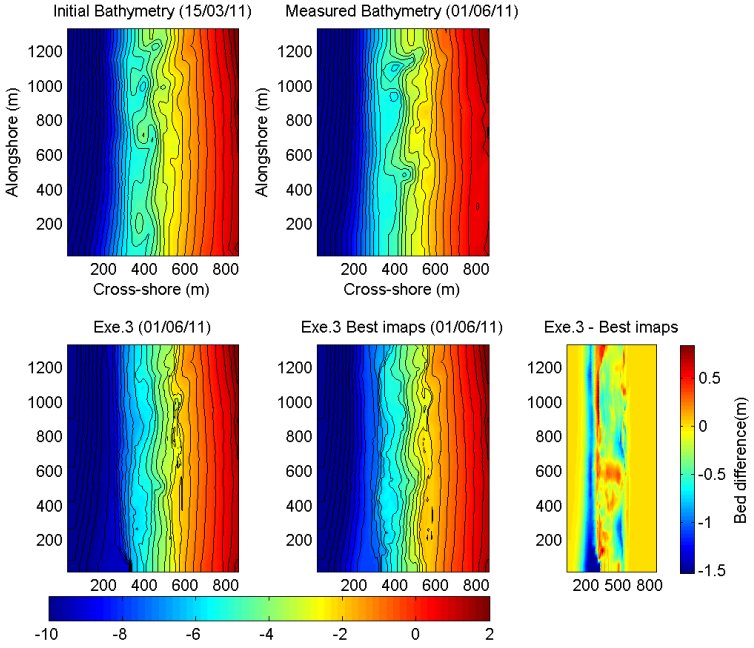

Figure 6-34. Resulting bathymetries using 1 imap per day. (Top) Measured bathymetries, initial (15/03/11) and current (01/06/11). (Bottom Left) Modelled bathymetry using all imaps (01/06/11). (Bottom centre) Modelled bathymetry best imaps (01/06/11). (Bottom right) Difference between modeled bathymetries with all imaps and with best imaps.

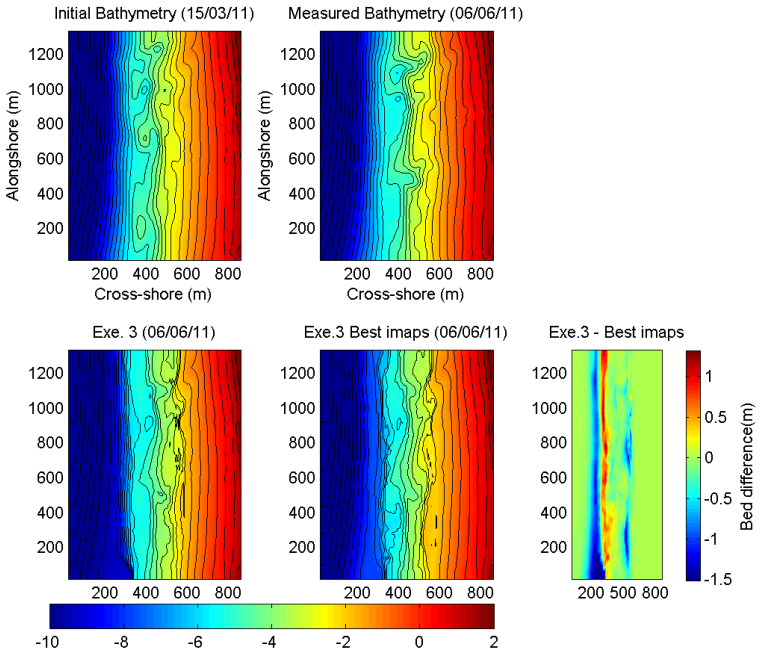

Figure 6-35. Resulting bathymetries using 1 imap per day. (Top) Measured bathymetries, initial (15/03/11) and current (06/06/11). (Bottom Left) Modelled bathymetry using all imaps (06/06/11). (Bottom centre) Modelled bathymetry best imaps (06/06/11). (Bottom right) Difference between modeled bathymetries with all imaps and with best imaps.

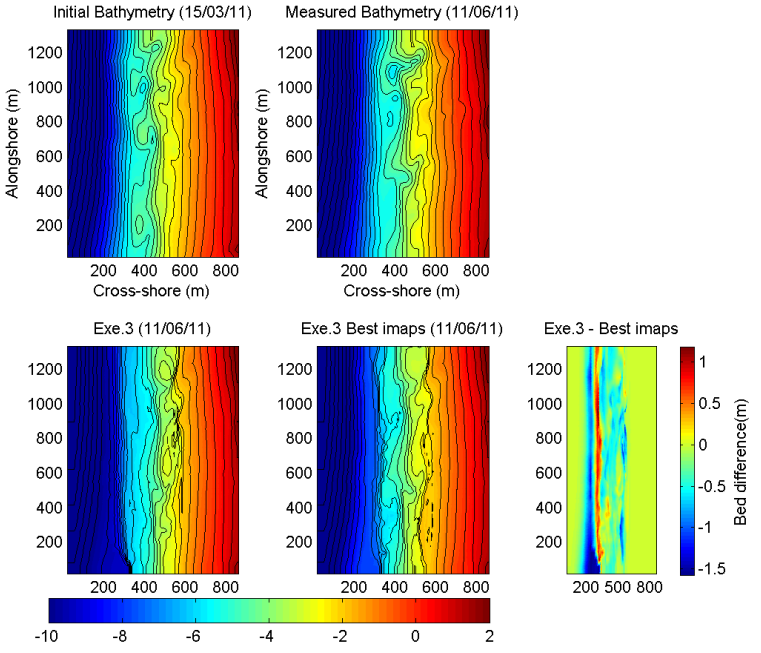

Figure 6-36. Resulting bathymetries using 1 imap per day. (Top) Measured bathymetries, initial (15/03/11) and current (11/06/11). (Bottom Left) Modelled bathymetry using all imaps (11/06/11). (Bottom centre) Modelled bathymetry best imaps (11/06/11). (Bottom right) Difference between modeled bathymetries with all imaps and with best imaps.

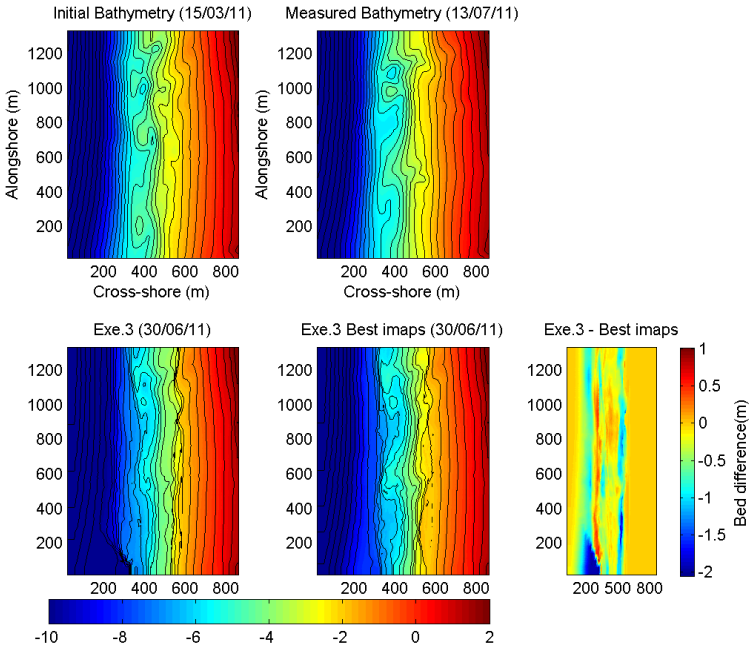

Figure 6-37. Resulting bathymetries using 1 imap per day. (Top) Measured bathymetries, initial (15/03/11) and current (13/07/11). (Bottom Left) Modelled bathymetry using all imaps (30/06/11). (Bottom centre) Modelled bathymetry best imaps (30/06/11). (Bottom right) Difference between modeled bathymetries with all imaps and with best imaps.

By visually assessing the modeled bathymetries on the 28th of April (Figure 6-33), a reduction in the predictive ability of the model is seen for the case where the "best" imaps are used. This is seen where in the bathymetry plots the general form of the contour lines are less representative of the real measured contour lines than the base case (using all imaps). Both of the main channels are less pronounced, and the large transverse bar at y=700 m is also lacking in definition. This might be due to the elimination of several imaps around the neap tide at the end of April.

The calculated bathymetries in the month of June show the opposite to what was observed on the 28th of April, namely an improvement in the calculated bathymetries when using the "best" imaps. The results on the 1st of June do not present very much change with respect to the base case, except for a slightly smoother shoreline, and a slightly less pronounced channel at y=500 m (Figure 6-34). The estimated bathymetry on the 6th of June presents very slight differences near the shoreline, and a lower offshore bar at around x=350 m, seeming like an overall improvement over the base case.

The results on the 11th of June (Figure 6-36) show a more notable improvement over the base case, with smoother shoreline features, and a more protruding transverse bar at y = 600 m. Similar to this, the estimated bathymetry on the 30th of June (Figure 6-37) shows a significant improvement over the base case, particularly in the representation of the transverse bar at y = 600 m, as well as a smoother transition between the shoreline and the surf zone (x = 500-600 m).

The resulting Brier skill scores for the case using the "best" available imaps are presented Figure 6-38 through Figure 6-41 in the upcoming section, alongside the results of the two cases that will now be described.

6.4.2 *Limiting forcing conditions*

From an operational point of view, it would be ideal to be able to define some limiting forcing conditions with which to choose the images to be used as input for the Beach Wizard model. Since it was found in the previous section that the quality of imaps is more important than the quality of images, the ability to systematically choose "good" imaps would be a very good addition to the model capabilities. This would be something that would most likely not be able to be widely applied, in the sense that it would have to be calibrated for different beaches, since different beaches will have different behaviors for different wave and tide conditions. However, the idea that a limiting wave height, period, direction, and/or tidal elevation can be defined to essentially eliminate images that will not represent the channels or other important morphological features should be looked into.

Given the fact that waves with higher periods will generally have higher probabilities of presenting rip currents, a limiting peak period will be defined in this section, where only periods above 7.5 s will be used. This was also somewhat noticed in the previous section, where the majority of the manually selected "good" imaps corresponded to days with long period waves (Figure 6-32). The other test that will be shown in this section corresponds to a run with a lower boundary limiting wave height of 85 cm. This is tried due to an observation that was found when running the first test cases during the present master thesis work, which was that for small waves more problems with the prediction at the shoreline (digging) arise, due to the waves

presenting shore-breaking rather than breaking on the outer bars. Due to time constraints, only these two simulations with limited forcing conditions were carried out, however, it is recommended to further investigate the possibility of defining functional limiting conditions.

The resulting bathymetries for the two cases using imaps chosen based on limited forcing conditions will not be presented here as bathymetry plots, since it is considered sufficient to briefly describe the observed results and present them in the form of calculated Brier skill scores. What was observed by restricting the imaps based on a wave height limit of 85 cm was a reduction in predictive ability, although for the 28th of April this reduction was extremely small (due to the fact that there were very few instances during April with wave heights below 85 cm). The observed differences concentrated mainly around the shoreline area, generally showing bed elevations that are too low with respect to the corresponding measured bathymetries.

The results obtained in the case where imaps were chosen based on a limiting peak period of 7.5 s showed similar results to the ones obtained from using a limiting wave height of 85 cm. The main observation is an under prediction of the bed level near the shoreline, and less accuracy in reproducing the general form of the main morphological features.

The BSS calculated for the two cases with limiting forcing conditions are presented in Figure 6-38 through Figure 6-41, alongside the skill scores calculated for both the base case and the case described in the previous section of this report (using the best quality imaps).

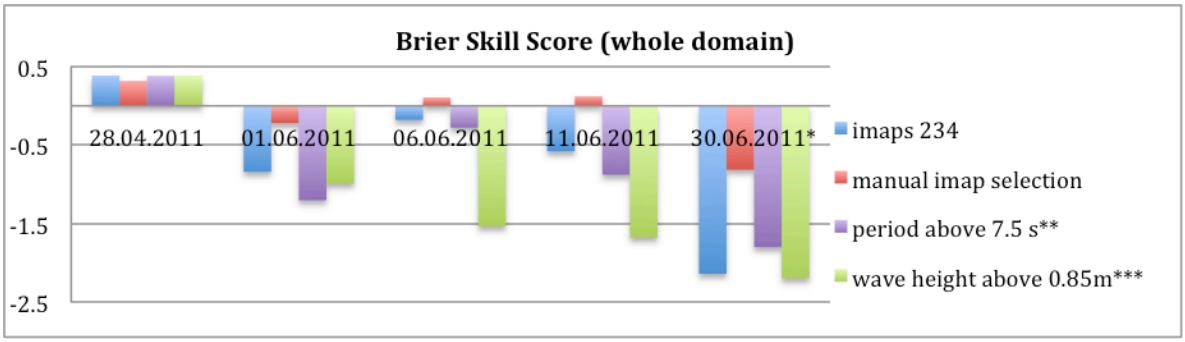

Figure 6-38. Brier skill scores over whole domain (excluding region below y=300m) for sensitivity on imap quality (manual imap selection) and limiting forcing conditions. *BSS calculated with modelled result on this date and measured bathymetry from 13/07/11. ** No imaps available on 06/06/11, 11/06/11 or 30/06/11; 05/06/11, 13/06/11, and 29/06/11 used instead. * No imaps available on 06/06/11 or 11/06/11; 07/06/11 and 09/06/11 used instead.**

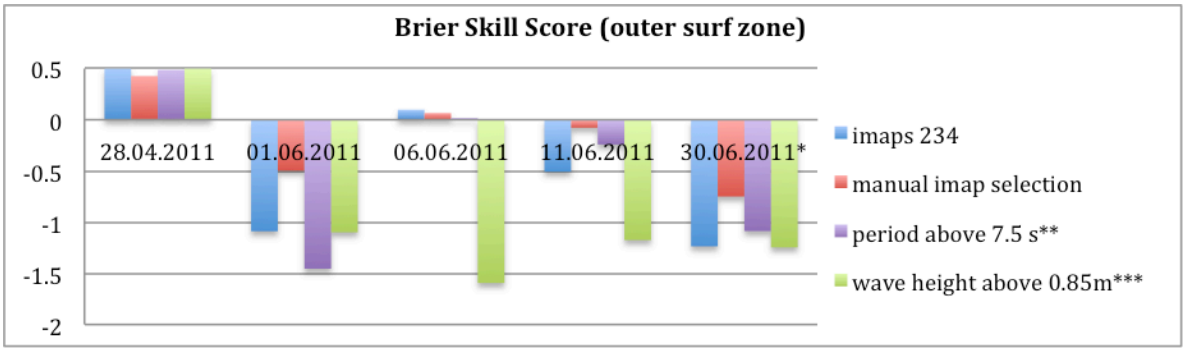

Figure 6-39. Brier skill scores on outer surf zone (x=250-450m, y=300-1340m) for sensitivity on imap quality (manual imap selection) and limiting forcing conditions. *BSS calculated with modelled result on this date and measured bathymetry from 13/07/11. ** No imaps available on 06/06/11, 11/06/11 or 30/06/11; 05/06/11, 13/06/11, and 29/06/11 used instead. * No imaps available on 06/06/11 or 11/06/11; 07/06/11 and 09/06/11 used instead.**

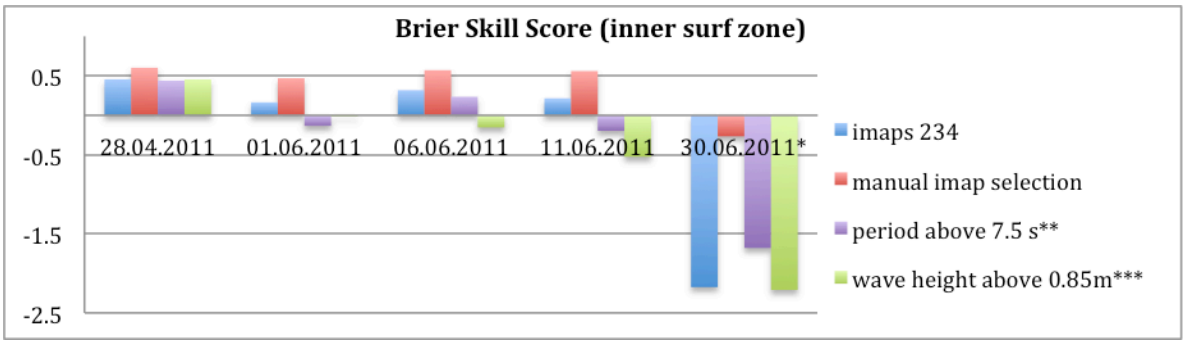

Figure 6-40. Brier skill scores on inner surf zone (x=450-600m, y=300-1340m) for sensitivity on imap quality (manual imap selection) and limiting forcing conditions. *BSS calculated with modelled result on this date and measured bathymetry from 13/07/11. ** No imaps available on 06/06/11, 11/06/11 or 30/06/11; 05/06/11, 13/06/11, and 29/06/11 used instead. * No imaps available on 06/06/11 or 11/06/11; 07/06/11 and 09/06/11 used instead.**

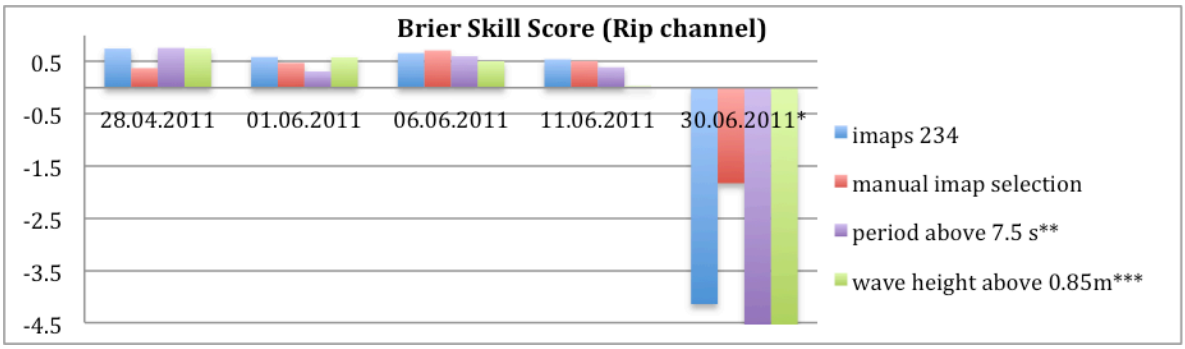

Figure 6-41. Brier skill scores at measured channel locations (Appendix D) for sensitivity on imap quality (manual imap selection) and limiting forcing conditions. *BSS calculated with modelled result on this date and measured bathymetry from 13/07/11. ** No imaps available on 06/06/11, 11/06/11 or 30/06/11; 05/06/11, 13/06/11, and 29/06/11 used instead. * No imaps available on 06/06/11 or 11/06/11; 07/06/11 and 09/06/11 used instead.**

The above presented Brier skill scores confirm what was described in the two previous sections of this report. What can be seen from the calculated BSS is that the

case using manually selected "good" imaps shows an increase in skill, while both the cases with limiting wave conditions generally present a reduction in model skill. For all three cases, very little variation is seen on the 28th of April, and this is attributed to the fact that April had many "good" imaps and relatively uniform wave conditions with long periods and wave heights higher than 1 m.

The resulting BSS over the whole domain for the manually selected "good" imaps case on the 6th and 11th of June present positive results, which can be looked at as a significant improvement over the base case which presents negative values. The case with manually selected "good" imaps also presents positive BSS over the inner surf zone for all dates except for the 30th of June, however, the BSS value on the 30th of June is quite small, and significantly better than the base case result.

In summary, it has been determined that the quality of imaps is quite important, and were able to obtain good estimations of bathymetry even though some large gaps were present between consecutive images at the end of May and at the end of June. As well as this, it was found that the imposed restrictions in wave height and period were not helpful in estimating bathymetries, however, varying the imposed limits might eventually lead to better results.

6.5 Overall results comparison

As to sum up all of the obtained results using different sets of images as input, here a brief summary presenting the obtained Brier skill scores is shown and discussed. Figure 6-42 through Figure 6-45 show the calculated BSS for all domain regions (as defined in Appendix D) and all imaps sensitivity runs.

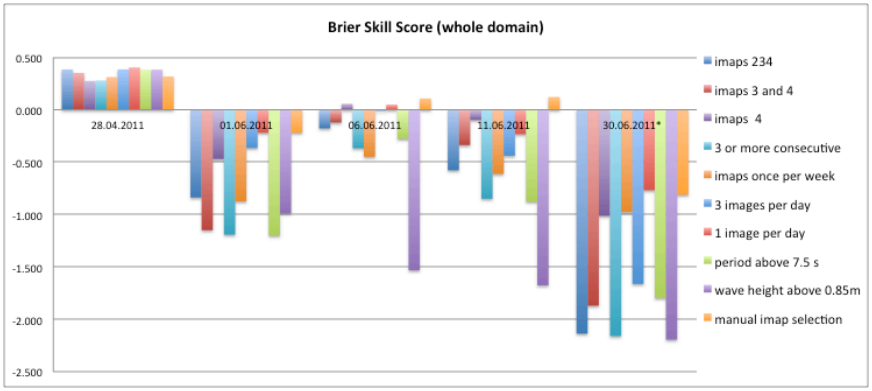

Figure 6-42. Brier skill scores calculated over the whole domain (excluding region below y=300m) for all imap sensitivity runs.

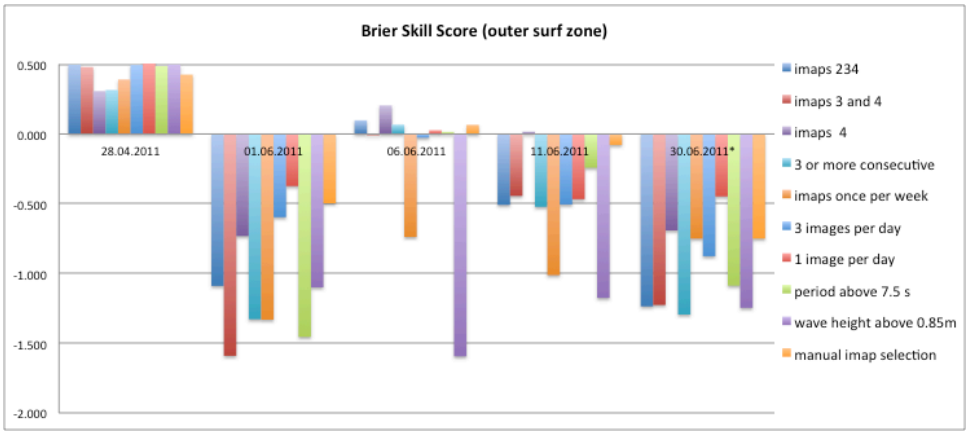

Figure 6-43. Brier skill scores calculated over the outer surf zone (x=250-450m, y=300-1340m) for all imap sensitivity runs.

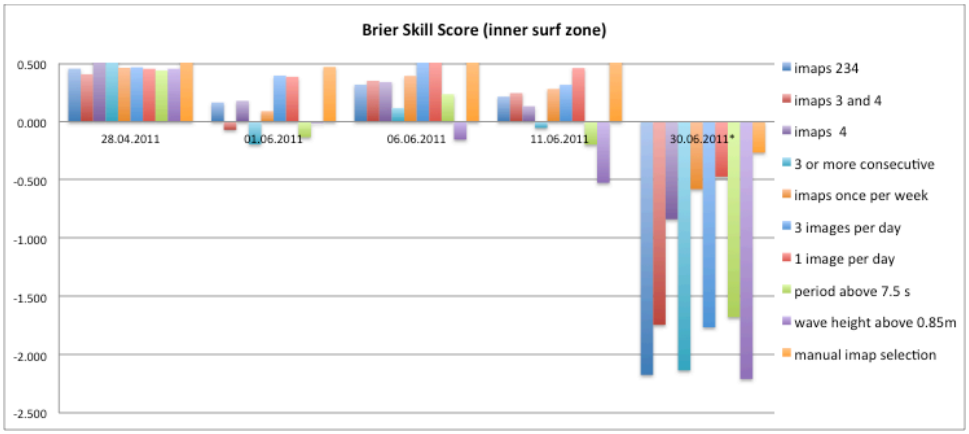

Figure 6-44. Brier skill scores calculated over the inner surf zone (x=450-600m) for all imap sensitivity runs.

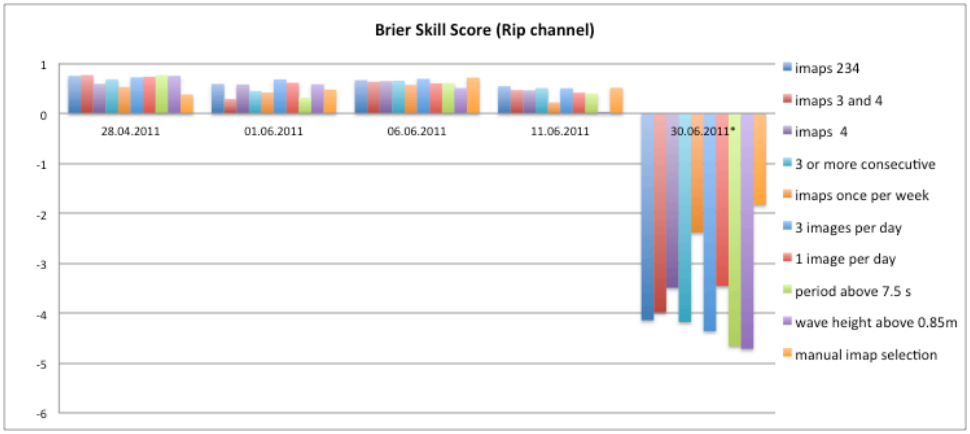

Figure 6-45. Brier skill scores calculated at specific rip channel locations (locations defined in Appendix D) for all imap sensitivity runs.

The first observation that can be made from the previous graphs is the fact that the results on the 28th of April seem less influenced by the variations in imaps used as input. This is due however to the fact that all of the BSS values on that date are positive, and given the formulation of the BSS (Equation 27), positive values have a maximum of 1 while negative values do not necessarily have a limit (if the difference between the initial and the measured bathymetry is zero then the BSS tends to -∞). This means that the same difference in RMS error will produce a smaller change in BSS if this value is positive rather than if it were negative.

The next observation that can be made is the variation in the BSS calculated for the different regions of the domain (whole domain, outer surf zone, inner surf zone, and measured channel locations). What these variations show is that the model provides better predictive skill in the nearshore zone and at the measured channel locations than over the whole domain or over the outer surf zone. The reason for this is that in the inner surf zone the majority of the major morphological features are present (part of the channels and transverse bars), therefore if the model is able to slightly resemble the general shape of the coastline, channels and transverse bars, then the resulting BSS will likely be positive. The same applies for the scores calculated at measured channel locations, given that the location of the channel on the initial bathymetry (15th of March) was several hundred meters to the north of the average location of the channel in April, May and June, then any reproduction of the channel in the correct measured location will be an improvement over the initial bathymetry (giving a positive BSS value).

After comparing all of the above presented BSS, it can be said that the cases that affect the model outcome most negatively are the cases which reduce the regularity of imaps (imaps used once per week, and days with two or less imaps removed) and the case which limits the wave height to 85 cm. As well as this, the results show that the scores for the cases with "good" images do not tend to significantly improve the model results overall, in some case actually reducing the skill. The cases that produced the best model skill are the case that used a single image per day, and the case where the best imaps were selected manually.

An additional model run was carried out which was not mentioned in this chapter, corresponding to a run using a longshore uniform flat bed as the initial bathymetry instead of using the measured bathymetry from the 15th of March 2011. This was carried out to determine the dependence of the modeled bathymetry on the initial bathymetry, but as it was not necessarily one of the objectives of the present thesis, it was not mentioned previously in this chapter. Said model run used a single imap per day as input (the same configuration as the case described in the previous sections) along with a flat bathymetry that was obtained by interpolating a straight line between the depth at x=600 m and x=250 m (maintaining the region outside x=200-600 m the same as the measured bathymetry on 15/03/11) and making it alongshore uniform. The resulting bathymetries from this configuration were very close to the results obtained with the same set of imaps and a measured initial bathymetry, showing variations in RMS error between these two in the order of centimeters (+/- 5 cm). This is a good result in that it demonstrates the models capability of producing good bathymetries without the need of having any measured bathymetries at all. The calculated BSS and RMS are presented in Appendix C-3.

6.6 Conclusions and Recommendations

The objective of the present chapter was to investigate the importance of a series of factors related to the video-derived input used in the Beach Wizard data-model assimilation process for the estimation of nearshore bathymetries. Specifically, these factors are the importance of image and intensity map quality, the importance of image spacing and frequency in time, and the importance of quantity of images used as input (all with respect to the model's ability to reproduce accurate bathymetries). The conclusions and recommendations presented here will be further elaborated on in the following chapter, which looks at the importance of these factors with respect to the modeling of rip currents using the estimated bathymetries, rather than simply analyzing the bathymetries themselves as is done in this chapter.

6.6.1 *Conclusions*

During the three month study period (April, May, and June 2011) two distinct periods were found, during which the skill of the model in estimating bathymetries varied. The first period corresponds to the month of April, which presents very regular wave conditions, characterized by long period swell waves; the second period covers the months of May and June during which various storm events are seen with highly varied wave heights, periods and directions. The skill of the model is consistently higher for the month of April than the months of May and June, possibly meaning that the varying wave conditions between these two periods is responsible for this differentiation.

The importance of imap quality was found to be more significant than image quality, meaning that in order to reproduce real bathymetries accurately it is more important to have good wave and tide conditions to obtain the best possible dissipation maps rather than having perfect image quality (clean lens, no sun glare, no fog, etc.). It was found that even if a certain image did not present perfect resolution or quality (maybe presenting a blurry patch or a streak through the image) it was still possible for the resulting intensity map produced with that image to have a positive effect on the predictive ability of the model.

Having a single image per day was found to be more useful than having many images in a single day once a week. What can be concluded from this is the importance of image frequency, implying that ideally large spaces in time (more than 3 days) with no images should be avoided, and having an image per day (even if it is not a perfect image) should improve the model results.

The impact of image quantity was found to be very low (as long as the frequency of available images is maintained at its maximum), due to the majority of the total bed change that occurs in a single day (over several images) being directly attributed to the first image in that day. This effect is again due to the increase in uncertainty between simulations, which is much larger from one day to the next (and increases significantly with increasing number of days between consecutive simulations) than if two consecutive simulations are only a few hours apart.

In manually selecting the best available dissipation maps to be used as input, it was found that it is possible to improve the model skill in this manner, and to some extent reduce the problems that arise when large temporal gaps with no available images are found. This means that a decision must be made whether it is easier to manually select the best possible imaps available (quite possibly eliminating entire days) or to choose a single best daily imap. From an operational point of view it is likely more convenient to select the best daily imaps and continually keep running the model, in this way reducing the large uncertainty increments that appear when there are several days with no images available and still have a certain degree of manual selection of "good" imaps.

6.6.2 *Recommendations*

The main recommendation for future work to be done with the ultimate goal of obtaining an operational model with as little necessary human interference as possible is in the selection process of imaps to be used as input. In the present thesis it was attempted to select the images to be used as input using a limiting wave height and period, however, due to time constraints this could not be tested in much detail. Given that the imap quality turned out to be one of the major factors influencing the quality of the estimated bathymetries, it is thought that the linking of imap quality with factors such as wave conditions, water levels, weather conditions, etc., would be of great use. Since what determines the quality of an imap is largely influenced by the kind of wave dissipation and the presence of rip channels and clear bar locations in the timex image, then it might be thought that a link between imap quality and the above mentioned conditions should be achievable.

The modification of the merging process of the individual timex images should be looked into, with the objective of solving the merge problem recurrently seen between the edges of camera 1 and camera 2's fields of view. This problem in image merging greatly reduced the amount of available good timex images, since for water levels higher than -1 m very few images were considered usable. Fixing this issue would allow for the use of images during neap tides, consequently eliminating the large gaps between consecutive images that were found around these dates.

7 RIP CURRENT MODELLING USING VIDEO-DERIVED BATHYMETRIES

In this section, hydrodynamic model computations are carried out using both the estimated bathymetries (using Beach Wizard) and the measured bathymetries in order to determine whether or not the estimated bathymetries are close enough to reality as to reproduce the nearshore flow conditions accurately. The comparison and quantification of the resulting rip current flows can be considered as a secondary model skill test alongside the previously calculated Brier skill scores on bathymetries. The idea behind this is that if an estimated bathymetry in fact presents the correct general patterns (even though it might present slight errors and sharper features) the resulting flow patterns over the bathymetry should to some extent replicate the flows over a real bathymetry. The utility of using rip current flows as a proxy for modeled bathymetry skill estimations lies in that using a skill test such as the Brier skill score may not necessarily show good results when considering overall shapes and patterns rather than total bed differences. The Brier skill score considers point-by-point differences in bed elevation, which means that it doesn't consider shapes or patterns in bathymetry. Because of this, even if an estimated bathymetry presents a clear improvement in shoreline shapes, channel and bar locations, etc., it will not produce a good Brier skill score if the total difference in bed elevation between the estimated and measured bathymetry is at all larger than the total difference between the initial and measured bathymetry.

The goal of the present chapter is then to determine whether or not updating bathymetries using Beach Wizard offers an improvement in accurately modeling rip currents over using an outdated measured bathymetry for said predictions. The effects of varying image input configurations (as described in the previous chapter) will also be looked at, ultimately quantifying the effects of said variations by means of rip current comparisons as opposed to direct bathymetry comparisons.

The contents of this chapter are comprised of firstly a description of the hydrodynamic model to be used along with the listing and justification of the model input configurations to be used (different estimated bathymetries obtained from the previous chapter); secondly a description of the criteria to be looked at regarding rip

current flows, considering a base case which will then be defined; and finally a comparison of the resulting rip current flows for all different tested bathymetries followed by the chapter's specific conclusions and recommendations.

7.1 Hydrodynamic model setup

The model to be used in this section is a non-stationary XBeach model, which was originally set up, calibrated, and validated for Perranporth beach by Austin et al. (in press). The model was calibrated and validated against measured Lagrangian and Eulerian current velocities, and was found to reproduce the rip current circulation patterns and velocities quite well. This finding will be the basis for the assumption made here, that is that if the current flows modeled on an estimated (with Beach Wizard) bathymetry resemble the flows modeled on a measured bathymetry, then the modeled flows over said estimated bathymetry are considered to indirectly resemble real flows under the same conditions.

In order to obtain comparable results, all model runs were forced with identical conditions. For this, the predicted tidal elevations from the 22nd of April 2011 are used along with the wave conditions obtained from the SWAN model for Perranporth (Austin et al. (in press)). In order to ensure that the wave fields are statistically identical in every simulation, the random number generator in XBeach was set to zero, in this manner reproducing the exact same wave field every time. The significant wave height of the chosen day is 1.37 m, and the tide is close to spring tide, ranging from -1.5 m at the start of the simulations down to -2.66 m half way through, and finally back up to -1.45 m at the end of the simulations. The simulations carried out have a duration of 4 hours, which was ultimately chosen as an acceptable length after having carried out a single 8 hour long run. The reason for carrying out a single 8 hour run was to determine the time during which rip currents are active at Perranporth, which was found to be approximately 4 hours or less, centered around low tide (which coincides with previous observations by Austin et al. 2009). With this, a 4 hour long simulation length was chosen for all cases, in this manner cutting down on model run time (by running for 4 hours in stead of 8) and enveloping the

period during which rip currents should be active. The model uses the "Roelvink_Daly" wave dissipation model with a the breaker parameter (beta) adjusted from its default to 0.05 (reduced slope on the roller surface).

The hydrodynamic model is run over a total of 6 measured bathymetries (15/03/11, 28/04/11, 01/06/11, 06/06/11, 11/06/11, and 13/07/11) and the modeled bathymetries on five of the 6 measured bathymetry dates (all except for the initial date on the 15/03/11) for 5 different Beach Wizard input configurations. The five Beach Wizard input configurations are the following, which follow the work carried out in the previous chapter and all use the best-obtained executable version (Exe. 3 with T_r=10 days).

- Base case: using all available imaps.
- 1 imap per day: to look at the importance of image quantity.
- Imaps once per week: to look at the importance of image input regularity or frequency.
- Imaps ranked 4: to look at the importance of image quality.
- Hand selected imaps: to look at the importance of imap quality.

These four Beach Wizard imap input configuration variations are considered to be the four cases that best describe the criteria (image quantity, quality, and frequency) set out to be analyzed in the previous chapter on image input sensitivity. In order to quantify the resulting rip current flows for the consequent comparison between the different cases and measured bathymetries, a set of criteria must be defined, and will be described along with an example case in the upcoming section.

7.2 Rip current flow quantification

Unfortunately no methods for easily quantitatively comparing flow patterns are currently available; therefore a series of criteria will be defined here for determining the skill in reproducing real nearshore flow patterns. From an operational point of view, the main points of interest to consider in describing rip currents can be seen as the following three points.

- Rip current strength

- Rip current location
- Rip current duration and timing

In other words, a good rip current forecasting system should be able to inform the user on when, where, and how strong a certain rip event will be. Similar to the reasoning in the previous two chapters, the skill of the Beach Wizard model will be seen as a comparative of the resulting rip current flows obtained using the modeled bathymetries and using the initial measured bathymetry from the start of the study period (15th of March 2011). This is to find whether or not using updated bathymetries for forecasting rip currents over the summer months shows any improvement over using a measured bathymetry from the beginning of the study period over the whole summer. With this in mind, several different velocity, location, and time variables will be quantified and rated with Brier skill scores (Equation 27) and RMS errors.

The process of rip current flow quantification that will be used will now be described using the base case bathymetry (resulting Beach Wizard bathymetries using all imaps as input) modeled on the 28th of April as a descriptive example. The process that will now be described is carried out for all five cases and all five analysis dates, resulting in an extensive amount of plots, figures and results to be looked at. Having said this, the plots for a single case and date will be shown, and finally all of the obtained results will be discussed and summarized in the form of BSS, RMS errors, and absolute magnitudes.

7.2.1 *Visual flow comparison and location*

The first step in the rip current quantification process involves the visual comparison of the absolute nearshore velocities over the measured and modeled bathymetries, and the definition of the rip current locations on each bathymetry. A single rip current location will be looked at for each bathymetry, being the one corresponding to the transverse bar and channel present approximately in the middle of the alongshore grid (the precise location varies for each date). Figure 7-1 shows the modeled flow results in the form of absolute 15 minute time averaged velocities, progressively advancing in time during the model simulations from top to bottom row. The red

asterisk in the figure marks the location of the maximum absolute rip current velocity on the measured bathymetry on the 28th of April, as to see more clearly the differences in location of the rip between the measured and modeled bathymetries.

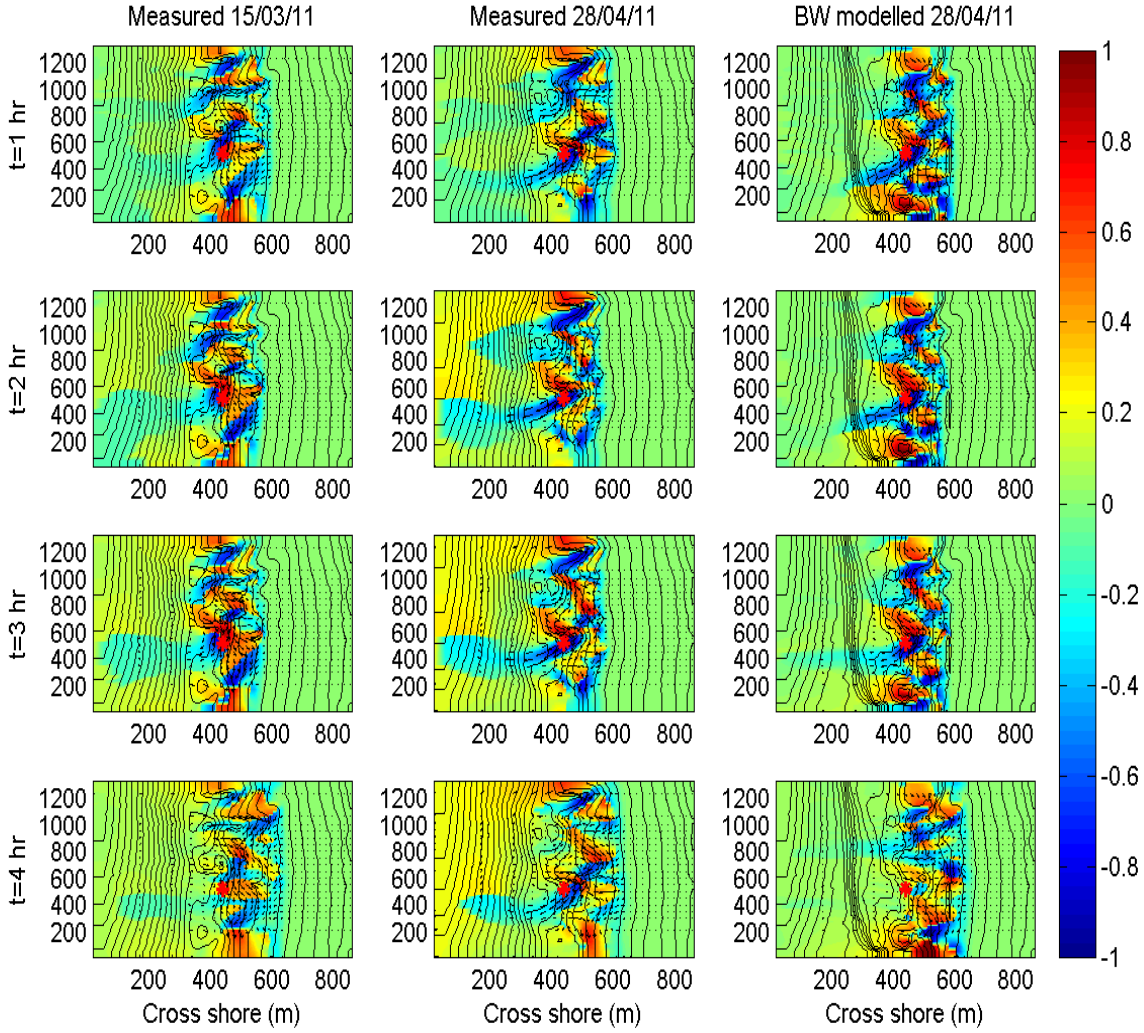

Figure 7-1. Plan view temporal evolution of rip currents. Advancing in time during simulation from top row to bottom row. Colour scale of absolute 15min time averaged velocities in m/s, where negative (blue) is with an offshore directed cross shore component and positive (red) an onshore directed cross shore component. (First column) Modelled flows over measured bathymetry on the 15th of March, (second column) modeled flows over measured bathymetry on the 28th of April, (third column) modeled flows over estimated bathymetry with base Beach Wizard input configuration. Red asterisk marks the location of the maximum rip current flow on the measured bathymetry on the 28th of April.

By comparing the three columns in Figure 7-1, it is clear that the flows over the measured and Beach Wizard bathymetry on the 28th of April show very similar features, with the main rip current (at approximately y = 500 m) appearing at very

similar locations with similar magnitudes as well. The column on the left shows the flows over the initial measured bathymetry (15th of March), and substantial differences between the flows on its date of measurement and the 28th of April (second column) can be seen.

The process of pinpointing the location of maximum flow velocities is done by manually defining a box that covers the bar/channel area on each measured date, and searching for the maximum absolute (with offshore directed cross shore component) velocity inside the region. The regions defined for the initial bathymetry (measured on 15th of March) and the measured and modeled bathymetry on the 28th of April are shown in Figure 7-2. It is clear from this figure that there is quite a spatial offset between the rip current locations on both measured bathymetry dates, and a very small spatial offset between the maximum rip location on the measured bathymetry and Beach Wizard modeled bathymetry (on the 28th of April).

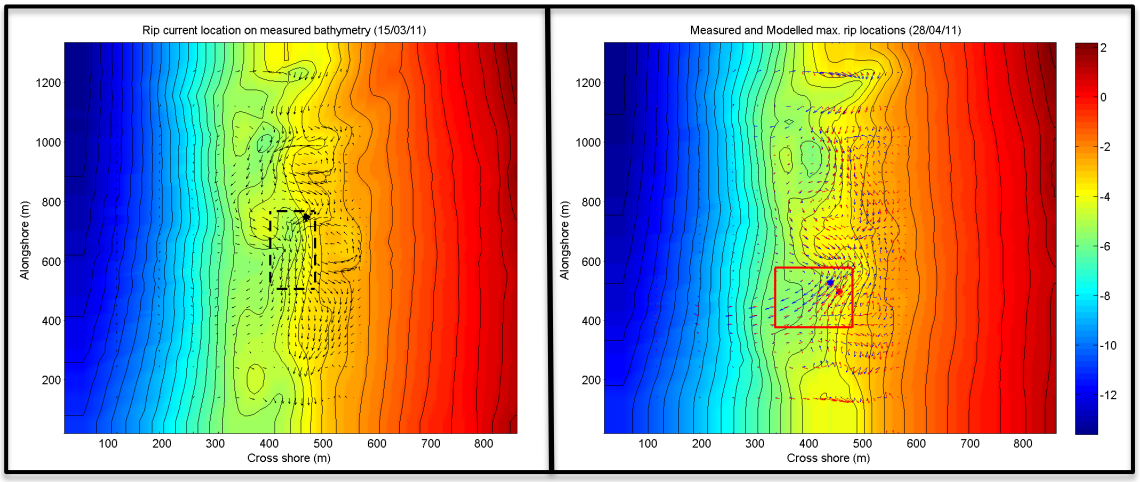

Figure 7-2. Rip current locations over measured bathymetries on 15th of March (left) and 28th of April (right). (Left) Rip channel location inside dashed black lines, maximum location at black asterisk, black arrows are absolute velocities. (Right) Rip location inside red lines, blue arrows are absolute velocities modeled with measured bathymetry and red arrows are absolute velocities modeled with Beach Wizard modeled bathymetry, blue asterisk is location of maximum "measured" rip current and red asterisk is location of "modeled" maximum rip current.

7.2.2 *Temporal modulation of rip current activity*

The temporal modulation of rip currents is quantified in two ways. What is sought out to be quantified here is the "peak" time and the duration of a given rip current event. In order to calculate these temporal indicators of rip current modulation, when a rip

current may be considered "active" must be defined as well as what velocity component will be used to describe the flow.

It was observed that for most of the analysis dates the mean (15-minute time averaged) cross shore component of the velocity at the time and location of the maximum absolute rip flow was quite small in comparison to the alongshore component. This is in part due to the maximum velocities generally being located close to the shoreline, where the alongshore feeder currents may be dominant, and as the flow moves offshore the crosshore component becomes dominant (however the absolute velocity is less as it moves offshore). Considering this finding, the rip current velocity to be used here in the analysis of the temporal modulation will be the absolute 15-minute time averaged velocities (offshore directed). These velocities are calculated as follows,

$$U_r = \sqrt{(u^2 + v^2)} \tag{30}$$

where U_r is the absolute rip velocity, u is the mean (15-min time averaged) cross shore (offshore directed) velocity component, and v is the mean (15-min time averaged) alongshore velocity component.

The "activation" of a given rip current will be defined as the time during which the absolute velocity is greater than $2/3$ of the maximum absolute velocity. This limit was defined based on the model results obtained on the measured bathymetries along with observations at Perranporth, which describe rip currents presenting themselves for a period of 3-4 hours centered around low tide. A limiting velocity of $2/3$ of the maximum velocity results in rip current durations generally between 3.5-4 hours, which coincides with field observations.

The "peak" time of a rip current is not simply defined as the time at which the maximum velocity is found, rather as the time corresponding to the weighted centre time of the activated rip current (following the above described definition of "activated"). The reason for using the weighted centre time as opposed to directly using the time of the maximum velocity is that in certain cases the velocity might go above the $2/3$ limit and then below and then back above it; so for the sake of providing a time around which a rip current could possibly present itself this

definition was found to be more suitable. The centre time is calculated as the centre of gravity of the velocity above 2/3 of the maximum absolute velocity, and uses the classical definition of centre of gravity as follows,

$$t_c = \frac{\int t * U_r dt}{\int U_r dt} \tag{31}$$

where t_c is the centre time, t is time and U_r is the absolute rip velocity above 2/3 of the maximum.

Figure 7-3 shows the temporal evolution of the maximum absolute rip velocity for the results using the initial measured bathymetry (black line), the measured bathymetry on the 28th of April (blue line), and the Beach Wizard-estimated bathymetry on the 28th of April (red line). The horizontal dashed lines are the 2/3 limiting velocity, the vertical lines are the centre time of each rip event, and the bottom portion of the figure shows the tide during the simulations.

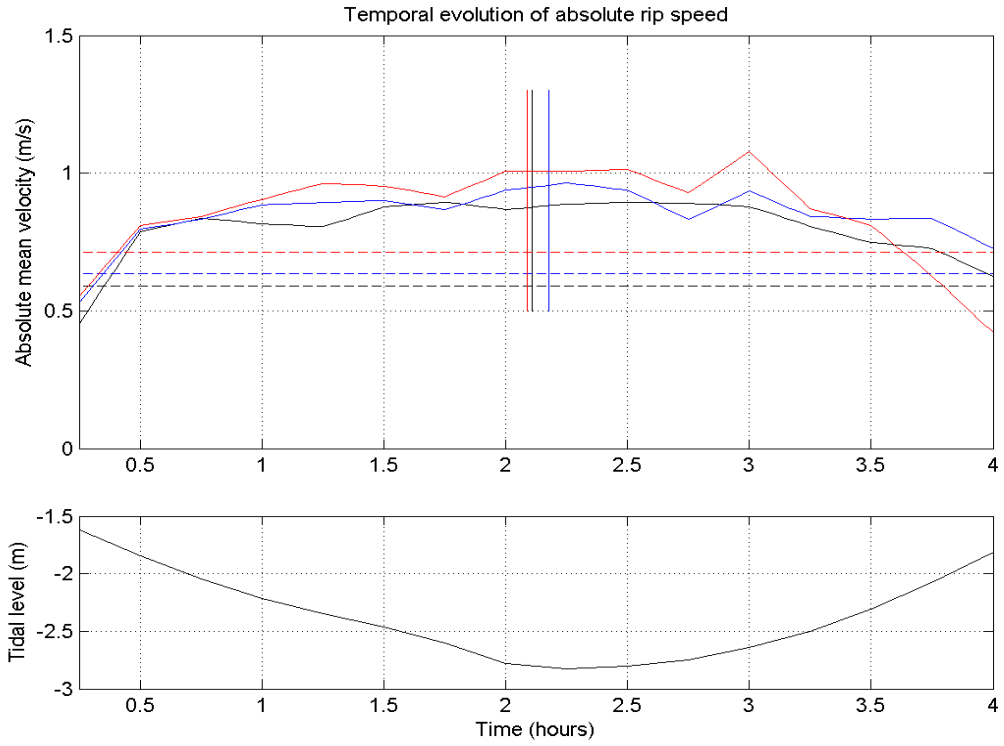

Figure 7-3. Temporal evolution of maximum rip current velocity for measured and modelled bathymetries. (Top) Maximum absolute 15 min time averaged velocities, black = from initial measured bathymetry (15/03/11), blue = from current measured bathymetry (28/04/11), red = from modeled current bathymetry (28/04/11); dashed lines = 2/3 of maximum velocities, vertical lines = center time of rip event. (Bottom) Tidal elevation.

Figure 7-3 shows very similar temporal evolution of the rip current for the three cases shown, as well as the fact that the rip current events are centered around low tide, with a duration of almost 4 hours.

7.2.3 *Rip current strength quantification*

For the quantification of rip current strengths, several different current velocities and components are analyzed. As it was mentioned previously, the main indicator to be used for rip current strength is the maximum absolute 15-minute time averaged velocity. This velocity however may not be a good representation of total rip current strength if only the maximum is analyzed, due to the possibility of a modeled velocity coming very close to the measured velocity for only a very short period of time during the time window of the rip current. For this reason, the average of said velocity over the time window of each rip current event will also be looked at, in this way quantifying the total rip event and not only an instantaneous maximum velocity.

In order to also remove the variable of direction from the velocities, cross shore components are also considered. With this task in mind, several measures of cross shore velocity were analyzed, ultimately deciding that the most representative measure of cross shore velocity for this purpose is the maximum (over 15-minute intervals) cross shore velocity at the location of the maximum absolute 15-minute time-averaged velocities. The reason for using maximum cross shore velocities rather than mean (15-minute time-averaged) cross shore velocities is that the latter tend to present very low values at the specific location of the maximum absolute velocities, while the maximum cross shore velocities present reasonable magnitudes at these locations.

Figure 7-4 presents the maximum cross shore velocities along an alongshore transect at the cross shore location of the maximum absolute velocity for five time instances during the simulation (progressively advancing in time from top to bottom). The red line corresponds to the maximum cross shore velocity over the base case Beach Wizard bathymetry on the 28th of April, and the blue line is the same but over the measured bathymetry on said date. This figure provides not only the visualization of

the magnitudes of the maximum cross shore velocities, but the alongshore distribution and temporal variation of these as well; with which the location of the rip current and the temporal modulation of the rip current can be compared between measured and modeled bathymetry cases. From this figure it's clear that all three factors (magnitude, alongshore location, and timing) are quite similar between both cases (measured and Beach Wizard modeled bathymetries), showing the main rip current as a peak in the velocities at around 400-500 m in alongshore direction.

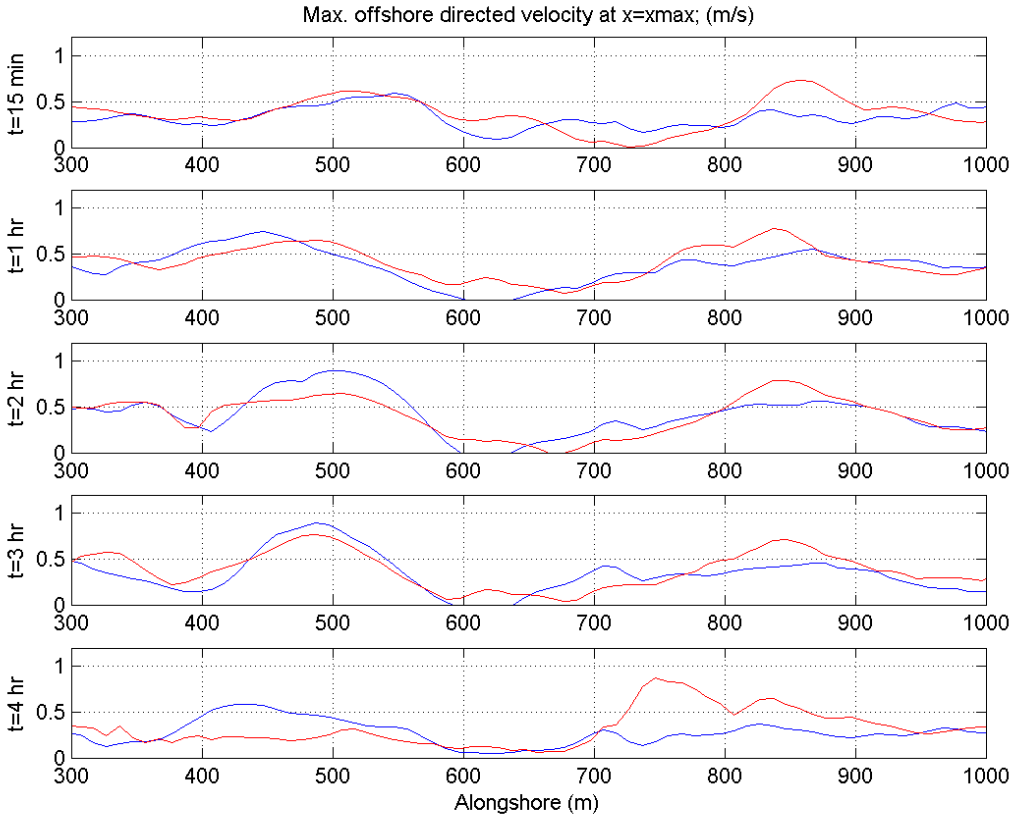

Figure 7-4. Alongshore profile of maximum cross shore velocities for five time instances in the simulation, progressively advancing in time from top to bottom. The cross shore location (xmax) of the alongshore profile corresponds to the location of the maximum absolute velocity. Red line = maximum cross shore velocity on Beach Wizard modeled bathymetry, blue line = maximum cross shore velocity on measured bathymetry, both on the 28th of April 2011.

Following the procedures described in the present and two previous sections of this report, the quantification of all three rip current descriptive indicators (strength, location, and timing) is carried out for all measured bathymetry dates and all five cases of Beach Wizard modeled bathymetries (with varying sets of imaps as input).

The results obtained will be presented and discussed in the upcoming section of this report.

7.3 Rip current flow quantification results

As it was mentioned in section 7.2.1, the initial phase in the analysis of the modeled rip current flows is a visual analysis of the overall patterns, flow directions, timing, and rip strengths by looking into the plan view plots of absolute mean velocities. By means of this simple visual observation method, some clear observations were made with respect to which seemed to be the best resulting dates and Beach Wizard cases and which were the worst. A brief description of these observations will be narrated here, and then quantified and compared for all cases following the process described in the three previous sections of this report.

The resulting flow velocities on the 28th of April showed to be the best looking results. The base case, the 1 imap per day case, and the hand selected imap case showed very similar results between them for this date, while the two other cases (imaps once per week, and imaps ranked 4) showed clearly worse flow patterns. The first three cases showed very good results compared to the flows calculated over the measured bathymetry on the 28th of April, presenting a clear rip currents with very similar direction, strength and location. The last two cases (imaps once per week, and imaps ranked 4) however, did not present clear rip currents at the location of the measured rip current.

The flows modeled for the 1st of June presented a slight reduction in apparent skill for most of the bathymetries used. The case with hand selected imaps seemingly presents the best flow patterns and rip current characteristics on the 1st of June, showing a clear rip current in the correct location with good direction and strength. The base case and the case with 1 imap per day show slightly worse flow patterns on this date, however, quite some resemblance of the modeled flows over the measured bathymetry is still observed. On this date, the case with imaps ranked 4 shows a clear improvement over the results on the 28th of April, now showing some similarities to the rip current over the measured bathymetry, but still showing worse flow patterns

and magnitudes than the cases with 1 imap per day and the case with hand selected imaps; and showing very similar flows to the results obtained from the base case.

On the 6th of June, the modeled flows show very similar characteristics to the observed on the 1st of June. The two best cases on this date are the case with 1 imap per day and the case with hand selected imaps, both showing good representation of the flows over the measured bathymetry. The base case shows worse results than the two best cases, and very similar results to the two worst cases (imaps once per week and imaps ranked 4) on the 1st of June. These three "worst" cases do not show good similarity to the flows modeled over the measured bathymetry on this date.

The results on the 11th of June seem to show some recovery over the results on the 6th of June, presenting generally better flow distribution and patterns. Similarly to the previous dates, the cases showing the best flows are the cases with 1 imap per day and hand selected imaps, with the latter showing even some improvement over the former. On this date the base case and the case with imaps once per week show similar flow patterns, with the main rip appearing in the correct location, but with possibly lower velocities and slightly different timing between the two and with respect to the flows over the measured bathymetry. The case with imaps ranked 4 shows the worst flow patterns, with the major rip current not extending through the surf zone as it does over the measured bathymetry, but rather presenting a confined circular cell closer to the shoreline.

The results obtained on the 30th of June are quite good for the case using hand selected imaps, and slightly worse for the case with 1 imap per day (but still good). The flow patterns obtained for the three other cases are not very good, since the bathymetries obtained for this date with those three cases showed a very uniform shoreline (missing a major transverse bar at approximately y=500 m), unlike the cases with 1 imap per day and hand selected imaps. The results obtained on this date however are compared to the results obtained with a measured bathymetry on the 13th of July (two weeks later), since this was the closest date with measured bathymetry. This obviously leaves room for some error, regardless of which the case with hand selected imaps in particular showed very good similarities in flow patterns.

7.3.1 *Rip current location and timing*

The resulting locations, centre rip times, and time windows for all measured and modeled bathymetries are summarized in Table 7-1. In this table the location refers to the alongshore location of the maximum absolute flow velocity, the centre time is the weighted centre time of the rip current event (while the absolute velocity is over 2/3 of the maximum), and the time window is the duration of said rip event. The total values of these are presented for the measured bathymetries, in meters and hours, and the differences between these and the calculated on all modeled bathymetry cases are shown as absolute differences, in meters and minutes.

Table 7-1. Rip current location and timing results. Location, centre time, and time window showed for modelled rips over measured bathymetries. Difference between the results from measured bathymetries and all modelled bathymetry cases shown as absolute differences. Location, centre time, and time window follow the definitions described in sections 7.2.1 and 7.2.2.

		Alongshore location (m)	Centre time (hours)	Time window (hours)
Measured bathymetry	15.03.2011	747	2.11	3.85
	28.04.2011	527	2.18	3.85
	01.06.2011	527	2.14	4.00
	06.06.2011	507	2.13	4.00
	11.06.2011	507	2.14	4.00
	30.06.2011	457	2.13	3.90
		Difference (m)	Difference (minutes)	Difference (minutes)
Base case	28.04.2011	30	1	3
	01.06.2011	10	4	6
	06.06.2011	10	6	3
	11.06.2011	10	5	3
	30.06.2011	40	7	3
1 imap per day	28.04.2011	40	1	3
	01.06.2011	20	4	6
	06.06.2011	20	6	3
	11.06.2011	0	5	3
	30.06.2011	10	7	3
Hand selected imaps	28.04.2011	50	13	15
	01.06.2011	30	2	0
	06.06.2011	30	7	6
	11.06.2011	20	0	3
	30.06.2011	100	10	3
Imaps once per week	28.04.2011	30	13	60
	01.06.2011	70	11	18
	06.06.2011	10	5	36
	11.06.2011	50	3	12
	30.06.2011	50	8	6
Imaps ranked 4	28.04.2011	10	14	21
	01.06.2011	2	0	6
	06.06.2011	10	0	45
	11.06.2011	0	1	48
	30.06.2011	50	0	6

It was decided that the use of a Brier skill score on the rip current timing indicators is not of much use, due to the fact that the values on measured and modeled bathymetries are generally very similar, as are the values on the initial measured date. The values shown in Table 7-1 show that the difference in the centre time of any rip event on the modeled bathymetries differs in no more than 14 minutes in any case, which from a practical (operational) point of view, is extremely close to reality. The values presented for the time window of the rip currents (time during which the rip is "active") vary very little for the base case, the 1 imap per day case, and the hand selected imaps case, with differences ranging from 3 to 6 minutes generally. The cases with imaps once per week and imaps ranked 4 however do show large differences reaching in several cases values between 0.5 and 1 hour.

With regards to the location of the rip currents, the use of modeled bathymetries as opposed to the initial measured bathymetry from the 15th of March showed great improvements. The difference between the location of the rip current on the initial measured bathymetry and the average position on the rest of the measured dates is in the order of 200-250 meters, while using the Beach Wizard modeled bathymetries replicates the correct location to within distances of 10-50 m in most cases. The calculation of Brier skill scores for the location of rip currents is also not very useful in this case, since all of the values will obviously be very large (all above 0.9) due to the very large difference in location between the initial and measured rip locations.

7.3.2 *Rip current strength*

As it was mentioned in section 7.2.3, the modeled rip current strengths will be quantified by means of three different velocity measures, namely the maximum absolute (15-minute time-averaged) velocity, the average of the maximum absolute velocity during the time window of each rip event, and the maximum cross shore velocity at the location of the maximum absolute velocities. These results will be compared and analyzed by presenting the magnitudes, calculated Brier skill scores, and RMS errors for each case and date during the study period.

Figure 7-5 through Figure 7-7 present the maximum absolute (15-minute time averaged) velocity magnitudes, Brier skill scores and RMS errors respectively for all cases and dates.

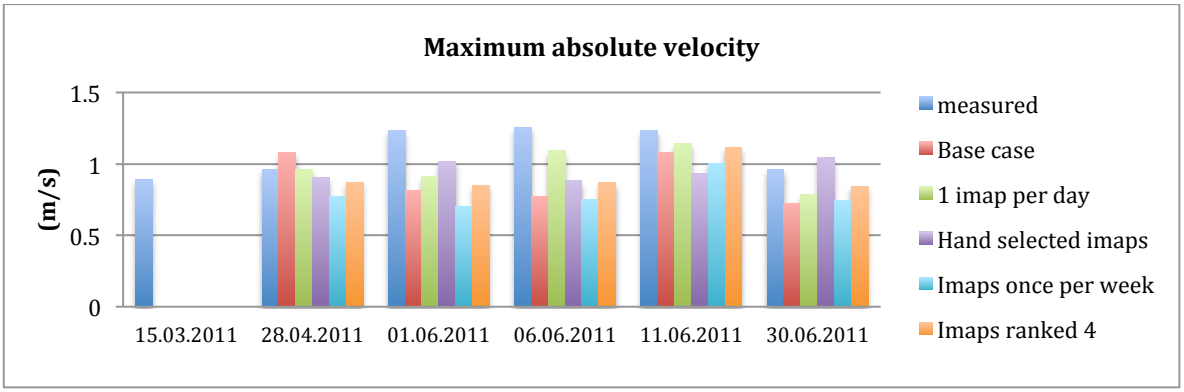

Figure 7-5. Maximum absolute (15-minute time averaged) velocity for all measured and modelled bathymetry cases.

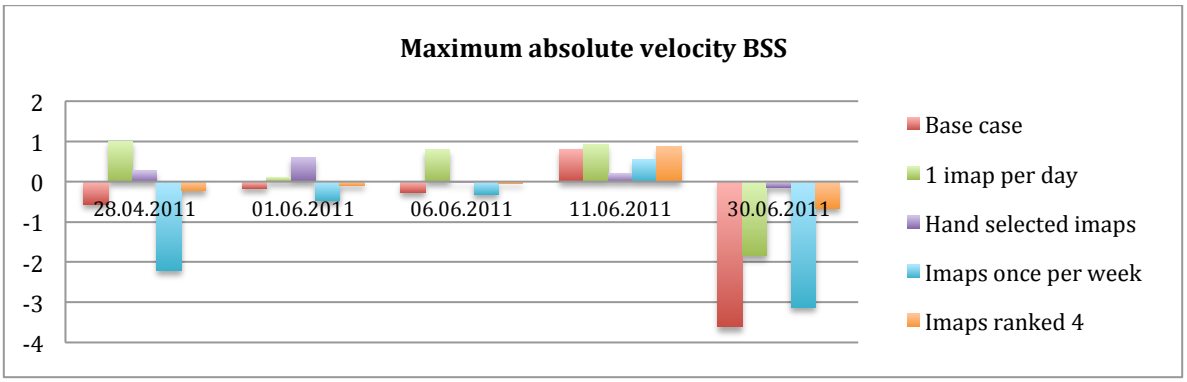

Figure 7-6. Brier skill score for maximum absolute (15-minute time averaged) velocity for all measured and modelled bathymetry cases. Using the results on the 15th of March as the "initial", and then the modeled case and measured results on each respective date.

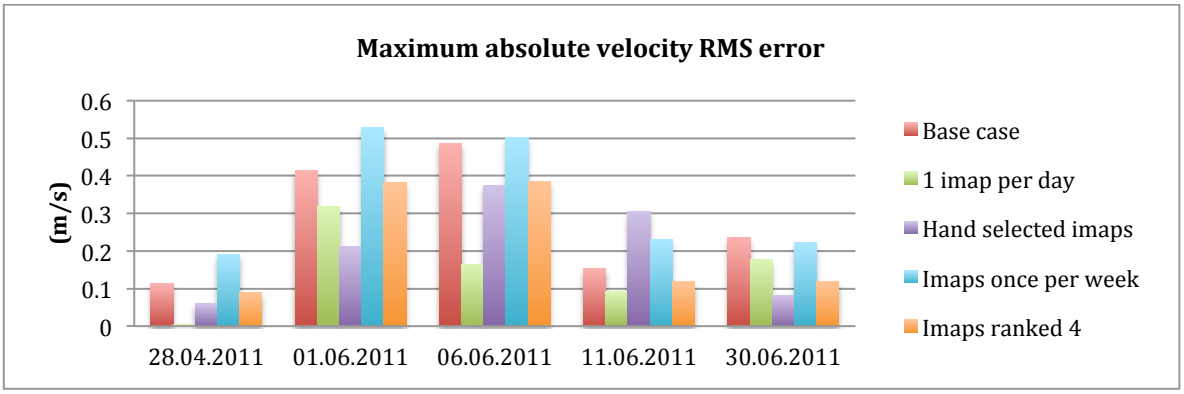

Figure 7-7. RMS error of maximum absolute (15-minute time averaged) velocity for all modelled bathymetry cases. Calculated as the RMS between the maximum absolute velocity results on measured and modeled bathymetries.

The above shown Brier skill scores and RMS errors calculated for the maximum absolute velocities show promising results. It was found that the case using 1 imap per day shows the best skill on the 28th of April, and the 6th and 11th of June, presenting high BSS on all these dates (above 0.8). As well as this, the results for this particular case show positive results on the 1st of June (with a positive BSS of 0.15) and a negative BSS on the 30th of June, but still presenting a small RMS error (of 0.15 m/s). The results obtained for the case with hand selected imaps also shows some positive skill scores (though not as high as for the 1 imap per day case) on the 28th of April, and the 1st and 11th of June. The RMS error for this case is very small on the 30th of June, still however presenting a very small negative BSS (due to the velocity on the initial bathymetry being very close to the velocity on the measured bathymetry). The case using imaps once per week consistently shows the worst results, followed by the case with imaps ranked 4 (both presenting poor resulting velocities. The base case presents good results on the 28th of April and the 11th of June, but overall doesn't compare well to the cases using a single imap per day and hand selected imaps.
Figure 7-8 through Figure 7-10 show the average absolute (15-minute time averaged) velocity magnitudes, Brier skill scores and RMS errors respectively.

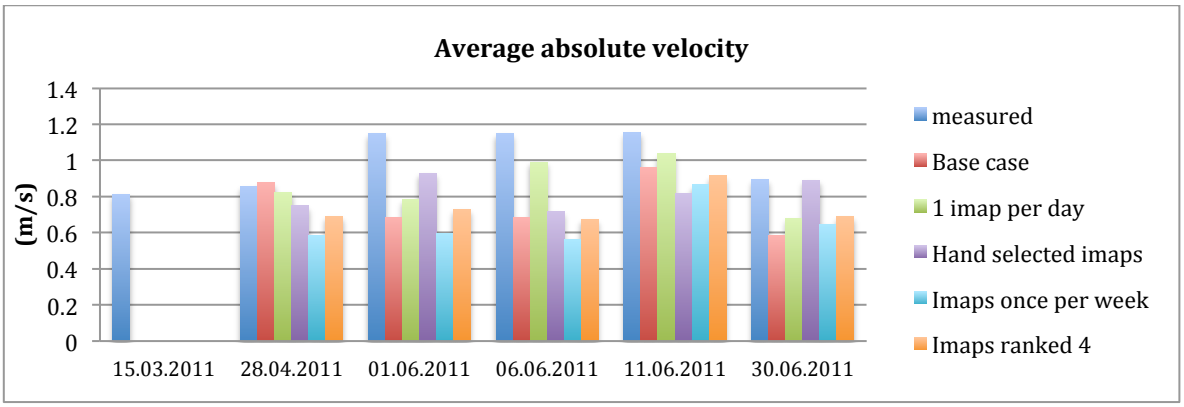

Figure 7-8. Average absolute (15-minute time averaged) velocity during rip event time window for all measured and modelled bathymetry cases.

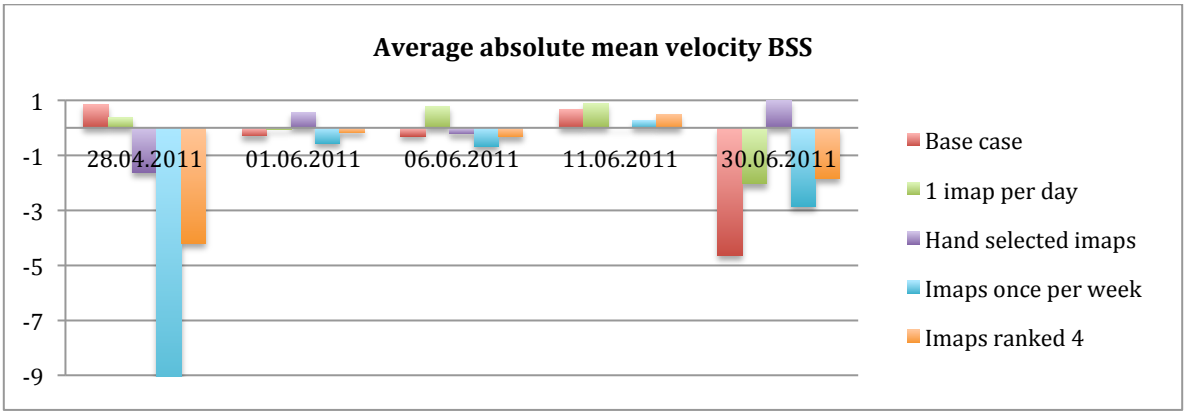

Figure 7-9. Brier skill score of average absolute (15-minute time averaged) velocity during rip event time window for all modelled bathymetry cases. Using the results on the 15th of March as the "initial", and then the modeled case and measured results on each respective date.

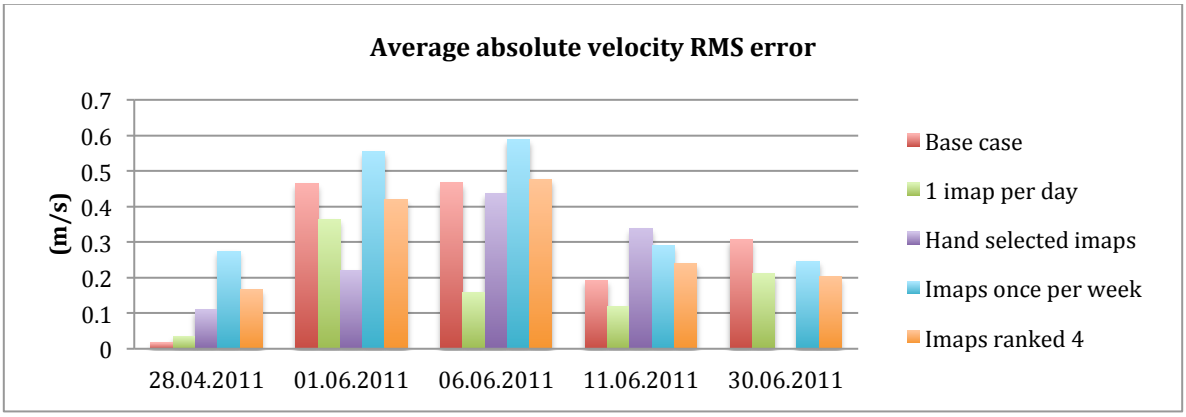

Figure 7-10. RMS error of average absolute (15-minute time averaged) velocity for all modelled bathymetry cases. Calculated as the RMS between the average absolute velocity results on measured and modeled bathymetries.

The results obtained for the average absolute velocities show very similar trends as the maximum absolute velocities did (as it might have been expected). The main difference observed is that the skill of the case using hand selected imaps corresponding to the average absolute velocities shows a large improvement on the 30th of June. As well as this, the base case shows very good skill on the 28th of April. Other than that, the general observation that the cases using 1 imap per day and using hand selected imaps show overall much better results than the other three cases.

Finally, Figure 7-11 through Figure 7-13 show the maximum offshore directed cross shore velocity magnitudes, Brier skill scores, and RMS errors respectively.

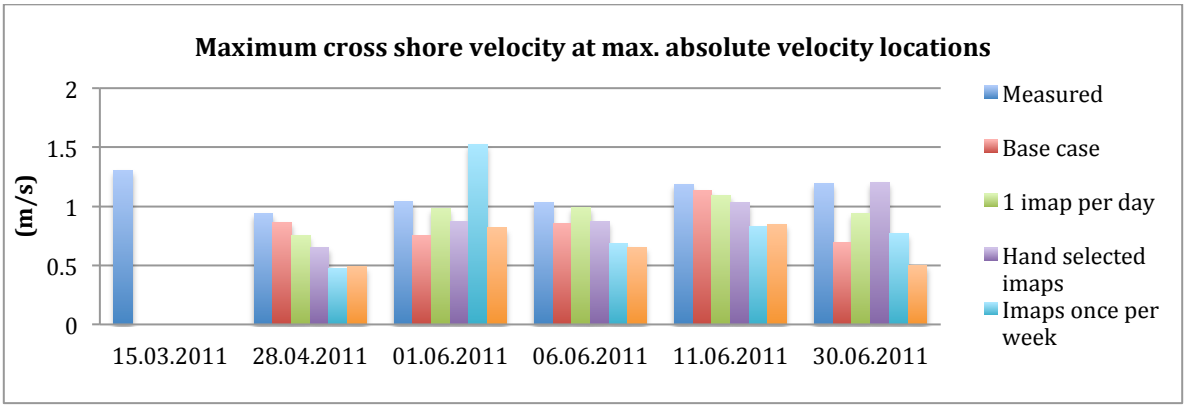

Figure 7-11. Maximum offshore directed cross shore velocity at respective maximum absolute velocity locations for all measured and modeled bathymetry cases.

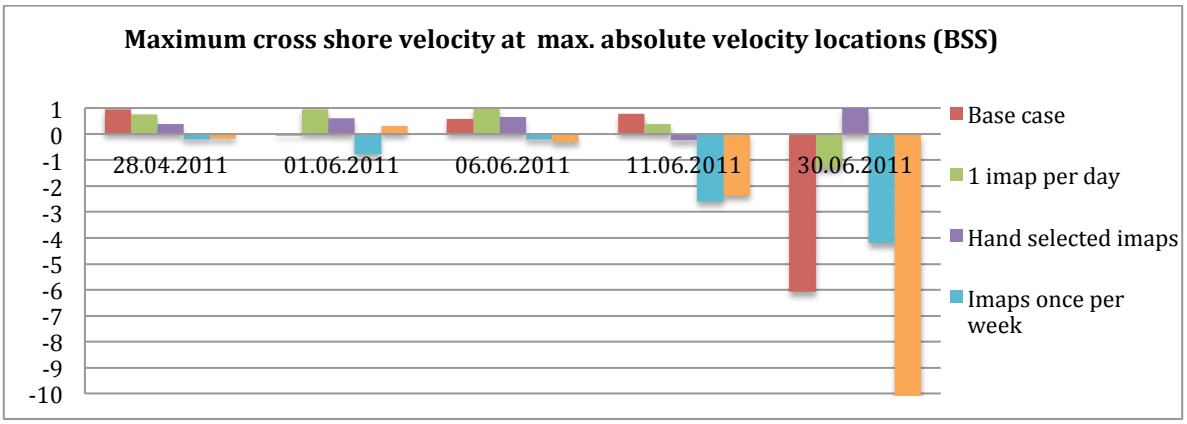

Figure 7-12. Brier skill score of maximum offshore directed cross shore velocity at respective maximum absolute velocity locations for all modelled bathymetry cases. Using the results on the 15th of March as the "initial", and then the modeled case and measured results on each respective date.

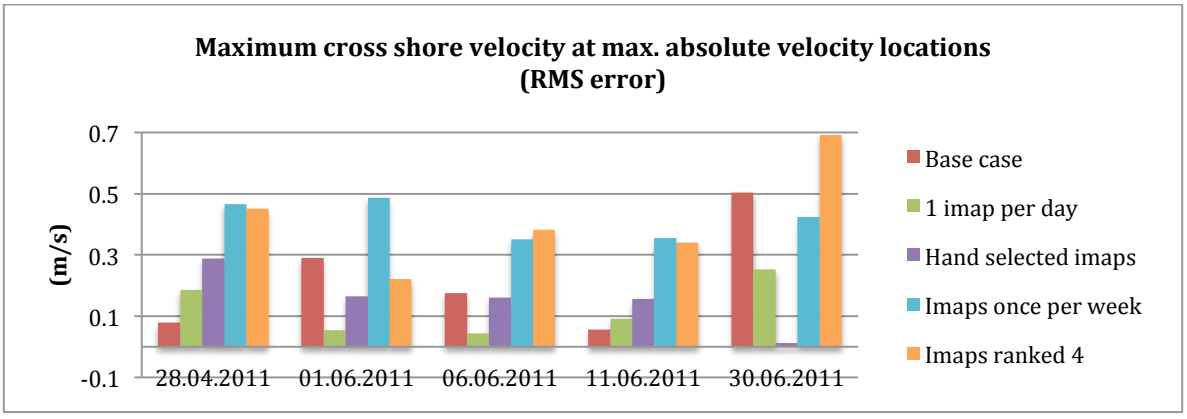

Figure 7-13. RMS error of maximum offshore directed cross shore velocity at respective maximum absolute velocity locations for all modelled bathymetry cases. Calculated as the RMS between the average absolute velocity results on measured and modeled bathymetries.

The results calculated with the maximum offshore directed cross shore velocity show the case using 1 imaps per day dominating the results, similarly to the previous two velocity measures. The case using 1 imap per day shows very good skill and low RMS errors on the 28th of April, and on the 1st, 6th and 11th of June. The case using hand selected imaps also shows good skill (with higher errors than the case using 1 imap per day) on all dates, except for the 11th of June, where the BSS is negative, but still very small, with an RMS error of only 0.15 m/s. The skill of the base case on the 28th of April and on the 6th and 11th of June are also quite good, presenting RMS errors of around 0.1 m/s. The overall results obtained by analyzing the maximum cross shore velocity back up the results obtained from the absolute velocities, all showing generally good skill for the cases using 1 imap per day and hand selected imaps, and much worse skill for the cases using imaps once per week and imaps ranked 4. The base case turns out to be a kind of middle ground between the best and worse cases, sometimes presenting good skill and sometimes bad.

7.4 Conclusions

The objective of the present chapter was to validate the bathymetry updating system with regards to rip current characteristics, as well as testing the variations in rip currents for different bathymetries obtained with varying video-derived input configurations. It was found that even if some irregularities and errors are present in the estimated bathymetries, the general nearshore flows can present a good resemblance of the flows modeled over real (measured) bathymetries. In other words, the estimated bathymetries having sharp features and some errors are capable of nicely reproducing real rip current flows as long as the general morphological features are present in these bathymetries. All in all, the capability of the Beach Wizard bed updating scheme for reproducing general morphological features is good enough to be implemented in an eventual rip current forecasting system. The improvement of using estimated bathymetries rather than using an outdated measured bathymetry (from the 15th of March) for the modeling of rip currents during April, May, and June was present during the entire study period, with a slight

reduction in skill for the months of May and June (still however viewed as an improvement).

It was found that the prediction of a given rip current's time of occurrence, duration, and location are greatly achievable using estimated bathymetries. The temporal parameters however, do not show a clear improvement over using the initial measured bathymetry from the 15th of March, due to the rip currents consistently occurring at the same time (with variations in the order of 10 minutes). The prediction of the location of a given rip current using estimated bathymetries shows a great improvement over using an outdated measured bathymetry, due to the main rip channels and bars migrating in alongshore direction with time. The three rip strength indicators chosen (maximum and average absolute velocity, and maximum cross shore velocity) showed a good characterization of the observed rip current flows, allowing for good comparisons between the different cases modeled.

The conclusions from the previous chapter regarding the importance of video derived input were reinforced in this chapter, finding that the best overall input configurations for Beach Wizard were the case using a single daily image and the case using hand selected ("best") imaps as input. This leads to the conclusion that both imap quality and regularity are more critical in providing realistic bathymetries (and rip current predictions) than image quality and quantity. For this reason, the eventual image selection process to be implemented in an operational manner for rip current forecasting would ideally involve the selection of the best daily imaps, avoiding large periods of time with no images used as input (ideally no more than a few days).

8 CONCLUSIONS AND RECOMMENDATIONS

8.1 Conclusions

This study had several specific objectives, which can be divided into four major groups, corresponding to the four major phases of work that were carried out. The first major phase of work is the initial model set-up and processing of images to be used as input. The second phase is the analysis of the behavior and functioning of the Beach Wizard bed updating system, along with addressing specific model formulations and parameter inputs. The next phase of work was the analysis of the importance of video-derived input (timex images) and forcing conditions for the optimal prediction of bathymetries. The final stage of work was the hydrodynamic modeling of nearshore flows as to validate the bed updating system with regards to rip current dynamics; as well as using the rip current flows as a measure of bathymetry accuracy (ultimately to back-up the conclusions obtained in the previous stage of work).

As well as the four mentioned major phases of work, an initial phase in which the characteristics of Perranporth beach and the natural temporal variability in bathymetries was studied. The objective of this initial phase was to determine the importance of having up to date bathymetrical information for the prediction of rip currents, i.e. assuming that using an accurate bathymetry will reproduce accurate currents, so if large variations in bathymetry are seen, then the importance of having up to date bathymetries is large. It was found that the bathymetry at Perranporth is in fact quite dynamic, particularly for timescales in the order of months, where the main channel and transverse bars were seen to migrate up to over 200 m in one month. The overall conclusions of the three major phases of work will now be presented.

8.1.1 *Image processing*

Two problems in the timex image merging process were observed. The first being a general error in which the resulting image intensities were wrong, presenting high intensities in the offshore region and/or low intensities on the dry beach region (these problems do not always occur). The second problem is a particular one along what is

believed to be the merge-line between cameras 1 and 2. This problem does not affect images corresponding to tidal levels below -1 m, but do present issues in many cases for higher tidal levels. This problem along the camera's merge-line produces a line of high intensity parallel to the shoreline, which Beach Wizard would perceive as wave breaking, generating erroneous bed changes. This second problem greatly reduces the amount of available images, leaving the periods around neap tides with very few available usable images.

As to address the issue of the overall image merging problem (where offshore intensities were high and/or onshore intensities are low), an interactive shoreline and surf zone detection system was applied in this work. This scheme allows the user to define the area of interest (where there is observed wave dissipation) manually.

8.1.2 *Beach Wizard model formulations and parameter settings*

The measurement error was found to be a very important factor in the bed updating scheme, as it directly influences the uncertainty and consequently the total amount of bed change that will take place. The measurement error was set to a percentage (15%) of the maximum observed dissipation rather than a fixed value, allowing images corresponding to different wave conditions to have the same relative importance.

The timescale parameter that controls the rate at which the prior bed uncertainty increases towards the natural uncertainty was found to affect the total amount of bed change quite a lot. An increase in the timescale parameter from the original 5 days to 10 days was finally chosen to be the best, reducing the increment in uncertainty between simulations significantly, and in this manner reducing total amount of bed change per simulation. This parameter should vary between different beaches, therefore the user must define this parameter by observing the general rates of change of the bathymetry at a given beach.

The implementation of a time dependent bed change factor was found to improve the model results, by reducing the effects of the two systematic estimation errors (shoreline digging and building). These systematic estimation errors are generated due to the model considering only local differences in modeled and observed

dissipation, not accounting for the "automatic" reaction of the dissipation near the shoreline due to changes in the bed level (and dissipation) farther offshore.

8.1.3 *Importance of video-derived input and forcing conditions*

It was found that the best estimated bathymetries were consistently at the end of April 2011, and a slight deterioration in model skill was seen for the following months of May and June. The difference observed between these two period was in the forcing conditions, particularly in that the month of April presented long swell waves with quite constant wave heights, periods and directions; as opposed to the months of May and June during which more variable conditions were observed, with shorter period waves and various storm events. What can be concluded from this is that the performance of Beach Wizard will generally be better for periods with long period uniform wave conditions, which produce nice uniform dissipation patterns and rip currents, allowing the model to reproduce more accurate bathymetries.

With respect to the importance of video-derived input (dissipation maps generated from Timex images), the same overall conclusions were obtained by directly comparing the resulting bathymetries for various test cases and comparing the generated nearshore flows modeled over the same bathymetries. The overall conclusions here are that imap quality is more important than image quality (as defined in sections 6.1 and 6.4.1), input regularity is quite important, and image quantity is not important as long as the regularity is maintained. It was found that the two best cases were the configuration using a single imap per day and the configuration using hand selected imaps ("best" imaps), with a slight favoring of the first mentioned case. This means that maintaining high regularity (images every day) of input even if each image is not perfect is preferable due to the fact that by doing this, the uncertainty between simulations does not have a chance to increase too high and produce harmful large bed changes. From an operational point of view, this was a good finding, since it means that choosing a single best daily image (avoiding gaps between images larger than 3 days when possible) should provide the best results in rip current forecasting.

8.1.4 *Rip current flow modeling on estimated bathymetries*

Using estimated bathymetries (product of Beach Wizard) in a non-stationary hydrodynamic XBeach model resulted in nearshore flows greatly resembling the nearshore flows modeled over measured bathymetries. Using updated bathymetries as opposed to an outdated measured bathymetry for the prediction of rip currents proved to be much more useful, particularly with respect to predicting the location of a given rip current. The prediction of the time of occurrence of a rip current and its duration were highly achievable using estimated bathymetries, resulting in differences in the order of minutes, which from an operational point of view is more than good enough. The rip current strength was also well predicted, in the majority of cases showing an improvement over using an outdated bathymetry in its place.

All in all, the capabilities of the Beach Wizard bed updating scheme are quite promising for its eventual implementation in an operational rip current forecasting system.

8.2 Recommendations

Due to time constraints on the present study, there were several ideas which could not be further tested or elaborated on, which may be recommended however to be considered for future work. In section 4.5 and 5.4.2 some specific recommendations are described concerning the image merging process and the Beach Wizard model formulations and parameter settings respectively. As well as this, section 6.6.2 describes some recommendations concerning the video-derived input for Beach Wizard. Here some of the more important recommendations will be mentioned and somewhat summarized, and is recommended to refer to the previously mentioned sections for further detail.

The main recommendations with respect to the specific parameters used in the Beach Wizard bed update scheme are for further improvement and testing of different configurations of the time dependent bed change factor implemented in this study; further testing of variations in the measurement error's definition; and further testing in what concerns the increase in bed uncertainty between simulations. This last one comes also from the finding which pointed out that the best results are obtained with

the highest possible regularity of images used as input (1 imap per day case), due to the fact that for small temporal spacing between images the increase in uncertainty between simulations is also small. It is recommended to test the impact of reducing the natural uncertainty (which is currently set to 1 m), which would likely allow for having larger spaces between consecutive images without having very large corresponding bed changes. From an operational point of view, it may be recommendable to look into "resetting" the model for cases where large periods of time with no available or usable images are found, and possibly starting over with the initial bathymetry or with a plane bed bathymetry with the same steepness as the real bathymetry. This might be helpful in that if any errors were accumulated, they could be essentially erased and the model can have a fresh start when new images are available.

Another important recommendation for the eventual implementation of a rip current forecasting model at Perranporth is to work out the problems concerning the merging of the three individual camera images, since this seriously restricts the total amount of images available. The problematic mergeline between cameras 1 and 2 (parallel to the shoreline) tends to produce errors in the merged images for water levels higher than -1 m, therefore leaving periods around neap tides with significantly less available images than around spring tides.

REFERENCES

Aarninkhof, S. G. J., P. P. Janssen & N. G. Plant (1997), Quantitative estimations of bar dynamics from video images. In: Proceedings Coastal Dynamics'97, New York: ASCE, pp. 365–374.

Aarninkhof, S.G.J., Turner, I.L., Dronkers, T.D.T., Caljouw, M., Nipius, L., (2003). A video-technique for mapping intertidal beach bathymetry. Coastal Engineering 49, 275–289.

Aarninkhof, S. (2003). Nearshore Bathymetry derived from Video imagery. Delft Hydraulics Select series 3/2003. Delft Univrsity Press. Delft.

Aarninkhof, S.G.J., Ruessink, B.G., Roelvink, J.A., (2005a). Nearshore subtidal bathymetry from time-exposure video images. Journal of Geophysical Research 110, C06011.

Aarninkhof, S.G.A., Wijnberg, K.M., Roelvink, J.A., Reniers, A.J.H.M., (2005b). 2DH- Quantication of surf zone bathymetry from video. Proc. Coastal Dynamics '05.

Andrews, D. G., & McIntyre, M. E. (1978). An exact theory of nonlinear waves on a Lagrangian-mean flow. *Journal of Fluid Mechanics*, *89*, 609-646.

Austin, M. J., Scott, T. M., Brown, J. W., Brown, J. A., & Macmahan, J. H. (2009). Macrotidal rip current experiment : circulation and dynamics. *Journal of Coastal Research*, (56).

Austin, M., Scott, T., Brown, Jeff, Brown, Jenna, MacMahan, J., Masselink, G., & Russell, P. (2010). Temporal observations of rip current circulation on a macro-tidal beach. *Continental Shelf Research*, *30*(9), 1149-1165.

Austin, MJ, Scott, TM, Russell, PE and Masselink, G, (in press). Rip current prediction: development, validation and evaluation of an operational tool. Journal of Coastal Research.

Baart, F., Kaaij, T. van der, Ormondt, M. van, Dongeren, A. van, Koningsveld, M. van, Roelvink, J. A., (2009). Real- time forecasting of morphological storm impacts: a case study in the Netherlands. Journal of coastal research, SI 56, 1617-1621.

Baldock, T. E., P. Holmes, S. Bunker, and P. Van Weert (1998), Cross-shore hydrodynamics within an unsaturated surf zone, Coastal Eng., 34, 173– 196.

Bowen, A.J., (1969). Rip currents: 1. Theoretical investigations. J. Geophys. Res. 74, 5467–5478.

Bowen, A.J., Inman, D.I., (1971). Edge waves and crescentic bars. J. Geophys. Res. 76, 8662–8671.

Bruneau, N., Castelle, B., Bonneton, P., Pedreros, R., Almar, R., Bonneton, N., Bretel, P., Parisot, J.-P., Se´ ne´ chal, N., (2009). Field observations of an evolving rip current on a meso-macrotidal well-developed inner bar and rip morphology. Continental Shelf Research 29, 1650–1662.

Dalrymple, R.A., Lozano, C.J., (1978). Wave–current interation models for rip currents. J. Geophys. Res. 83 (C12), 6063–6071.

Daly, C. (2009). Low Frequency Waves in the Shoaling and Nearshore Zone - A Validation of XBeach. Section of Hydraulic Engineering, Department of Coastal Engineering. Delft, Delft University of Technology. Erasmus Mundus Master in Coastal and Marine Engineering and Managerment (CoMEM).

Dean, R.G., (1977). Equilibrium beach profiles: U.S. Atlantic and Gulf coasts. Ocean Engineering Report No. 12, Department of Civil Engineering. University of Delaware, Newark, DE.

Galappatti, R., Vreugdenhil, C.B., (1985). A depth integrated model for suspended transport. J. Hydraul. Res. 23 (4), 359–377.

Haller, M. C., & Dalrymple, R. A. (2001). Rip current instabilities. *Journal of Fluid Mechanics*, *433*, 161-192.

Hatfield, J., Williamson, A., Sherker, S., Brander, R. Improving Beach Safety: The Science of the

Surf (SOS) research Project. World conference on drowning prevention, paper 169.

Holman, R.A., (1981). Infragravity energy in the surfzone. J. Geophys. Res. 86, 6442 – 6450.

Holman, R.A., Stanley, J., (2007). The history and technical capabilities of Argus. Coastal Engineering 54, 477–491.

Jacobs, R.P.M. (2010). Non-hydrostatic computations of nearshore hydrodynamics. MSc thesis Delft University of Technology.

Lippmann, T.C., Holman, R.A., (1989). Quantification of sand bar morphology: a video technique based on wave dissipation. Journal of Geophysical Research 94 (C1), 995–1011.

Longuet-Higgins, M.S., Stewart, R.W., (1964). Radiation stress in wáter waves, a physical discussion with applications. Deep-Sea Res. 11 (4), 529 – 563.

Longuet-Higgins, M. S., (1969). 'On the transport of mass by time-varying ocean currents'. *Deep-Sea Res.*

Longuet-Higgins, M. S., (1986). 'Eulerian and Lagrangian aspects of surface waves', *J. Fluid Mech.*, **173**, 683-707.

MacMahan, J., A. J. H. M. Reniers, E. B. Thornton, and T. Stanton. (2004). Infragravity rip current pulsations. Journal of Geophysical Research. 109 (C01033)

MacMahan, J.H., Thornton, E.B. and Reniers, A.J.H.M.,(2006). Rip current review. Coastal Engineering, 53, 191-208.

McKenzie, R. (1958). Rip current systems. Journal of Geology, 66: 103-113.

Munk, W.H., (1949a). Surf beats. Trans. Am. Geophys. Union 30,849 – 854.

Munk, W.H., (1949b). The solitary wave theory and application to surf problems. Ann. N. Y.

Acad. Sci. 51 (3), 376–424.

Phillips, O.M., (1977). The Dynamics of the Upper Ocean 2nd ed. Cambridge Univ. Press, New York. 336 pp.

Poate, T. Kingston, K.K., Masselink, G. and Russell. P.E., (2009). Response of high-energy, macrotidal beaches to seasonal changes in wave conditions: examples from North Cornwall. Journal of Coastal Research, SI 56, 747-75

Reniers, a J. H. M. (2004). Morphodynamic modeling of an embayed beach under wave group forcing. *Journal of Geophysical Research*, *109*(C1), 1-22.

Reniers, A.J.H.M., MacMahan, J., Thornton, E.B., Stanton, T.P., (2006). Modelling infragravity motions on a rip-channel beach. Coast. Eng. 53, 209–222

Reniers, A., MacMahan, J., Thornton, E.B. and Stanton, T.P., (2007). Modeling of very low frequency motions during RIPEX. Journal of Geophysical Research.

Roelvink, J. a. (1993). Dissipation in random wave groups incident on a beach. *Coastal Engineering*, *19*, 127-150.

Roelvink, D., Reniers, A., van Dongeren, A., van Thiel de Vries, J., McCall, R., & Lescinski, J. (2009). Modelling storm impacts on beaches, dunes and barrier islands. *Coastal Engineering*, *56*, 1133-1152.

Scott, T. R., & Mason, D. C. (2007). Data assimilation for a coastal area morphodynamic model: Morecambe Bay. *Coastal Engineering*, *54*(2), 91-109.

Scott, T., Russel, P., Masselink, G., & Wooler, A. (2009). Rip current variability and hazard along a macro-tidal coast. *Journal of Coastal Research*, (56), 895-899.

Sembiring, L.E. (2010). Application of Beach Wizard for Coastal Operational Model System. MSc Thesis wse-he-cepd-10.08. UNESCO-IHE Institute for water education.

Shepard, F. P., Emery, K. O. & La Fond, E. C. (1941). Rip currents: a process of geological

importance. J. Geol. 49, 337–369

Short, A. D., and C. L. Hogan. (1994). Rip currents and beach hazards: Their impact on public safety and implications for coastal management. Journal Coastal Research, Special Issue No. 12: 197-209.

Short, A.D. and Brander, R., (1999). Regional variation in rip density. *Journal of Coastal Research*, 15, 813-822.

Soulsby, R.L., (1997). Dynamics of Marine Sands. Thomas Telford, London.

Stockdon, H.F., Holman, R.A., (2000). Estimation of wave phase speed and nearshore bathymetry from video imagery. Journal of Geophysical Research 105,
22015–22033.

Stokes, G.G. (1847). "On the theory of oscillatory waves". Transactions of the Cambridge Philosophical Society **8**: 441–455.

Sutherland, J., Peet, A. H., & Soulsby, R. L. (2004). Evaluating the performance of morphological models. Coastal Engineering, 51(8-9), 917-939.

Thornton, E.B., MacMahan, J.H., Sallenger Jr., A.H., (2007). Rip currents, mega cusps and eroding dunes. Mar. Geol. 240, 151–167.

Van Dongeren, A., Plant, N., Cohen, A., Roelvink, D., Haller, M.C., Catalan, P., (2008). Beach Wizard: Nearshore bathymetry estimation through assimilation of model computations and remote observations. Coastal Engineering 55, 1016-1027.

Van Rijn, L.C., Walstra, D.J.R., Grasmeijer, B., Sutherland, J., Pan, S., Sierra, J.P., (2003). The predictability of cross-shore bed evolution of sandy beaches at the time scale of storms and seasons using process-based profile models. Coastal Engineering 47, 295–327.

Wijnberg, K.M., Roelvink, J.A., Aarninkhof, S.G.J., (2004). Bed variability in the surf zone at the

storm- and seasonal time scale, mapped by Argus-video techniques. Rijkswaterstaat, RIKZ, Z3781.

Winter, G. (2011). Rip Current Characteristics at the Dutch Coast: Egmond and Zee. MSc thesis Delft University of Technology.

Wright, L.D., Guza, R.T., Short, A.D., (1982). Dynamics of a high energy dissipative surf-zone. Mar. Geol. 45, 41–62.

Wright, L. D. and Short, A. D., (1984). Morphodynamic variability of surf zones and beaches – A synthesis. *Marine Geology*, 56 (1-4),

APPENDIX

A. MEASURED BATHYMETRIES

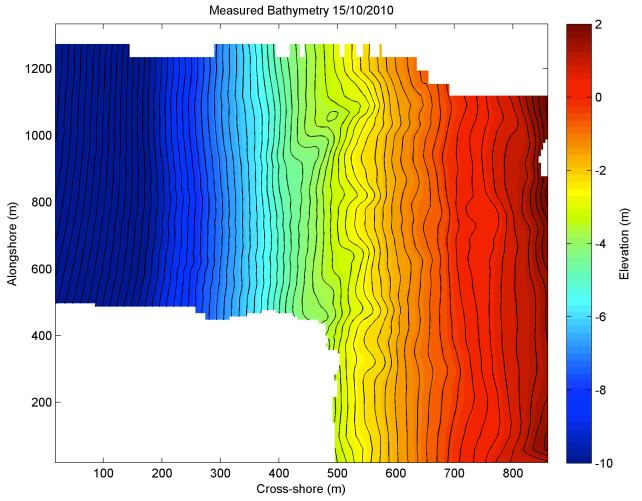

Figure A-1. Measured bathymetry Perranporth 15/10/2010Figure

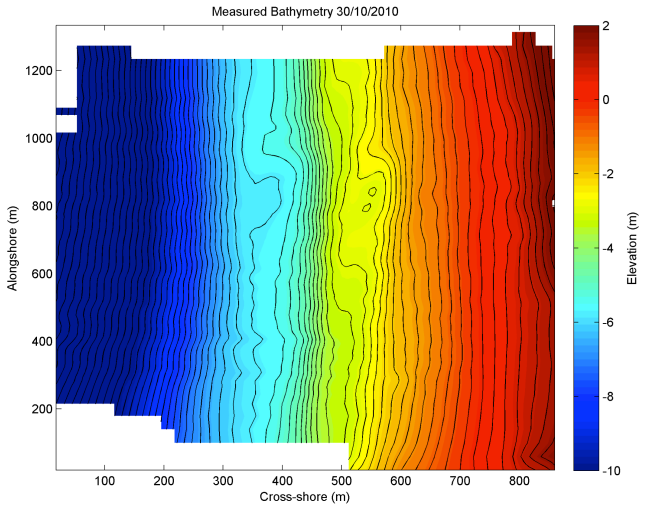

Figure A-2. Measured bathymetry Perranporth 30/10/2010

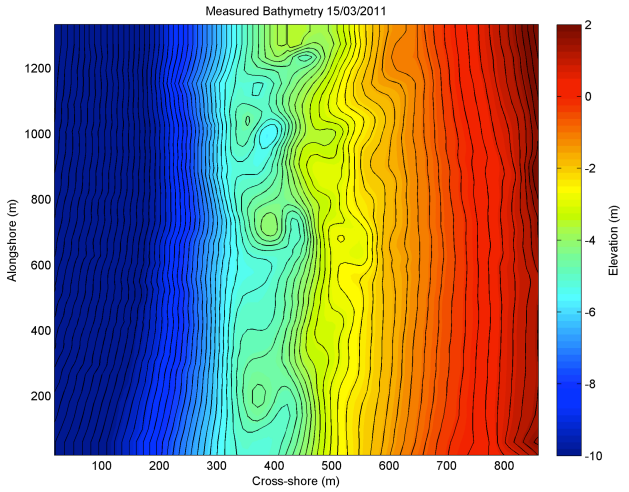

Figure A-3. Measured bathymetry Perranporth 15/03/2011

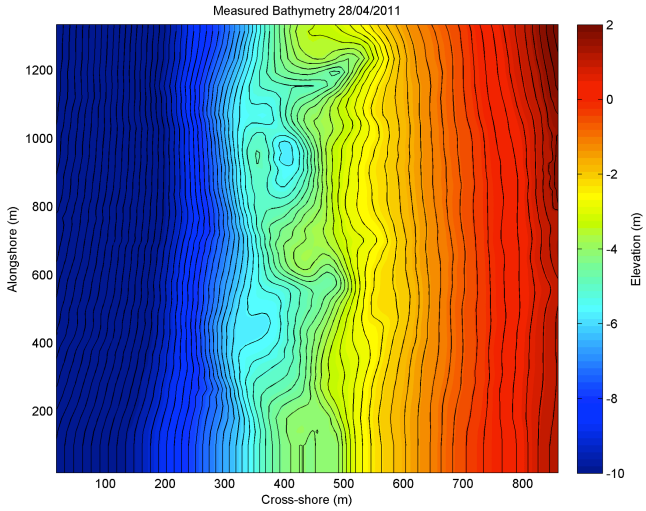

Figure A-4. Measured bathymetry 28/04/2011

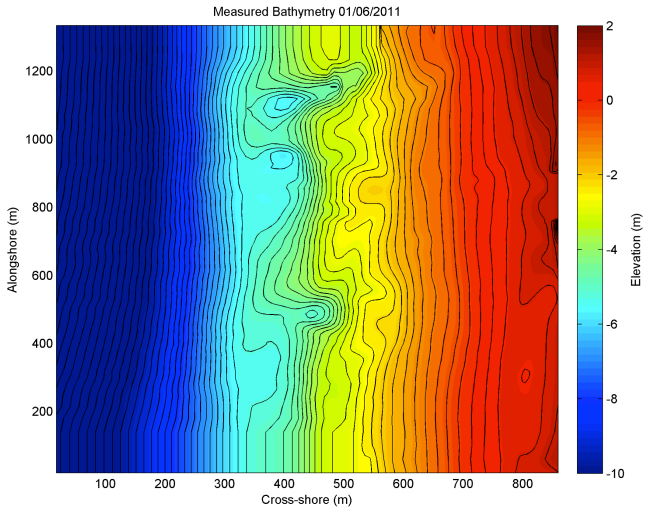

Figure A-5. Measured bathymetry Perranporth 01/06/2011

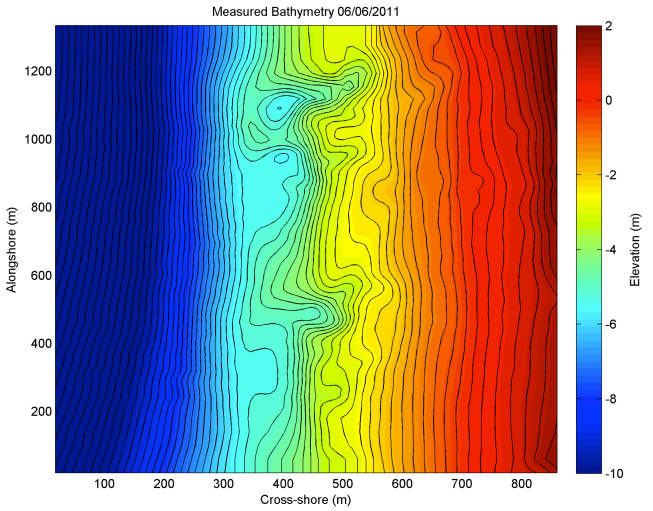

Figure A-6. Measured bathymetry Perranporth 06/06/2011

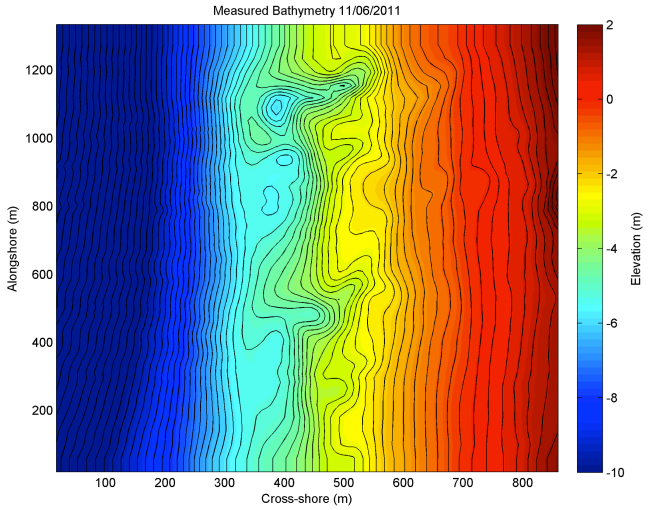

Figure A-7. Measured bathymetry Perranporth 11/06/2011

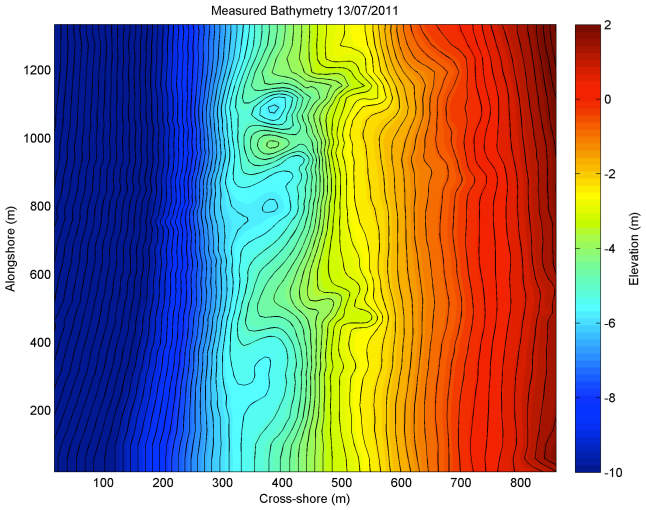

Figure A-8. Measured bathymetry Perranporth 13/07/2011

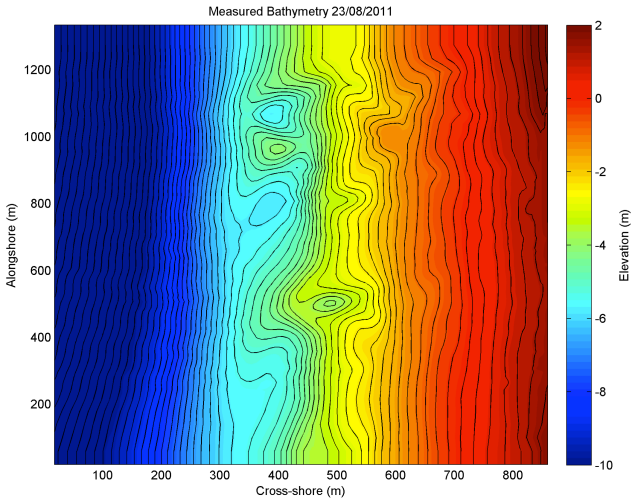

Figure A-9. Measured bathymetry Perranporth 23/08/2011

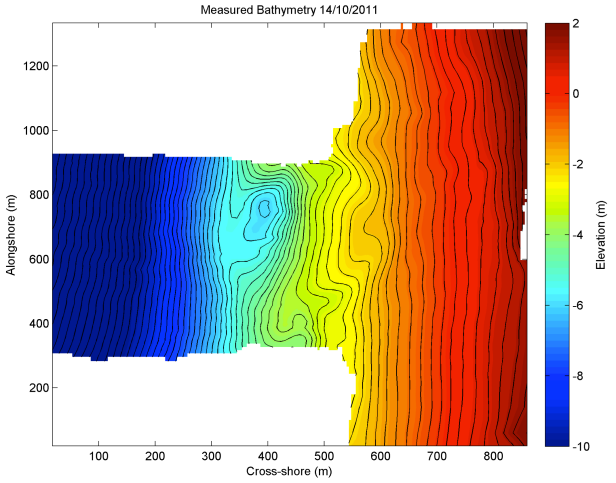

Figure A-10. Measured bathymetry Perranporth 14/10/2011

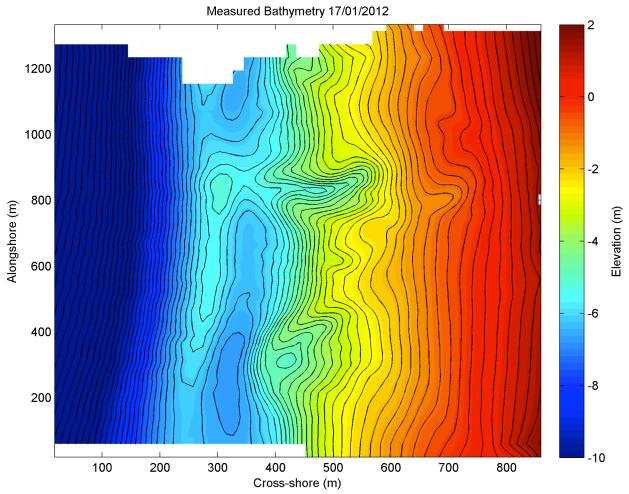

Figure A-11. Measured bathymetry Perranporth 17/01/2011

B. MODEL SENSITIVITY RESULTS

The resulting bathymetry plots for the best obtained model setup are presented here, as well as a summary of all calculated BSS and RMS errors for the variations in the model and parameter settings.

B-1. Bahtymetry plots using executable 3 and Tr=10 days

All figures present the initial bathymetry (which is the measured bathymetry on the 15th of March 2011), the current measured bathymetry (labeled with "Measured Bathymetry" and the corresponding date), the modelled bathymetry with executable 2 (labelles "Exe.2" with the corresponding date), the modelled bathymetry with executable 3 and Tr=10 days (labeled "Exe.3 w/Tr=10"), two difference plots between the current measured bathymetry and each modeled bathymetry.

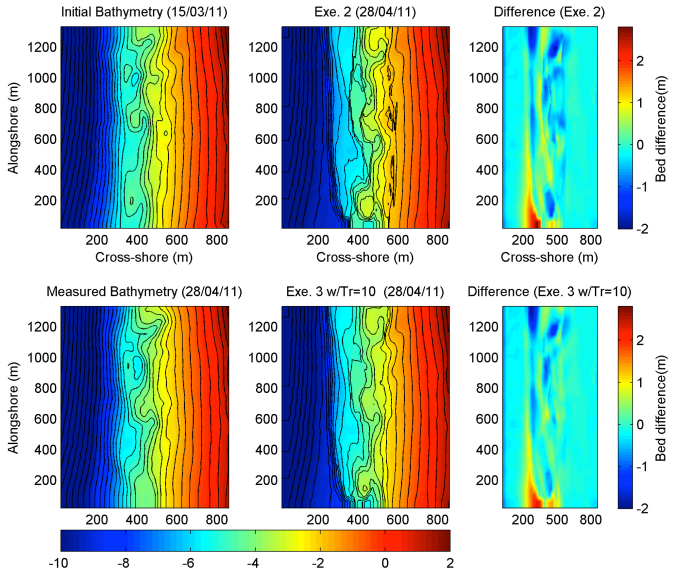

Figure B-1. Resulting bathymetries with best obtained executable version (Exe. 3 with Tr=10 days) on 28th of April.

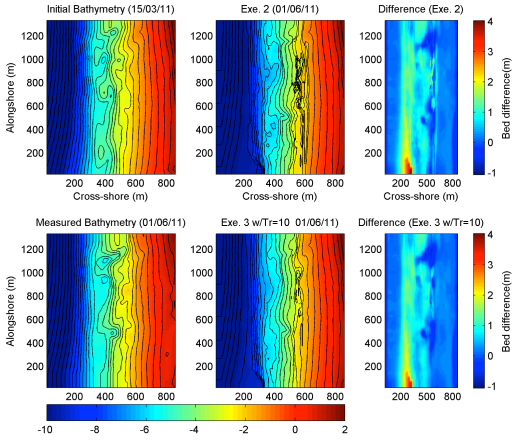

Figure B-2. Resulting bathymetries with best obtained executable version (Exe. 3 with Tr=10 days) on the 1st of June.

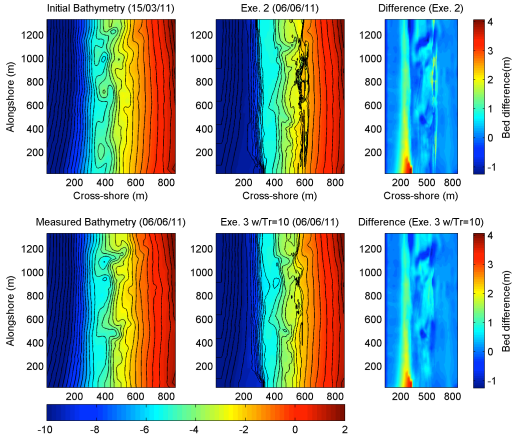

Figure B-3. Resulting bathymetries with best obtained executable version (Exe. 3 with Tr=10 days) on 6th of June.

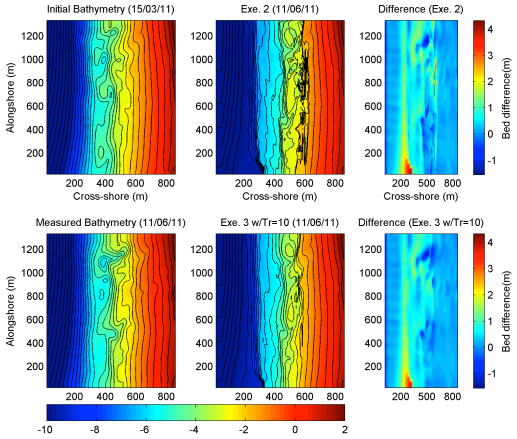

Figure B-4. Resulting bathymetries with best obtained executable version (Exe. 3 with Tr=10 days) on 11th of June.

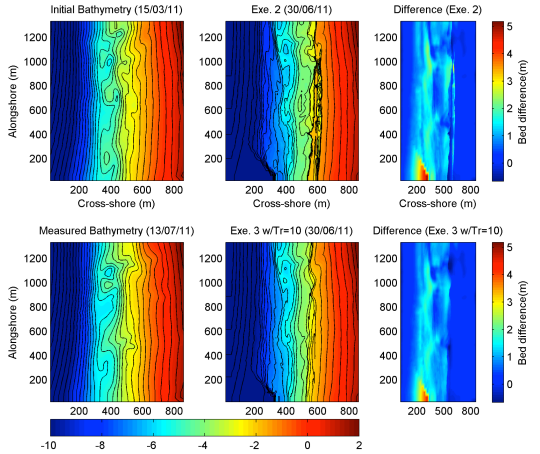

Figure B-5. Resulting bathymetries with best obtained executable version (Exe. 3 with Tr=10 days) on 30th of June.

B-2 BSS and RMS error results

Table B-1. BSS and RMS error results for model and parameter sensitivity analysis calculated over whole domain.

Whole Domain	28.04.2011		01.06.2011		06.06.2011		11.06.2011		30.06.2011*	
	BSS	*RMS error*	*BSS*	*RMS error*	*BSS*	*RMS error*	*BSS*	*RMS error*	*BSS*	*RMS error*
Exe. 1	-0.404	0.410	-5.800	0.971	-5.970	0.974	-6.080	0.993	-6.626	1.057
Exe. 2	0.027	0.334	-1.381	0.590	-0.489	0.451	-1.364	0.566	-3.865	0.815
Exe. 2 with Tr=10 days	0.225	0.299	-0.972	0.539	-0.251	0.412	-0.873	0.505	-2.832	0.734
Exe. 2 with Tr=15 days	0.327	0.276	-1.020	0.537	-0.515	0.454	-0.952	0.513	-2.417	0.697
Exe. 3	0.322	0.279	-0.907	0.528	-0.034	0.376	-0.637	0.473	-2.583	0.716
Exe. 3 (with 0.65*t)	0.303	0.284	-0.928	0.532	-0.028	0.375	-0.652	0.476	-2.666	0.723
Exe. 3 with Tr=10 days	0.384	0.263	-0.838	0.512	-0.178	0.402	-0.578	0.464	-2.137	0.673

Table B-2. BSS and RMS error results for model and parameter sensitivity analysis calculated over outer surf zone area.

Outer surf zone (x = 250-450)	28.04.2011		01.06.2011		06.06.2011		11.06.2011		30.06.2011*	
	BSS	*RMS error*	*BSS*	*RMS error*	*BSS*	*RMS error*	*BSS*	*RMS error*	*BSS*	*RMS error*
Exe. 1	-0.162	0.660	-2.957	1.198	-1.611	1.012	-1.838	1.036	-1.754	1.248
Exe. 2	0.341	0.514	-1.475	0.962	0.173	0.571	-0.781	0.834	-1.576	1.182
Exe. 2 with Tr=10 days	0.449	0.451	-1.232	0.909	0.126	0.588	-0.648	0.798	-1.318	1.135
Exe. 2 with Tr=15 days	0.491	0.431	-1.095	0.877	0.012	0.620	-0.675	0.793	-1.128	1.095
Exe. 3	0.425	0.462	-1.304	0.926	0.174	0.572	-0.605	0.796	-1.507	1.173
Exe. 3 (with 0.65*t)	0.417	0.468	-1.331	0.931	0.174	0.572	-0.628	0.801	-1.509	1.173
Exe. 3 with Tr=10 days	0.498	0.425	-1.089	0.877	0.098	0.598	-0.508	0.764	-1.236	1.121

Table B-3. BSS and RMS error results for model and parameter sensitivity analysis calculated over inner surf zone area.

inner surf zone (x = 450-600)	28.04.2011		01.06.2011		06.06.2011		11.06.2011		30.06.2011*	
	BSS	*RMS error*	*BSS*	*RMS error*	*BSS*	*RMS error*	*BSS*	*RMS error*	*BSS*	*RMS error*
Exe. 1	0.190	0.501	-5.465	1.511	-5.968	1.617	-5.234	1.622	-8.770	1.541
Exe. 2	0.047	0.397	-0.059	0.652	0.159	0.539	-0.158	0.611	-4.181	1.028
Exe. 2 with Tr=10 days	0.142	0.353	0.160	0.576	0.246	0.508	0.013	0.580	-3.432	0.956
Exe. 2 with Tr=15 days	0.289	0.306	-0.093	0.615	-0.037	0.603	-0.068	0.624	-2.937	0.903
Exe. 3	0.396	0.272	0.281	0.517	0.467	0.396	0.220	0.481	-2.562	0.855
Exe. 3 (with 0.65*t)	0.368	0.282	0.274	0.524	0.474	0.393	0.220	0.483	-2.724	0.876
Exe. 3 with Tr=10 days	0.455	0.266	0.165	0.535	0.318	0.476	0.215	0.501	-2.174	0.800

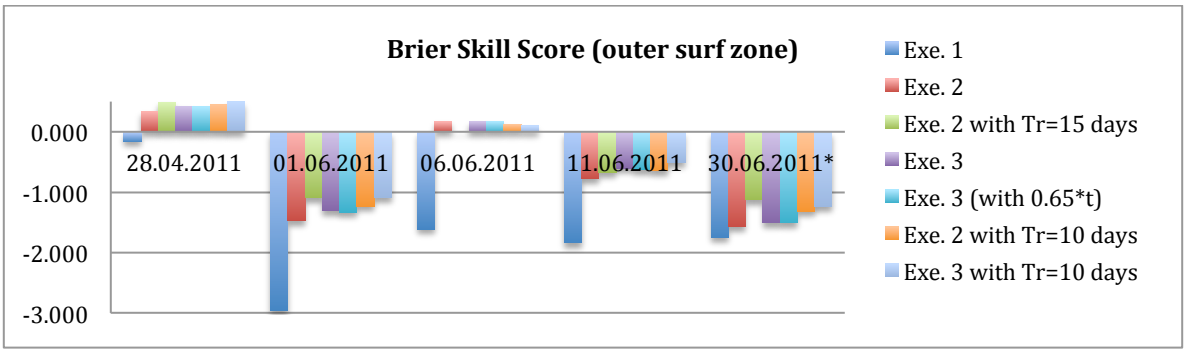

Figure B-6. Brier skill scores over outer surf zone for model settings and parameter sensitivity.

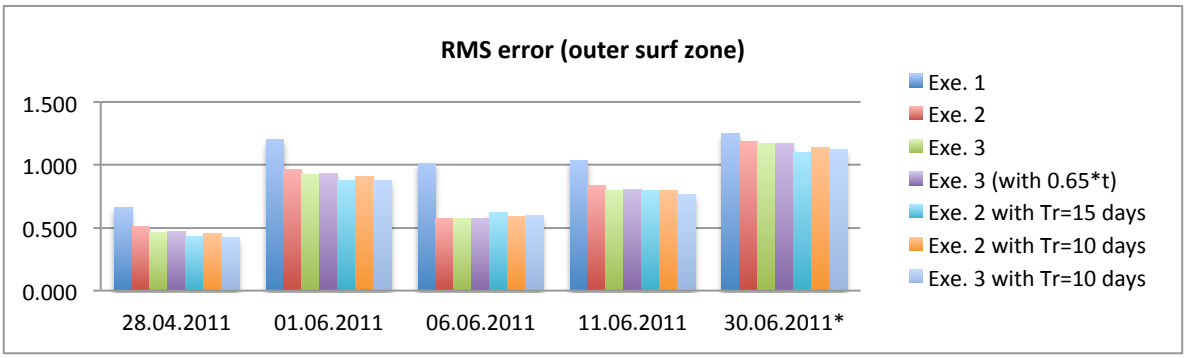

Figure B-7. RMS errors over outer surf zone for model settings and parameter sensitivity.

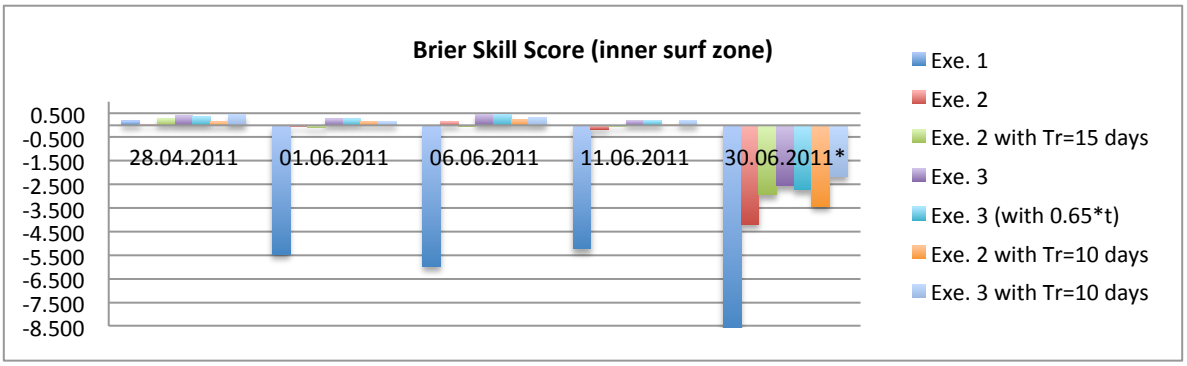

Figure B-8. Brier skill scores over inner surf zone for model settings and parameter sensitivity.

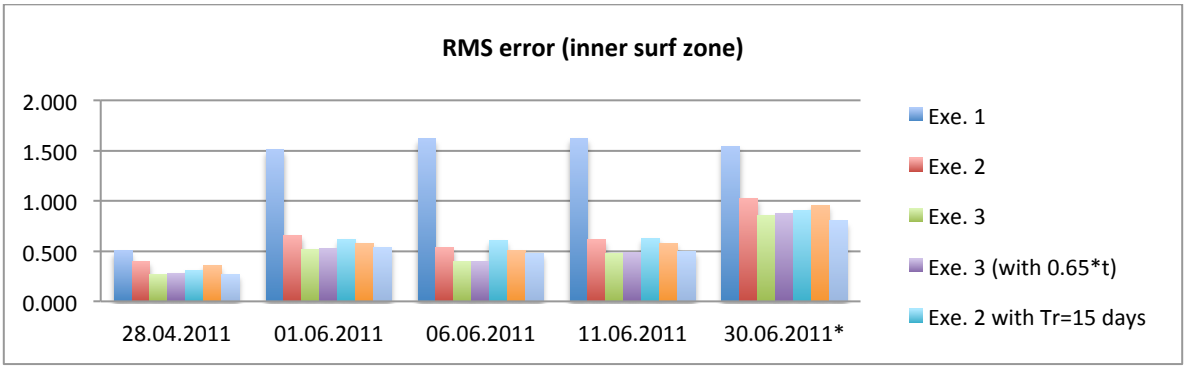

Figure B-9. RMS errors over inner surf zone for model settings and parameter sensitivity.

C. IMAP SENSITIVITY RESULTS

The figures presented here correspond to the resulting bathymetries for varying combinations of imap inputs. All figures present the initial bathymetry (which is the measured bathymetry on the 15th of March 2011), the current measured bathymetry (labeled with "Measured" and the corresponding date), the modelled bathymetry with executable 3 and all imaps (labeled Exe. 3 with corresponding date), the modelled bathymetry with a changed set of imaps, and a difference plot between the modeled bathymetry with all imaps and the varied set of imaps. In some cases the dates labeled on the measured bathymetry and the modeled bathymetries wont coincide, that is due to the fact that by removing certain imaps in some cases the dates with measured bathymetries will not have available imaps; therefore the closest modeled date to the measured date is chosen.

C-1. Bathymetry plots using imaps ranked 3 and 4

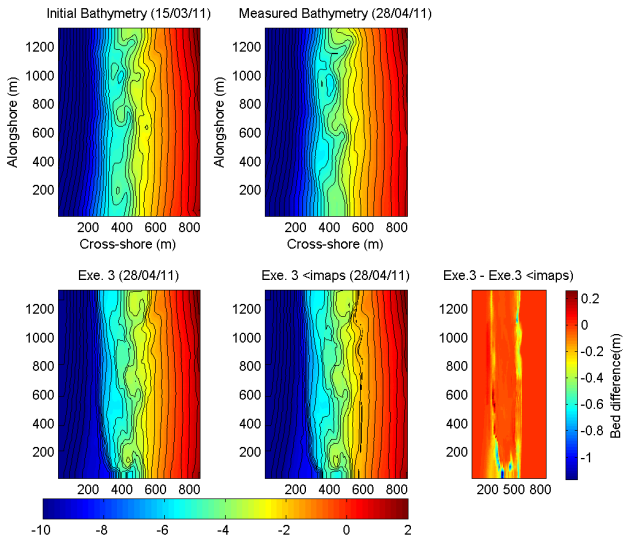

Figure C-1. Resulting bathymetries on the 28th of April using only imaps ranked 3 and 4.

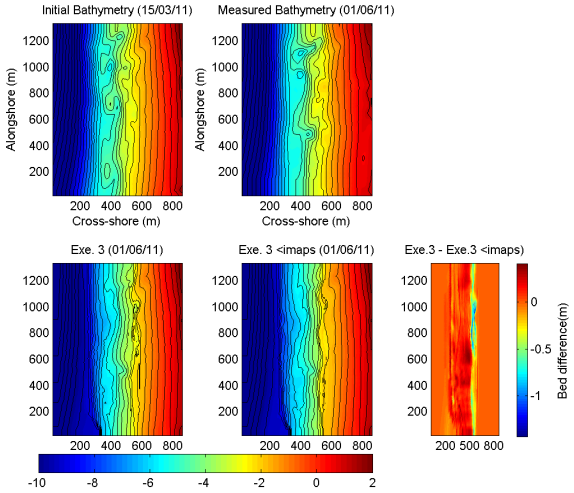

Figure C-2. Resulting bathymetries on the 1st of June using only imaps ranked 3 and 4.

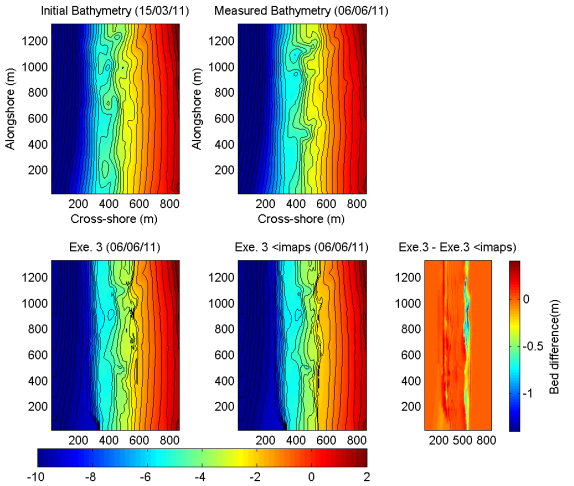

Figure C-3. Resulting bathymetries on the 6th of June using only imaps ranked 3 and 4.

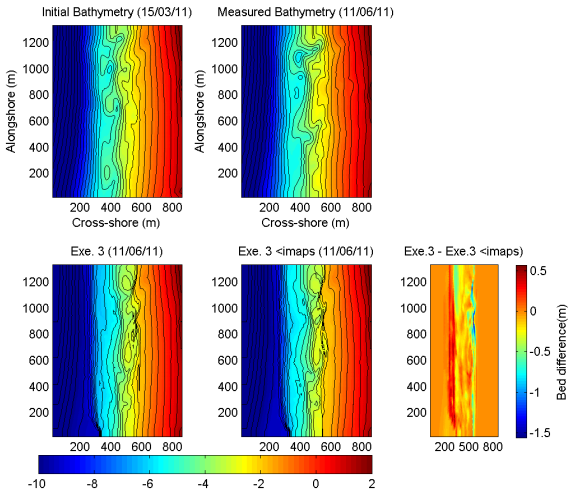

Figure C-4. Resulting bathymetries on the 11th of June using only imaps ranked 3 and 4.

C-2. Bathymetry plots using three or more consecutive daily imaps

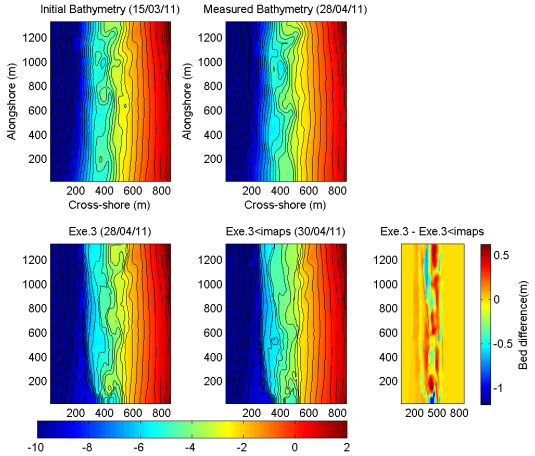

Figure C-5. Resulting bathymetries on the 30th of April using only imaps from days with more than 2 images.

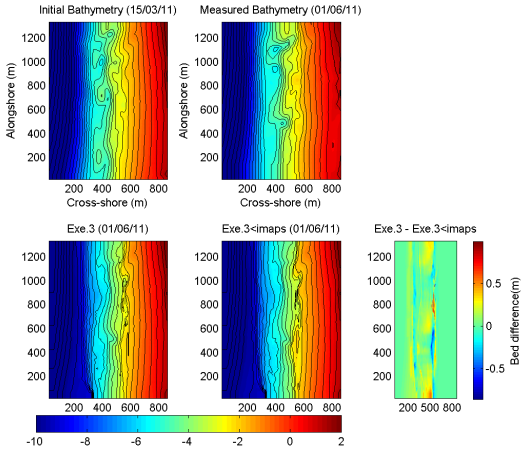

Figure C-6. Resulting bathymetries on the 1st of June using only imaps from days with more than 2 images.

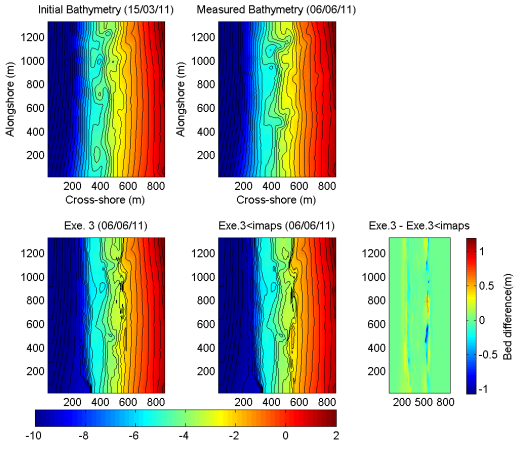

Figure C-7. Resulting bathymetries on the 6th of June using only imaps from days with more than 2 images.

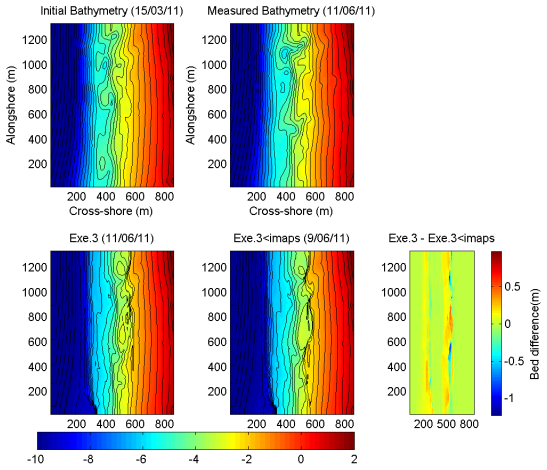

Figure C-8. Resulting bathymetries on the 9th of June using only imaps from days with more than 2 images.

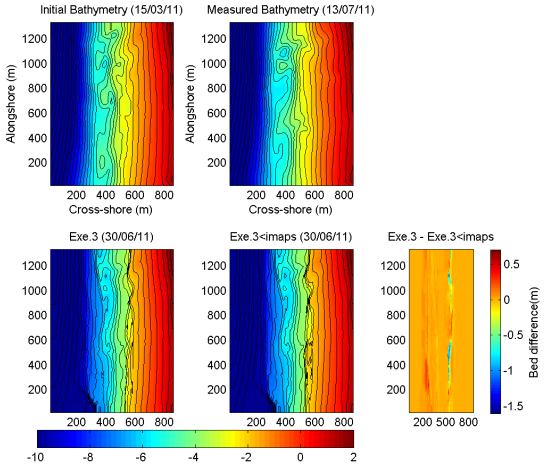

Figure C-9. Resulting bathymetries on the 30th of June using only imaps from days with more than 2 images.

C-3. BSS and RMS error results

Table C-1. BSS and RMS results calculated over whole domain for imap sensitivity model runs.

Whole Domain	28.04.2011		01.06.2011		06.06.2011		11.06.2011		30.06.2011*	
	BSS	*RMS error*	*BSS*	*RMS error*	*BSS*	*RMS error*	*BSS*	*RMS error*	*BSS*	*RMS error*
imaps 234	0.384	0.263	-0.838	0.512	-0.178	0.402	-0.578	0.464	-2.137	0.673
imaps 3 and 4	0.352	0.269	-1.150	0.552	-0.122	0.394	-0.337	0.429	-1.870	0.651
imaps 4	0.275	0.287	-0.471	0.449	0.058	0.358	-0.098	0.385	-1.012	0.553
3 or more consecutive	0.279	0.288	-1.193	0.554	-0.368	0.431	-0.850	0.501	-2.160	0.677
imaps once per week	0.312	0.273	-0.874	0.502	-0.449	0.439	-0.612	0.478	-0.976	0.533
3 images per day	0.386	0.262	-0.365	0.441	-0.004	0.372	-0.439	0.442	-1.663	0.626
1 image per day	0.403	0.257	-0.220	0.412	0.049	0.362	-0.233	0.412	-0.768	0.524
manual imap selection	0.317	0.280	-0.219	0.420	0.108	0.354	0.122	0.349	-0.812	0.507
period above 7.5 s	0.381	0.263	-1.201	0.559	-0.277	0.422	-0.876	0.508	-1.797	0.650
wave height above 0.85m	0.382	0.264	-0.988	0.530	-1.532	0.591	-1.676	0.605	-2.194	0.689
1 imap per day, initial flat bed	0.001	0.338	-0.147	0.445	0.006	0.416	-0.202	0.457	-0.780	0.555

Table C-2. BSS and RMS results calculated over the outer surf zone for imap sensitivity model runs.

Outer surf zone (x = 250-450)	28.04.2011		01.06.2011		06.06.2011		11.06.2011		30.06.2011*	
	BSS	*RMS error*	*BSS*	*RMS error*	*BSS*	*RMS error*	*BSS*	*RMS error*	*BSS*	*RMS error*
imaps 234	0.498	0.425	-1.089	0.877	0.098	0.598	-0.508	0.764	-1.236	1.121
imaps 3 and 4	0.480	0.428	-1.591	0.972	-0.008	0.631	-0.444	0.739	-1.226	1.119
imaps 4	0.308	0.483	-0.732	0.783	0.205	0.559	0.018	0.604	-0.692	0.985
3 or more consecutive	0.316	0.492	-1.329	0.925	0.068	0.614	-0.522	0.772	-1.295	1.133
imaps once per week	0.391	0.451	-1.332	0.904	-0.739	0.806	-1.012	0.877	-0.750	0.972
3 images per day	0.494	0.420	-0.597	0.766	-0.026	0.626	-0.505	0.756	-0.876	1.049
1 image per day	0.542	0.396	-0.374	0.704	0.028	0.610	-0.467	0.738	-0.448	0.948
manual imap selection	0.426	0.449	-0.497	0.741	0.066	0.593	-0.078	0.620	-0.750	0.945
period above 7.5 s	0.487	0.428	-1.455	0.952	0.016	0.633	-0.242	0.706	-1.087	1.112
wave height above 0.85m	0.499	0.425	-1.100	0.878	-1.594	1.004	-1.175	0.912	-1.247	1.149
1 imap per day, initial flat bed	0.304	0.411	-0.203	0.698	0.047	0.606	-0.433	0.735	-1.191	0.939

Table C-3. BSS and RMS results calculated over the inner surf zone for imap sensitivity model runs.

inner surf zone (x = 450-600)	28.04.2011		01.06.2011		06.06.2011		11.06.2011		30.06.2011*	
	BSS	*RMS error*	*BSS*	*RMS error*	*BSS*	*RMS error*	*BSS*	*RMS error*	*BSS*	*RMS error*
imaps 234	0.455	0.266	0.165	0.535	0.318	0.476	0.215	0.501	-2.174	0.800
imaps 3 and 4	0.408	0.275	-0.070	0.572	0.351	0.428	0.246	0.413	-1.745	0.744
imaps 4	0.588	0.257	0.179	0.454	0.340	0.406	0.133	0.439	-0.838	0.612
3 or more consecutive	0.547	0.265	-0.194	0.627	0.118	0.539	-0.054	0.600	-2.135	0.797
imaps once per week	0.462	0.230	0.091	0.480	0.393	0.386	0.281	0.439	-0.580	0.550
3 images per day	0.467	0.261	0.395	0.432	0.525	0.372	0.317	0.461	-1.766	0.744
1 image per day	0.454	0.256	0.385	0.414	0.521	0.648	0.460	0.386	-0.472	0.541
manual imap selection	0.602	0.274	0.470	0.402	0.571	0.356	0.560	0.308	-0.266	0.497
period above 7.5 s	0.439	0.260	-0.133	0.617	0.236	0.507	-0.196	0.682	-1.678	0.737
wave height above 0.85m	0.455	0.267	-0.010	0.587	-0.154	0.655	-0.525	0.775	-2.209	0.813
1 imap per day, initial flat bed	-0.148	0.2825	-0.14	0.4206	0.078	0.3821	0.037	0.4048	-2.26	0.5515

Table C-4. BSS and RMS results calculated at corresponding measured rip channel locations for imap sensitivity model runs.

At Rip channel	28.04.2011		01.06.2011		06.06.2011		11.06.2011		30.06.2011*	
	BSS	*RMS error*	*BSS*	*RMS error*	*BSS*	*RMS error*	*BSS*	*RMS error*	*BSS*	*RMS error*
imaps 234	0.751	0.2742	0.589	0.4782	0.665	0.3739	0.543	0.4095	-4.144	0.9349
imaps 3 and 4	0.766	0.2652	0.29	0.6521	0.634	0.401	0.465	0.4262	-3.985	0.9201
imaps 4	0.591	0.3546	0.579	0.4284	0.645	0.3937	0.461	0.4499	-3.495	0.8708
3 or more consecutive	0.683	0.3065	0.448	0.5548	0.652	0.3866	0.508	0.4416	-4.181	0.9379
imaps once per week	0.529	0.3728	0.417	0.5339	0.569	0.428	0.222	0.5572	-2.389	0.744
3 images per day	0.721	0.2968	0.678	0.4082	0.692	0.3665	0.502	0.4357	-4.361	0.9565
1 image per day	0.733	0.2828	0.612	0.4719	0.6	0.4647	0.414	0.47	-3.461	0.868
manual imap selection	0.377	0.4355	0.475	0.5624	0.715	0.3561	0.512	0.3813	-1.83	0.6874
period above 7.5 s	0.762	0.2678	0.313	0.6409	0.603	0.4442	0.393	0.5283	-4.656	0.9823
wave height above 0.85m	0.75	0.2746	0.583	0.4818	0.508	0.5318	0.031	0.6323	-4.716	0.9897
1 imap per day, initial flat bed	0.351	0.3013	0.053	0.4812	0.051	0.4751	-0.69	0.4836	-5.84	0.8886

D. BSS AND RMS ERROR CALCULATION DOMAINS

Here the domains over which the Brier skill scores and RMS error were calculated will be shown for each measured bathymetry date. The red dashed line box is the location of the rip channel, the "whole domain" refers to the entire area above the horizontal black dashed line, the "outer surf zone" is the area between the vertical red and black dashed lines (and above the horizontal black dashed line), and the "inner surf zone" is the area between the vertical black and blue dashed lines.

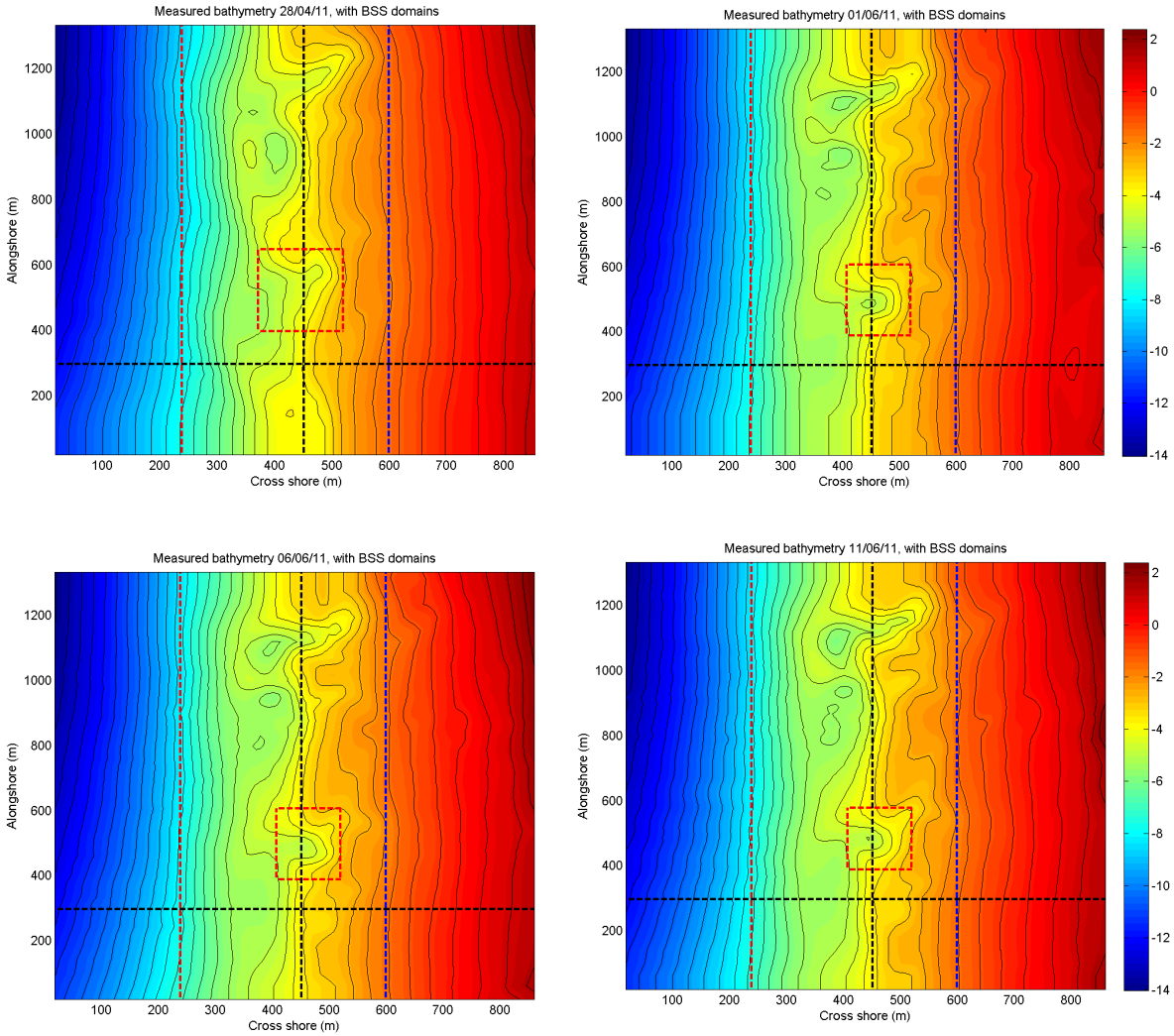

Figure D-1. Calculation domains for BSS and RMS errors for 28/04/11, 01/06/11, 06/06/11, and 11/06/11.

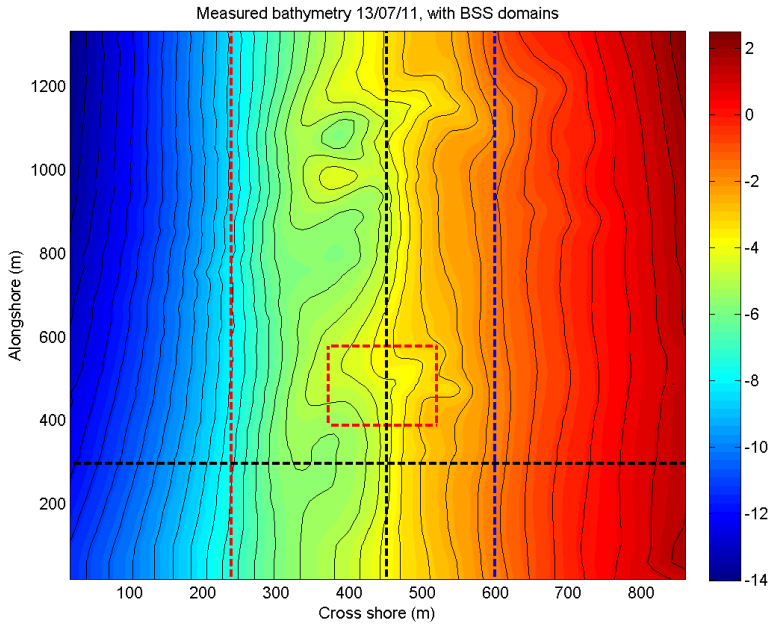

Figure D-2. Calculation domains for BSS and RMS errors for 30/06/11.

E. GRADIENT FORMULATIONS

For the case in which the source is wave dissipation, f in Equation (15) (from section 2.3.1 in the present report) will be substituted by D_r. The gradient which is of interest is dD_r/dh, however, this gradient cannot be computed analytically. Because of this, the derivative of the organized wave field will be used in its place, namely dD_w/dh. The formula of Baldock et al. (1998) is used for the computation of the dissipation rate of organized wave motion. The computation of the gradient in question is calculated as follows:

$$\frac{dD_w}{dh} = \frac{dD_w}{d\Gamma}\frac{d\Gamma}{dH_b}\frac{dH_b}{dh} \tag{E-1}$$

in which

$$D_w = \frac{1}{4}\rho g f_p H_{rms}^2 e^{-\Gamma}(1+\Gamma)$$

$$\Gamma = (\frac{H_b}{H_{rms}})^2$$

$$H_b = \frac{0.88}{k}tanh(\frac{\gamma kh}{0.88})$$

$$\gamma = 0.29 + 0.76kh$$

Therefore,

$$\frac{\partial D_w}{\partial \Gamma} = -\frac{1}{4}\rho g f_p H_{rms}^2 \Gamma e^{-\Gamma} \tag{E-3}$$

$$\frac{\partial \Gamma}{\partial H_b} = 2\frac{H_b}{H_{rms}^2} \tag{E-4}$$

$$\begin{aligned}\frac{\partial H_b}{\partial h} = & \frac{1}{\cosh^2(\frac{0.29kh + 0.76(kh)^2}{0.88})} \\ & [(0.29 + 2*0.76kh)(\frac{-kh}{\sinh kh\cosh kh + kh} + 1)] + \\ & \frac{0.88\tanh(\frac{0.29kh + 0.76(kh)^2}{0.88})}{\sinh kh\cosh kh + kh}\end{aligned} \tag{E-5}$$

By inserting Equations (E-3), (E-4), and (E-5) into Equation (E-1) the gradient of organized wave dissipation is found.